MICROBIAL PARTNERS IN HEALTH: BROADENING OUR UNDERSTANDING OF HOST-MICROBIOME RELATIONSHIPS

A Dissertation Presented for the

Doctor of Philosophy

Degree

The University of Tennessee, Knoxville

Sarah Stuart Chewning

December 2018

Copyright © 2018 by Sarah Stuart Chewning
All rights reserved.

DEDICATION

To God be the glory.

For Zack who showed me that with faith and perseverance, my dreams can come true.

“It was not by accident that the greatest thinkers of all ages were deeply religious souls."

-Max Planck

"I was taught that the way of progress was neither swift nor easy." -Marie Curie

ACKNOWLEDGEMENTS

I had a crazy idea. I was going to quit my job, that paid well, and go back to school—full time—and live like a student again. I've never taken the easy path, and I'm honestly not sure why. What I am certain of is that embarking on this journey was the absolute right decision. It was a decision made with much prayer, doubt, and finally, resolution. Jesus intentionally designed every part of this plan and surrounded me with people and places for my good and His glory.

I thank Sarah. She took a chance on me in so many ways. She was continually patient, gracious and supportive through emotionally, physically and psychologically brutal life circumstances. She kept me on track, gave me time when needed most, and challenged me in ways no one else could. Sarah taught me how to be a good scientist. She taught me to accept scientific rejection and push forward. She taught me I could accomplish things I doubted. She was a gift and I am grateful.

I thank David. He's been a dear friend, a reflection of Christ's Truth, a steady support, and the scientist by my side for many of these years.

Thank you to my committee, Alison Buchan, Gladys Alexandre, Chunlei Su, and again Sarah Lebeis, for support, guidance and patience. You have individually and collectively taught me how to be a good scientist and have led by example.

My dearest girls Karen, April, Sam, Beth, Margo and Katie, you are a source of joy, Truth, generosity and rest.

I thank my parents, with God, you molded and guided me. You are a constant, steadfast source of love and grace. You have consistently given me the best and I am grateful.

Finally, I thank the love of my life, the one for which "it" was all worth, Zack. You have shown me what God intended love on this Earth to be. Your selflessness, encouragement, grace, and love reflect His goodness. You are a good man. I am grateful.

ABSTRACT

While microbes inhabit a wide array of environments, their ability to live within host tissue and become tolerated as part of a select microbial community is perhaps one of the most impressive feats of microbial resilience and survival. Host microbiome establishment and maintenance requires both host-microbe and microbe-microbe interactions. Among plant hosts, benefits from associated microbiomes are known to include improved growth, development and resistance to abiotic and biotic stresses. Mammalian microbiomes are known to improve host digestion, influence inflammation and even improve immune response to pathogens. While host-associated microbial communities across all domains of life are incredibly diverse, a growing number of studies are finding host-specific taxonomic trends, suggesting microbiome conservation and evolutionary selection. However, we have come to recognize that there is often functional redundancy between taxa. Therefore, investigative focus on microbiome composition potentially neglects pivotal and influential microbial players. Shifting focus to function over form creates the opportunity to tease apart the driving forces of unique microbiome constituents. This allows for identification of strains and genes of interest as well as microbial selections. To that end, here we describe the relationships between hosts and microbiomes as well as between microbes in two vastly different host systems (Figure 1.1). First, we suggest that plant root-associated *Streptomyces* isolates harboring genes encoding an enzyme and its co-factor are more tolerant of phenolic compounds generated by roots. Next, we address the capability of these *Streptomyces* isolates to employ their metabolic repertoires to influence the composition of the root microbiome. Finally, we define a previously under-described role for the gut microbiome in malaria immunology and suggest that gut microbial composition can modulate the severity of malarial disease. Together, these findings demonstrate the broad implications of microbiome composition across diverse hosts and environments, revealing unexplored opportunities for therapeutic interventions aimed at improving plant and human health.

TABLE OF CONTENTS

CHAPTER ONE - INTRODUCTION....1
I. MICROBIOMES ACROSS HOST SPECIES....3
I. THE PLANT ROOT MICROBIOME....5
Plant-microbe interactions....5
Microbe-microbe interactions....9
II. THE MAMMALIAN GUT MICROBIOME....10
Chronic diseases....11
Infectious diseases....14
III. OBJECTIVES....16
IV. REFERENCES....17
V. APPENDIX: FIGURES....29
CHAPTER TWO - ROOT-ASSOCIATED STREPTOMYCES ISOLATES HARBORING MEL GENES DEMONSTRATE ENHANCED PLANT COLONIZATION....30
I. ABSTRACT....32
I. INTRODUCTION....33
II. MATERIALS AND METHODS....35
Streptomyces culture preparation....35
Extracellular pigment extraction....36
Liquid-chromatography mass spectrometry....36
Pangenomic visualization....37
Phylogenetic trees and identification of mel operons....38
Tyrosinase Assay....38
Phenolic compound challenges on agar....39
Salicylic acid challenge in liquid media....40
Seed sterilization and germination....40
Plant colonization experiments....41
Statistical analysis....42
III. RESULTS....42
Melanin production is associated with root-enriched Streptomyces strains....42
Genomes of melanin-producing strains contain genes essential for melanin production....43
Enzyme kinetics differentiate tyrosinase activity between Streptomyces strains....44
Survival and growth in the presence of phenolic compounds is improved in better colonizers....45
Seedling colonization is Streptomyces strain and tyrosinase identity dependent....47
IV. DISCUSSION....48
Streptomyces' metabolic potential in the root microbiome....48
Streptomyces' employ distinct tyrosinase enzymes....48

Comparative genomics inform benchtop experimentation....49
A new role for a common microbial product....50
V. ACKNOWLEDGEMENTS....51
VI. REFERENCES....52
VII. APPENDIX: TABLES....58
VIII. APPENDIX: FIGURES....60
CHAPTER THREE - MULTI-SCALE DESIGN TRANSLATES COMPARATIVE GENOMIC PREDICTIONS AND IN VITRO MICROBIAL INTERACTIONS INTO DEFINED ROOT MICROBIOME ASSEMBLAGES....70
I. ABSTRACT....72
I. INTRODUCTION....73
II. MATERIALS AND METHODS....76
Genome comparison and biosynthetic gene cluster identification....76
Bacterial culture preparations....76
Molten overlay experiments....77
Co-culture assays....77
Seed sterilization and germination....78
Vertical plate assays....78
Colorimetric auxin assay....78
Wild soil slurry preparation....79
Plant inoculations....79
Plant growth and harvest....79
DNA extraction and 16S rRNA gene community sequencing....80
16S rRNA gene amplicon QIIME 2 analysis....80
Statistical analyses....81
III. RESULTS....82
Identification of biosynthetic gene clusters from bacterial genomes predict microbe-microbe interactions during root microbiome assemblage....82
In vitro microbe-microbe challenges suggest Streptomyces strains can both co-exist and also compete....83
Root phenotypes are Streptomyces strain-specific....85
Root morphology phenotypes are not solely dependent on microbial indole-3-acetic acid production....86
16S rRNA gene amplicon sequencing of A. thaliana with three distinct inoculation events indicates inoculum complexity contributes to community assembly....87
IV. DISCUSSION....90
V. ACKNOWLEDGEMENTS....93
VI. REFERENCES....94
VII. APPENDIX: TABLES....99

VIII. APPENDIX: FIGURES 106
CHAPTER FOUR - COMPOSITION OF THE GUT MICROBIOME REGULATES THE SEVERITY OF MALARIA 120
I. ABSTRACT 122
II. INTRODUCTION 123
III. MATERIALS AND METHODS 124
Animals and housing 124
Diets 124
Plasmodium infection 125
Evaluation of parasitemia 125
Enumeration of red blood cells and parasitized red blood cells 125
Cecum transplant 126
Gut microbiota analysis 126
Metabolomics analysis 127
Yogurt treatment 129
Isolation and sequencing of Lactobacillus 129
Cellular immune response 130
Detection of P. *yoelii* $MSP1_{19}$-specific antibodies 130
Statistical analysis 131
IV. RESULTS 131
Mice from different vendors exhibit differential susceptibility to malaria. 131
Gut bacterial community structure and function are different in resistant and susceptible mice. 133
Differences in the gut microbiome shape susceptibility to malaria. 134
Decreased parasite burden in mice treated with Lactobacillus and Bifidobacterium. 134
Severity of malaria tracts with the magnitude of the host immune response. 135
V. DISCUSSION 136
VI. ACKNOWLEDGEMENTS 140
VII. REFERENCES 141
VIII. APPENDIX: FIGURES 146
CHAPTER FIVE - CONCLUSIONS AND FUTURE DIRECTIONS 178
I. REFERENCES 185
VITA 189

LIST OF TABLES

Table 2.S1. Strains referenced in this study. 58
Table 2.S2. Streptomyces' genome investigation reveals divergent properties and biosynthetic predictions..... 59
Table 3.1. Strains included in SynCom*, coculture^, and/or comparative genomics# 99
Table 3.2. Genome statistic and biosynthetic gene proportion. 100
Table 3.3. Co-culture cross spots indicate microbe-microbe growth influences..... 101
Table 3.4. 16S rRNA amplicon community sequencing root microbiome sample information. 105

LIST OF FIGURES

Figure 1.1. Host-microbiome interactions triad.....29
Figure 2.1. Streptomyces strains 299 and 303 produce a pigment consistent with synthetic melanin. 60
Figure 1.2. Phylogenetic and pangenomic comparison of *Streptomyces spp*. indicate distinct phylogeny and overlapping genes consistent with melanin production……...……...61
Figure 2.3. Strain-specific tyrosinase activity and kojic acid (KA) inhibition is demonstrated via dopachrome production from L-DOPA with the addition of cell and extracellular 299, 303, CL18 and 136 protein extracts. 62
Figure 2.4. Phenolic compound tolerance differs by *Streptomyces* strain. 64
Figure 2.5. Differential colonization of *Arabidopsis thaliana* seedlings by *Streptomyces* strains. 65
Figure 2.S1. *Streptomyces* strains 299, 303, CL18 and 136 do not alters plant biomass, even 8 weeks after inoculation. ……..66
Figure 2.S2. Intracellular and extracellular protein extracts from 303 are inhibited by kojic acid (KA).....67
Figure 2.S3. Challenge of all strains with catechol and benzoate indicate variable differences in CFU formation. 68
Figure 2.S4. Colonization of *Arabidopsis thaliana* seedlings by *Streptomyces* strains when grown with melanin compounds indicates no differences……..69
Figure 3.1. antiSMASH strain genome analysis reveals unique biosynthetic gene clusters and potential metabolites……..106
Figure 3.2. *Streptomyces* interactions demonstrate potential growth inhibition. 107
Figure 3.3. *Streptomyces* spp. differentially influence *A. thaliana* root morphology.....108
Figure 3.4. Microbial auxin production does not fully explain root phenotypes. 109
Figure 3.5. Experimental schematic for 16S rRNA amplicon sequencing samples. 110
Figure 3.6. Alpha diversity indicates species richness by root microbiome sample. 111
Figure 3.7. Principle coordinate analysis (PCoA) generated via weighted UniFrac distances shows diversity between samples. 112

Figure 3.8. Relative abundance of phyla in root microbiome samples with Wild secondary inoculum differ. 113
Figure 3.9. Relative abundance of families from samples secondarily inoculated with SynCom are different than the SynCom inoculum. 114
Figure 3.10. Relative abundance of Actinobacteria families in all samples. 115
Figure 3.11. Relative abundances of Alphaproteobacteria families. 117
Figure 3.12. Gammaproteobacteria family relative abundances. 119
Figure 4.1. Plasmodium parasite burden, morbidity and mortality vary by mouse vendor and diet. 146
Figure 4.2. Susceptibility to malaria correlates with differences in cecal bacteria populations. 147
Figure 4.3. Gut microbiome shapes susceptibility to severe malaria. 148
Figure 4.4. Susceptible mice treated with yogurt have decreased parasitemia and morbidity. 149
Figure 4.5. Resistant Jax mice have an elevated cellular and humoral immune response to Plasmodium. 150
Figure 4.S1. Differential anemia and circulating parasitized red blood cells between mice from different vendors. 151
Figure 4.S2. Similar susceptibility to parasitized red blood cell infection between C57BL/6 mice from different vendors. 152
Figure 4.S3. C57BL/6 mice from Charles River are susceptible to high P. yoelii parasite burden. 153
Figure 4.S4. Modulation of malaria pathogenesis by the gut microbiota is generalizable to another mouse strain and Plasmodium species. 154
Figure 4.S5. Inversion of Jax and NCI in-house diets minimally effects severity of P. yoelii infection. 155
Figure 4.S6. Susceptibility to malaria correlates with differences in the gut microbial community structure. 156
Figure 4.S7. Jackson mice fed Teklad 22/5 diet exhibit defined changes in cecal bacterial populations. 157
Figure 4.S8. Distinct bacterial community structure in Jackson mice fed separate diets. 158

Figure 4.S9. Changes in the gut microbial community structure correlate with changes in the gut and plasma metabolome in resistant and susceptible mice. 159
Figure 4.S10. Germ-free mice colonized wtih cecal content have similar bacterial diversity as donor sample. 161
Figure 4.S11. Lactobacillus and Bifidobacterium are among the bacteria that drive differences between the gut-associated bacterial communities of resistant and susceptible mice. 162
Figure 4.S12. Phylogenetic tree of bacteria isolated from stool samples and lab-cultured yogurt. 163
Figure 4.S13. Treatment of gut microbiota intact mice with yogurt has a modest effect on parasite burden. 164
Figure 4.S14. Gating strategy for T cell and B cell populations in Jax and NCI mice infected with P. *yoelii*. 165
Figure 4.S15. Sequencing and diversity metrics from Jax, Har, NCI, and Tac mice. 166
Figure 4.S16. Variability in each sample type for PLS-DA. 168
Figure 4.S17. Average small intestine metabolite ion counts and relative standard deviations (RSD) for Jax (n=5) and NCI (n=5) mice. 169
Figure 4.S18. Average cecum metabolite ion counts and relative standard deviations (RSD) for Jax (n=4) and NCI (n=5) mice. 172
Figure 4.S19. Average plasma metabolite ion counts and relative standard deviations (RSD) for Jax (n=5) and NCI (n=5) mice. 175

CHAPTER ONE - INTRODUCTION

A VERSION OF THIS CHAPTER WAS PREVIOUSLY PUBLISHED

Sarah Stuart Sloan and Sarah L. Lebeis. "Under the influences: effects of distinct biotic interactions on root microbiomes." *Current Opinion in Plant Biology* 26 (2015): 32-36.

Two individuals significantly contributed to this manuscript, Sarah Stuart Chewning (Sloan) and Sarah L. Lebeis. SSC and SLL both conceived of the topics covered and wrote the manuscript.

I. MICROBIOMES ACROSS HOST SPECIES

Microbiomes are formed when organisms assemble in communities. Often these microbial communities live in close proximity to, or even within, complex host organisms. Dynamic relationships develop between hosts and their microbiomes as well as among the microbial constituents [1]. Generally, maintenance of microbiome stability is fundamentally beneficial to the host. In addition to protection from biotic stress, microbiomes also extend the host metabolic repertoire, nutrient acquisition and protection from abiotic stress [2-4]. Included here in describing host-microbiome and microbe-microbe dynamics are both the microbial organism and their respective genomes. Recent improvements in sequencing technologies, data analysis techniques, and study design allow definition of the microbiota and potential functional implications of these intimate and important relationships with increasing accuracy. Interestingly, microbiome studies are revealing patterns across various host species, providing valuable insight into microbiome influence on host development, metabolism, innate immunity, and even pathogen resistance [1, 5-9]. These patterns are likely multivariate and may suggest evolutionary influences, as well as host and microbial assemblage pressures [1, 10-14]. While taxonomic characterizations are an essential foundation, transcriptional and protein community studies are now shedding light on functional overlaps and drilling down dominant species-specific tasks that may have once been unappreciated or overlooked.

Regardless of host, most microbiomes are extremely diverse and often differ greatly from the microbes inhabiting their surrounding environment [15]. Interestingly the concept of a core microbiome is recognized within various hosts including invertebrates, humans, plants and others [9, 16-22]. Host selection is known to play a key role in selection of this core, with the host immune system being a fundamental component of selective pressure, employing a variety of host-specific immune strategies influential in shaping the microbiome [23-25]. For example, when infected with a pathogen, the model plant *Arabidopsis thaliana* alters its root microbiome to selectively incorporate disease-suppressive and growth-promoting microbes [26]. Similarly, microbes in the gut can control pathogens by preferentially altering the environment via consuming nutrients the pathogen needs to replicate and survive [27]. In general, microbiome disruption can lead to dysbiosis and ultimately pathogenesis [28]. However, in addition to the microbiome,

homeostasis is reliant on host genetics and the environment, which can be disrupted by alteration of even one host gene [16]. Studies of germ-free animals demonstrate host microbiome importance for health and wellness including immune development [29, 30]. As we continue to gain insights into the complexities of microbiomes, the delicate yet resilient relationships between hosts, their microbiomes and microbes themselves become ever more evident.

Importantly, the stable host genome is off-set by the rapid evolutionary capability of the inhabiting microbial genomes. While potentially risky, the perceived host benefit must outweigh the inevitable risk of microbial evolution to pathogenicity. As microbiomes can assemble with and without hosts, assimilation and maintenance with plants and animals suggests mutual benefit [2-4, 31]. Although assemblage patterns are evident and resulting core microbiomes have been identified, the importance of individual taxa cannot be overlooked [15]. Interestingly, as yet, substantial taxonomic overlaps between plant roots and the mammalian gut have not been identified [3]. However, when microbiomes from diverse environments, including plants, were introduced into the guts of germ-free mice, the microbes successfully established residency and competed [32], suggesting the potential for discovery of common taxa. It is also essential to recognize that in general, taxonomic abundance does not necessarily correlate with functional influence. In fact, transient or rare microbiome taxa sometimes disproportionately influence their host [33].

In summary, microbiome assemblage requires host and microbe tolerance and energy, which transcends to which domain of life the host belongs [1, 3, 15]. The host immune system must tolerate non-self and microbiome members must tolerate one another. In many cases, the relationships between a host and its microbiome are crucial for hosts to thrive [11, 34]. In other cases, bacterial dysbiosis is associated with a variety of disease and immune complications [35-39]. Microbiomes have been implicated in modulating host immune responses [19, 24, 40-45] and inclusion or exclusion of certain taxa within the microbiome can influence disease severity in mammals [41, 46, 47] and plants [2, 39]. Despite host and environmental pressures, microbial assemblages that have survived, thrived and evolved to become paramount in many domains of life, leading to the suggestion of the holobiont [16]. Thus, definition of general microbiome traits,

including composition and function are necessary for identification of knowledge gaps and potential areas for investigation.

I. THE PLANT ROOT MICROBIOME

Root microbiomes are formed from diverse microbial soil surroundings with extraordinary uniformity, suggesting consistent mechanisms of community assembly. Complex soil communities house incredible potential for agricultural application and are known to contribute to plant health and protection [48]. Strategies to harness this potential with minimal environmental impact are underway [49-51]. In addition to expanding our understanding of microbiome establishment from complex soil communities, collections of plant-specific microbiomes are being established by laboratories across the world with varying goals for elucidating their forms and function [31, 50, 52-55]. Comparing datasets provides powerful insights into the overlap of plant microbiomes, as well as the impacts of surrounding plants and microbes on root microbiomes and long-term soil conditioning.

The relationship between a plant and its microbiome may promote plant productivity by improving accessibility to nutrients, producing plant growth stimulating factors, outcompeting invading pathogens, and inducing protection against infection and various abiotic stresses [2, 3, 26, 56]. Only particular taxa are assembled and maintained within the phyllosphere (above-ground plant tissue), rhizosphere (surrounding the root) and root microbiomes. While there are overlaps, these plant fractions are known to house distinct sets of microbes [2, 57-59]. The composition of the whole (internal and closely adhering) root microbiome is influenced by various biotic interactions, but of particular interest here is its relevance to plant-microbe and microbe-microbe relationships (Figure 1.1). Here we specifically address how recent studies tease apart the impact of these biotic interactions on plant root microbiome composition.

Plant-microbe interactions

While whole root microbiomes impact plant ecology with both negative feedback from plant pathogens and positive feedback from beneficial microbes, plants condition the soil microbiota [60, 61]. In fact, the pathogens of seasonal crops grown in monoculture fields are among the

considerations used to decide which crops will be in rotation with each other [60]. Specifically, pea and oat are often used as break crops in rotation schemes to promote yield of crops such as wheat [62]. When the rhizosphere communities of these three crops were examined in a common soil, it was revealed that both pea and oat appeared to exert strong selection on eukaryotic microbial communities [63]. Conversely, it has been suggested that plants can act as master manipulators, modulating microbial behaviors to their advantage [64, 65], and further that plant selection of co-residents can be influenced by "metabolic complementation," in which plants may search for organisms that selectively supplement their carbon and nutrient profiles [58].

Unique plant root exudate profiles result in preferential selection of microbial partners and the formation of "biased rhizospheres" [66], with both positive (e.g. carbon sources) and negative rhizosphere inputs (e.g. root antimicrobials). Thus, metagenomic studies in rice found that endophytic root bacteria contain several groups of genes involved in: motility, plant polymer degradation, iron acquisition (e.g. siderophores), quorum-sensing, and detoxification of reactive oxygen species [67]. This targeted utilization of natural rhizosphere ecology has proven valuable in bio-energy, agriculture and bio-energy [68] potentially altering critical plant phenotypes. Hence, when rhizospheres were selected over ten generations in *A. thaliana*, promotion of either early or late flowering time was observed [69]. This control over plant traits was even transferable by inoculating other genotypes with the microbiome [69], highlighting the tight interaction of plant and microbe adaptation. In addition, plant immune system inducing beneficial microbes were shown to stimulate the plant transcription factor MYB72, resulting in the production of coumarins, a class of phenolic compounds that include scopoletin, which was shown to influence microbiome composition [70]. Further, a root exudate and microbiome assembly study in the grass *Avena barbata* demonstrated metabolic harmony between root exudates and microbiome uptake, suggesting a mechanism for rhizosphere microbiome assembly [71]. Attracting preferred bacteria, fungi and other microbes to the host root is largely influenced by the plant root itself via release of volatiles and other metabolites [72]. Plant-mediated regulation of exudates such as malic acid and flavonoids were shown to recruit bacterial species capable of helping plants tolerate environmental stress [73, 74]. To better understand the dynamics of these relationships, time course studies have been carried out that connect changes in *A. thaliana* rhizosphere communities

at four developmental stages with differences in the composition of root exudates at those times, especially sugars and phenolic compounds [75, 76]. Additional work to weave together the mechanisms and intricate relationships between individual root exudates to control rhizosphere community formation will require further understanding of plant-microbe interactions.

Realization of common immune targets for extraordinarily diverse plant pathogen effectors [77, 78] facilitated a parsed and often targeted approach to understanding plant-microbe interactions. Rhizobia, nitrogen-fixing soil microbes that commonly associate with plant roots, are known to use type 3 secreted effector (T3E) proteins to promote establishment of plant beneficial nitrogen-fixing nodules and suppress the plant immune response [79]. Interestingly, T3Es are also used by pathogenic microbes, but for infection, not establishment of beneficial relationships [79]. While there is a need to explore host-beneficial and host-pathogen interactions concordantly [80], there is strong evidence that both beneficial and pathogenic microbes can activate a number of plant immune responses, including: programmed cell death, cell wall thickening, antimicrobial compound expression, reactive oxygen species generation, and defense phytohormones production individually [81, 82]. Plant hormonal modulators that integrate induction of immune system output responses [83] such as salicylic acid-jasomonic acid crosstalk often a common target to facilitate colonization.

As obligate mutualistic biotrophs, arbuscular mycorrhizal (AM) fungi are reliant on plant hosts for survival while plants can gain fitness benefits from the cortical invasion [84]. In order for the plant-mycorrhizal relationship to become established, either the plant immune system must adapt to colonization or the fungus must evade or modify the inevitable host immune attack during and post-colonization [84]. Symbiosis is most often achieved via modulation of the host immune response, first with initiation of microbe-associated molecular pattern (MAMP) triggered immunity (MTI) [85], then with defense-related gene suppression. Recent studies suggest that alteration of MAMP-triggered defense-related phytohormone synthesis is essential to allow establishment of AM symbioses [86]. Specifically, salicylic acid (SA) and jasmonic acid (JA), known antagonistic plant defenders, are dynamically regulated to achieve colonization [72, 83, 84]. A phytohormone with both beneficial and detrimental effects, stringlolactone (SL), is

important in AM colonization and is also known to cue parasitic plants and increase susceptibility to pathogenic fungi and bacteria [87]. Other mechanisms involve utilization of host enzymes, such as chitinases to remodel fungal cell walls to allow for symbiont establishment [88]. *Glomus intraradices*, an AM colonizer, secretes specific effector proteins, such as SP7, which directly interferes with the transcription factor ERF19, leading to suppression of effector-triggered genes to allow colonization [89]. The molecular crosstalk of host and symbiont illustrate the importance of this evolutionarily driven relationship.

Following colonization, beneficial microbes can also induce immune "priming", which refers to acceleration of subsequent defense responses to pathogens [90], even in distal tissues. Thus, protective rhizobacteria trigger induced systemic resistance (ISR) and AM can produce mycorrhizal induced resistance (MIR) [84, 85]. In addition, the discovery of mycorrhizae helper bacteria (MHB), demonstrates the ability of select *Pseudomonas* strains to aid in mycorrhizal colonization, seemingly benefitting the host plant, fungus and bacteria [91]. Specific MHB are known to protect from pathogens, aid in nutrient acquisition and assist with nitrogen fixation [92]. Also significant in mediating the plant-microbe relationship is systemic induced susceptibility (SIS) [93]. Prior plant infection with a pathogenic strain of Pseudomonas, *P. syringae*, results in SIS to a species of moth larva [93]. Together, these findings suggest that certain bacterial strains can be beneficially selected for plant inoculation, subsequent mycorrhizae establishment, and result in improved host competition [91], or manipulated for pathogenic infection [93], highlighting the integration of immune suppression and priming by AM in mutualistic relationships.

Interestingly, a recent survey of global fungal diversity revealed that plant and fungal diversity could not be directly correlated [94]. Another study found that while alpha diversity, or the number of types of archaeal, bacterial, and fungal species within samples did not correlate with plant alpha diversity, plant beta diversity, or the comparison of types of microbes between samples, was significantly correlated with bacterial and fungal beta diversity [95]. The ancient symbiotic relationship between plants and microbes reveals that plants and fungi have long shared biological niches, suggesting plants engage in careful and intentional selection of their microbial partners.

Microbe-microbe interactions

Simultaneously exploring fungal, archaeal, and bacterial root microbiome composition through genomic profiles can allow for further understanding of the most effective methods for distinguishing microbial life, niches in which organisms live and grow, host benefit or detriment, and general ecological diversity indices. For these reasons, Shakya et al. [96] compared metagenomic and gene-specific techniques for identification of mixed synthetic archaeal/bacterial communities and found that metagenomic data were more representative than amplicon sequencing by both 454 and Illumina technology [96]. This idea has also been demonstrated with the uncoupling of fungal and microbe diversity from the predictive indicators host species and soil origin. Multiplex 454 amplicon sequencing of four loci from three unique plant species grown in soils from three exclusive geographic sites revealed that fungal community composition is more influenced by soil rather than plant host species whereas the inverse is true for bacterial community composition [97]. Further, microbial gene dynamics (i.e. loss, lateral transfer, etc.) have also been identified as a driver of microbiome contouring [98], demonstrating another mechanisms microbes may use to influence other members of root microbiomes.

While understanding colonization by a single microbe is helpful in deciphering colonization and functional root microbiome mechanisms, such relationships do not depict environmentally relevant scenarios. A comparison of plants colonized with *Streptomyces* mixtures of 1-, 4-, 8-, or 16-species revealed bacterial co-associations unique to individual plant species [64]. An additional strategy examines co-association matrices; these studies are capable of eliminating the inherent noise of relative abundance amplicon census surveys, since they require microbes to be present in multiple samples for a co-occurrence to be identified [54, 64, 99]. Community-level co-association studies have been successfully applied to human microbiota to show that dominate commensal bacteria likely compete with each other, while potential pathogens might co-occur, possibly due to habitat sharing [100]. A similar approach was used to examine the composition of the rhizoplane and root endosphere of lettuce cultivars [54]. In this case, more positive interactions were revealed than negative interactions. In fact, only a single negative interaction between Streptomycetaceae and Acidobacteriaceae was discovered [54]. Streptomycetaceae, which belongs to the order Actinomycetales, is commonly enriched in root endosphere (within root) compared to rhizosphere

and surrounding soil, while Acidobacteria is depleted in *A. thaliana* and other Brassicaeceae grown in diverse soils [18, 19, 101]. A study of the maize root microbiome used a novel approach to identify *Entrobacter cloacae* as a keystone species and further describe specific community assembly mechanisms via selective removal of individual strains [102]. A genomic approach to exploring selection pressures among a variety of Actinobacteria genera revealed different evolutionary rates in secretory protein gene evolution between species, suggesting a 'genetic marker' indicative of host tolerance [103]. Together these data potentially highlight a specific root microbiome control mechanism used by Streptomycetaceae and other Actinobacteria to exclude microbes from the root endosphere.

Among the positive interactions between microbiota in the lettuce root tissue, many existed between closely related taxa [54]. The validation for these findings was performed using fluorescent *in situ* hybridization (FISH), and two major observations were made: 1) mixed colonies on the surface of the root, indicating possible symbiosis between the microbes and 2) segregated colonies in close proximity, suggesting habitat sharing [54]. These studies demonstrate that models based on census data can be validated and provide additional insight into how microbes might inhibit or promote co-resident microbe growth in the root microbiome.

II. THE MAMMALIAN GUT MICROBIOME

Genes comprising the human microbiome and other mammals are known to exponentially outnumber those of its hosts [104]. Therefore, not surprisingly, the trillions of cells housing these genes perform functions critical for human life. Countless organisms assemble and inhabit various mammalian body structures and organs [4, 30]. Like plants, mammalian microbiomes have been implicated in a number of essential functions, including nutrient acquisition and metabolism, protection from pathogens, and protection from abiotic stress (Figure 1.1) [3]. The gut microbiome has been linked to many of these functions, with likely the most studied being that of immune modulation and development of disease [4]. As has been described in plant microbiome dynamics via systemic induced susceptibility, individual gut microbes, and even a distinct microbial genes, can lead to problematic vulnerabilities and shifts [105]. In contrast, inflammation in the mammalian gut microbiome can be reduced by altering the metabolic potential of a single family

via introduction of a specific cofactor [106]. Thus, the host immune-gut commensal balance is critical to maintain homeostasis. A recent study of long-term drivers of mammalian gut microbial composition found that host phylogeny was predictive of more recent bacterial lineages, while host dietary shift predicted acquisition of ancient bacterial clades [107]. Interestingly, this study found distinct older clades associated with herbivory as opposed to more recent clades linked with carnivory [107]. These findings prompt questions about the implications of these shifts on host health and, in particular host immune adaptation to the introduction of new bacterial clades. The human microbiome project has characterized common gut microbiome taxa [104] and other studies have explored dysbiosis and its implications on a variety of gastrointestinal diseases [106, 108, 109]. Continuously, new studies are emerging exploring links between the gut microbiome and diseases, either chronic or infectious.

The mammalian gut microbiome is known to be an influential determinant in various physiological and disease outcomes, including liver diseases [38] irritable bowel disorders [110], osteoporosis [111], obesity [112], allergy/asthma [113], influenza [114], and even malaria [46]. Gut dysbiosis has been implicated in many of these diseases, including identification of specific taxa found to be either protective or contributory. Furthermore, probiotics, consisting of one or various combinations of bacterial isolates, continue to be studied for their therapeutic potential with promising and ever evolving findings [30, 115]. In many cases, mechanisms remain unknown, but recent studies are beginning to reveal potential disease-contributory and protective mechanisms between isolates and the host immune system [4].

Chronic diseases

As the population grows and ages, long term illness afflicts a greater proportion of these individuals, opening the door for identification of opportunities to harness the power of the gut microbiome for intervention and prevention. It is known that genes responsible for gut development and immunity influence the composition of the gut microbiome [116]. In alignment with the concept of symbiotic plant-microbe co-evolution [16], the human body is considered a holobiont in which its microbiomes, and thus including the gut microbiome, function as one unit, with neither the microbes nor gut functioning autonomously [20]. Therefore not surprisingly, the

gut microbiome is established immediately following birth and continues to adapt and change according to varying environmental stimuli, stresses and host diet [20]. Considering its early establishment and therefore potential for longitudinal impact, it is essential we understand connections between the gut microbiome and progression to chronic disease. Several select chronic diseases with known links to gut microbiome dynamics are addressed here.

Crohn's disease and other inflammatory diseases of the intestinal tract are known to be associated with gut dysbiosis [106, 117]. While these are likely among the most studied diseases linked with gut dysbiosis, the inherent complexities of the gut-microbe system leave room for further exploration and development of effective interventions. Depletion of commensal taxa from the phyla Bacteroidetes and Firmicutes has long been associated with various disease states, and inflammatory bowel diseases (IBD) in particular [117]. Interestingly, as compared to plants, addition of members from the Actinobacteria and Proteobacteria phyla is associated with IBD risk [116]. Individual genes and immune proteins/processes have been identified as regulators of IBD. For example, mice lacking *nod2*, a gene involved in innate immune regulation, are more susceptible to IBD, and specifically Crohn's disease [118]. In addition, recent study of the gut microbiome and the innate immune signaling complex, NLRP6 found that plant-derived flavones, and specifically apigenin, is protective against colitis via apigenin-mediated modulation of gut microbe inflammation and proliferation [119]. Interestingly, our prior understanding of the concurrence of general dysbiosis and IBD pathology expanded to include more targeted volatile disruptive events. Recent studies of dysbiosis and inflammatory bowel disease (IBD) found that IBD is characterized by abnormal violent fluctuations of the gut microbiome, rather than general dysbiosis [109, 120]. A longitudinal cohort study of clinical data from 29 IBD patients and healthy individuals allowed for statistical establishment of a healthy gut microbiome plane (HP) [120]. IBD patients sporadically, but sometimes drastically, deviated from the HP, further informing gut microbiome-disease dynamics [120]. Overall, complex dynamics regulate the host gut microbiome and potential IBDs, with host genetic variations becoming increasingly significant [116]. However, our expanding knowledge has proven incredibly useful in treatment and therapeutic interventions.

While it is not surprising that the gut microbiome plays an essential role in modulating localized infections and pathology, increasingly evident is the influence of the gut microbiome in distal pathologies. It is thought that microbiome-derived metabolites like short chain fatty acids (SCFAs), such as butyrate, play an essential role in signaling to these sites [121]. One example of this is lung disease. Study of the gut-lung axis is newly emerging, but thus far, trends strongly suggest that gut microbiota extend their metabolic reach to the lung [37, 121, 122]. Specifically, a recent review describes the role of SCFAs originating in the gut microbiota, as stimulators of signaling to immune cells essential in protection from lung and airway inflammation [123]. Similarly, Gray *et al.* described the importance of the exposure of neonatal mice to commensal microbes for lung mucosal immunity development and protection against various infections [124]. A recent study of pneumonia in newborns implicates the importance of the gut microbiome in establishing mucosal lung immunity [125]. Several of these studies are summarized in a new review of the gut-lung axis that describes a shared mucosal immune system in which signals are transmitted from gut microbiota to the lungs and airways, resulting in immune modulation, response and largely protective phenotypes [126]. While there is still much to be explored, new studies are defining the roles of specific metabolite and genes involved in signaling and development of mucosal immunity [121].

Finally, of recent interest is the connection between the gut microbiome and osteoporosis. Studies describing the impacts of gut composition on bone health are beginning to take shape and mounting evidence suggests the importance of intestinal microbes and post-menopausal osteoporosis (PMO) [111]. In fact, it is know that the gut microbiome is responsible for bone physiology, with SCFAs essential in immune signaling and promotion of bone formation and resorption [121]. SCFAs are thought to influence proteins involved in calcium absorption [111]. Beyond PMO, links between healthy bone formation and the gut microbiome are emerging. Bone formation is influenced by the production of insulin-like growth factor 1 (IGF-1), a hormone known for involvement in skeletal formation [127, 128]. Specifically, gut microbiome colonization is correlated with IGF-1 production and was found to be directly associated with SCFA availability [129]. These studies provide valuable opportunities for probiotic and other therapeutic interventions. In particular, highlighted here are the complexities of mammalian physiology and the interwoven dependencies

of the gut microbiome across systems. Of particular interest and common to many of the diseases described is the necessity for gut microbiome metabolites in distal immune response.

Infectious diseases

Infectious diseases are highly studied and use a variety of animal models and systems. The opportunities to study the role of the gut microbiome in infectious pathologies are broad and ongoing. Multitudes of data exist in many facets of immunology describing these phenotypes. Despite the abundance of data, new niches are being explored, leading to valuable insights and therapies. As in plants, protection from pathogens is among the most valuable of the benefits from host-microbe assimilation. Described here are examples of a viral, bacteria and parasitic infection whose severity or infectivity is modulated in some way by the gut microbiome, the final example, malaria, will be described fully in Chapter IV.

Influenza is a serious viral respiratory infection, causing annual morbidity and mortality involving 3 to 5 million people. Immunologic studies of mice treated with a broad spectrum antibiotic cocktail in their drinking water demonstrated the significance of the gut microbiome in mediating infection from influenza [130]. mRNA expression of TLR7, an innate immune receptor important in recognizing viruses and expressing pro-inflammatory cytokines, was decreased in mice treated with the broad spectrum antibiotic neomycin, suggesting the importance of the gut microbiome in effective pulmonary immune function [131]. Additionally, various sets of immune modulated, compromised and specific pathogen free (SPF) mice were shown to develop incomplete immunity when administered seasonal influenza vaccine [132]. This was discovered to be a result of decreased TLR5 expression, an innate immune receptor essential to bacterial flagellin recognition. In summary, commensal gut microbes activated the TLR5 pathway, resulting in reduced immunoglobulin G (IgG) and IgM antibody responses, and therefore incomplete protection from influenza virus [132]. Together, these studies demonstrate the significance of the gut microbiome on a specific respiratory pathogen and suggest a role for therapies resulting in minimal gut disturbance, and careful administration of vaccines post antibiotic treatments.

Nosocomial infections with *Clostridium difficile* ravage immunocompromised patients, with significant detrimental outcomes, including spread of infection to other patients and increased morbidity and mortality. The infection is most often associated with antibiotic treatment in combination with hospitalization. Controlling these infections is essential to improving outcomes for hospitalized and other patients. While part of the normal gut flora, *C. difficile* can become problematic during gut dysbiosis [133-135]. Importantly, presence and absence of select taxa are known to be influential in *C. difficile* infection [136, 137], and profiling of the gut microbiome via16S rRNA gene sequencing has shed light on distinct strains of the bacterium associated with varying pathologies and risks for initial and reinfection [138] Evidence suggests that the cause of significant infection and inability of the immune system to adequately control the infection is related to the absence of key gut metabolites and bacterial components important in stimulating immune function [134]. Some of these include SCFAs and a variety of other nutrients [133]. Modulation of the gut taxa allowing exploitation by *C. difficile* can be devastating, and therapies to prevent and control infection are continuously emerging. Among the most controversial of these is fecal microbiota transplant (FMT). Mounting evidence lauds the benefits of recolonization, but additional studies are needed to fully explore the options for effective and simulated FMT [139].

Parasitic infections plague much of the population, particularly in the developing world, with *Plasmodium* infection, which causes malaria, being a very significant public health burden. There are few studies of the gut microbiome and malaria infections, but newer studies have described associations between decreased severity of malarial illness and specific taxa, such as *Bifidobacterium, Streptococcus,* and *Lactobacillus,* and even specific strains such as *Eshcheria coli* O86:B7 [46, 140]. Interestingly, *Plasmodium* and *E. coli* O86:B7 both stimulate production of the same antibody, therefore inducing cross-reactivity [135, 141, 142]. Generally, many studies suggest that the host immune system and gut microbiome insight corollary efforts to mediate the parasitic infection. A recent review of the gut microbiome's influence on malarial illness found trends consistent with *Plasmodium*'s ability to reversibly alter the composition of the gut microbiome [142]. Fundamental dynamics of malarial infection makes identification of any one mechanism of this relationship difficult to tease out. Mammalian *Plasmodium* infection is multivariate, and the immune system is stimulated to regulate multiple malarial antigens at varying

stages of infection, presenting significant challenges for vaccine. Thus, it is essential that we continue to examine the potential for microbiome-related therapies in malaria prevention.

III. OBJECTIVES

Microbiome studies broadly designed to characterize operational taxonomic unit (OTU) or amplicon sequence variant (ASV) relative abundances have provided characterization of these abundances and allowed for hypothesis generation. More focused studies of microbiome community members can suggest functional influences of bacterial members. While undeniably complex, the contribution of individual strains should not be overlooked. Multidimensional studies (i.e. *in vitro*, *in vivo*, and *in silico*) taking into account individual strain roles may redefine host-microbe or microbe-microbe relationships in the context of a microbiome. The following chapters address some of the microbiome assembly cues shared across kingdoms, as well as a detailed look at dynamics within the plant root microbiome and a foray into the complexities of the influence of the mammalian gut microbiome on a pathogenic infection.

The use of co-occurrence matrices and mixed synthetic communities to explore microbe-microbe and host-microbe interactions is proving more feasible and can be used as a tool of comparison to environmentally relevant analyses. Technical advances in 'omics approaches have vastly expanded our understanding of microbiome composition and function [143]. The declining cost of sequencing has substantially contributed to improved comparative genomics [144]. Continued reduction in costs associated with sequencing will allow for consistent contribution to sequence databases and the corollary improvement of genome and metagenome comparisons. As this access to multi-kingdom microbiome datasets improves, the integration of these datasets will provide powerful insights into the physiology of microbiomes. Aligning these data and mining large datasets for overlapping functions will allow for identification of impacts that other plants and microbes have on root microbiomes and long-term soil conditioning with mammalian microbiomes, and how taxa within mammalian microbiomes contribute to disease severity, will allow the development of sustainable, tractable, therapies improving crop health and productivity as well as reducing disease burdens worldwide.

IV. REFERENCES

1. Borer, E.T., et al., *The world within: Quantifying the determinants and outcomes of a host's microbiome.* Basic and Applied Ecology, 2013. **14**(7): p. 533-539.
2. Liu, H.W., et al., *Inner Plant Values: Diversity, Colonization and Benefits from Endophytic Bacteria.* Frontiers in Microbiology, 2017. **8**.
3. Hacquard, S., et al., *Microbiota and Host Nutrition across Plant and Animal Kingdoms.* Cell Host Microbe, 2015. **17**(5): p. 603-16.
4. Liang, D., et al., *Involvement of gut microbiome in human health and disease: brief overview, knowledge gaps and research opportunities.* Gut Pathogens, 2018. **10**.
5. Edwards, J., et al., *Structure, variation, and assembly of the root-associated microbiomes of rice.* Proc Natl Acad Sci U S A, 2015. **112**(8): p. E911-20.
6. Niu, B., et al., *Simplified and representative bacterial community of maize roots.* Proc Natl Acad Sci U S A, 2017. **114**(12): p. E2450-E2459.
7. Schreiter, S., et al., *Effect of the soil type on the microbiome in the rhizosphere of field-grown lettuce.* Front Microbiol, 2014. **5**: p. 144.
8. Rakoff-Nahoum, S., et al., *Recognition of commensal microflora by toll-like receptors is required for intestinal homeostasis.* Cell, 2004. **118**(2): p. 229-41.
9. Wolz, C.R.M., et al., *Effects of host species and environment on the skin microbiome of Plethodontid salamanders.* Journal of Animal Ecology, 2018. **87**(2): p. 341-353.
10. Ursell, L.K., et al., *Defining the human microbiome.* Nutrition Reviews, 2012. **70**: p. S38-S44.
11. Blaser, M.J., *Who are we? Indigenous microbes and the ecology of human diseases.* Embo Reports, 2006. **7**(10): p. 956-960.
12. Berg, G., et al., *Unraveling the plant microbiome: looking back and future perspectives.* Front Microbiol, 2014. **5**: p. 148.
13. Bouffaud, M.L., et al., *Root microbiome relates to plant host evolution in maize and other Poaceae.* Environ Microbiol, 2014. **16**(9): p. 2804-14.
14. Paredes, S.H. and S.L. Lebeis, *Giving back to the community: microbial mechanisms of plant-soil interactions.* Functional Ecology, 2016. **30**(7): p. 1043-1052.

15. Adair, K.L. and A.E. Douglas, *Making a microbiome: the many determinants of host-associated microbial community composition.* Current Opinion in Microbiology, 2017. **35**: p. 23-29.
16. Rosenberg, E. and I. Zilber-Rosenberg, *The hologenome concept of evolution after 10 years.* Microbiome, 2018. **6**.
17. Ley, R.E., et al., *Worlds within worlds: evolution of the vertebrate gut microbiota.* Nature Reviews Microbiology, 2008. **6**(10): p. 776-788.
18. Lundberg, D.S., et al., *Defining the core Arabidopsis thaliana root microbiome.* Nature, 2012. **488**(7409): p. 86-90.
19. Bulgarelli, D., et al., *Revealing structure and assembly cues for Arabidopsis root-inhabiting bacterial microbiota.* Nature, 2012. **488**(7409): p. 91-5.
20. Milani, C., et al., *The First Microbial Colonizers of the Human Gut: Composition, Activities, and Health Implications of the Infant Gut Microbiota.* Microbiology and Molecular Biology Reviews, 2017. **81**(4).
21. Yeoh, Y.K., et al., *Evolutionary conservation of a core root microbiome across plant phyla along a tropical soil chronosequence.* Nat Commun, 2017. **8**(1): p. 215.
22. Yeoh, Y.K., et al., *The core root microbiome of sugarcanes cultivated under varying nitrogen fertilizer application.* Environ Microbiol, 2016. **18**(5): p. 1338-51.
23. King, K.C., et al., *Rapid evolution of microbe-mediated protection against pathogens in a worm host.* Isme Journal, 2016. **10**(8): p. 1915-1924.
24. Lebeis, S.L., et al., *PLANT MICROBIOME. Salicylic acid modulates colonization of the root microbiome by specific bacterial taxa.* Science, 2015. **349**(6250): p. 860-4.
25. Yoo, B.B. and S.K. Mazmanian, *The Enteric Network: Interactions between the Immune and Nervous Systems of the Gut.* Immunity, 2017. **46**(6): p. 910-926.
26. Berendsen, R.L., et al., *Disease-induced assemblage of a plant-beneficial bacterial consortium.* Isme Journal, 2018. **12**(6): p. 1496-1507.
27. Kamada, N., et al., *Control of pathogens and pathobionts by the gut microbiota.* Nat Immunol, 2013. **14**(7): p. 685-90.
28. Littman, D.R. and E.G. Pamer, *Role of the commensal microbiota in normal and pathogenic host immune responses.* Cell Host Microbe, 2011. **10**(4): p. 311-23.

29. Atarashi, K., et al., *Induction of colonic regulatory T cells by indigenous Clostridium species.* Science, 2011. **331**(6015): p. 337-41.
30. Ericsson, A.C. and C.L. Franklin, *Manipulating the Gut Microbiota: Methods and Challenges.* Ilar Journal, 2015. **56**(2): p. 205-217.
31. Fitzpatrick, C.R., et al., *Assembly and ecological function of the root microbiome across angiosperm plant species.* Proc Natl Acad Sci U S A, 2018. **115**(6): p. E1157-E1165.
32. Seedorf, H., et al., *Bacteria from Diverse Habitats Colonize and Compete in the Mouse Gut.* Cell, 2014. **159**(2): p. 253-266.
33. Shade, A. and J.A. Gilbert, *Temporal patterns of rarity provide a more complete view of microbial diversity.* Trends Microbiol, 2015. **23**(6): p. 335-40.
34. Berendsen, R.L., C.M. Pieterse, and P.A. Bakker, *The rhizosphere microbiome and plant health.* Trends Plant Sci, 2012. **17**(8): p. 478-86.
35. Huttenhower, C., et al., *Structure, function and diversity of the healthy human microbiome.* Nature, 2012. **486**(7402): p. 207-214.
36. Jiang, W., M.M. Lederman, and P. Hunt, *Plasma levels of bacterial DNA correlate with immune activation and the magnitude of immune restoration in persons with antiretroviral-treated HIV infection (vol 199, pg 1177, 2009).* Journal of Infectious Diseases, 2009. **200**(1): p. 160-160.
37. O'Dwyer, D.N., R.P. Dickson, and B.B. Moore, *The Lung Microbiome, Immunity, and the Pathogenesis of Chronic Lung Disease.* Journal of Immunology, 2016. **196**(12): p. 4839-4847.
38. Chen, Y., et al., *Characterization of Fecal Microbial Communities in Patients with Liver Cirrhosis.* Hepatology, 2011. **54**(2): p. 562-572.
39. Klein, E., et al., *Soil suppressiveness to fusarium disease: shifts in root microbiome associated with reduction of pathogen root colonization.* Phytopathology, 2013. **103**(1): p. 23-33.
40. Round, J.L., et al., *The Toll-like receptor 2 pathway establishes colonization by a commensal of the human microbiota.* Science, 2011. **332**(6032): p. 974-7.
41. Chappert, P., et al., *Specific gut commensal flora locally alters T cell tuning to endogenous ligands.* Immunity, 2013. **38**(6): p. 1198-210.

42. Suzuki, K., et al., *The sensing of environmental stimuli by follicular dendritic cells promotes immunoglobulin A generation in the gut.* Immunity, 2010. **33**(1): p. 71-83.
43. Franchi, L., R. Munoz-Planillo, and G. Nunez, *Sensing and reacting to microbes through the inflammasomes.* Nat Immunol, 2012. **13**(4): p. 325-32.
44. Lebeis, S.L., *The potential for give and take in plant-microbiome relationships.* Front Plant Sci, 2014. **5**: p. 287.
45. Mine, A., M. Sato, and K. Tsuda, *Toward a systems understanding of plant-microbe interactions.* Front Plant Sci, 2014. **5**: p. 423.
46. Villarino, N.F., et al., *Composition of the gut microbiota modulates the severity of malaria.* Proceedings of the National Academy of Sciences of the United States of America, 2016. **113**(8): p. 2235-2240.
47. Hummelen, R. and J. Hemsworth, *YOGURT, AND PRE- AND PROBIOTICS TO REDUCE THE PROGRESSION OF HIV.* Yogurt in Health and Disease Prevention, 2017: p. 525-532.
48. Mauchline, T.H. and J.G. Malone, *Life in earth - the root microbiome to the rescue?* Current Opinion in Microbiology, 2017. **37**: p. 23-28.
49. Andreote, F.D. and M. Silva, *Microbial communities associated with plants: learning from nature to apply it in agriculture.* Current Opinion in Microbiology, 2017. **37**: p. 29-34.
50. Finkel, O.M., et al., *Understanding and exploiting plant beneficial microbes.* Current Opinion in Plant Biology, 2017. **38**: p. 155-163.
51. Viaene, T., et al., *Streptomyces as a plant's best friend?* FEMS Microbiol Ecol, 2016. **92**(8).
52. Felice, L., et al., *Soil Streptomyces communities in a prairie establishment reflect interactions between soil edaphic characteristics and plant host.* Plant and Soil, 2015. **386**(1-2): p. 89-98.
53. Bonaldi, M., et al., *Colonization of lettuce rhizosphere and roots by tagged Streptomyces.* Front Microbiol, 2015. **6**: p. 25.
54. Cardinale, M., et al., *Bacterial networks and co-occurrence relationships in the lettuce root microbiota.* Environmental microbiology, 2015.

55. Bulgarelli, D., et al., *Structure and function of the bacterial root microbiota in wild and domesticated barley.* Cell Host Microbe, 2015. **17**(3): p. 392-403.
56. Xu, L., et al., *Correction for Xu et al., Drought delays development of the sorghum root microbiome and enriches for monoderm bacteria.* Proc Natl Acad Sci U S A, 2018. **115**(21): p. E4952.
57. Vorholt, J.A., *Microbial life in the phyllosphere.* Nat Rev Microbiol, 2012. **10**(12): p. 828-40.
58. Andreote, F.D., T. Gumiere, and A. Durrer, *Exploring interactions of plant microbiomes.* Scientia Agricola, 2014. **71**(6): p. 528-539.
59. Bulgarelli, D., et al., *Structure and functions of the bacterial microbiota of plants.* Annu Rev Plant Biol, 2013. **64**: p. 807-38.
60. Bever, J.D., L.M. Broadhurst, and P.H. Thrall, *Microbial phylotype composition and diversity predicts plant productivity and plant-soil feedbacks.* Ecol Lett, 2013. **16**(2): p. 167-74.
61. Guttman, D., A.C. McHardy, and P. Schulze-Lefert, *Microbial genome-enabled insights into plant-microorganism interactions.* Nat Rev Genet, 2014.
62. Seymour, M., et al., *Break-crop benefits to wheat in Western Australia–insights from over three decades of research.* Crop and Pasture Science, 2012. **63**(1): p. 1-16.
63. Turner, T.R., et al., *Comparative metatranscriptomics reveals kingdom level changes in the rhizosphere microbiome of plants.* ISME J, 2013. **7**(12): p. 2248-58.
64. Bakker, M.G., et al., *Diffuse symbioses: roles of plant-plant, plant-microbe and microbe-microbe interactions in structuring the soil microbiome.* Mol Ecol, 2014. **23**(6): p. 1571-83.
65. Goh, C.H., et al., *The impact of beneficial plant-associated microbes on plant phenotypic plasticity.* J Chem Ecol, 2013. **39**(7): p. 826-39.
66. Hartmann, M., et al., *Bacterial, archaeal and eukaryal community structures throughout soil horizons of harvested and naturally disturbed forest stands.* Environ Microbiol, 2009. **11**(12): p. 3045-62.

67. Sessitsch, A., et al., *Functional characteristics of an endophyte community colonizing rice roots as revealed by metagenomic analysis.* Mol Plant Microbe Interact, 2012. **25**(1): p. 28-36.
68. Philippot, L., et al., *Going back to the roots: the microbial ecology of the rhizosphere.* Nat Rev Microbiol, 2013. **11**(11): p. 789-99.
69. Panke-Buisse, K., et al., *Selection on soil microbiomes reveals reproducible impacts on plant function.* ISME J, 2014.
70. Stringlis, I.A., et al., *MYB72-dependent coumarin exudation shapes root microbiome assembly to promote plant health.* Proceedings of the National Academy of Sciences of the United States of America, 2018. **115**(22): p. E5213-E5222.
71. Zhalnina, K., et al., *Dynamic root exudate chemistry and microbial substrate preferences drive patterns in rhizosphere microbial community assembly.* Nat Microbiol, 2018. **3**(4): p. 470-480.
72. Hause, B. and S. Schaarschmidt, *The role of jasmonates in mutualistic symbioses between plants and soil-born microorganisms.* Phytochemistry, 2009. **70**(13-14): p. 1589-99.
73. Coronado, C., et al., *ALFALFA ROOT FLAVONOID PRODUCTION IS NITROGEN REGULATED.* Plant Physiology, 1995. **108**(2): p. 533-542.
74. Rudrappa, T., et al., *Root-Secreted Malic Acid Recruits Beneficial Soil Bacteria.* Plant Physiology, 2008. **148**(3): p. 1547-1556.
75. Chaparro, J.M., et al., *Root exudation of phytochemicals in Arabidopsis follows specific patterns that are developmentally programmed and correlate with soil microbial functions.* PLoS One, 2013. **8**(2): p. e55731.
76. Chaparro, J.M., D.V. Badri, and J.M. Vivanco, *Rhizosphere microbiome assemblage is affected by plant development.* ISME J, 2014. **8**(4): p. 790-803.
77. Selin, C., et al., *Elucidating the Role of Effectors in Plant-Fungal Interactions: Progress and Challenges.* Frontiers in Microbiology, 2016. **7**.
78. Mukhtar, M.S., et al., *Independently Evolved Virulence Effectors Converge onto Hubs in a Plant Immune System Network.* Science, 2011. **333**(6042): p. 596-601.
79. Miwa, H. and S. Okazaki, *How effectors promote beneficial interactions.* Current Opinion in Plant Biology, 2017. **38**: p. 148-154.

80. Lakshmanan, V., G. Selvaraj, and H.P. Bais, *Functional soil microbiome: belowground solutions to an aboveground problem.* Plant Physiol, 2014. **166**(2): p. 689-700.
81. Dodds, P.N. and J.P. Rathjen, *Plant immunity: towards an integrated view of plant-pathogen interactions.* Nat Rev Genet, 2010. **11**(8): p. 539-48.
82. Jones, J.D. and J.L. Dangl, *The plant immune system.* Nature, 2006. **444**(7117): p. 323-9.
83. Pieterse, C.M., et al., *Hormonal modulation of plant immunity.* Annu Rev Cell Dev Biol, 2012. **28**: p. 489-521.
84. Pozo, M.J. and C. Azcon-Aguilar, *Unraveling mycorrhiza-induced resistance.* Curr Opin Plant Biol, 2007. **10**(4): p. 393-8.
85. Zamioudis, C. and C.M. Pieterse, *Modulation of host immunity by beneficial microbes.* Mol Plant Microbe Interact, 2012. **25**(2): p. 139-50.
86. Fernandez, I., et al., *Defense related phytohormones regulation in arbuscular mycorrhizal symbioses depends on the partner genotypes.* J Chem Ecol, 2014. **40**(7): p. 791-803.
87. Lopez-Raez, J.A., K. Shirasu, and E. Foo, *Strigolactones in Plant Interactions with Beneficial and Detrimental Organisms: The Yin and Yang.* Trends in Plant Science, 2017. **22**(6): p. 527-537.
88. Ruzicka, D., et al., *Inside arbuscular mycorrhizal roots–Molecular probes to understand the symbiosis.* The Plant Genome, 2013. **6**(2).
89. Kloppholz, S., H. Kuhn, and N. Requena, *A secreted fungal effector of Glomus intraradices promotes symbiotic biotrophy.* Curr Biol, 2011. **21**(14): p. 1204-9.
90. Conrath, U., *Systemic acquired resistance.* Plant Signal Behav, 2006. **1**(4): p. 179-84.
91. Labbe, J.L., et al., *Newly identified helper bacteria stimulate ectomycorrhizal formation in Populus.* Front Plant Sci, 2014. **5**: p. 579.
92. Frey-Klett, P., J. Garbaye, and M. Tarkka, *The mycorrhiza helper bacteria revisited.* New Phytologist, 2007. **176**(1): p. 22-36.
93. Groen, S.C., et al., *Pathogen-Triggered Ethylene Signaling Mediates Systemic-Induced Susceptibility to Herbivory in Arabidopsis.* Plant Cell, 2013. **25**(11): p. 4755-4766.
94. Tedersoo, L., et al., *Fungal biogeography. Global diversity and geography of soil fungi.* Science, 2014. **346**(6213): p. 1256688.

95. Prober, S.M., et al., *Plant diversity predicts beta but not alpha diversity of soil microbes across grasslands worldwide.* Ecol Lett, 2015. **18**(1): p. 85-95.
96. Shakya, M., et al., *Comparative metagenomic and rRNA microbial diversity characterization using archaeal and bacterial synthetic communities.* Environ Microbiol, 2013. **15**(6): p. 1882-99.
97. Bonito, G., et al., *Plant host and soil origin influence fungal and bacterial assemblages in the roots of woody plants.* Mol Ecol, 2014. **23**(13): p. 3356-70.
98. Boon, E., et al., *Interactions in the microbiome: communities of organisms and communities of genes.* FEMS Microbiol Rev, 2014. **38**(1): p. 90-118.
99. Zuppinger-Dingley, D., et al., *Selection for niche differentiation in plant communities increases biodiversity effects.* Nature, 2014.
100. Faust, K., et al., *Microbial co-occurrence relationships in the human microbiome.* PLoS Comput Biol, 2012. **8**(7): p. e1002606.
101. Schlaeppi, K., et al., *Quantitative divergence of the bacterial root microbiota in Arabidopsis thaliana relatives.* Proc Natl Acad Sci U S A, 2013.
102. Niu, B., et al., *Simplified and representative bacterial community of maize roots.* Proceedings of the National Academy of Sciences of the United States of America, 2017. **114**(12): p. E2450-E2459.
103. Thakur, S., et al., *Contrasted evolutionary constraints on secreted and non-secreted proteomes of selected Actinobacteria.* BMC Genomics, 2013. **14**: p. 474.
104. Nelson, K.E., et al., *A Catalog of Reference Genomes from the Human Microbiome.* Science, 2010. **328**(5981): p. 994-999.
105. Roche-Lima, A., et al., *The Presence of Genotoxic and/or Pro-inflammatory Bacterial Genes in Gut Metagenomic Databases and Their Possible Link With Inflammatory Bowel Diseases.* Frontiers in Genetics, 2018. **9**.
106. Zhu, W.H., et al., *Precision editing of the gut microbiota ameliorates colitis.* Nature, 2018. **553**(7687): p. 208-+.
107. Groussin, M., et al., *Unraveling the processes shaping mammalian gut microbiomes over evolutionary time.* Nature Communications, 2017. **8**.

108. Winter, S.E., C.A. Lopez, and A.J. Baumler, *The dynamics of gut-associated microbial communities during inflammation.* EMBO Rep, 2013. **14**(4): p. 319-27.
109. Shi, N., et al., *Interaction between the gut microbiome and mucosal immune system.* Military Medical Research, 2017. **4**.
110. Shreiner, A.B., J.Y. Kao, and V.B. Young, *The gut microbiome in health and in disease.* Curr Opin Gastroenterol, 2015. **31**(1): p. 69-75.
111. Xu, X., et al., *Intestinal microbiota: a potential target for the treatment of postmenopausal osteoporosis.* Bone Research, 2017. **5**.
112. Koleva, P.T., S.L. Bridgman, and A.L. Kozyrskyj, *The infant gut microbiome: evidence for obesity risk and dietary intervention.* Nutrients, 2015. **7**(4): p. 2237-60.
113. Fujimura, K.E. and S.V. Lynch, *Microbiota in allergy and asthma and the emerging relationship with the gut microbiome.* Cell Host Microbe, 2015. **17**(5): p. 592-602.
114. Steed, A.L., et al., *The microbial metabolite desaminotyrosine protects from influenza through type I interferon.* Science, 2017. **357**(6350): p. 498-502.
115. Gibson, G.R., et al., *The International Scientific Association for Probiotics and Prebiotics (ISAPP) consensus statement on the definition and scope of prebiotics.* Nature Reviews Gastroenterology & Hepatology, 2017. **14**(8): p. 491-502.
116. Hall, A.B., A.C. Tolonen, and R.J. Xavier, *Human genetic variation and the gut microbiome in disease.* Nature Reviews Genetics, 2017. **18**(11).
117. Frank, D.N., et al., *Molecular-phylogenetic characterization of microbial community imbalances in human inflammatory bowel diseases.* Proceedings of the National Academy of Sciences of the United States of America, 2007. **104**(34): p. 13780-13785.
118. Petnicki-Ocwieja, T., et al., *Nod2 is required for the regulation of commensal microbiota in the intestine.* Proc Natl Acad Sci U S A, 2009. **106**(37): p. 15813-8.
119. Radulovic, K., et al., *A dietary flavone confers communicable protection against colitis through NLRP6 signaling independently of inflammasome activation.* Mucosal Immunology, 2018. **11**(3): p. 811-819.
120. Halfvarson, J., et al., *Dynamics of the human gut microbiome in inflammatory bowel disease.* Nature Microbiology, 2017. **2**(5).

121. Feng, Q.Q., W.D. Chen, and Y.D. Wang, *Gut Microbiota: An Integral Moderator in Health and Disease.* Frontiers in Microbiology, 2018. **9**.
122. Ubags, N.D.J. and B.J. Marsland, *Mechanistic insight into the function of the microbiome in lung diseases.* European Respiratory Journal, 2017. **50**(3).
123. Tremblay, J., et al., *Primer and platform effects on 16S rRNA tag sequencing.* Front Microbiol, 2015. **6**: p. 771.
124. Gray, J., et al., *Intestinal commensal bacteria mediate lung mucosal immunity and promote resistance of newborn mice to infection.* Science Translational Medicine, 2017. **9**(376).
125. Tamburini, S. and J.C. Clemente, *Neonatal gut microbiota induces lung immunity against pneumonia.* Nature Reviews Gastroenterology & Hepatology, 2017. **14**(5): p. 263-+.
126. Budden, K.F., et al., *Emerging pathogenic links between microbiota and the gut-lung axis.* Nature Reviews Microbiology, 2017. **15**(1): p. 55-63.
127. Yan, J., et al., *Gut microbiota induce IGF-1 and promote bone formation and growth.* Proceedings of the National Academy of Sciences of the United States of America, 2016. **113**(47): p. E7554-E7563.
128. Bakker, A.D., et al., *Mechanical Stimulation and IGF-1 Enhance mRNA Translation Rate in Osteoblasts Via Activation of the AKT-mTOR Pathway.* Journal of Cellular Physiology, 2016. **231**(6): p. 1283-1290.
129. El Qaidi, S., et al., *The vitamin B(6) biosynthesis pathway in Streptococcus pneumoniae is controlled by pyridoxal 5'-phosphate and the transcription factor PdxR and has an impact on ear infection.* J Bacteriol, 2013. **195**(10): p. 2187-96.
130. Ichinohe, T., et al., *Microbiota regulates immune defense against respiratory tract influenza A virus infection.* Proceedings of the National Academy of Sciences of the United States of America, 2011. **108**(13): p. 5354-5359.
131. Wu, S., et al., *Microbiota Regulates the TLR7 Signaling Pathway Against Respiratory Tract Influenza A Virus Infection.* Current Microbiology, 2013. **67**(4): p. 414-422.
132. Oh, J.Z., et al., *TLR5-Mediated Sensing of Gut Microbiota Is Necessary for Antibody Responses to Seasonal Influenza Vaccination.* Immunity, 2014. **41**(3): p. 478-492.

133. Koenigsknecht, M.J., et al., *Dynamics and Establishment of Clostridium difficile Infection in the Murine Gastrointestinal Tract.* Infection and Immunity, 2015. **83**(3): p. 934-941.
134. Theriot, C.M., et al., *Antibiotic-induced shifts in the mouse gut microbiome and metabolome increase susceptibility to Clostridium difficile infection.* Nature Communications, 2014. **5**.
135. Denny, J.E., W.L. Powell, and N.W. Schmidt, *Local and Long-Distance Calling: Conversations between the Gut Microbiota and Intra- and Extra-Gastrointestinal Tract Infections.* Frontiers in Cellular and Infection Microbiology, 2016. **6**.
136. Samarkos, M., E. Mastrogianni, and K. Olga, *The role of gut microbiota in Clostridium difficile infection.* European Journal of Internal Medicine, 2018. **50**: p. 28-32.
137. Schubert, A.M., H. Sinani, and P.D. Schloss, *Antibiotic-Induced Alterations of the Murine Gut Microbiota and Subsequent Effects on Colonization Resistance against Clostridium difficile.* Mbio, 2015. **6**(4).
138. Daquigan, N., et al., *High-resolution profiling of the gut microbiome reveals the extent of Clostridium difficile burden.* Npj Biofilms and Microbiomes, 2017. **3**.
139. El Hage, R., E. Hernandez-Sanabria, and T. Van de Wiele, *Emerging Trends in "Smart Probiotics": Functional Consideration for the Development of Novel Health and Industrial Applications.* Frontiers in Microbiology, 2017. **8**.
140. Waldman, A.J. and E.P. Balskus, *The Human Microbiota, Infectious Disease, and Global Health: Challenges and Opportunities.* Acs Infectious Diseases, 2018. **4**(1): p. 14-26.
141. Yilmaz, B., et al., *Gut Microbiota Elicits a Protective Immune Response against Malaria Transmission.* Cell, 2014. **159**(6): p. 1277-1289.
142. Ippolito, M.M., et al., *Malaria and the microbiome: a systematic review.* Clinical infectious diseases : an official publication of the Infectious Diseases Society of America, 2018.
143. Hadrich, D., *Microbiome Research Is Becoming the Key to Better Understanding Health and Nutrition.* Frontiers in Genetics, 2018. **9**.

144. Schuster, S.C., *Next-generation sequencing transforms today's biology.* Nature Methods, 2008. **5**(1): p. 16-18.

V. APPENDIX: FIGURES

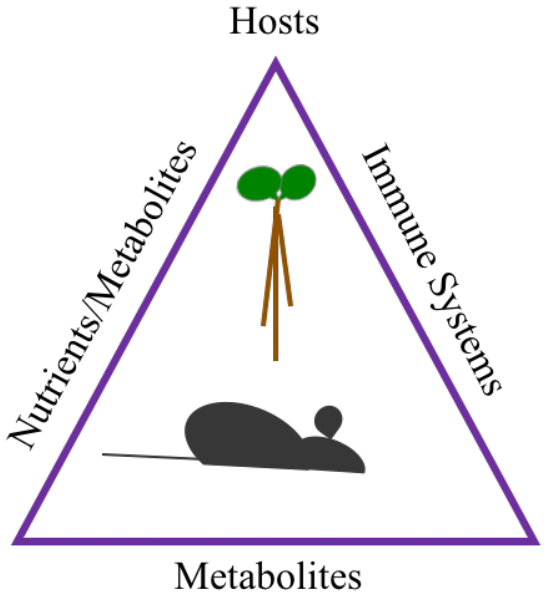


Figure 2.1. Model of host-microbiome interactions.

Combinations of host-microbiome and microbe-microbe interactions shape the microbiome and subsequently influence host growth, health and disease states.

CHAPTER TWO - ROOT-ASSOCIATED *STREPTOMYCES* ISOLATES HARBORING *MEL* GENES DEMONSTRATE ENHANCED PLANT COLONIZATION

A VERSION OF THIS CHAPTER IN PREPARATION TO BE SUBMITTED FOR PUBLICATION

Sarah Stuart Chewning, David L. Grant, Bridget S. O'Banion, Brandon J. Kennedy, Shawn R. Campagna, and Sarah L. Lebeis. "Root-associated *Streptomyces* isolates harboring *mel* genes demonstrate enhanced plant colonization." *Current Biology*

Sarah Stuart Chewning, David L. Grant, Bridget S. O'Banion, Brandon J. Kennedy, Shawn R. Campagna, and Sarah L. Lebeis. "Root-associated *Streptomyces* isolates harboring *mel* genes demonstrate enhanced plant colonization."

Five individuals contributed to this chapter: Sarah Stuart Chewning, David L. Grant, Bridget S. O'Banion, Brandon J. Kennedy, and Sarah L. Lebeis. SSC, DGL, and SLL conceived the experiments. BJK performed the chemical analysis in Figure 2.1 in the laboratory of SRC. SSC performed experiments shown in Figures 2.1, 2.2, 2.4, 2.5. 2.S1. 2.S3, and 2.S4 and assisted with experiments in Figures 2.3 and 2.S3. DLG performed the experiments in Figure 2.3, and 2.S2 and assisted with experiments in Figures 2.1, 2.4, 2.S1, 2.S3 and 2.S4. BSO generated the phylogenies used in Figure 2.2. SSC, BSO, BJK, and SLL analyzed the data. SSC, BSO, and SLL wrote the manuscript.

I. ABSTRACT

Streptomyces assemble into the root microbiomes of a wide variety of plants grown in soils worldwide, suggesting their ability to survive during root microbiome assembly by an array of robust molecular mechanisms. A previous student found that among four non-pathogenic, root-associated *Streptomyces* strains, only two colonized *Arabidopsis thaliana* roots consistently when inoculated in a complex bacterial synthetic community. Here we characterize genomic and biochemical differences between these four non-pathogenic root-associated *Streptomyces* strains. Notably, *in vitro* studies provide evidence that the two isolates with more successful root colonization produce melanin. Genome investigation of these strains identified two copies of the gene that encodes *Streptomyces* tyrosinase, an enzyme necessary for extracellular melanin biosynthesis, but which oxidizes other plant-relevant phenolic compounds. Enzymatic assays of whole cell extracts and supernatants revealed tyrosinase activity, which could be inhibited with the chemical inhibitor kojic acid (KA), indicating that these isolates produced functional extracellular and intracellular enzymes. When challenged *in vitro* with phenolic compounds present in root exudates, salicylic acid (SA) and ferulic acid (FA), strains harboring two functional tyrosinases demonstrated increased protection. Monoinoculation of *A. thaliana* seedlings with each of four *Streptomyces* strains demonstrated that melanin-producing *Streptomyces* also had significantly more seedling colonization, which was significantly lower with the addition of KA. Overall, we observe a previously unappreciated consequence of microbial melanin production and/or tyrosinase activity to increase seedling colonization of *Streptomyces* isolates, which we propose protects against plant-produced phenolic compounds. These findings emphasize the importance of considering innovative roles for previously characterized natural products within the context of the microbiome.

I. INTRODUCTION

The mechanisms of plant microbiome assembly are complicated and interweaving with both hosts and microbes driving composition [1]. The microbial members of these communities likely efficiently scavenge resources and nutrients [2, 3], withstand abiotic and biotic assault [4, 5], and/or act aggressively toward competing microbes [6]. Microbiome assembly is likely influenced by cooperation and competition between microbes vying for niches within the root. Additionally, negotiation of the host immune system requires specific microbial abilities, as well as host accommodation. Hosts drive microbiome composition by recruiting subsets of the soil microbial reservoir, resulting in host-specific microbiome assemblages that are often rich in certain taxa and deplete in others. While defined assemblages facilitate the detection of community composition shifts, which may result in a net benefit or cost to the host and other microbes [7], it is still critical to define the finer scale influence of individual members on host health [1, 8]. Understanding incentives for specific host-microbiome establishment will facilitate consistent community manipulation to improve plant health and growth through defined agricultural practices [5, 9].

Deciphering the mechanisms that promote colonization of individual microbial strains within a complex microbial inoculum is essential for the development of successful biological products to improve plant health. Although Streptomycetaceae are not a dominant root-associated family, they are consistently enriched within the roots of various plant species compared to the surrounding soil and are highly regarded for their metabolic potential [10-16]. While strains of *Streptomyces scabiei* and *Streptomyces ipomoeae* are plant pathogens [17], most other strains are non-pathogenic and consistent root microbiome members. Many *Streptomyces* contribute or are correlated to agriculturally important traits, such as drought resistance, improved plant growth, disease resistance through exhibition of distinct biocontrol capabilities, and plant growth-promoting rhizobacteria (PGPR) [18-20]. Because they need to be present to exert sustainable direct or indirect influence on plant health, it is critical to tease apart unique mechanisms that facilitate *Streptomyces* root colonization. Further, we must define *Streptomyces* strain-specific mechanisms that might potentiate survival advantages during root microbiome assembly.

Previous experiments inoculated axenic *Arabidopsis thaliana* with a synthetic community of 38 taxonomically diverse bacterial isolates, which included four *Streptomyces* isolates, and found that their colonization of 6-8 week-old *A. thaliana* roots differed [21]. Specifically, two *Streptomyces* isolates, 299 and 303, were found to be significantly more abundant in the endophytic compartment (EC) than inoculum and were thus indicated as "EC-enriched". One other *Streptomyces* isolate, CL18, did not significantly change in abundance in root compared to the inoculum while the fourth, 136, was significantly less abundant in the roots than in the inoculum [21]. These phenotypes were influenced by salicylic acid (SA), a phenolic compound, which inhibits microbial growth [22, 23], acts as a plant defense phytohormone [24, 25], and is measurable in root tissue, seedlings and exudates [21, 26-28]. Isolate 136 colonized significantly better in *pad4* plants, which are unable to trigger SA accumulation, while 303 displayed significantly increased levels of root colonization in plants sprayed with exogenous SA [21]. Thus, *Streptomyces* colonization appears to be influence by at least one phenolic compound present in the root-soil interface. Here we explore distinct phenotypic and genomic characteristics of these four non-pathogenic *A. thaliana* root-associated *Streptomyces* strains (Table 2.S1). We investigate the strain-specific kinetics and products of an enzyme present in the two EC-enriched strains, 299 and 303, but not CL18 or 136. Further, we suggest inhibition of this enzyme can influence protection against phenolic compounds during root association. These studies present a unique opportunity to elucidate microbial determinants of root-associated strains within a single genus.

Streptomyces' fall within the Actinobacteria phylum, a group with vast and varied metabolic potential [29]. We propose that one influential product made by plant colonizing *Streptomyces* strains is melanin, a pigment ranging in color from tan to black. Melanin is also produced by other bacterial taxa, fungi, plants, insects, and mammals [30-34]. While function and synthesis vary by organism, it is generally hypothesized to provide protection from stresses such as reactive oxygen species (ROS), antibiotics, and antimicrobial peptides [34-36], thereby providing a potential survival advantage [37]. The production of melanin in *Streptomyces* is conferred by the *melC* operon, which contains two genes, *melC1* and *melC2*. *melC2* encodes a tyrosinase enzyme critical for oxidizing compounds at multiple steps during melanin production from tyrosine [38-40]. *melC1* encodes a helper protein that adds the required copper ions for tyrosinase function and

contains a secretion signal that facilitates the export of both MelC1 and MelC2 proteins into the extracellular space, where the MelC2 enzyme participates in melanin production [41, 42]. A previous study discovered that a collection of melanin producing *Streptomyces* isolates contained two predicted copies of the *melC* operon, each containing the two required genes [35]. The second copy of the operon (termed *melD*) resulted in an intracellular enzyme, oxidizing phenolic compounds within the cell and preventing toxic ROS generation [35]. Here we describe that our *Streptomyces* isolates capable of producing melanin also possess both a *melC* and a *melD* operon, exhibit increased resistance to phenolic compounds, and that the well-defined chemical tyrosinase inhibitor, kojic acid (KA) [43, 44] is capable of preventing enzymatic activity. Ultimately, this strategy could contribute to self-preservation and subsequent enhanced opportunity for root colonization by *Streptomyces* strains. The experimental system we use allows us to determine the potential survival advantage of *mel*-harboring isolates via hypothesized protective tyrosinase or melanin activities. Advancing our understanding of how *Streptomyces spp*. colonize the *A. thaliana* root microbiome will provide future opportunities to understand their activities in the root microbiome and determine if they manipulate microbiome composition to improve plant health, growth, and ultimately yield.

II. MATERIALS AND METHODS

Streptomyces culture preparation

Streptomyces isolates were grown in Lysogeny Broth (LB) at 30 ^{o}C with shaking at 150 rpm for four to seven days. Cultures were vortexed vigorously for 5 seconds and beaten with 3 mm glass beads for 2.5 minutes to disrupt bacterial aggregates. A spectrophotometer measured the optical density at 600 nm (OD_{600}) and cultures were normalized to an OD_{600} of 0.01. 100 μL of all normalized isolate resuspensions were plated on LB solid media, incubated at 28 ^{o}C for four to seven days and colony forming units (CFUs) were counted. Inoculum ranged from $1x10^2$ to $3x10^4$ CFU/mL. LB medium was used because each of the isolates has extremely consistent and differential colony morphology when grown on this medium, which allows us to accurately detect contamination with another *Streptomyces* or other faster growing bacteria.

Extracellular pigment extraction

Pigment extraction from the two pigment-producing strains was adapted from Drewnowska *et al* [45]. Two hundred mL of cultures of 299 and 303 were split between four, 50 mL sterile conical tubes each and centrifuged for 15 min at 3200 x *g* (4000 rpm). Supernatants of both isolates were transferred to two 100 mL glass bottles respectively. The pH of the supernatants was adjusted to 2.0 via addition of 1 M HCl. Samples were incubated at room temperature for one week in the dark. Following incubation, the acidified supernatants were boiled in the glass bottles for one hour at 240 °C. Cooled supernatants from each isolate were transferred to four, 50 mL conical tubes and centrifuged for 15 minutes at 3200 x *g*. After supernatants were removed, approximately 1 mL pellets remained in each tube. Pellets were resuspended and combined into a single 15 mL tube per isolate. The two tubes were then centrifuged again for 7 minutes at 3200 x *g* and supernatants were discarded. Pellets were washed and centrifuged for 7 minutes at 3200 x *g* three times in 15 mL of 0.1 M HCl and a final time in 15 mL of water. After each wash, supernatants were discarded. After washing, 10 mL of absolute ethanol was added to the 15 mL tubes containing the pellets and resuspended. The tubes were placed in a boiling water bath for 10 minutes and then removed and incubated at room temperature for one day. Following incubation, the suspensions were centrifuged for 7 minutes at 3200 x *g* and the supernatant was discarded. The pellets were washed twice with absolute ethanol and centrifuged for seven minutes at 3200 x *g* between washings. After the second wash, the pellets were allowed to air dry.

Liquid-chromatography mass spectrometry

Pigment pellets were digested following the protocol established by Ito *et al*. [46]. Briefly, approximately 1 mg portions of the dried pigments were weighed and transferred to glass vials (4 dr) for digestion. The solid samples were suspended in 100 µL of HPLC-grade H_2O, which was then sonicated for 2 minutes to increase dispersion of pigments in the aqueous solution. To the suspension of pigment in H_2O, 30 µL 30% H_2O_2 and 375 µL of 1 M K_2CO_3 was added. The vials were capped and secured on an orbital shaker set to ~200 rpm to digest at room temperature for about 20 hours. At this time, excess peroxide was destroyed with the addition of 50 µL 10% Na_2SO_3 and the sample was acidified with 140 µL 6N HCl. These digested and quenched samples were centrifuged at 4000 rpm for 5 min and 300 µL of supernatant was transferred into an

autosampler vial. The LC-MS analyses were performed on an Ultimate 3000 UPLC system (Thermo Scientific, Pittsburgh, PA) coupled to an Exactive™ Plus Orbitrap mass spectrometer. Separations were conducted on an Accucore HILIC HPLC column (150 x 2.1 mm; 2.6 µm particle size, Thermo Scientific) kept at 25 °C and 10 µL of sample was injected onto the column for each analysis. The chromatographic method employed used 0.1% formic acid in ACN and 0.1% formic acid in H_2O as mobile phases A and B, respectively. The chromatographic conditions were as follows: 0 minutes, 80% A; 10 minutes, 80% A; 10.1 minutes, 100% A; 20 minutes, 80% A; 25 minutes, 80% A. The MS experiments were all conducted in negative ion mode using an electrospray ionization (ESI) source. The ESI parameters used were a spray voltage of -4.0 kV, an aux gas flow rate of 10 units, sheath gas flow rate of 25 units, and capillary temperature set to 320 °C. The mass spectrometer scan range was set to 120-1800 m/z with a resolution of 140,000 and an automatic gain control (AGC) target of $3.0x10^6$, and maximum injection time of 200 ms. The high-resolution mass spectrometric data was analyzed and processed using the MAVEN [47] software and Microsoft Excel to generate the bar graphs. Extracted ion chromatograms (EICs) were generated in MAVEN [47] with an extraction window of 10 ppm.

Pangenomic visualization.

Genomes for strains 299, 303, CL18, 136, and *Streptomyces scabiei* 87.22 (Table 2.S1 and 2.S2) were downloaded from JGI IMG/M ER [48]. Genomes were mined using JGI IMG/M ER query tools and Anvi'o v2.1.0 (a platform used to analyze and visualize genomic data)[49]. Pangenomic analysis was performed with Anvi'o, as outlined by Eren *et al* [29]. Homologs were identified using similarity searches through NCBI's BLASTP and protein clusters were resolved with the MCL algorithm (inflation parameter 10)[50] using the minbit scoring method (score 0.5). Annotations were done with Pfam [51] and SUPERFAMILY [52]. Manual "binning" of protein clusters shared between subsets of genomes facilitated identification of group-specific gene clusters. Analyses resulted in a visual representation of the pangenome and a database of protein family annotations from the Pfam database [51].

Phylogenetic trees and identification of mel operons

A concatenated alignment of the amino acid sequences of five housekeeping genes (*trpB*, *gyrB*, *rpoB*, *atpD*, and *recA)* from ten *Streptomyces* strains and one *Kitasatospora* strain, which represents another genus in Streptomycetaceae (Table 2.S1), was used to build a Maximum Likelihood (RAxML v7.2.8) phylogenetic tree using 100 bootstrap replicates [53]. Alignment (using MAFFT v7.017 [54] and tree-building was performed in Geneious version R7 (http://www.geneious.com) (48). Melanin genes (*melC1* (SCAB85691), *melC2* (SCAB85681), *melD1* (SCAB59231), *melD2* (SCAB59241)) from *Streptomyces scabiei* 87.22 identified by Yang *et al.* were used as queries for NCBI BLASTP searches to identify melanin genes in all strains [35]. A separate concatenated alignment (MAFFT v7.394)[54] of amino acid sequences of the *melC2*, *melD2, melC1,* and *melD1* genes from ten *Streptomyces* strains (Supplemental Table 1) was used to build a Maximum Likelihood tree using RAxML-HPC Black Box using 500 bootstrap replicates (version 8.2.10). Alignment and tree-building was done through CIPRES Science Gateway V. 3.3 [55]. Housekeeping and *mel* trees were visualized in iTOL [56]. All seven strains encoded the extracellular *melC2* gene, whereas only six strains encoded the intracellular *melD2* (Figure 2D).

Tyrosinase Assay

Enzymatic oxidation of L-3,4-dihydroxyphenylalanine (L-DOPA) by tyrosinase was monitored spectrophotometrically [57] using the BioTek® Synergy® Multi-Detection Microplate Reader. Synthesis of Dopachrome was monitored at an absorbance of 475 nm. To prepare the assay, liquid cultures of each *Streptomyces* isolate were grown in 100 mL standard glucose-minimal salts medium with Tiger's Milk (MMT) at 30 ^{o}C with shaking for 5-7 days, according to Keiser *et al* [58]. Approximately 20 mL of each culture was harvested and split between two, 15 mL conical tubes, which were centrifuged for 7 minutes at 3200 x *g*. Supernatants were collected and kept on ice while pellets were resuspended and washed with 10 mL of 0.1 M sodium phosphate (131 mg $Na_2HPO_4 \bullet 7H_2O$ / 70 mg $NaH_2PO_4 \bullet H_2O$) pH 6.8. Resuspended cells were then centrifuged for 7 minutes at 3200 x *g* and supernatants were discarded. Following resuspension of cell pellets in 10 mL of 0.1 M sodium phosphate pH 6.8, suspensions were split between two tubes and sterile glass beads were added to each 15 mL tube and bead beaten for 5 minutes at 1500 rpm. Bead beaten

cell extracts were then combined in one 15 mL tube and sonicated with a microtip for six cycles of 15 seconds of sonication at an amplitude of 15 and 45 seconds rest on ice. Cells were then centrifuged for 7 minutes at 3200 x *g* and supernatants were collected, which was considered the cell extract fraction. For protein extracts, these cell extracts and culture supernatants were then treated with 70% ammonium sulfate ($(NH_4)_2SO_4$) and incubated on ice until dissolved. After dissolution, both cell and extracellular protein extracts were centrifuged at 4 ^oC for 30 minutes at 3200 x *g*. Supernatants were discarded and protein pellets were resuspended in 2.5 mL of 0.1 M sodium phosphate. To remove the salt from the protein pellets, samples were applied to PD 10 desalting columns and allowed to pass through via gravity. Before application, columns were washed with 4 applications of 0.1 M sodium phosphate pH 6.8. After desalting, total protein concentrations were determined via the microtiter Bio-Rad Protein Assay. Extracellular extract protein concentrations ranged from 26.4 μg/mL to 601.8 μg/mL while intracellular extract protein concentrations range from 453.3 μg/mL to 1201.9 μg/mL. Samples were loaded into a 96-well microtiter plates, which included: 100 μL cell extract or extracellular extract all resuspended in 0.1 M sodium phosphate, 100 μL 6.8 mM L-DOPA, and additions with and without, 5 mM of a tyrosinase inhibitor KA [44]. KA is known to inhibit the enzymatic activity of tyrosinase [43, 44]. KA has been shown to have a competitive inhibitory effect on monophenolase activity via copper chelation. Additionally, KA is known to have a mixed inhibitory effect on dephenolase activity of tyrosinase and likely inhibits tyrosinase via copper chelation at the enzyme's active site [43]. Controls included three replicates wells without protein containing combinations of 0.1 M sodium phosphate, L-DOPA, and 5mM KA. Absorbance at 475 nm was measured every minute for 8-10 hours.

Phenolic compound challenges on agar

To determine strain resistance to phenolic compounds, standard glucose-minimal salts medium (MM) was prepared according to Keiser *et al*. [58] with the addition of 0.01 g copper (II) sulfate ($CuSO_4$) and 100 mL of phosphate buffer (138 g/L NaH_2PO_4 and 142 g/L Na_2HPO_4) per liter. Filter sterilized phenolic compounds were added to cooled, autoclaved media at concentrations of either 0, 0.125, 0.5, 1, or 5 mM for salicylic acid (SA), catechol, and ferulic acid (FA) or 0, 2, 5, 6, 8, 10 and 12 mM for benzoate. 25 mL of phenol-containing agar was pipetted or poured onto

petri dishes. Once solid, 100 μL of *Streptomyces* strains 299, 303, CL18 and 136 standardized to OD_{600} of 0.01 (see above) and diluted 1:10 was pipetted onto solidified plates and spread with sterile beads (CFU range: $4x10^3$ to $4x10^4$). Plates were incubated at 30 °C and checked daily for CFU formation. CFUs were counted and recorded.

Salicylic acid challenge in liquid media

Liquid cultures of each isolate were prepared as described above with the exception of growth medium type. Cultures were grown in MM with copper (II) sulfate ($CuSO_4$), rather than solid LB. A spectrophotometer measured the optical density at 600 nm (OD_{600}) and cultures were normalized to an OD_{600} of 0.1. 100 μL of all normalized isolate resuspensions was added to sterile 125 mL flasks containing 75 mL MM and concentrations of either 0.0 mM or 0.5 mM SA. These concentrations were chosen based on results from solid media as well previous findings from Lebeis *et al* [21]. In addition, a separate complete set of flasks was inoculated exactly as described, with the addition of 1.5 mM KA. Three technical replicates were prepared. Erlenmeyer flasks were incubated at 30 °C with shaking at 125 rpm for 6 days. After the 6-day incubation, biomass was collected via 10 second vacuum filtration of each 75 mL culture on 0.2 μm filter paper. Filters were allowed to dry overnight. Three filter paper controls with filtered media only were weighed and biomass was calculated based on the difference between the average of the control filter paper and those with culture.

Seed sterilization and germination

For all seedling experiments, we used Col-0 accession, wild-type (WT) *A. thaliana* plants. *sid2* seedlings, which cannot produce SA [59] were obtained from the Arabidopsis Biological Resource Center (ABRC) seed collection at The Ohio State University. All seeds were surface sterilized via treatment in 70% ethanol with 0.1% Triton-X100 for one minute, 10% household bleach with 0.1% Triton-X100 for 15 minutes, and three washes with sterile distilled water. Seeds were stratified for 3 days in the dark at 4 °C and subsequently germinated at 24 °C with 18 hours of light for 6-days on agar plates containing half strength (2.22 g/L) Murashige & Skoog (MS) vitamins, 1% sucrose, and 1% Phytoagar (Bioworld).

Plant colonization experiments

To inoculate plates, 150 µL of individual isolate resuspensions were spread on prepared half strength MS 150 mm x 150 mm square agar plates with no sucrose. Plates were allowed to dry and four to five seedlings were aseptically transferred onto each plate with flame-sterilized tweezers. Plates were sealed with Parafilm® M Laboratory Film and randomly stacked vertically in open wire trays, which were grown at 24 ºC with 18 hours of light for 14 days. Every two days, root length was observed, phenotype was assessed, and plates were shuffled. After 14 days, the seedlings from each plate were aseptically harvested and pooled in sterile previously weighed 1.5 mL centrifuge tubes. Tubes were weighed again after tissue was added to determine seedling biomass. To quantify internal levels of colonization, roots were rinsed and vortexed 5 seconds three times with sterile distilled water to determine combined level of colonization for internal and tightly attached external bacteria. Alternatively, seedlings were surface sterilized by treating with freshly made 10% household bleach with 0.01% Triton-X100 for 15 minutes. Seedlings were then rinsed with sterile distilled water, residual bleach was neutralized with sterile 2.5% sodium thiosulfate ($Na_2S_2O_3 \bullet 5H_2O$) for 5 minutes, and finally washed with sterile distilled water twice more. For homogenization of weighed seedlings, sterile 3 mm garnet or glass beads were aseptically transferred to tubes containing the pooled, surface sterilized whole seedlings in each tube, 1 mL of sterile water was added to each tube, and samples were homogenized in a 2010 Geno/Grinder® at 1500 rpm for 2.5 minutes. 100 µL of homogenized tissue was spread on LB plates and incubated at 28 ºC for 4-7 days. CFUs were counted and recorded. For experiments in pots, 64 mL of sterile calcined clay (Pro's Choice Rapid Dry) in three-inch square pots was inoculated with 49mL normalized culture suspended in half strength MS buffered with sterile 2-(N-morpholino) ethanesulfonic acid (MES). Six-day old seedlings were aseptically transferred to inoculated pots. An additional 1mL of suspended inoculum was used to bury the seedling roots. Plants were watered every 2-3 days from the top with sterile distilled water and grown in growth chambers (Percival, model: AR41L3C8) with 10 hours of light at 22ºC and 14 hours of dark at 18ºC. Beginning at six weeks of growth, plants were aseptically harvested when inflorescence began to emerge. Whole plants were submerged in 25mL of sterile harvesting phosphate buffer with 0.01% Silwet (Lehle Seeds) and vortexed vigorously for ten seconds. Roots and rosettes were separated with sterile forceps and transferred to sterile centrifuge tubes and weighed. Roots were

either rinsed three times with sterile distilled water, or treated with bleach to remove external microbes, as aforementioned. Sterile glass or garnet beads were added to each tube containing roots, which were homogenized as described above. Once homogenized, 100μL of tissue was spread on LB plates and incubated at 28ºC for four to seven days. CFUs were counted and recorded.

Statistical analysis

Enzyme assay, phenolic compound challenge, culture biomass, and seeding colonization and plant biomass, results were statistically analyzed with Prism version 7.0a for Mac (GraphPad Software, La Jolla California USA, www.graphpad.com) using the nonparametric Kruskal-Wallis test, including one-way ANOVA followed by Dunn's multiple comparisons. When appropriate, analysis included two-way ANOVA and Tukey's multiple comparisons, or the Wilcoxon matched-pairs signed rank test or multiple t-test with Holm-Sidak multiple correction method.

III. RESULTS

Melanin production is associated with root-enriched Streptomyces strains

While Streptomycetaceae are not a dominant root-associated family, they are consistently present within the roots of various plant species [10-16, 18]. In previously reported findings, when *A. thaliana* was inoculated with a defined bacterial community of isolates and grown for 6-8 weeks, two *Streptomyces* isolates, 299 and 303, displayed enriched root endophytic compartment colonization while another two, CL18 and 136, did not [21]. Strikingly, 299 and 303 liquid and solid media, but not the bacteria themselves, developed distinct pigmentation *in vitro*, which never appear in CL18 or 136 cultures (Figure 2.1A). Pigment produced by strain 299 was delayed and lighter in color than that produced by 303 (Figure 1A). The brown/black pigmentation suggested the potential production of melanin.

To determine its identity, pigment was extracted from 299 and 303 spent liquid media. LC-MS analysis of pigments extracted from 299 and 303 indicated molecular similarity to a synthetic melanin standard by the presence of three distinct melanin degradation products (pyrrole-2,3-

dicarboxylic acid (PDCA), pyrrole-2,3,5-tricarboxylic acid (PTCA), 1,3-thiazole-4,5-dicarboxylic acid (TDCA)) (Figure 2.1B-C). In addition, while both extracted pigment samples were consistent with synthetic melanin, the normalized relative intensities of melanin degradation products from isolates 299 and 303 were not identical, consistent with pigment distinctions observed in liquid (Figure 2.1A) and solid media (data not shown). Overall, our findings suggest that when grown in/on LB and MM, 299 and 303 produce an extracellular pigment, which CL18 and 136 do not, and this pigment is melanin. We next sought to determine if pigment production was associated with genome distinctions between the four *Streptomyces* strains.

Genomes of melanin-producing strains contain genes essential for melanin production

A phylogenetic tree constructed from a concatenated alignment of five housekeeping genes indicated our four non-pathogenic, root-associated *Streptomyces* strains showed phylogenetic similarity with a variety of previously characterized soil-derived *Streptomyces*, with 136 diverging the most from 299, 303, and CL18 (Figure 2.2A and Table 2.S1). Included in this comparison for its robust colonization of *A. thaliana* roots and melanin pigment production, *Streptomyces scabiei* 87.22 proved more closely related to 299 and 303 than CL18 or 136, although neither 299 nor 303 showed evidence of pathology even 6-8 weeks post-infection (Figure 2.S1). Thus, we set out to determine genome regions and more specifically, individual genes shared by phenotypically similar strains.

Besides the genome of *S. scabiei* 87.22, which is complete, all genomes were estimated to be >99% complete by Anvi'o identification of four sets of bacterial single-copy gene collections [29]. Annotations were assigned using the Pfam and [51] SUPERFAMILY [52] databases (Figure 2.2B-C). Interestingly, 299, 303, and *S. scabiei* 87.22 had larger genomes than CL18 and 136 (Table 2.S2), leaving room for exploration of genes and potential gene products involved in root association (Figure 2.2B-C). Comparative genomics of our four isolates and *S. scabiei* 87.22 revealed homologous genes shared among different subsets of all of the genomes. Specifically, we investigated homologous regions shared among 299, 303 and *S. scabiei*, but not CL18 or 136 (Figure 2.2B). The cluster unique to 299, 303 and *S. scabiei* 87.22 (Figure 2.2B-C) indicated the presence of two genes encoding tyrosinase in the genomes of 299 and 303 and one such gene in

the genome of *S. scabiei* 87.22, although BLASTP searches returned two copies for *S. scabiei* 87.22 (Figure 2.2C pink boxes). While Pfam annotations identified only one copy of the tyrosinase co-factor MelC1 in 299, 303 and *S. scabiei* 87.22 genomes, BLASTP searches returned two copies of this helper gene for each of these isolates respectively. The annotated co-factor is the helper protein responsible for copper ion addition to tyrosinase allowing enzymatic function [35]. As discussed, tyrosinase is an enzyme critical to melanin production, aligning with our previous finding of extracellular melanin production, suggesting that at least one tyrosinase/co-factor pair is active in 299 and 303. However, we needed to investigate the potential role an active second tyrosinase/co-factor pair might confer.

To further characterize the genes encoding tyrosinases and their co-factors, proteins identified in Anvi'o (Figure 2.2B-C), we searched for the presence of distinct *melC* and *melD* operons in select *Streptomyces* genomes with a BLASTP search using *S. scabiei* 87.22 protein sequences identified by Yang *et al* as queries [35]. Tyrosinase genes (Figure 2.2D bottom) and helper genes with at least 97% homology (Figure 2.2D top) were identified in six additional *Streptomyces* strains that produce a brown pigment in the medium (Table 2.S1). Components of the melanin operon were not identified in the genomes of CL18 or 136. A phylogenetic tree of the tyrosinase genes from only *Streptomyces* genomes encoding two copies shows general clustering and divergence of the two genes (Figure 2.2D bottom and Table 2.S1). This was also true for the annotated tyrosinase helper genes (Figure 2.2D top). Finally, the predicted *melC1* and *melC2* genes were contiguous within each genome, which was also true for the *melD1* and *melD2* genes. While 299 and 303 tyrosinase and helper genes share homology, they were not identical, which correlates with the strain-specific melanin pigments produced (Figure 2.1A, C). Together, these findings necessitated investigation of strain-specific tyrosinase kinetics.

Enzyme kinetics differentiate tyrosinase activity between Streptomyces strains

We next sought to determine if 299 and 303 did indeed produce functional intracellular and extracellular tyrosinases by performing an enzymatic activity assay on whole cell extracts and culture supernatants. Whole cell (intracellular) and supernatant (extracellular) protein extracts from all four strains were combined with tyrosinase substrate L-DOPA, and enzymatic activities were observed as production of Dopachrome via spectrophotometry absorbance at 475 nm. While

strain 303 showed enzymatic activity in both intracellular and extracellular protein extracts (Figure 2.3B), strain 299 did not demonstrate statistically significant tyrosinase activity using this assay (Figure 2.3E) without the addition of copper sulfate (data not shown). However, both 303 and 299 produced melanin (Figure 2.1), indicating that each of their extracellular tyrosinase is active at least *in vitro*. CL18 and 136 extracts did not show any activity above the L-DOPA alone control and neither strain produced a pigment *in vitro* (Figure 2.3, 2.S2, 1.1A). Interestingly, the tyrosinase activity demonstrated in both 303 intracellular and extracellular protein extract could be significantly inhibited by KA (Figure 2.3B, 2.3E, 2.S2). Together, our results support our earlier findings that while 299 and 303 both produce melanin, the tyrosinase required for its production has different activity (Figure 2.3), resulting in distinguishable melanins (Figure 2.1).

Survival and growth in the presence of phenolic compounds is improved in better colonizers

Microorganisms living close to and within plant roots must contend with root exudates, potentially including phenolic compounds such as salicylic acid (SA) and ferulic acid (FA), which inhibit *Streptomyces* growth [35]. Thus, SA is measurable in *A. thaliana* roots and seedlings while both SA and FA are present in root exudates of *A. thaliana* and *Avena barbata* [21, 27, 28]. Specifically, this evidence suggests that plant-associated strains living on or near roots may need to resist phenolic root exudates to successfully colonize. Beyond their role in melanin production, tyrosinase enzymes encoded by *Streptomyces* are capable of oxidizing various phenolic compounds, including SA and FA, into their quinone form [35]. To determine *Streptomyces* isolate phenolic compound tolerance, we compared growth of all isolates on solid medium with the addition of varying concentrations of SA, FA, catechol, and benzoate (Figure 2.4A and 2.S3). As seen on the left in Figure 2.4A, at a concentration of 0.5mM SA, 303 grew significantly better than 299, CL18 and 136. When challenged with FA, a lignin degradation product [60], at a concentration of 0.125mM, 303 survived significantly better than 299, CL18 and 136 (Figure 2.4A right). At 0.5mM FA, 303 grew better than both CL18 and 136, but not 299 (Figure 2.4A right) while at 1mM, 303 grew better than all other strains. Catechol challenge only at the lowest concentration (0.125mM) resulted in significant growth differences, in which 299 grew better than 303, CL18 and 136 (Figure 2.S3). We propose that differential results between 299 and 303 phenolic compound stress tolerance may be due to variable tyrosinase substrate preferences, which

have been demonstrated even between MelD2 and MelC2 of the same *Streptomyces* strains [35]. Notably, 303 also encodes enzymes in a previously characterized *Streptomyces* SA degradation pathway and can use SA as its sole carbon source [21]. Similar genes were not found in the genomes of 299, CL18 and 136 [21]. Therefore, we needed to further distinguish if the increased colony forming units on solid medium was due to increased growth of 303, or increased protection of the oxidative stress induced by SA.

To determine if the apparent protection of 303 against SA *in vitro* is mediated directly by bacterial tyrosinase activity, we added the tyrosinase inhibitor KA (1.5 mM) to liquid minimal medium (MM) with the significant concentration of 0.5 mM SA and measured biomass accumulation after 6 days. Interestingly, biomass comparisons of 299 and 303 indicated that biomass was not influenced by SA presence at the concentrations tested (Figure 2.4B), suggesting that these strains do not have increased growth under these *in vitro* conditions, but rather are protected from phenolic compounds. Because only 303 contained a functional intracellular tyrosinase, both solid and liquid media challenges indicate that intracellular activity does not necessarily mediate oxidative stress protection (Figure 4A-B). While this protection correlates with extracellular tyrosinase activity, it was not eliminated under these conditions with the addition of 1.5 mM KA (Figure 4B), which was sufficient to inhibit enzymatic activity (Figure 2.3B and E). Of note, addition of KA halted visible 299 and 303 pigment production (data not shown). Thus, we could not conclude that extracellular tyrosinase activity independent of melanin production protects 299 and 303 from SA induced stress. Likewise, the addition of synthetic melanin to CL18 and 136 cultures grown with SA did not affect biomass (Figure 2.4C). However, our evidence suggested that together tyrosinase and melanin can protect these strains from phenol-induced oxidative stress. Thus, our *in vitro* growth experiments propose that neither tyrosinase nor melanin pigment alone are sufficient to provide *Streptomyces* with protection from SA, suggesting that both may be necessary to increase plant colonization. Additionally, we cannot rule out other mechanisms of protection, such as the tyrosinase-independent functional SA degradation pathway in strain 303 [21] or other tyrosinase products. To determine if tyrosinase-dependent protection from phenolic compounds might increase survivability near the root, we performed seedling colonization assays.

Seedling colonization is Streptomyces strain and tyrosinase identity dependent

In a mixed bacterial community, the presence of predicted *mel* operons positively correlates to root enrichment of our two melanin-producing strains 299 and 303 [21], suggesting a potential role for tyrosinase or products of its enzymatic activity (such as melanin) in host colonization. Thus, to distinguish influences of mixed bacterial communities from individual strain capabilities, *Streptomyces* isolates 299, 303, CL18, and 136 were screened for their ability to colonize 6-day old *A. thaliana* seedlings as the sole inoculum for 14 days (Figure 2.5A). After two weeks, seedlings were colonized with significantly more of isolate 299 and 303 than 136, whereas CL18 colonization was not significantly different than any other isolate (Figure 2.5A). This pattern was also observed in bleached seedlings (Figure 2.S4A). Thus, in addition to increased root colonization of mature plants in a competitive context, 299 and 303 also colonize seedlings better than 136 14 days following monoinoculations, while CL18 is not significantly different from others (Figure 2.5A)[21]. Importantly, monoinoculated plants show no signs of pathology or change in biomass even after 6-8 weeks of growth (Figure 2.S1), confirming that they are not pathogens.

We hypothesized that tyrosinase or its products could influence seedling colonization via conferring protection from common phenolic compounds in root tissues, seedlings, and exudates [21, 27, 28]. Thus, we again performed the monoinoculations described above, but introduced the tyrosinase inhibitor KA [43] to the assay to prohibit immediate tyrosinase-conferred protection. When KA (1.5 mM) was spread on plates prior to addition of each isolate, only seedling colonization by 303 was influenced by KA ($p<0.0705$)(Figure 2.5B), which correlates with the inhibition of intracellular and extracellular 303 tyrosinase activity (Figure 2.3B,E). Synthetic and bacterially-derived melanin were added to monoinoculations to determine if CL18 or 136 colonization would improve, but it did not at 7 days (Figure 2.S4B-C). Together with the previous finding that *in vitro* liquid growth of 303 with SA remained unchanged when tyrosinase was inhibited (Figure 2.4B), our results do not distinguish the importance of tyrosinase activity from melanin production in the context of seedling colonization.

To determine if SA production by seedlings influences *Streptomyces* isolate colonization, wild-type Col-0 and *sid2 A. thaliana* seedlings, which are unable to biosynthesize SA, were inoculated with each of the four isolates (Figure 2.5C). While there were no significant differences in level of colonization for 299, 303, and 136, CL18 colonized significantly better in *sid2* seedlings, indicating that SA production partially limits its colonization (Figure 2.5C). Together these experiments demonstrate that *Streptomyces* isolates are differentially sensitive to SA during seedling colonization, representing at least one mechanism that influences their level of colonization.

IV. DISCUSSION

Streptomyces' metabolic potential in the root microbiome

Streptomyces are capable of colonizing the roots of a wide variety of plant species [11-16, 21] in geographically and geologically diverse soils [62], emphasizing the need to understand their assembly into the root microbiome. Select *Streptomyces* strains have been identified as plant growth promoting and even disease suppressive [18], highlighting their potential applications in agriculture. Yet, likely due to their complex arsenal of natural products, including a variety of small molecules and antimicrobials such as volatile organic compounds, indole acetic acid, hydrogen sulfide, ammonia, and many currently uncharacterized products. Although microbial activities associated with root colonization for other more predominant taxa, such as Proteobacteria, have been uncovered, specific functions involving root microbiome assembly mechanisms for less abundant microbes, such as *Streptomyces spp.* is largely unexplored [18, 19, 63, 64]. Overall, these studies shed light on the root microbiome colonization potential of specific *Streptomyces* strains and represent a shift towards defining multiple functional mechanisms microbes use for colonization from a complex microbial inoculum.

Streptomyces' employ distinct tyrosinase enzymes

Based on our ability to distinguish *Streptomyces* strains by degree of seedling colonization, we hypothesized genomic differences would explain strain variation. Our comparative genomic analyses suggest distinct differences between our *Streptomyces* isolates. These findings highlight

that functional conclusions based on genus-level abundance from 16S rRNA gene amplicon studies inadequately capture the organisms' potential, as previously described for plant-associated *Pseudomonas* strains [65]. Further, including the plant pathogen *S. scabiei* 87.22 in our genomic comparisons revealed shared genetic factors contributing to increased seedling colonization in our non-pathogenic, melanin-producing *Streptomyces* isolates. In addition to these findings, Beausejour and Beaulieu [61] found that melanin plays a role in *S. scabiei* 87.22 virulence and colonization. Genomic analyses identified potential phenolic compound resistance genes in 299 and 303, leading to *in vitro* challenges with phenolic compounds that induce ROS production [66,67]. On solid media, 303 was able to withstand SA and FA better than CL18 and 136 (Figure 2.4A), while 299 grew better than all other strains when challenged with the lowest concentration of catechol (Figure 2.S3). In SA-containing inoculated liquid media, KA did not significantly influence 299 or 303 biomass accumulation, suggesting that there are other mechanisms to alleviate SA induced stress, such as the previously identified SA degradation pathway in 303 [21]. Taken together, our genomic, *in vitro,* and *in vivo* findings emphasize 299 and 303 differential enzymatic structures, substrates and products, supporting strain-specific survival mechanisms. Further, neutralizing phenolic compounds is likely just one of many potential selective pressures imposed by the plant host.

Comparative genomics inform benchtop experimentation

As critical genome features in plant microbiomes continue to be defined, we propose the discovery power added via incorporation of genomic tools (i.e. comparative genomics) into benchtop exploration of microbial functional similarities and differences found to be predictive of colonization or host health. Studies are required to further define strain-specific *Streptomyces* natural products conferring potential survival advantages, which might also impact host or microbiome co-inhabitant growth. The presence of *Streptomyces* in the core root microbiome from a diverse collection of plants [11-16] suggests strong selection for microbiome members with a diverse arsenal of secondary metabolic functions. This highlights the necessity to define the activities associated with strains in this genus.

A new role for a common microbial product

Here we offer an approach to begin to disentangle phylum and family level generalizations about bacterial functions and roles within the host microbiome. We have used this approach to define a new role for a widely studied enzyme, tyrosinase, and one of its products, melanin. Together, melanin pigment production and tyrosinase gene identification unique to genomes of root-enriched strains suggests melanin or the tyrosinase enzyme required for its production may influence host colonization. We propose that during plant colonization, melanin-producing strains are protected against phenolic compounds commonly found in the root-soil interface [26-28, 60, 68, 69]. The impact of this finding is particularly interesting given that it is produced by a range of other soil isolated fungi and bacteria. Defining this new context for melanin production will ultimately inform our understanding the complex processes of root microbiome assembly and manipulation.

As we look for new strategies to tackle the challenges of climate change-induced crop decline, we look toward the potential of the plant microbiome. Recently, plant drought resistance bacterial community studies have identified Actinobacteria and *Streptomyces* as root enriched in drought conditions [19, 20]. We propose that continued strain-level investigation of overlapping genome regions and robust *in vitro* and *in vivo* studies will help further inform results from microbiome studies. Thus, we suggest the power of moving beyond taxonomic identification and abundances to distinct strain gene comparisons and product exploration. Together our findings provide opportunities for harnessing their power to improve plant health and more broadly enhance agricultural applications and crop productivity.

V. ACKNOWLEDGEMENTS

This work was supported by the University of Tennessee, Knoxville. We thank current and former members of the Lebeis laboratory for useful discussions, especially Katherine Moccia, Caleb Whitley, Lizzy Denison, and Jake Massey. We also thank Sur Hererra Paredes and David Baltrus for critical comments on the manuscript. The chemical analysis of melanin was performed at the Biological and Small Molecule Mass Spectrometry Core at the University of Tennessee. The four strains of *Streptomyces* were originally isolated in the laboratory of Jeffery Dangl at the University of North Carolina.

VI. REFERENCES

1. Coyte, K.Z., J. Schluter, and K.R. Foster, *The ecology of the microbiome: Networks, competition, and stability.* Science, 2015. **350**(6261): p. 663-6.
2. Hibbing, M.E., et al., *Bacterial competition: surviving and thriving in the microbial jungle.* Nat Rev Microbiol, 2010. **8**(1): p. 15-25.
3. Wei, Z., et al., *Trophic network architecture of root-associated bacterial communities determines pathogen invasion and plant health.* Nat Commun, 2015. **6**: p. 8413.
4. Jousset, A., et al., *Intraspecific genotypic richness and relatedness predict the invasibility of microbial communities.* ISME J, 2011. **5**(7): p. 1108-14.
5. Lareen, A., F. Burton, and P. Schafer, *Plant root-microbe communication in shaping root microbiomes.* Plant Mol Biol, 2016. **90**(6): p. 575-87.
6. Fiegna, F. and G.J. Velicer, *Exploitative and hierarchical antagonism in a cooperative bacterium.* PLoS Biol, 2005. **3**(11): p. e370.
7. Lakshmanan, V., G. Selvaraj, and H.P. Bais, *Functional soil microbiome: belowground solutions to an aboveground problem.* Plant Physiol, 2014. **166**(2): p. 689-700.
8. van der Heijden, M.G. and M. Hartmann, *Networking in the Plant Microbiome.* PLoS Biol, 2016. **14**(2): p. e1002378.
9. Sheth, R.U., et al., *Manipulating Bacterial Communities by in situ Microbiome Engineering.* Trends Genet, 2016. **32**(4): p. 189-200.
10. Seipke, R.F., M. Kaltenpoth, and M.I. Hutchings, *Streptomyces as symbionts: an emerging and widespread theme?* FEMS Microbiol Rev, 2012. **36**(4): p. 862-76.
11. Lundberg, D.S., et al., *Defining the core Arabidopsis thaliana root microbiome.* Nature, 2012. **488**(7409): p. 86-90.
12. Bulgarelli, D., et al., *Revealing structure and assembly cues for Arabidopsis root-inhabiting bacterial microbiota.* Nature, 2012. **488**(7409): p. 91-5.
13. Peiffer, J.A., et al., *Diversity and heritability of the maize rhizosphere microbiome under field conditions.* Proc Natl Acad Sci U S A, 2013. **110**(16): p. 6548-53.
14. Edwards, J., et al., *Structure, variation, and assembly of the root-associated microbiomes of rice.* Proc Natl Acad Sci U S A, 2015. **112**(8): p. E911-20.

15. Yeoh, Y.K., et al., *The core root microbiome of sugarcanes cultivated under varying nitrogen fertilizer application.* Environ Microbiol, 2016. **18**(5): p. 1338-51.
16. Bonaldi, M., et al., *Colonization of lettuce rhizosphere and roots by tagged Streptomyces.* Front Microbiol, 2015. **6**: p. 25.
17. Bignell, D.R., J.K. Fyans, and Z. Cheng, *Phytotoxins produced by plant pathogenic Streptomyces species.* J Appl Microbiol, 2014. **116**(2): p. 223-35.
18. Viaene, T., et al., *Streptomyces as a plant's best friend?* FEMS Microbiol Ecol, 2016. **92**(8).
19. Fitzpatrick, C.R., et al., *Assembly and ecological function of the root microbiome across angiosperm plant species.* Proc Natl Acad Sci U S A, 2018. **115**(6): p. E1157-E1165.
20. Xu, L., et al., *Correction for Xu et al., Drought delays development of the sorghum root microbiome and enriches for monoderm bacteria.* Proc Natl Acad Sci U S A, 2018. **115**(21): p. E4952.
21. Lebeis, S.L., et al., *PLANT MICROBIOME. Salicylic acid modulates colonization of the root microbiome by specific bacterial taxa.* Science, 2015. **349**(6250): p. 860-4.
22. Bosund, I., et al., *The Bacteriostatic Action of Benzoic and Salicylic Acids. II. The Effect on Acetate Metabolism.* Acta Chemica Scandinavica, 1960. **14**(1): p. 111-125.
23. Yang, L., et al., *Salicylic acid biosynthesis is enhanced and contributes to increased biotrophic pathogen resistance in Arabidopsis hybrids.* Nat Commun, 2015. **6**: p. 7309.
24. Rivas-San Vicente, M. and J. Plasencia, *Salicylic acid beyond defence: its role in plant growth and development.* J Exp Bot, 2011. **62**(10): p. 3321-38.
25. Studham, M.E. and G.C. MacIntosh, *Phytohormone signaling pathway analysis method for comparing hormone responses in plant-pest interactions.* BMC Res Notes, 2012. **5**: p. 392.
26. Strehmel, N., et al., *Profiling of secondary metabolites in root exudates of Arabidopsis thaliana.* Phytochemistry, 2014. **108**: p. 35-46.
27. Zhalnina, K., et al., *Dynamic root exudate chemistry and microbial substrate preferences drive patterns in rhizosphere microbial community assembly.* Nat Microbiol, 2018. **3**(4): p. 470-480.

28. Chaparro, J.M., et al., *Root exudation of phytochemicals in Arabidopsis follows specific patterns that are developmentally programmed and correlate with soil microbial functions.* PLoS One, 2013. **8**(2): p. e55731.
29. Barka, E.A., et al., *Taxonomy, Physiology, and Natural Products of Actinobacteria.* Microbiol Mol Biol Rev, 2016. **80**(1): p. 1-43.
30. Eisenman, H.C. and A. Casadevall, *Synthesis and assembly of fungal melanin.* Appl Microbiol Biotechnol, 2012. **93**(3): p. 931-40.
31. Valverde, P., et al., *Variants of the melanocyte-stimulating hormone receptor gene are associated with red hair and fair skin in humans.* Nat Genet, 1995. **11**(3): p. 328-30.
32. Zhang, L., et al., *Genetic Basis of Melanin Pigmentation in Butterfly Wings.* Genetics, 2017. **205**(4): p. 1537-1550.
33. Emami, S.A., et al., *Inhibitory effects of different fractions of Nepeta satureioides on melanin synthesis through reducing oxidative stress.* Res Pharm Sci, 2017. **12**(2): p. 160-167.
34. Manivasagan, P., et al., *Actinobacterial melanins: current status and perspective for the future.* World J Microbiol Biotechnol, 2013. **29**(10): p. 1737-50.
35. Yang, H.Y. and C.W. Chen, *Extracellular and intracellular polyphenol oxidases cause opposite effects on sensitivity of Streptomyces to phenolics: a case of double-edged sword.* PLoS One, 2009. **4**(10): p. e7462.
36. Brenner, M. and V.J. Hearing, *The protective role of melanin against UV damage in human skin.* Photochem Photobiol, 2008. **84**(3): p. 539-49.
37. Nosanchuk, J.D. and A. Casadevall, *The contribution of melanin to microbial pathogenesis.* Cell Microbiol, 2003. **5**(4): p. 203-23.
38. Bernan, V., et al., *The nucleotide sequence of the tyrosinase gene from Streptomyces antibioticus and characterization of the gene product.* Gene, 1985. **37**(1-3): p. 101-10.
39. Katz, E., C.J. Thompson, and D.A. Hopwood, *Cloning and expression of the tyrosinase gene from Streptomyces antibioticus in Streptomyces lividans.* J Gen Microbiol, 1983. **129**(9): p. 2703-14.
40. Lee, Y.H.W., et al., *A Trans-Acting Gene Is Required for the Phenotypic-Expression of a Tyrosinase Gene in Streptomyces.* Gene, 1988. **65**(1): p. 71-81.

41. Chen, L.Y., et al., *Copper Transfer and Activation of the Streptomyces Apotyrosinase Are Mediated through a Complex-Formation between Apotyrosinase and Its Transactivator Melc1.* Journal of Biological Chemistry, 1992. **267**(28): p. 20100-20107.
42. Leu, W.M., et al., *Secretion of the Streptomyces Tyrosinase Is Mediated through Its Transactivator Protein, Melc1.* Journal of Biological Chemistry, 1992. **267**(28): p. 20108-20113.
43. Chang, T.S., *An updated review of tyrosinase inhibitors.* Int J Mol Sci, 2009. **10**(6): p. 2440-75.
44. Chen, J.S., C.I. Wei, and M.R. Marshall, *Inhibition-Mechanism of Kojic Acid on Polyphenol Oxidase.* Journal of Agricultural and Food Chemistry, 1991. **39**(11): p. 1897-1901.
45. Drewnowska, J.M., et al., *Melanin-Like Pigment Synthesis by Soil Bacillus weihenstephanensis Isolates from Northeastern Poland.* PLoS One, 2015. **10**(4): p. e0125428.
46. Ito, S. and K. Wakamatsu, *Chemical degradation of melanins: application to identification of dopamine-melanin.* Pigment Cell Res, 1998. **11**(2): p. 120-6.
47. Clasquin MF, M.E., Rabinowitz JD. , *LC-MS Data Processing with MAVEN: A Metabolmic Analysis and Visualization Engine.* Curr Protoc Bioinformatics, 2012. **37**(14.11): p. 14.11.1-14.11.23.
48. Chen, I.A., et al., *IMG/M: integrated genome and metagenome comparative data analysis system.* Nucleic Acids Res, 2017. **45**(D1): p. D507-D516.
49. Eren, A.M., et al., *Anvi'o: an advanced analysis and visualization platform for 'omics data.* PeerJ, 2015. **3**: p. e1319.
50. Enright, A.J., S. Van Dongen, and C.A. Ouzounis, *An efficient algorithm for large-scale detection of protein families.* Nucleic Acids Res, 2002. **30**(7): p. 1575-84.
51. Finn, R.D., et al., *The Pfam protein families database: towards a more sustainable future.* Nucleic Acids Res, 2016. **44**(D1): p. D279-85.
52. Gough, J., et al., *Assignment of homology to genome sequences using a library of hidden Markov models that represent all proteins of known structure.* J Mol Biol, 2001. **313**(4): p. 903-19.

53. Kearse, M., et al., *Geneious Basic: an integrated and extendable desktop software platform for the organization and analysis of sequence data.* Bioinformatics, 2012. **28**(12): p. 1647-9.
54. Katoh, K., et al., *MAFFT: a novel method for rapid multiple sequence alignment based on fast Fourier transform.* Nucleic Acids Res, 2002. **30**(14): p. 3059-66.
55. Miller, M.A., W. Pfeiffer, and T. Schwartz. *Creating the CIPRES Science Gateway for inference of large phylogenetic trees*. in *Proceedings of the Gateway Computing Environments Workshop (GCE)*. 2010. New Orleans, LA.
56. Ciccarelli, F.D., et al., *Toward automatic reconstruction of a highly resolved tree of life.* Science, 2006. **311**(5765): p. 1283-7.
57. Claus, H. and H. Decker, *Bacterial tyrosinases.* Syst Appl Microbiol, 2006. **29**(1): p. 3-14.
58. Kieser T, B.M., Buttner MJ, Chater KF, Hopwood DA., *Practical Streptomyces Genetics*, ed. J.I. Foundation. 2000, Norwich, England: Crowes.
59. Dewdney, J., et al., *Three unique mutants of Arabidopsis identify eds loci required for limiting growth of a biotrophic fungal pathogen.* Plant J, 2000. **24**(2): p. 205-18.
60. Kirby, R., *Actinomycetes and lignin degradation.* Adv Appl Microbiol, 2006. **58**: p. 125-68.
61. Beausejour, J. and C. Beaulieu, *Characterization of Streptomyces scabies mutants deficient in melanin biosynthesis.* Can J Microbiol, 2004. **50**(9): p. 705-9.
62. Choudoir, M.J., J.R. Doroghazi, and D.H. Buckley, *Latitude delineates patterns of biogeography in terrestrial Streptomyces.* Environ Microbiol, 2016. **18**(12): p. 4931-4945.
63. Jones, S.E., et al., *Streptomyces exploration is triggered by fungal interactions and volatile signals.* Elife, 2017. **6**: p. e21738.
64. Yandigeri, M.S., et al., *Drought-tolerant endophytic actinobacteria promote growth of wheat (Triticum aestivum) under water stress conditions.* Plant Growth Regulation, 2012. **68**(3): p. 411-420.

65. Blakney, A.J. and C.L. Patten, *A plant growth-promoting pseudomonad is closely related to the Pseudomonas syringae complex of plant pathogens.* FEMS Microbiol Ecol, 2011. **77**(3): p. 546-57.
66. Bosund, I., K. Tilander, J. Åselius, S. Refn and G. Westin (1960). "The Bacteriostatic Action of Benzoic and Salicylic Acids. II. The Effect on Acetate Metabolism." Acta Chemica Scandinavica **14**(1): 111-125.
67. Cheng, A. X., J. Y. Gou, X. H. Yu, H. Yang, X. Fang, X. Y. Chen and C. J. Liu (2013). "Characterization and ectopic expression of a populus hydroxyacid hydroxycinnamoyltransferase." Mol Plant **6**(6): 1889-1903.
68. Hartmann, A., et al., *Plant-driven selection of microbes.* Plant and Soil, 2009. **321**(1-2): p. 235-257.
69. Bakker, M.G., et al., *Harnessing the rhizosphere microbiome through plant breeding and agricultural management.* Plant and Soil, 2012. **360**(1-2): p. 1-13.
70. Greco, G., Ed. (2014). Neuromelanin and Parkinson's Disease. Handbook of Neurotoxicity. New York, NY, Springer.

VII. APPENDIX: TABLES

Table 2.S1. Strains referenced in this study.

This table provides a link between the Streptomyces strains that were used in these experiments and the identification numbers for the permanent draft genomes on the IMG/ER (https://img.jgi.doe.gov/mer/)

Strain Abbreviation	Strain name	IMG Genome ID	NCBI Database Hyperlink	Figure references
299	*Streptomyces canus* 299MFChir4.1	2521172643	NA	1,2,3,4
303	*Streptomyces sp.* 303MFCol5.2	2521172626	NA	1,2,3,4
CL18	*Streptomyces sp.*UNC401CLCol	2522572047	NA	1,2,3,4
136	*Streptomyces sp.* 136MFCol5.1	2636416059	NA	1,2,3,4
S. scabiei	*Streptomyces scabiei* 87.22	646564576	NA	3,4,5
OV308	*Streptomyces mirabilis* OV308	2582581313	NA	5
YR139	*Streptomyces mirabilis* YR139	2582581314	NA	5
OK006	Actinobacteria bacterium OK006	2639763183	NA	5
OK461	*Streptomyces mirabilis* OK461	2616644814	NA	5
S. glaucscens	*Streptomyces glaucscens* NRRL B-2706	NA	Streptomyces glaucscens NRRL B-2706	3
S. galbus	*Streptomyces galbus* NRRL B-2283	NA	Streptomyces galbus NRRL B-2283	3
S. tranashiensis	*Streptomyces tanashiensis* SCTC 19972	NA	Streptomyces tanashiensis SCTC 19972	3
S. avermitilis	*Streptomyces avermitilis*MA-4680	NA	Streptomyces avermitilis MA-4680	3
S. coelicolor	*Streptomyces coelicolor* A3(2)	NA	Streptomyces coelicolor A3(2)	3
S. lincolnesis	*Streptomyces lincolnesis* NRRL ISP-5355	NA	Streptomyces lincolnesis NRRL ISP-5355	3

Table 2.S2. Streptomyces' genome investigation reveals divergent properties and biosynthetic predictions.

Genome features include estimated size, GC content, number of scaffolds in the permanent draft genome, and estimated gene numbers.

Streptomyces Isolate	Genome Size (MB)	G+C Content	Contigs	Protein Coding Genes	Total Genes
299	10.5	70%	116	9620	9710
303	9.5	71%	77	8387	8480
CL18	7.3	72%	49	6591	6677
136	7.8	70%	31	6905	6991
Streptomyces scabiei NCPPB 4086	10.5	71%	295	9050	9151

VIII. APPENDIX: FIGURES

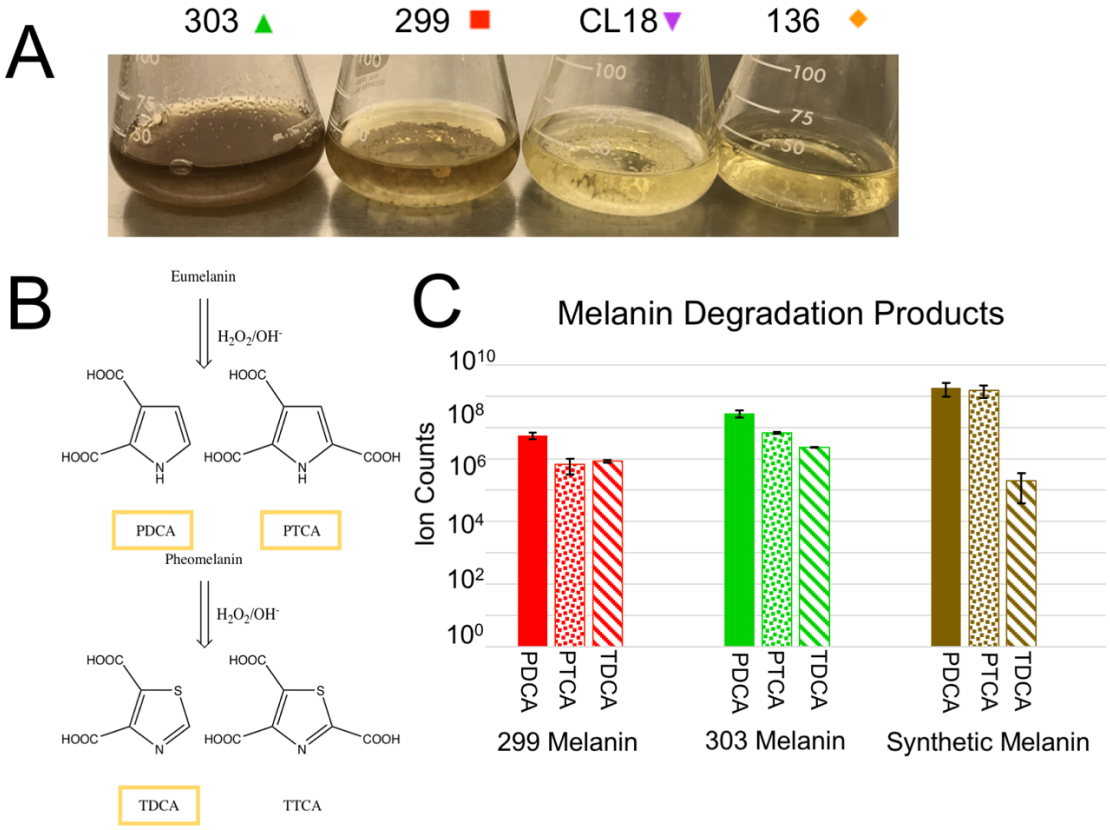


Figure 2.1. Streptomyces strains 299 and 303 produce a pigment consistent with synthetic melanin.

(A) 299 and 303 cultures on the left and middle left produce an extracellular pigment in the LB medium. (B) A schematic showing the products expected from eumelanin degradation, including pyrrole-2,3-dicarboxylic acid (PDCA), pyrrole-2,3,5-tricarboxylic acid (PTCA), and 1,3-thiazole-4,5-carboxylic acid (TDCA). The figure was adapted from Greco, G. [70]. (C) LC-MS of pigmented bacterial extracts indicate degradation components were present consistent with melanin (n=3, blanks subtracted, normalized to mass digested, mean displayed, and standard deviation indicated by error bars).

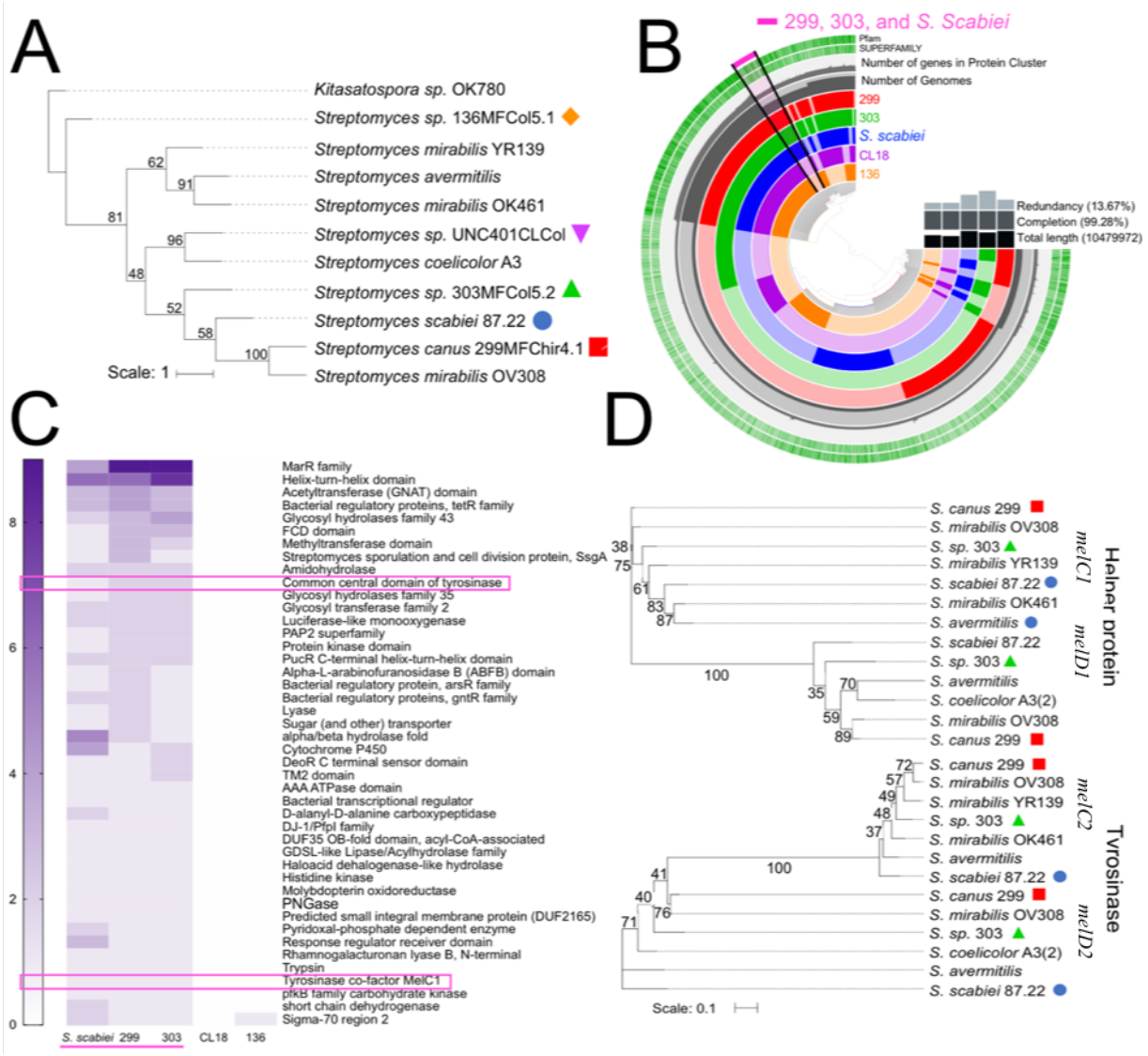


Figure 3.2. Phylogenetic and pangenomic comparison of *Streptomyces* spp. indicate distinct phylogeny and overlapping genes consistent with melanin production.

(A) Concatenated alignment of the 5 amino acid sequences for housekeeping genes *trpB*, *gyrB*, *rpoB*, *atpD*, and *recA* from 8 *Streptomyces* strains and one outgroup (*Kitasatospora sp.* OK780) (Maximum Likelihood, bootstrap consensus values based on 100 replicates) (B) Pangenomic comparison of *Streptomyces* isolates (listed from inside out: 136 (orange), CL18 (purple), *S. scabiei* (blue), 303 (green), and 299 (red). The fan with the pink bar on the end highlights those genes only present in *S. scabiei*, 303, and 299 genomes. (C) Heat map of Pfams predicted from Anvi'o (pink indicates tyrosinase Pfams). The scale on the left indicates how many copies (0-9).

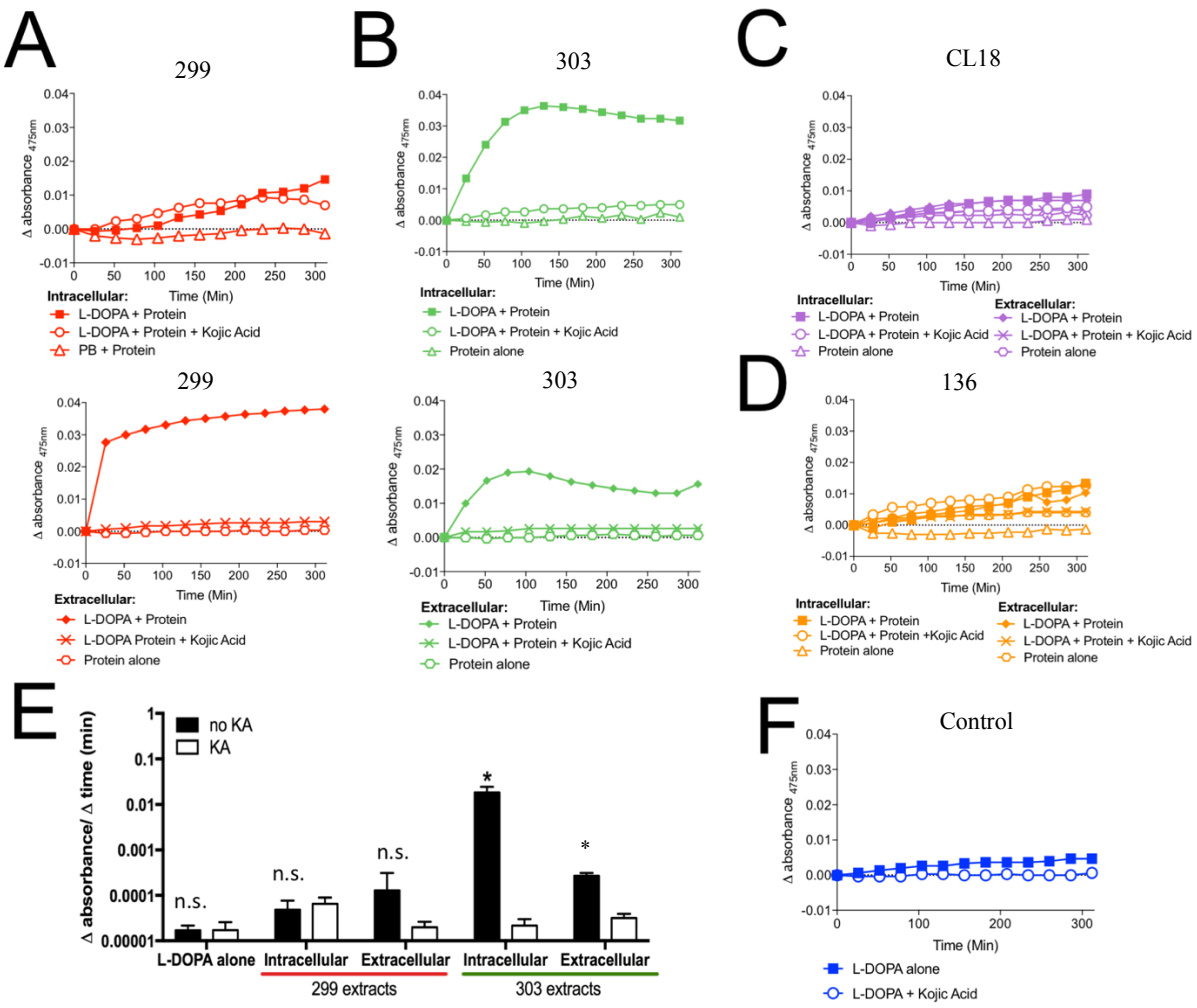


Figure 2.3. Strain-specific tyrosinase activity and kojic acid (KA) inhibition is demonstrated via dopachrome production from L-DOPA with the addition of cell and extracellular 299, 303, CL18 and 136 protein extracts.

Dopachrome production as observed by the mean change in absorbance from the time 0 absorbance at 475 nm for 3 replicates for L-DOPE with protein extracts from 299 (A, red: 1143.3 µg/mL intracellular protein (top) and 601.8 µg/mL extracellular protein (bottom)) 303 (B, green: 903.3 µg/mL intracellular protein (top) and 475.5 µg /mL extracellular protein (bottom)), CL18 (C, purple: 1201.9 µg/mL intracellular protein (top) and 62.3 µg/mL extracellular protein (bottom)), or 136 (D, orange: 453.3 µg/mL intracellular protein (top) and 26.4 µg/mL extracellular protein (bottom)) with and without the addition of the tyrosinase inhibitor, kojic acid (KA). Control E) Tyrosinase kinetics determined by the maximum spectrophotometric change in absorbance divided

by the time required for the change indicating enzyme (tyrosinase) and substrate (L-DOPA) binding for 299 (above the red bar) and 303 (above the green bar) intracellular and extracellular extract, as well as the L-DOPA alone controls. * indicates KA samples were significantly lower at $p<0.05$, multiple t-test with Holm-Sidak multiple correction method. (F) The mean change in absorbance from time 0 absorbance at 475 nm for 3 replicates of L-DOPA alone with no protein addition.

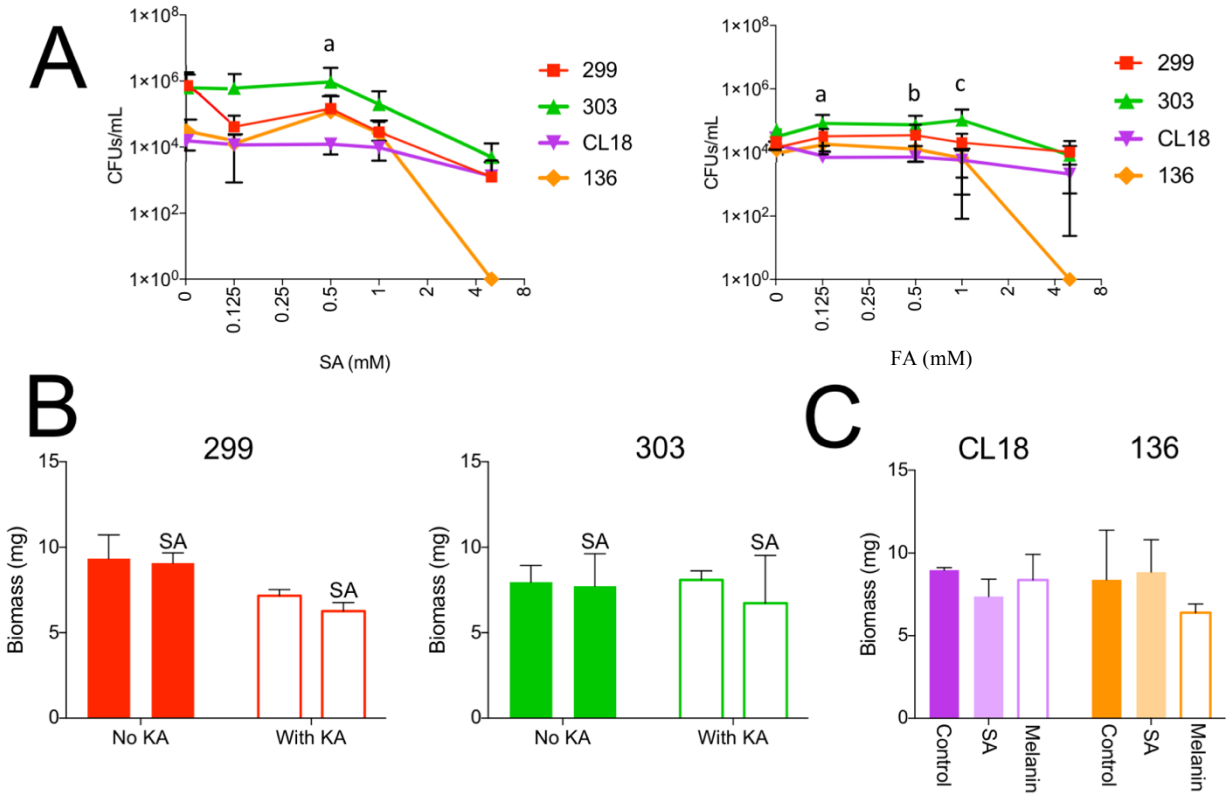


Figure 2.4. Phenolic compound tolerance differs by *Streptomyces* strain.

(A) CFUs after 5-7 days of growth on solid glucose minimal medium containing the indicated concentration of salicylic acid (SA, left) or ferulic acid (FA, right). "a" indicates 303 was significantly different than 299, CL18, and 136. "b" indicates 303 was significantly different than CL18 and 136 (n=12, Kruskal-Wallis, Tukey's multiple comparison, ($p<0.05$)) (B) Biomass of 75mL liquid culture grown for 6 days in MM with and without kojic acid, with and without SA (0.5mM) (n=3). (C) Biomass of 75mL liquid cultures grown for 6 days in MM, MM with SA (0.5mM), or MM with synthetic melanin (20mg/mL) (n=3) (Figure 2.S3).

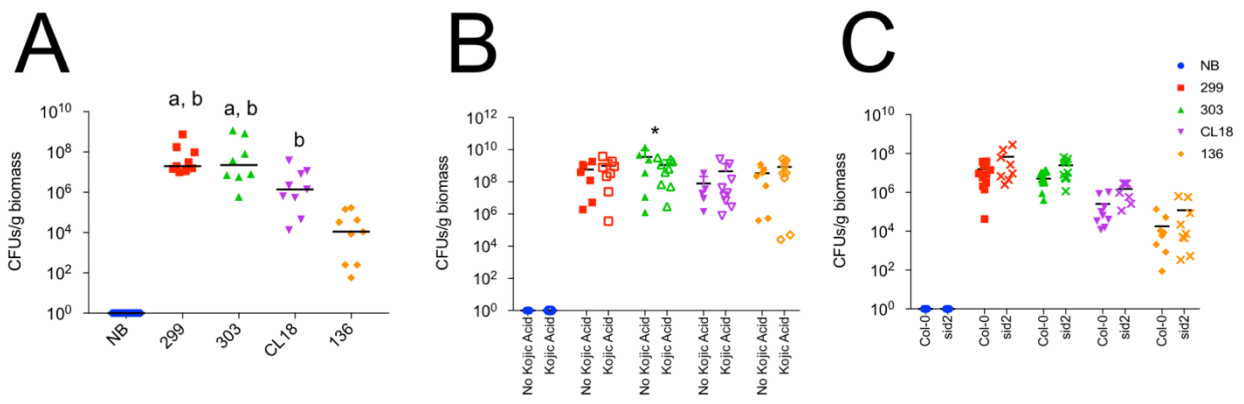


Figure 2.5. Differential colonization of *Arabidopsis thaliana* seedlings by *Streptomyces* strains.

(A) 7 day old sterile, wild-type (WT) *A. thaliana* seedlings were inoculated with nothing (blue), 299 (red), 303 (green), CL18 (purple), or 136 (orange) for 7 days to determine level of *Streptomyces* strain colonization. "a" indicates significantly different from 136 ($p<0.05$). "b" indicates significantly different from no bacteria (NB) ($p<0.05$), Dunn's multiple comparison) (B) WT seedlings again inoculated with each *Streptomyces* strain in the presence (open symbols) and absence (closed symbols) of kojic acid. * indicates significantly different seedling colonization with and without kojic acid ($p<0.05$), Holm-Sidak multiple t-test (C) WT seedlings and *sid2* seedlings ("x" symbols), which are unable to biosynthesize SA, were inoculated with each *Streptomyces* strain.

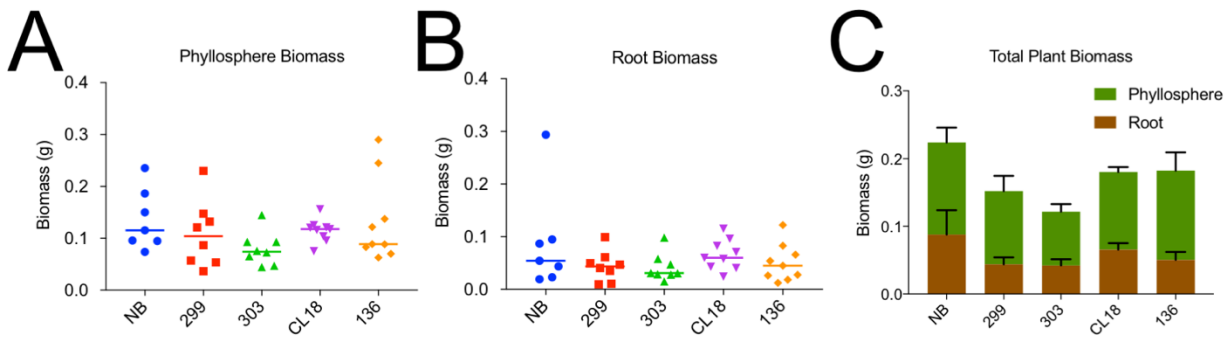


Figure 2.S1. *Streptomyces* strains 299, 303, CL18, and 136 do not alter plant biomass, even 8 weeks after inoculation.

Biomass of: (A) above-ground biomass (phyllosphere), (B) below-ground root, and (C) total plant material was measured in plants grown for 6-8 weeks in sterile clay substrate inoculated with a single Streptomyces strain (n=7-10). No significant differences were observed.

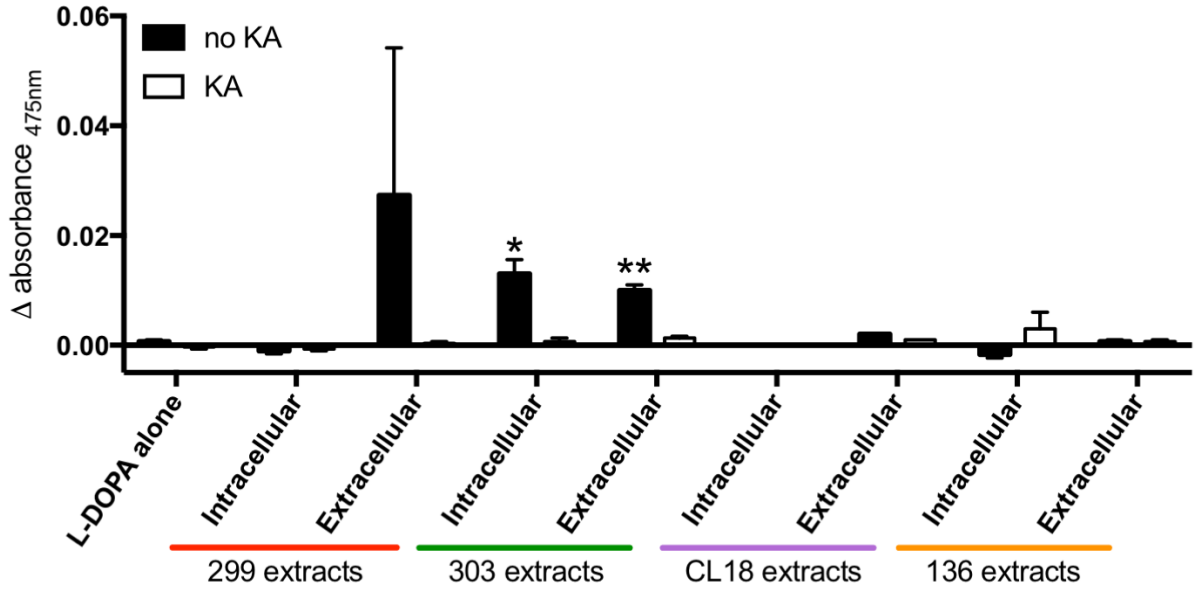


Figure 2.S2. Intracellular and extracellular protein extracts from 303 are inhibited by kojic acid (KA).

The mean change in absorbance at 475 nm 25 minutes into the assay with the standard error of the mean shown for intracellular and extracellular protein extracts from 299 (red bar), 303 (green bar), CL18 (purple bar), and 136 (orange bar) cultures with (white bars) or without (black bars) the addition of tyrosinase inhibitor, kojic acid (KA). * indicates KA samples are significantly lower absorbance than those without, $p<0.002$, multiple t-tests, Benjamini, Krieger, and Yeutieli multiple test correction. ** indicates KA samples are significantly lower absorbance than those without, $p<0.0002$, multiple t-tests, Benjamini, Krieger, and Yeutieli multiple test correction.

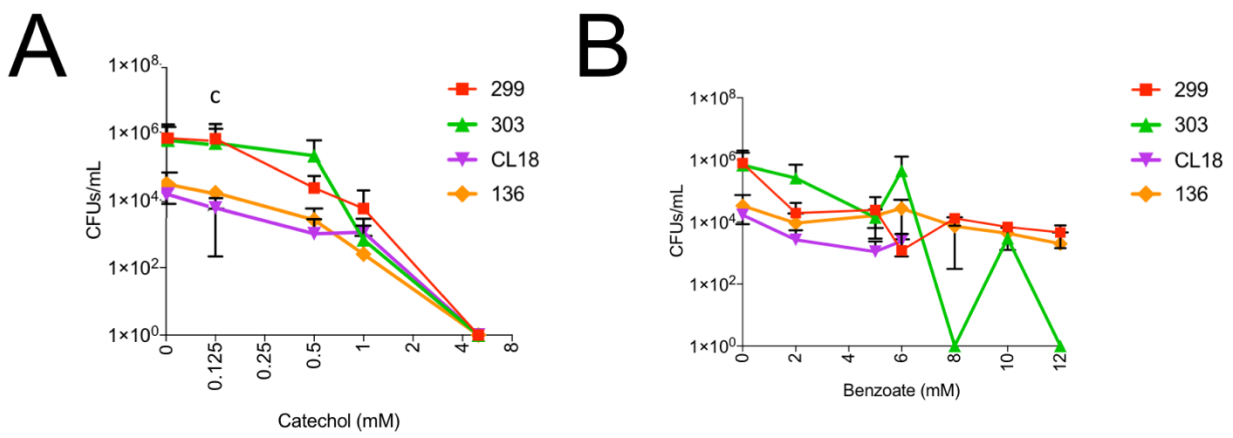


Figure 2.S3. Challenge of all strains with catechol and benzoate indicate variable differences in CFU formation.

CFUs after 5-7 days of growth on solid glucose minimal medium containing the indicated concentration of catechol (A) or benzoate (B) were measured. "c" indicates 299 was significantly different than CL18 and 136 (n=9-12, Kruskal-Wallis, Tukey's multiple comparison, ($p<0.05$))

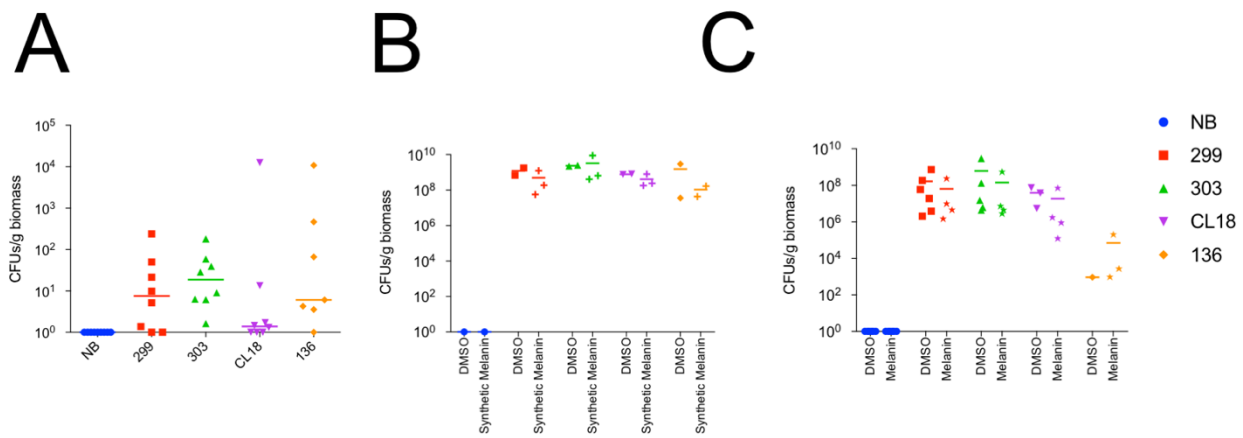


Figure 2.S4. Colonization of *Arabidopsis thaliana* seedlings by *Streptomyces* strains when grown with melanin compounds indicates no differences (n=3, 7 days germination, 7 days seedling growth)

(A) Monoinoculated seedlings rinsed with bleach (B) Monoinoculated seedlings grown in the presence of 4 mg/mL synthetic melanin (DMSO, melanin solvent control) (C) Monoinoculated seedlings grown in the presence of bacterial-derived melanin (DMSO, melanin solvent control).

CHAPTER THREE - MULTI-SCALE DESIGN TRANSLATES COMPARATIVE GENOMIC PREDICTIONS AND *IN VITRO* MICROBIAL INTERACTIONS INTO DEFINED ROOT MICROBIOME ASSEMBLAGES

A VERSION OF THIS CHAPTER IS IN PREPARATION TO BE SUBMITTED FOR PUBLICATION

Sarah Stuart Chewning, David L. Grant, Andrew Willems, Bridget S. O'Banion, and Sarah L. Lebeis. "Multi-scale design translates comparative genomic predictions and *in vitro* microbial interactions into defined root microbiome assemblages".

Three individuals significantly contributed to this chapter: Sarah Stuart Chewning, David L. Grant, and Sarah L. Lebeis. In addition, Andrew J. Willems and Bridget S. O'Banion contributed. Conceived experiments: SSC, DLG and SLL. SSC performed the experiments for Figures 3.2-3.12 and Table 3.3. DGL performed the experiments for Table 3.3 and Figure 3.2. SSC performed the analysis to generate Figures 3.1, 3.8-3.12. AJW performed the analysis to generate Figures 3.6-3.12. Wrote the chapter: SSC, AJW, and SLL.

I. ABSTRACT

Complex interactions of hosts and microbiomes continue to prove difficult to define. In part, this is due to the nature of the interaction, but investigative approach has also proved a limiting factor. *Streptomyces* are metabolically productive, ubiquitous soil-dwelling organisms known to inhabit the microbiome of a wide variety of plant cultivars. When introduced to plants, certain taxa promote growth, induce disease suppression, and even improve drought tolerance. Their multifactorial benefits offer exciting opportunities for agricultural applications, but they require careful testing of their effect, prior to deployment. Here we explore activities of four *Streptomyces* isolates in root microbiome assembly using a combination of approaches encompassing comparative genomics, *in vitro* co-culture challenges, and *in vivo* colonization with a low complexity bacterial synthetic community (SynCom) or a high complexity microbial community derived from wild soil (Wild). We discovered the vast and sometimes divergent biosynthetic potential of these four *Streptomyces* strains and other root-associated taxa is not necessarily correlated with competitiveness either in co-culture or with a complex community *in vivo*. Two of our *Streptomyces* isolates had biosynthetic gene clusters for indole; when tested *in vitro*, these strains proved capable of making indole acetic acid (IAA). Interestingly, *in vitro* competition assays between the *Streptomyces* isolates as well as with other non-*Streptomyces* isolates indicated that resistance and susceptibility phenotypes do not always correlate with *in vivo* competitive colonization phenotypes with the same isolates. As Amplicon Sequence Variant (ASV) sample divergence and even phyla data did not provide the resolution necessary to detect potential differences, analysis and comparison of individual and averaged ASV relative abundances emphasized the importance of family-level investigation of samples. Our methods help tease apart plant and environment selective influence from microbe-microbe competition on microbiome assemblage. Overall, our findings confirm *Streptomyces* as consistent members of root microbiomes and suggest that nuance strain-level influences can be better targeted and detected using multiple levels of resolution and provide valuable avenues for additional root microbiome research.

I. INTRODUCTION

As sessile organisms, plants are reliant on their surrounding environment, including air, soil and water, for microbial introduction. Significantly, soils are among the most microbially diverse environments on Earth, serving as rich inocula for host plants [1]. The selection process for host microbiome inclusion is mediated by microbe-microbe and host-microbe interactions [2]. The endosphere (internal) and rhizosphere (external) root-associated microenvironments present varying levels of host-microbe and microbe-microbe selection pressures, which significantly shape microbial inclusion from soil to within plant root [3]. The resulting bacterial assemblages have significant influence on host health and growth [4]. The limited internal root microbial diversity relative to surrounding soil presents an unique opportunity for studies manipulating soil microbiomes to achieve optimal plant health [5]. The assembled organisms must both invade and also persist, surviving host immune pressures, competition for resources, and environmental changes [5, 6]. Greater microbial diversity is correlated with increased nutrient acquisition, metabolism and plant growth [7], which would result from complex microbiome assembly processes. Community construction dynamics are teased apart via progressive individual and community-level approaches, including next-generation sequencing technologies, co-occurrence network analyses, molecular techniques and pangenomic analyses. These efforts are shedding new light on potential mechanisms driving community assemblies and resistance.

To meet agricultural demands, fundamental strategies harnessing the power of microbiome manipulation and maintenance must be made. Thus far, multiple microbiome studies including those exploring the influence of the host immune system [8], diversity [7], pathogen resistance [9], disease suppressive soils [10], beneficial consortia [5] and many others are contributing to our understanding of microbiome establishment. For example, via a randomly barcoded transposon mutagenesis sequencing (RB-TnSeq) screen of *Pseudomonas simiae,* 115 bacterial genes important for *Arabidopsis thaliana* root colonization were identified, including 44 unannotated genes [11]. To determine functions of these genes, the researchers compared their findings to a RB-TnSeq library screening using 90 distinct *in vitro* conditions representing a proportion of the environmental root colonization conditions [11]. Salicylic acid (SA), a plant phytohormone that helps protect against microbe-induced stress, influenced bacterial commensal root colonization of

A. thaliana [8]. In addition, previous work performed by our lab suggests genes involved in tyrosinase production, an enzyme important for production of melanin, were *Streptomyces*-strain specific and influenced tolerance to common phenolic root exudates (Chapter 2). While studies of whole microbiomes and individual strains are essential, neither allows for simultaneous discovery of complex community dynamics while also the fine resolution necessary to determine roles of individual microbes. Thus, the remaining options suggest refined study of a set of microbes or use of a synthetic community (SynCom).

16S rRNA gene survey studies suggest common members of root microbiomes across a variety of plant species [12-18]. While soil type is known to be the primary determinant of root-associated plant microbiomes and is considered the major inoculum, plant phylogeny has also proven to be an influential determinant of microbiome taxa [19]. Further, the root microbiome is distinct from that of other plant fractions, independent of host genotype [20]. Plant microbiome studies focused on determining relative abundances of all taxa or those belonging to a core potentially overlook the contribution of less abundant, but influential taxa. To provide tractable and reproducible findings, recently highlighted is the value added via use of lower complexity SynCom rather than high complexity mixed communities [21]. Lower complexity studies, including use of reductionist approaches, which often include pared-down designs such as host-mediated selection of SynCom members [15], allow for mechanistic interspecies studies. Marriage of previous knowledge gained from studies of conserved core endophytes with value gained from lower complexity studies allows for intentional construction and investigation of SynCom and resulting tractable plant-microbe and microbe-microbe interactions.

Access to genome repositories, sequencing technologies and protein/metabolite predictive applications allows intentional selection of microbes to include in *in vitro* and *in vivo* plant-microbe and microbe-microbe interaction studies. Because plant roots winnow soil bacteria from the rhizosphere to include a distinct set of endophytes, the withstanding organisms are commonly defined in complex microbiome studies. This set includes: Actinobacteria, Proteobacteria, Bacteroidetes, and Firmicutes [12, 14, 17, 22]. Among the Actinobacteria, common, but low abundance, residents of various soil and root microbiomes are bacteria in the Streptomycetaceae

family, including *Streptomyces spp*. [13, 23, 24]. *Streptomyces'* metabolic capabilities [25], contribution to disease suppressive soils [26, 27], and plant growth-promoting potential [28] suggest their function as root microbiome members may exceed their numbers. Further, their distinct biocontrol capabilities against plant pathogens [29] elude to root microbiome sculpting potential. Thus, defining their role in microbe-microbe interactions provides an interesting comparison of *in vitro* interaction potential that can be compared to plant monoinoculation phenotypes. These findings can then be compared to more complex studies of sustainability and sculpting potential while competing with a low complexity SynCom and an inoculum made from a slurry of wild soil (Wild).

Here we take a multi-faceted approach to determine plant microbiome interactions and functions that contribute to community assembly. Capitalizing on access to varying levels of inoculum complexity, we apply our previous findings to inform novel microbe-microbe and plant-microbe studies of four *Streptomyces* strains with discriminate root colonization abilities. These strains were previously included in microbiome studies of axenic *A. thaliana* colonization with a complex SynCom of 38 taxonomically diverse soil isolates [8]. In addition, monoinoculation studies indicated distinct *A. thaliana* root colonization phenotypes consistent with the complex SynCom studies (Chapter 2). Using an 11-member SynCom, we examine host and microbe interactions and phenotypes. Consistent with previous suggestions of benefit [21], we find that lower complexity SynCom lends to more resolute conclusions about microbe-microbe and plant-microbe interactions whereas our studies with a wild soil slurry were valuable for additional hypothesis generation. Thus, each method yielded new information. We individually competed select SynCom isolates with the four *Streptomyces* strains *in vitro* followed by *in vivo* inoculations with communities of increasing complexity to determine if the microbe-microbe interactions we predict *in silico* and observe *in vitro* actually occur during root microbiome assemblage. This approach provided valuable distinctions allowing separation of microbe-driven and plant-driven pressures, setting the stage for targeted functional studies. Together with *in silico* genomic tools, our findings suggest the value of tiered-approach microbiome studies to optimize opportunities for conclusive determinants of microbiome assembly.

II. MATERIALS AND METHODS

Genome comparison and biosynthetic gene cluster identification

Genomes of all strains for which we had genomes (i.e. 299, 303, CL18, 136, 181, 273, 40, 50, CL11 and *Streptomyces scabiei* 87.22) were downloaded from JGI IMG/M ER [30]. Genomes were mined using JGI IMG/M ER query tools and the antibiotics and Secondary Metabolites Analysis Shell (antiSMASH, v4), with all options selected (i.e. ClusterFinder, KnownClusterBlast, smCoG analysis, whole-genome Pfam analysis, ClusterBlast, ActiveSiteFinder, SubClusterBlast, Detect TTA codons) [31]. AntiSMASH utilizes profile Hidden Markov Models of genes to identify all gene clusters encoding potential secondary metabolites from all known chemical classes. Gene clusters were generated from complete IMG fasta nucleic acid sequences of genomes from 299, 303, CL18, 136, and *Streptomyces scabiei* 87.22.

Bacterial culture preparations

Streptomyces isolates were grown in Lysogeny Broth (LB) at 30^{o}C with shaking at 150 rpm for 4-7 days. Cultures were vortexed and bead beaten to disrupt bacterial aggregates. All other isolates were grown in LB at 30^{o}C with shaking at 150 rpm for 1-2 days. A spectrophotometer measured the optical density at 600nm (OD_{600}) and cultures were normalized to an OD_{600} of 0.01. 100µL of all normalized isolate resuspensions were plated on LB, incubated at 28^{o}C for 4-7 days and colony forming units (CFUs) were counted. Inoculum ranged from $1x10^{2}$ to $3x10^{4}$ CFU/mL. SynCom inoculum was created by growing each member until turbid (1-2 days), normalizing to an OD_{600} of 0.01, and creating a mixed inoculum of containing 1mL of each member. Frozen stocks of this SynCom were created with 200µL of the mixed bacterial community and 200µL 40% glycerol, snap frozen in liquid nitrogen, and stored at -80 ^{o}C. Prior to experimental inclusion, a frozen stock was thawed and grown in LB at 30^{o}C with shaking at 150 rpm for 2 days. After 2 days, mixed culture was normalized to an OD_{600} of 0.01.

Molten overlay experiments

To create two-layer agar plates, 1.5% and 0.75% LB agar was prepared. For the bottom layer, 5mL of sterile 1.5% agar was pipetted into 50mm petri dishes. While the bottom agar was solidifying, log growth phase *Streptomyces* cultures were prepared for top layer inoculation by bead beating 1mL of each culture in sterile centrifuge tubes with sterile 3 mm glass beads. The OD_{600} was measured using a spectrophotometer. These measurements were used to calculate the volume of culture to add to 0.75% LB agar to achieve an OD_{600} of 0.01, which was the same concentration used for our vertical plate assays. The appropriate volume of culture was added to the cooled (approximately 50°C), but not solidified 0.75% LB agar. Culture additions were mixed well into the agar by pipetting. 5mL of each inoculated 0.75% agar was pipetted onto the top of the solidified 1.5% LB agar in each petri dish. After the top layer solidified, 15µL of prepared challenge isolates (standardized to OD_{600} of 0.01) were spotted on top of the 0.75% agar layer. These spots were allowed to dry and all petri dishes were incubated at 30°C and checked daily for growth. Zones of inhibition (ZOI) were measured at 5-7 days.

Co-culture assays

Streptomyces isolates were grown as described above in LB liquid medium. After 4-7 days incubation, 2 mL of each culture were taken and bead beaten with 3 mm glass beads for 2.5 minutes using the Geno/Grinder SPEX Sample Prep. Optical density at 600 nm (OD_{600}) was measured using a spectrophotometer and cultures were normalized to an OD_{600} of 0.1. Using a Rainin Pipet-Lite XLS multichannel, five 2µL spots of each *Streptomyces* isolate were placed onto solid LB medium 1 cm apart from each other. The plate was then incubated overnight at 28 ^{o}C. After 16-20 hours, the challenge isolates were normalized to an OD_{600} of 0.1 without bead beating due to the turbidity of cultures. The Rainin multichannel pipet was used to place four 2µL spots of the challenge isolates 1 cm apart and perpendicular to the *Streptomyces* spots. Plates were placed back into the incubator at 28 ^{o}C for one week. After one week, the plates were removed, scanned and ImageJ was used to measure colony sizes (ImageJ).

Seed sterilization and germination

For all experiments, we used Col-0 accession, wild-type (WT) A. thaliana plants. For the auxin insensitivity experiment, we also used two genotypes, axr4-2 [32] and axr1-7axr4-2 double mutant [32], obtained from the Arabidopsis Biological Resource Center (ABRC) seed collection at The Ohio State University. All seeds were surface sterilized via treatment in 70% ethanol with 0.1% Triton-X100 for 1 minute, 10% household bleach with 0.1% Triton-X100 for 15 minutes, and three washes with sterile distilled water. Seeds were stratified for 3 days in the dark at 4 oC and subsequently germinated at 24 oC with 10 hours of light for 6-7 days on agar plates containing half strength (2.22g/L) Murashige & Skoog (MS) vitamins, 1% sucrose, and 1% Phytoagar (Bioworld).

Vertical plate assays

To inoculate plates for 14 day experiments, 150µL of individual *Streptomyces* isolate resuspensions were spread on 150 mm x 150 mm prepared half strength MS square agar plates with no sucrose. Plates were allowed to dry and 4-5 6-day old axenic seedlings were aseptically transferred onto each plate with flame-sterilized tweezers. Plates were sealed with Parafilm® M Laboratory Film and randomly stacked vertically in open wire trays, which were grown at 24 ^{o}C with 18 hours of light for 14 days. Every two days, root length was observed, plant health was assessed, and plates were shuffled. Finally, plates were scanned and roots measured.

Colorimetric auxin assay

Indole-3-acetic acid production was determined as described by Szkop et al [33]. Briefly, *Streptomyces* isolates were grown in 35mL of LB broth with 1% Tryptophan added at 30^{o}C with shaking at 150 rpm for 4-7 days. After incubation, cells were removed from culture by centrifugation at 4,000 x *g* for 10 minutes. After centrifugation, 1mL of supernatant was removed from each tube and incubated with 2mL of Salkowski reagent in the dark at room temperature for 30 minutes. Following incubation, 100µL of each supernatant mixture or uninoculated medium was added to a clear, flat-bottom 96-well plate and absorbance was measured at λ = 530 nm for each sample (n=6 per condition).

Wild soil slurry preparation

Wild soils were collected from a field on the campus of Oak Ridge National Lab in Oak Ridge, TN and an aliquot was prepared via filling a sterile conical tube to 20 mL. Soils were A glass bottle containing 100 mL of water and a stir bar were sterilized by autoclave. Once cooled, the 20 mL of soil was added to the water and placed on a stir plate to stir uninterrupted for 1.5 hours. The soil settled for 1-2 minutes and 250µL aliquots of the suspended slurry were added to sterile freezer stock tubes with 250µL 60% glycerol, snap frozen in liquid nitrogen, and stored at -80 ^{o}C. The day of secondary inoculations, freezer stocks were thawed and spun at 13,000 x g for 1 minutes. Glycerol supernatants were removed and the wild soil slurry (Wild) pellet was resuspended in 2mL sterile water. Optical density at 600nm (OD_{600}) was measured using a spectrophotometer and Wild inocula were normalized in half strength MS buffered with sterile 2-(N-morpholino) ethanesulfonic acid MES to an OD_{600} of 0.01. These resuspensions were then used as secondary inocula as described below.

Plant inoculations

For primary inoculation of seedings, vertical plate assays were performed as described above, except 100 µL of each isolate resuspension were spread on 100 mm x 100 mm plates containing half strength MS square agar plates with no sucrose. Following 7 days of vertical growth, seedlings were aseptically transferred to individual three-inch square pots, with 64 mL of sterile calcined clay (Pro's Choice Rapid Dry) inoculated with secondary inocula of 49 mL MES normalized Wild or SynCom. Control no bacteria (NB) pots contained only sterile MES. An additional 1mL of suspended inoculum was used to bury the seedling roots. For experiments in which there was not primary inoculation, 6-day old sterile seedlings were aseptically transferred directly from germination plates to individual three-inch square pots, with 64 mL of sterile calcined clay (Pro's Choice Rapid Dry) 49 mL MES.

Plant growth and harvest

Plants were watered every 2-3 days from the top with sterile distilled water and grown in growth chambers (Percival, model: AR41L3C8) with 10 hours of light at 22^{o}C and 14 hours of dark at 18^{o}C. After 8 weeks of growth, plants were aseptically harvested when inflorescence began to

emerge. Whole plants were submerged in 25mL of sterile harvesting phosphate buffer with 0.01% Silwet (Lehle Seeds) and vortexed vigorously for 10 seconds. Roots and rosettes were separated with sterile forceps and transferred to sterile centrifuge tubes and weighed. Roots were rinsed three times with sterile distilled water and snap frozen. Once snap frozen, roots were lyophilized overnight (LABCONCO FreeZone 6 catalog number 7753020 ; drying chamber: short clear chamber with valves, catalog number 7318802). After lyophilizing, roots were homogenized via bead beating in the Geno/Grinder SPEX Sample Prep with sterile 3mm glass beads or garnet beads for 2.5 minutes.

DNA extraction and 16S rRNA gene community sequencing

DNA was extracted from homogenized plant roots using the Mo Bio PowerSoil kit (now a Qiagen product). DNA concentration was determined with the Quant-iT PicoGreen dsDNA Assay Kit and fluorospectrometer. The University of Tennessee, Knoxville Genomics Core performed library preparation and sequenced the samples. Based on previous findings of high-quality reads, 16S rRNA gene barcoded V4 (515F, 806R) primer sets with Illumina adapters were utilized for PCR reactions and sequenced via Illumina MiSeq® pyrosequencing [24, 34, 35]. Polymerase chain reaction (PCR) was performed in triplicate and with a negative control to ensure absence of contamination. A mixture of two peptide nucleic acid (PNA) blockers, which bind to plant host plastid and mitochondrial 16S rRNA genes, were used to minimize amplification of plant DNA.

16S rRNA gene amplicon QIIME 2 analysis

The *in silico* tool used to perform the 16S rRNA gene microbial analysis was QIIME 2. QIIME 2 is an open source, extensible, and decentralized microbiome analysis package with a focus on data and analysis transparency [36](www.qiime2.org). Data were imported into the .qza file format using the QIIME tools import command. The software package FastQC was used to visualize the quality metrics of the sequences and determine the appropriate places to trim and truncate the reads in order to ensure the highest quality reads. From the visualizations, it was determined that the first 15 base pairs should be trimmed from the beginning of the reads while all reads should be truncated at 250 base pairs. To perform trimming and truncating, the QIIME dada2 [37] denoise-paired command was run and two tables, an Amplicon Sequence Variant (ASV) table and a representative

sequences table, were generated [38]. The QIIME alignment MAFFT and QIIME alignment mask commands were run to perform a multiple sequence alignment of the representative sequences file and to mask any highly variable regions seen in the alignment. The QIIME phylogeny FASTREE command was run to generate an unrooted phylogenetic tree. The QIIME phylogeny midpoint-root command was run to create a mid-point rooted phylogenetic tree. The QIIME diversity core-metrics-phylogenetic command was carried out with a uniform sampling depth of 2,000, allowing inclusion of 98% of samples, which generated alpha and beta diversity metrics, as well as plotting capabilities (e.g. Shannon's diversity index, weighted UniFrac, principal coordinate analyses). Taxonomy was generated by building a Naïve-Bayes classifier. This classifier was built by first importing raw SILVA V132 taxonomy and sequence files. The classifier files were imported and files trimmed to the standard 16S forward and 16S reverse Illumina primers with a truncation length of 250 base pairs. The classifier was trained to the new reference sequences with the QIIME feature-classifier fit-classifier-naive-bayes command and then used to build taxonomy using the QIIME feature-classifier classify-sklearn command on the representative sequences file. Although mitochondrial and plastid PNA blocker were used, plant reads remained, and thus manually removed. Taxonomy visualization was achieved via the QIIME metadata tabulate command.

Statistical analyses

Molten overlay, root growth, auxin production, 16S rRNA gene amplicon sequencing, results were statistically analyzed with Prism version 7.0 for Mac (GraphPad Software, La Jolla California USA, www.graphpad.com) using the nonparametric Kruskal-Wallis test, including one-way ANOVA followed by Dunn's multiple comparisons. When appropriate, analysis included two-way ANOVA and Tukey's multiple comparisons. Molten overlay growth influence was analyzed visually in ImageJ [39] and then statistically compared by 2-way ANOVA, Dunnett's multiple test correct using GraphPad Prism v. 7.0.

III. RESULTS

Identification of biosynthetic gene clusters from bacterial genomes predict microbe-microbe interactions during root microbiome assemblage

Because we sought to better understand how microbe-microbe interactions influence community dynamics, we included in our genomic and experimental studies isolates from our collection from a 38-isolate complex SynCom designed by Lebeis et al. [8], as well as new isolates from lab collection (Table 3.1). Among those were four *Streptomyces* isolates 299, 303, CL18, and 136, which colonize *A. thaliana* roots and seedlings at various degrees as part of the 38-member SynCom and in monoinoculation (Chapter 2). We also included a common root pathogen *Streptomyces scabiei* 87.22, as it is known for robust root colonization and disease induction in plants [40]. To predict how they would interact in subsequent *in vitro* and *in vivo* studies, in our *in silico* genome investigations, we included 5 of the 11 isolates from our SynCom with completed draft genomes (Table 3.1).

Isolate genome sequences were downloaded from where they are curated at the U.S. Department of Energy's Joint Genomes Institute, Integrated Microbial Genomes and Microbiome Samples (JGI IMG/M ER) database and analysis tool (Table 3.2) and analyzed with the Antibiotic and Secondary Metabolite Analysis Shell (antiSMASH) [31] to identify predicted microbial products (Figure 3.1). Interestingly, the strains that previously colonized roots better when in a 38-member SynCom (299 and 303) had larger genomes and a greater percentage of genes predicted to be involved in biosynthetic gene clusters (BGCs) than those that did not (CL18 and 136) (Table 3.2). In comparison, *S. scabiei* 87.22 had a genome size between that of 299 and 303, but the largest proportion of predicted biosynthetic genes.

Previous pangenomic comparisons of our 4 *Streptomyces* strains (Chapter 2) potentiated biosynthetic similarities between 299 and 303. In addition, phylogeny showed similarity with previously characterized soil-derived *Streptomyces*, with 136 diverging the most from 299, 303, and CL18 (Chapter 2). Previously described monocolonization trends led us to hypothesize that 299 and 303 may have overlapping genomic characteristics (Chapter 2). In addition,

Actinobacteria are known to share intra-phylum primary and secondary metabolic pathways often requiring the same nutrients for synthesis of precursors and products [41]. Thus, we suspected 299 and 303 might harbor similar biosynthetic genes allowing employment of strategies to acquire physical space and nutrients within the plant root. Interestingly, antiSMASH predicted largely similar biosynthetic clusters between the genomes of 299 and 303, including several involved in biotic and abiotic stress, as well as candidate antimicrobial gene clusters with the potential of influencing microbial growth (Figure 3.1). Interestingly, 303 was predicted to have distinct indole and phenazine clusters (Figure 3.1). Obvious antimicrobial clusters suggested the possibility of productive findings from competitive microbial assays.

In addition to the four *Streptomyces* strains, we compared the genomes and biosynthetic potential of 6 additional isolates, one of which was an Actinobacteria, four Proteobacteria, one in the phylum Firmicutes and the last Bacteroidetes (Table 3.1). Interestingly, the pathogen and robust root colonizer, *S. scabiei* 87.22 was predicted to have the most biosynthetic clusters in common with 299 and 303 (Figure 3.1). Many of the non-*Streptomyces* isolates either had few clusters (e.g. the *Paenibacillus* isolate 181) or more putative clusters (e.g. the *Pseudomonas* isolate 50). This can be attributed either to reduced biosynthetic potential or lack of annotation. While not providing conspicuous evidence of select gene clusters correlated with microbiome assembly, the results set precedence for multiple avenues of investigation, and potential plant-microbe and microbe-microbe interactions. Thus, we next designed challenge experiments to determine isolates' susceptibility and inhibitory capabilities.

In vitro microbe-microbe challenges suggest Streptomyces strains can both co-exist and also compete

To determine *Streptomyces* interaction with other strains of similar biosynthetic potential as well as with non-Actinobacteria endophytic commensals of varying biosynthetic potential (Figure 3.1), we designed co-culture molten overlays and cross-spots on agar to determine microbe-microbe growth influence *in vitro*. We hypothesized that these *in vitro* binary microbial challenges may inform more complex community level interactions during plant colonization. Because both 299 and 303 colonized *A. thaliana* roots similarly (Chapter 2) and shared predicted gene clusters (Figure 3.1), we suspected these two isolates might employ strategies to acquire physical space

and nutrients within the plant root. Thus, microbial competition experiments were intended to inform growth inhibition between strains.

Molten overlays allowed for metabolite perfusion through the semi-solid agar and potentially induced production of metabolites unique to a reduced oxygen environment. We previously found that our four *Streptomyces* strains were capable of growing anaerobically (data not shown) and thus, each of the 4 isolates was inoculated into LB media and challenged with another isolate spotted on the solid agar surface. Interestingly, when spotted on the surface, 303 influenced each competing *Streptomyces* isolate's growth (Dunnett's multiple comparison test, $p<0.05$) (Figure 3.2). 299 grew well when spotted on 303-inoculated agar but did not grow well when 303 was spotted on agar inoculated with 299 (Figure 3.2), highlighting that antibiosis varies with growth conditions. Isolates CL18 and 136 did not appear to prohibit the growth of other strains tested. We then challenged each *Streptomyces* strain with the other 3 via co-culture cross spotting on agar plates. Among all interactions tested, only 303 minimally inhibited CL18 (Table 3.3), suggesting differential metabolite biosynthesis by oxygen availability.

To determine if *Streptomyces* might influence or be influenced by the growth of other members of our bacterial collection, we then co-cultured our four *Streptomyces* strains on agar and some of the 11 soil-resident bacterial isolates from our collection, several of which were previously included in a study of root microbiome colonization (Table 3.1) and include members of the phyla Proteobacteria, Firmicutes, Bacteroidetes and Deinococcus-Thermus (Table 3.1 and Table 3.2). Previously defined colonization phenotypes for the 11 isolates ranged from robust to poor with several others unknown (Table 3.2). Co-culture cross-spots indicated that *Paenibacillus* strain 181 inhibited the growth of all 4 *Streptomyces* isolates (Table 3.3). This finding was especially interesting as 181 is from the family Paenibacillaceae, which has been linked to disease suppressive soils [42]. However, when included in a 38-member SynCom, this particular strain doesn't colonize roots well [8]. Additionally, 299, 303, and CL18 inhibited growth of isolate 2, from the family Rhizobiaceae (Table 3.3). In previous complex SynCom experiments of *A. thaliana* in which 299 and 303 are known to colonize the root, *Rhizobium* strain 2 also robustly colonize the root [8], suggesting that either microenvironments separating the organisms allow co-

colonization or the plant and other organisms are influencing colonization capabilities. Additionally, only CL18 inhibited the growth of the Burkholderiaceae CL11 (Table 3.3). This was particularly interesting as compared to the other 3 *Streptomyces* strains, CL18 has only one unique predicted biosynthetic gene cluster, an oligosaccharide, which could be a result of incomplete biosynthetic cluster characterization or related to this product. Growth of *Bacillus* strain A415 was inhibited by both 303 and CL18 (Table 3.3), highlighting exciting future directions potentiated by these results. Also of note, 136 co-culture with *E. coli* resulted in a very distinct and unique pigment production (Table 3.3). Overall, *Streptomyces* strains are capable of influencing growth of competing intra- and extra-genus microbes, helping to inform intentional construction of community level studies. Despite their metabolic repertoire, including antimicrobial products, *in vitro, Streptomyces* did not consistently out-compete each other or other strains. This led us to believe that *Streptomyces*-microbe interactions were not representative of their behavior in a more complex community, such as a SynCom or root microbiome.

Root phenotypes are Streptomyces strain-specific

Streptomycetaceae root colonization has been well documented in a variety of plant systems species [29, 43, 44]. Besides influencing the growth of other microbes, *Streptomyces* may produce compounds that influence the health of their plant host. Our lab previously described *Streptomyces* isolate-specific monocolonization of *A. thaliana* seedlings with strains 299, 303, CL18 and 136 (Chapter 2). Additionally, when these strains were included in a 38-member mixed bacterial community, they differentially colonized *A. thaliana* roots [8]. Significantly, plant root structure and function are often linked, creating unique root-microbe interactions and trigger a variety of host responses [45]. Thus, we hypothesized root-associated colonization distinctions may correlate with root structural differences. Accordingly, we established two week plant-microbe colonization of *A. thaliana* seedlings inoculated with each of the four *Streptomyces* strains to reveal distinct isolate-induced root phenotypes (Figure 3.3). As compared to control uninoculated seedlings and those inoculated with isolate CL18, seedlings grown with 299 and 303 resulted in more lateral roots, commonly referred to as cluster roots, and less primary root growth (Figure 3.3A and 3.3B). Interestingly, seedlings grown with 136 resulted in primary roots that were longer than those associated with 299 and 303 but had more lateral root growth than those associated with

CL18 (Figure 3.3A). To quantify the ability of different *Streptomyces* isolates to affect plant root growth, we measured primary root length every other day for 14 days. Beginning at 4 days after inoculation, statistical analysis revealed a significant difference ($p<0.05$, Figure 3.3B) in primary root length from the uninoculated control in isolates 299, 303 and 136. However, root biomass, leaf biomass, and leaf size did not significantly differ between control and inoculated plants, even after 8 weeks of growth (Chapter 2), suggesting that *Streptomyces* strains do not individually influence plant biomass accumulation in the conditions tested. Importantly, plant growth, biomass, and survival after 8 weeks of growth suggests that these isolates are not pathogens.

Root morphology phenotypes are not solely dependent on microbial indole-3-acetic acid production

Plant- and microbe-derived auxins are known to increase lateral root growth and inhibit primary root growth [46]. Hence, the phenotype of plants colonized with 299, 303, and 136 appeared to mimic the effects produced by auxin exposure (Fig 3.3A). To determine if the microbially-produced auxin compound indole-3-acetic acid (IAA) drove root morphology phenotypes, the colorimetric IAA assay described by Szkop et al. was performed on the supernatant of each isolate grown in liquid media supplemented with tryptophan [33]. 303 produced significantly more IAA than 299, CL18, and 136, although 299 produces significantly more auxin than the media control (Figure 3.4A). Further, although 299 and 303 are both capable of IAA production (Figure 3.4A), only 303 is also predicted to synthesize indole in our AntiSMASH results (Figure 3.1), which is a tryptophan-independent precursor for IAA. Together, these findings suggest 299 and 303 may produce an auxin compound capable of influencing root structure.

We performed monoinoculation with each of the four *Streptomyces* strains in Col-0 and two additional *A. thaliana* genotypes, *axr4* and *axr1/axr4*, which have decreased auxin sensitivity [32]. As compared to wild-type, observed patterns in root morphology phenotypes induced by each strain were remarkably consistent for all plant genotypes (Figure 3.4B), indicating that microbially-produced IAA detection via *axr1* and *axr4* pathways are not solely responsible for altered root morphology observed following 303 or 299 binary associations. Interestingly, 136 did not appear to produce auxin *in vitro* and induced similar root morphology changes in all *A. thaliana* genotypes, indicating that its influence is independent of auxin. These results provide evidence

that microbially-derived IAA does not fully explain the root morphology differences between seedlings inoculated with each isolate in the binary associations. Together with our previous monoinoculation and co-culture findings, we next moved beyond individual interactions to determine if genomic analyses or one on one interactions were indicative of isolate phenotypes in assembly from a larger microbial community.

16S rRNA gene amplicon sequencing of A. thaliana with three distinct inoculation events indicates inoculum complexity contributes to community assembly

Recently spotlighted are the potential benefits of varying levels of SynCom complexity and correlation with robust experimental conclusions [21]. Thus, we chose three distinct *A. thaliana* seedling inoculation points with varying levels of complexity (Figure 3.5) to extend application of our earlier *in silico, in vitro,* and monoinoculation *in vivo* experimental findings. We hypothesized that due to the biosynthetic potential of our *Streptomyces* strains; pre-inoculation with each strain could influence the community assemblage. To test this hypothesis, we first grew sterile *A. thaliana* seedlings as described earlier on vertical plates with a single *Streptomyces* strain, as well as a no inoculum control, providing the first inoculation event. After 6 days, individual seedlings were transferred to pots containing sterile calcined clay that received secondary inoculation with nothing, a SynCom of the 11 bacterial isolates (Table 3.2) or our Wild inoculum, providing the second inoculation event. Figure 3.5 provides an experimental schematic of each point of inoculation, the inoculum, and the time between inoculations. Plants were grown open-air in the same plant growth chamber for 6 to 8 weeks, providing the third inoculation event, and the assembled root microbiome was determined.

There were a total of 143 samples included in our analysis, grouped according to primary (e.g. no bacteria (NB), 299, 303, CL18, or 136) and secondary (e.g. NB, SynCom, or Wild) inoculum, resulting in 15 types of root microbiomes (Table 3.4). Also included in our analysis for comparison were the SynCom and Wild inoculum. PCR blanks were run for quality control and generated less than 100 reads. Samples ranged in read depth from 8,8375 reads to 10,976 reads (Table 3.4). We calculated diversity among samples via Shannon's Index testing alpha diversity (Figure 3.6). Wild soil inoculum had highest diversity, as expected. We found that in general, samples with secondary

inoculum of wild soil were distinct from those inoculated with SynCom or only open air (Figure 3.6). Interestingly, with the exception of primary inoculation with 303 or NB, all samples inoculated with 299, CL18 or 136 and with secondary inoculum of either SynCom or Wild were significantly different from one another, suggesting that primary inoculation with 303 influences post-secondary and tertiary inoculation sample diversity (Figure 3.6). Thus, we suspected that primary inoculation with 303 may influence species richness and closer investigation of phyla and families may provide additional insight into *Streptomyces*-specific root microbiome assemblages.

We next used a weighted UniFrac distance matrix to generate a principle coordinate analysis (PCoA) for comparison of different types of samples (Figure 3.7). Figure 3.7.A includes all samples color-coded by secondary inoculum. In general, when inoculation with SynCom (purple) and Wild (blue) the root microbiome communities shifted. Because SynCom and Wild root microbiomes are distinct, we suggest that in this setting, community structure was influenced by the secondary inocula. Root microbiome samples labeled orange (NB, no secondary inoculum) were generally scattered. We next separated root microbiome samples by secondary inoculum and color-coded samples by primary inoculum (Figures 3.7B-D). Primary inoculation with neither of our four *Streptomyces* isolates nor absence of primary inoculum (NB) altered root microbiome community assemblage.

We then analyzed average relative abundances of each root microbiome sample type at varying taxonomic levels. To start, we determined the relative abundance of phyla in each root microbiome sample type (Figure 3.8). At this higher taxonomic level, root microbiome relative abundance of Proteobacteria was significantly different from Wild inoculum for 299 and 136 primary inoculum and Wild secondary inoculum samples (Figure 3.8). Interestingly, these were the only sample types in which Actinobacteria relative abundance did not differ significantly from Wild (Figure 3.8). Next, we selectively created a subset of those samples inoculated with SynCom, allowing us to compare sample compositions to a defined set of SynCom families (Figure 3.9). Interestingly, relative abundances of Burkholderiaceae and Enterobacteriaceae in all root microbiome samples differed significantly from SynCom inoculum (Figure 3.9). Specifically, Enterobacteriaceae, consisting of *E. coli* in our SynCom (Table 3.1), are known to be poor colonizers and thus were

not surprisingly significantly different in root microbiome samples. Burkholderiaceae are known to colonize well (Table 3.1), which is reflected in their relative abundances in root microbiome samples (Figure 3.9). In general, the relative abundances in SynCom inoculum itself did not reflect sample root microbiome SynCom inclusion, suggesting influence of other microbes (i.e. tertiary open-air inoculum), plant influence in shaping the microbiome, or a combination of both (Figure 3.9).

Next, we sought to understand relative abundances of select families across all sample types for Actinobacteria, Alphaproteobacteria and Gammaproteobacteria. Among Actinobacteria, Micrococcaceae were more abundant in all root microbiome samples than in Wild inoculum alone (Figure 3.10A). We then considered one of our central early hypotheses, that select *Streptomyces* modulate colonization of other isolates. Looking at individual family abundances within each sample, we found that Streptomycetaceae relative abundance significantly differed by primary inoculum (Figure 3.10A). 299 colonized significantly better than CL18 or 136 and 303 better than 136 when secondary inoculum was SynCom (Figure 3.10B), providing evidence that regardless of microbial competition, these two isolates seem to colonize better than our other *Streptomyces* strains. Next, we assessed Alphaproteobacteria relative abundances by family and sample type (Figure 3.11A-D). Among families of Alphaproteobacteria, as compared to SynCom and Wild inocula, relative abundances of Beijerinckiaceae generally varied by primary inoculation with 303, CL18 and 136 and secondary inoculation with Wild or NB (Figure 3.11A). Interestingly, as this family was not included in our SynCom and has extremely low relative abundance in Wild inoculum, we suspect that either this family comes from tertiary inoculation in open air or prefers growth conditions present within the plant. Not surprisingly, those samples with SynCom secondary inoculum had overall greater relative abundances of Rhizobiaceae as compared to NB or Wild secondary inoculum (Figure 3.11B). Because robust colonizer Rhizobiaceae isolate 2, was included in the SynCom, we expected colonization of this family in these samples. However, of note, SynCom inoculum alone did not have significantly more Rhizobiaceae, suggesting Rhizobiaceae in our samples prefer growth *in planta* (Figure 3.11B). Finally, we compared family relative abundances among Gammaproteobacteria (Figure 3.11A-B). Enterobacteriaceae and Burkholderiaceae abundances were significantly different from abundances in other samples

(Figure 3.11A). As compared to SynCom inoculum alone, samples with Wild or SynCom secondary inoculation had different abundances of Enterobacteriaceae (Figure 3.11A). SynCom inoculum relative abundance of Burkholderiaceae was different from all other samples with NB, SynCom and Wild secondary inoculum (Figure 3.11A). While not statistically significant, distinct and selective presence of Moraxellaceae in specific root microbiome sample types (Figure 3.11B) suggests a previously unexplored relationship with our root-associated *Streptomyces* strains that will be investigated further with isolate co-culture experiments.

Collectively, our *in silico*, *in vitro*, and *in vivo* studies of *Streptomyces* provide evidence that while not the most abundant microbiome members, biosynthetically rich *Streptomyces* species persist when challenged 1) individually with other organisms of the same species 2) selectively in co-culture studies with vastly divergent taxa (e.g. *E. coli*, Burkholderiaceae, etc.) 3) with a SynCom of few, but diverse bacteria and 4) with more complex Wild inoculum. In addition, we found that *in vitro Streptomyces* co-culture phenotypes were not always indicative of *in vivo* relative abundances, suggesting colonization capability is likely a more important determinant of isolate inclusion in root microbiomes than survival in co-culture.

IV. DISCUSSION

Actinobacteria and specifically *Streptomyces* and their abundant metabolic products are being evaluated for implementation in agricultural practice [47]. Root colonization and manipulation of plant-microbiome assembly are in their spheres of influence [28]. They are known to be cosmopolitan organisms, colonizing the roots of a wide variety of plant species [44, 48-50] in geographically and geologically diverse soils [13, 24]. Disease suppressive capabilities are plant growth promotion round out *Streptomyces* potency making them ripe for a wide variety of applications [29]. Their potential has not gone unnoticed, yet their complexity has limited definitive mechanisms of assembly and isolate-level functional applications. We suggest that the role of individual *Streptomyces* strains should not be overlooked and exploiting the power of one can pack a hearty metabolic punch, influencing the entirety of the microbiome.

Previous *Streptomyces* colonization experiments, both monoinoculation and SynCom, indicated strain-specific colonization capabilities, prompting comparative genomic analyses and analysis of predicted secondary metabolite products. Our comparative genomic analyses suggest distinct differences in secondary metabolism may differentiate colonization capabilities between strains. These findings highlight that functional conclusions based on genus-level grouping inadequately capture the organisms' potential, as previously described for plant-associated *Pseudomonas* strains [51]. Further, including the plant pathogen *S. scabiei* 87.22 in our genomic comparisons revealed shared genetic factors contributing to increased root colonization in our non-pathogenic competitive colonizers. Discovering vast differences in genomes and biosynthetic products invoked anticipation of complex *in vitro* microbe-microbe interactions.

Our *in vitro* co-culture experiments reveal *Streptomyces* strains influence each other's growth and other strains, yet largely inhibitory phenotypes were not represented in the 16S rRNA amplicon community studies in which ASVs representing both are present in the same root samples. For example, in co-culture experiments, 299, 303 and CL18 inhibited growth of the Rhizobiaceae isolate 2 (Table 3.3), yet relative abundance data did not reflect this inhibition (Figure 3.11A-B). Interestingly, these findings suggest the dominant influence of the host, the environment, and likely the collective microbiome. While monoinoculation interactions are essential to tease apart fundamental microbe-microbe interactions, our findings emphasize that they are not always indicative or even suggestive of phenotypes in the context of a host or more diverse community. For these reasons, we suggest that a multi-tiered approach including various levels of comparison, competition, and colonization are necessary for more representative applications.

Perhaps of greatest significance is our use of multiple levels of complexity to study microbiome interactions. The use of monoinoculation, low complexity SynCom, wild soil and open air inocula allows for otherwise obscure distinctions not evident in the absence of one or more of these approaches or lower resolution. We found that in general, isolates that are historically good colonizers (Table 3.1) maintain their colonization phenotype despite primary inoculation with our *Streptomyces* strains. This suggests that microbe-microbe competition in the context of the microbiome likely influences resulting abundances. However, despite competition, 299 and 303

withstood metabolic pressures from other SynCom members (Table 3.1), and persisted, ultimately maintaining their previous attributes as good colonizers, although when compared to others, not the most abundant. Thus, reliance on relative abundances, especially when competed with a highly complex SynCom or wild soil, may negate the role of the less abundant, but important taxa. *Streptomyces'* large repertoire of secondary metabolites may amplify their importance and motivates understanding the roles for previously identified low abundance taxa in microbiomes as potential keystone community members. Recently, an *Enterobacteria* strain was defined as a keystone member in maize synthetic community experiments [52]. While the influence of soil type is often a primary root-microbiome determinant [53], this study reiterates that there is still room to explore novel drivers of microbiome establishment and stability, such as those inherent to metabolically rich *Streptomyces spp*.

Community balance may hinge on one or a small number of influential species. Their influence on community structure may not be reflected in abundance matrices and thus overlooked or underestimated [52, 54-56]. Previously emphasized reductionist approaches or additional use of lower complexity SynCom may help to inform the roles of individual taxa with higher resolution. Recent emphasis on the need to build more sustainable agroecosystems [57] highlights the importance of maximizing benefits of microbiomes and the vast utility they provide. We propose multi-tiered and multi-disciplinary microbiome studies are an essential component in achieving these goals. Advancing our understanding of how *Streptomyces spp*. potentiate colonization and sculpt the *A. thaliana* root microbiome will provide additional opportunities to manipulate microbiome composition to achieve tractable and sustainable agricultural applications.

V. ACKNOWLEDGEMENTS

The four strains of *Streptomyces* as well as several SynCom isolates were originally isolated in the laboratory of Jeffery Dangl at the University of North Carolina.

VI. REFERENCES

1. Fierer, N. and R.B. Jackson, *The diversity and biogeography of soil bacterial communities.* Proceedings of the National Academy of Sciences of the United States of America, 2006. **103**(3): p. 626-631.
2. Coyte, K.Z., J. Schluter, and K.R. Foster, *The ecology of the microbiome: Networks, competition, and stability.* Science, 2015. **350**(6261): p. 663-6.
3. Bai, Y., et al., *Functional overlap of the Arabidopsis leaf and root microbiota.* Nature, 2015. **528**(7582): p. 364-9.
4. Gopal, M., A. Gupta, and G.V. Thomas, *Bespoke microbiome therapy to manage plant diseases.* Front Microbiol, 2013. **4**: p. 355.
5. Finkel, O.M., et al., *Understanding and exploiting plant beneficial microbes.* Current Opinion in Plant Biology, 2017. **38**: p. 155-163.
6. Pieterse, C.M.J., et al., *Induced Systemic Resistance by Beneficial Microbes.* Annual Review of Phytopathology, Vol 52, 2014. **52**: p. 347-375.
7. Weidner, S., et al., *Bacterial diversity amplifies nutrient-based plant-soil feedbacks.* Functional Ecology, 2015. **29**(10): p. 1341-1349.
8. Lebeis, S.L., et al., *Salicylic acid modulates colonization of the root microbiome by specific bacterial taxa.* Science, 2015. **349**(6250): p. 860-864.
9. Wei, Z., et al., *Trophic network architecture of root-associated bacterial communities determines pathogen invasion and plant health.* Nat Commun, 2015. **6**: p. 8413.
10. Cha, J.Y., et al., *Microbial and biochemical basis of a Fusarium wilt-suppressive soil.* ISME J, 2016. **10**(1): p. 119-29.
11. Cole, B.J., et al., *Genome-wide identification of bacterial plant colonization genes.* PLoS Biology, 2017. **15**(9): p. e2002860.
12. Lundberg, D.S., et al., *Defining the core Arabidopsis thaliana root microbiome.* Nature, 2012. **488**(7409): p. 86-90.
13. Bulgarelli, D., et al., *Revealing structure and assembly cues for Arabidopsis root-inhabiting bacterial microbiota.* Nature, 2012. **488**(7409): p. 91-95.
14. Bonaldi, M., et al., *Colonization of lettuce rhizosphere and roots by tagged Streptomyces.* Front Microbiol, 2015. **6**: p. 25.

15. Niu, B., et al., *Simplified and representative bacterial community of maize roots.* Proc Natl Acad Sci U S A, 2017. **114**(12): p. E2450-E2459.
16. Gottel, N.R., et al., *Distinct microbial communities within the endosphere and rhizosphere of Populus deltoides roots across contrasting soil types.* Appl Environ Microbiol, 2011. **77**(17): p. 5934-44.
17. Bulgarelli, D., et al., *Structure and function of the bacterial root microbiota in wild and domesticated barley.* Cell Host Microbe, 2015. **17**(3): p. 392-403.
18. Fitzpatrick, C.R., et al., *Assembly and ecological function of the root microbiome across angiosperm plant species.* Proc Natl Acad Sci U S A, 2018. **115**(6): p. E1157-E1165.
19. Yeoh, Y.K., et al., *Evolutionary conservation of a core root microbiome across plant phyla along a tropical soil chronosequence.* Nat Commun, 2017. **8**(1): p. 215.
20. Wagner, M.R., et al., *Host genotype and age shape the leaf and root microbiomes of a wild perennial plant.* Nature Communications, 2016. **7**.
21. Vorholt, J.A., et al., *Establishing Causality: Opportunities of Synthetic Communities for Plant Microbiome Research.* Cell Host & Microbe, 2017. **22**(2): p. 142-155.
22. Liu, H.W., et al., *Inner Plant Values: Diversity, Colonization and Benefits from Endophytic Bacteria.* Frontiers in Microbiology, 2017. **8**.
23. Seipke, R.F., M. Kaltenpoth, and M.I. Hutchings, *Streptomyces as symbionts: an emerging and widespread theme?* Fems Microbiology Reviews, 2012. **36**(4): p. 862-876.
24. Lundberg, D.S., et al., *Defining the core Arabidopsis thaliana root microbiome.* Nature, 2012. **488**(7409): p. 86-+.
25. Challis, G.L. and D.A. Hopwood, *Synergy and contingency as driving forces for the evolution of multiple secondary metabolite production by Streptomyces species.* Proc Natl Acad Sci U S A, 2003. **100 Suppl 2**: p. 14555-61.
26. Schlatter, D., et al., *Disease Suppressive Soils: New Insights from the Soil Microbiome.* Phytopathology, 2017. **107**(11): p. 1284-1297.
27. Poudel, R., et al., *Microbiome Networks: A Systems Framework for Identifying Candidate Microbial Assemblages for Disease Management.* Phytopathology, 2016. **106**(10): p. 1083-1096.

28. Viaene, T., et al., *Streptomyces as a plant's best friend?* FEMS Microbiol Ecol, 2016. **92**(8).
29. Viaene, T., et al., *Streptomyces as a plant's best friend?* FEMS Microbiology Ecology, 2016. **92**(8).
30. Chen, I.M.A., et al., *IMG/M: integrated genome and metagenome comparative data analysis system.* Nucleic Acids Research, 2017. **45**(D1): p. D507-D516.
31. Blin, K., et al., *The antiSMASH database, a comprehensive database of microbial secondary metabolite biosynthetic gene clusters.* Nucleic Acids Research, 2017. **45**(D1): p. D555-D559.
32. Hobbie, L. and M. Estelle, *The axr4 auxin-resistant mutants of Arabidopsis-thaliana define a gene important for root gravitropism and lateral root initiation.* Plant Journal, 1995. **7**(2): p. 211-220.
33. Szkop, M., P. Sikora, and S. Orzechowski, *A novel, simple, and sensitive colorimetric method to determine aromatic amino acid aminotransferase activity using the Salkowski reagent.* Folia Microbiologica, 2012. **57**(1): p. 1-4.
34. Caporaso, J.G., et al., *Global patterns of 16S rRNA diversity at a depth of millions of sequences per sample.* Proceedings of the National Academy of Sciences of the United States of America, 2011. **108**: p. 4516-4522.
35. Tremblay, J., et al., *Primer and platform effects on 16S rRNA tag sequencing.* Frontiers in Microbiology, 2015. **6**.
36. Caporaso, J.G., et al., *QIIME allows analysis of high-throughput community sequencing data.* Nature Methods, 2010. **7**(5): p. 335-336.
37. Callahan, B.J., et al., *DADA2: High-resolution sample inference from Illumina amplicon data.* Nature Methods, 2016. **13**(7): p. 581-+.
38. Callahan, B.J., P.J. McMurdie, and S.P. Holmes, *Exact sequence variants should replace operational taxonomic units in marker-gene data analysis.* Isme Journal, 2017. **11**(12): p. 2639-2643.
39. Schneider, C.A. and W.S.E. Rasband, K. W., *NIH Image to ImageJ: 25 years of image analysis.* Nature Methods, 2012. **9**(7): p. 671-675.

40. Fyans, J.K., L. Bown, and D.R. Bignell, *Isolation and Characterization of Plant-Pathogenic Streptomyces Species Associated with Common Scab-Infected Potato Tubers in Newfoundland.* Phytopathology, 2016. **106**(2): p. 123-31.
41. Finn, R.D., et al., *The Pfam protein families database: towards a more sustainable future.* Nucleic Acids Research, 2017. **44**(D1).
42. Klein, E., et al., *Soil suppressiveness to fusarium disease: shifts in root microbiome associated with reduction of pathogen root colonization.* Phytopathology, 2013. **103**(1): p. 23-33.
43. Bonaldi, M., et al., *Colonization of lettuce rhizosphere and roots by tagged Streptomyces.* Frontiers in Microbiology, 2015. **6**.
44. Yeoh, Y.K., et al., *The core root microbiome of sugarcanes cultivated under varying nitrogen fertilizer application.* Environmental Microbiology, 2016. **18**(5): p. 1338-1351.
45. Farrar, K., D. Bryant, and N. Cope-Selby, *Understanding and engineering beneficial plant-microbe interactions: plant growth promotion in energy crops.* Plant Biotechnol J, 2014. **12**(9): p. 1193-206.
46. Fu, S.F., et al., *Indole-3-acetic acid: A widespread physiological code in interactions of fungi with other organisms.* Plant Signal Behav, 2015. **10**(8).
47. Xu, L., et al., *Correction for Xu et al., Drought delays development of the sorghum root microbiome and enriches for monoderm bacteria.* Proc Natl Acad Sci U S A, 2018. **115**(21): p. E4952.
48. Bulgarelli, D., et al., *Structure and Function of the Bacterial Root Microbiota in Wild and Domesticated Barley.* Cell Host & Microbe, 2015. **17**(3): p. 392-403.
49. Mahyarudin, I. Rusmana, and Y. Lestari, *Metagenomic of actinomycetes based on 16S rRNA and nifH genes in soil and roots of four Indonesian rice cultivars using PCR-DGGE.* Hayati Journal of Biosciences, 2015. **22**(3): p. 113-121.
50. de Araujo, J.M., A.C. da Silva, and J.L. Azevedo, *Isolation of endophytic actinomycetes from roots and leaves of maize (Zea may L.).* Brazilian Archives of Biology and Technology, 2000. **43**(4): p. 447-451.
51. Ozen, A.I. and D.W. Ussery, *Defining the Pseudomonas genus: where do we draw the line with Azotobacter?* Microb Ecol, 2012. **63**(2): p. 239-48.

52. Niu, B., et al., *Simplified and representative bacterial community of maize roots.* Proceedings of the National Academy of Sciences of the United States of America, 2017. **114**(12): p. E2450-E2459.
53. Yeoh, Y.K., et al., *Evolutionary conservation of a core root microbiome across plant phyla along a tropical soil chronosequence.* Nature Communications, 2017. **8**.
54. Paine, R.T., *Food Web Complexity and Species Diversity.* American Naturalist, 1966. **100**(910): p. 65-+.
55. Richardson, J.L., *The Organismic Community - Resilience of an Embattled Ecological Concept.* Bioscience, 1980. **30**(7): p. 465-471.
56. Berry, D. and S. Widder, *Deciphering microbial interactions and detecting keystone species with co-occurrence networks.* Frontiers in Microbiology, 2014. **5**.
57. Toju, H., et al., *Core microbiomes for sustainable agroecosystems.* Nature Plants, 2018. **4**(5): p. 247-257.

VII. APPENDIX: TABLES

Table 3.1. Strains included in SynCom[*], coculture[^], and/or comparative genomics[#]

List of bacteria isolated from *A. thaliana* used in these studies, which include representatives from 4 phyla: 7 Proteobacteria (purple), 2 Firmicutes (green), 1 Bacteroidetes (blue), and 1 Deinococcus-Thermus (pink). Six of these isolates have permanent draft genome sequences available at the *U.S. Department of Energy's Joint Genomes Institute, Integrated Microbial Genomes and Microbiome Samples (JGI IMG/M ER)*

Phylum	Family	Genera	Label	EC Enrichment	Colonization	Strain name	IMG Genome ID
Proteobacteria	Rhizobiaceae	*Rhizobium*	2[*^#]	Enriched	Robust	Rhizobium sp. 2MFCol3.1	2517572231
	Burkholderiaceae	*Burkholderia*	CL11[*^#]		Robust	Burkholderia CL11	2546825541
	Burkholderiaceae	*Burkholderia*	TN8[*^]		Unknown		
	Pseudomonadaceae	*Pseudomonas*	TN19[*^]		Unknown		
	Enterobacteriaceae	*Escherichia*	E. coli[*^]	Deplete	Poor		
	Pseudomonadaceae	*Pseudomonas*	50[*^#]	Deplete	Sporadic	Pseudomonas sp. KD5	2228664007
	Calobacteriaceae	*Brevundimonas*	374[*]		Sporadic	Brevundimonas sp.	2596583649
Firmicutes	Paenibacilliaceae	*Paenibacillus*	181[*^#]		Sporadic	Paenibacillus sp. 181MFCol5.1	2639762524
	Bacilliaceae	*Bacillus*	A415[^]				
Bacteroidetes	Weeksellaceae	*Flavobacterium*	40[*^#]		Sporadic	Flavobacterium sp. 40S8	2563366720
Deinococcus	Deinococcaceae	*Deinococcus*	TN56[*^]		Poor		

Table 3.2. Genome statistic and biosynthetic gene proportion.

Genome features in our isolates including: estimated genes and the percent that are predicted to be in biosynthetic gene clusters.

Isolate	Phylum	Protein Coding Genes	Total Genes	*Biosynthetic Clusters	Genes in BCs	% Biosynthetic Genes
299	Actinobacteria	9620	9710	120	1490	15.35
303	Actinobacteria	8387	8480	101	1432	16.89
CL18	Actinobacteria	6591	6677	69	742	11.11
136	Actinobacteria	6905	6991	47	755	10.80
2	Proteobacteria	6294	6365	29	303	4.76
40	Bacteroidetes	4727	4820	27	276	5.73
50	Proteobacteria	5832	5920	28	272	4.59
181	Firmicutes	4949	5066	36	464	9.16
CL11	Proteobacteria	7562	7478	48	604	8.08
Streptomyces scabiei NCPPB 4086	Actinobacteria	9050	9151	92	1638	17.90

*Includes all clusters capable of producing biosynthetic products (i.e. not limited to antibiotics and secondary metabolites)

Table 3.3. Co-culture cross spots indicate microbe-microbe growth influences.

Isolates were co-cultured on solid LB plates. Were each Streptomyces isolate was inoculated 2-3 days before each non-Streptomyces isolate. Differential growth patterns were observed. If no inhibition was observed, (NI) is noted in the table.

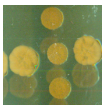
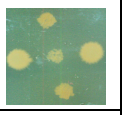
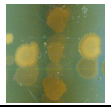
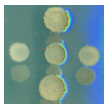
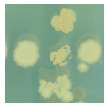
***Streptomyces* strain**	**Challenge strain**	**Colonization Phenotype**	**Challenge Family**	***Inhibition Direction**	***Level of Inhibition**	**Phenotype**
299	CL18		Streptomycetaceae	NI	NI	NI
303	CL18		Streptomycetaceae	303--|CL18	Minimal	
136	CL18		Streptomycetaceae	NI	NI	NI
303	136		Streptomycetaceae	NI	NI	NI
299	136		Streptomycetaceae	NI	NI	NI
303	299		Streptomycetaceae	NI	NI	NI
299	181	Sporadic	Paenibacillaceae	299|--181	Intermediate	
303	181	Sporadic	Paenibacillaceae	303|--181	Intermediate	
CL18	181	Sporadic	Paenibacillaceae	CL18|--181	Intermediate	
136	181	Sporadic	Paenibacillaceae	136|--181	Intermediate	
299	TN19	Unknown	Pseudomonadaceae	NI	NI	NI

Table 3.3. Continued

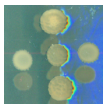
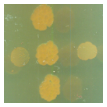
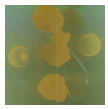
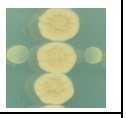
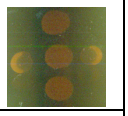
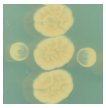
Streptomyces strain	Challenge strain	Colonization Phenotype	Challenge Family	*Inhibition Direction	*Level of Inhibition	Phenotype
303	TN19	Unknown	Pseudomonadaceae	NI	NI	NI
CL18	TN19	Unknown	Pseudomonadaceae	CL18|--TN19	Intermediate	
136	TN19	Unknown	Pseudomonadaceae	NI	NI	NI
299	2	Robust	Rhizobiaceae	299 --|2	Intermediate	
303	2	Robust	Rhizobiaceae	303--|2	Major	
CL18	2	Robust	Rhizobiaceae	CL18--|2	Major	
136	2	Robust	Rhizobiaceae	NI	NI	NI
299	A415	Robust	Intrasporangiaceae	NI	NI	NI
303	A415	Robust	Intrasporangiaceae	303--|A415	Major	
CL18	A415	Robust	Intrasporangiaceae	CL18-|A415	Major	
136	A415	Robust	Intrasporangiaceae	NI	NI	NI
299	CL11	Robust?	Burkholderiaceae	NI	NI	NI

Table 3.3. Continued

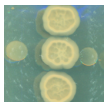
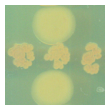
Streptomyces strain	Challenge strain	Colonization Phenotype	Challenge Family	*Inhibition Direction	*Level of Inhibition	Phenotype
303	CL11	Robust?	Burkholderiaceae	NI	NI	NI
CL18	CL11	Robust?	Burkholderiaceae	CL18-|CL11	Major	
136	CL11	Robust?	Burkholderiaceae	NI	NI	NI
299	E. coli	Poor	Enterobacteriaceae	NI	NI	NI
303	E. coli	Poor	Enterobacteriaceae	NI	NI	NI
CL18	E. coli	Poor	Enterobacteriaceae	NI	NI	NI
136	E. coli	Poor	Enterobacteriaceae		Color Change	
299	TN56	Poor	Deinococcaceae	NI	NI	NI
303	TN56	Poor	Deinococcaceae	NI	NI	NI
CL18	TN56	Poor	Deinococcaceae	NI	NI	NI
136	TN56	Poor	Deinococcaceae	NI	NI	NI
299	40	Sporadic	Flavobacteriaceae	NI	NI	NI

Table 3.3. Continued

Streptomyces strain	Challenge strain	Colonization Phenotype	Challenge Family	*Inhibition Direction	*Level of Inhibition	Phenotype
303	40	Sporadic	Flavobacteriaceae	NI	NI	NI
CL18	40	Sporadic	Flavobacteriaceae	NI	NI	NI
136	40	Sporadic	Flavobacteriaceae	NI	NI	NI
299	50	Sporadic	Pseudomonadaceae	NI	NI	NI
303	50	Sporadic	Pseudomonadaceae	NI	NI	NI
CL18	50	Sporadic	Pseudomonadaceae	NI	NI	NI
136	50	Sporadic	Pseudomonadaceae	NI	NI	NI

*Level "NI" = no inhibition

Table 3.4.16S rRNA amplicon community sequencing root microbiome sample information.

The total number of replicates for each type of sample, as well as basic information about the samples, including: average, minimum, and maximum number of reads in our sequencing run.

Sample Type	N	Average Reads	Minimum Reads	Maximum Reads	Read Range
NB/NB	9	88375.44444	23861	176400	152539
299/NB	6	107704.6	61047	208813	147766
303/NB	9	104922.6667	39464	176113	136649
CL18/NB	6	78786.66667	28494	147048	118554
136/NB	4	101045.75	47954	156785	108831
SynCom	3	78187.66667	62150	98170	36020
NB/SynCom	11	109765.3636	38600	243232	204632
299/SynCom	15	71306.33333	13781	140184	126403
303/SynCom	14	67878.42857	11852	199865	188013
CL18/SynCom	14	65215.28571	38643	144613	105970
136/SynCom	16	79271.3125	17790	167139	149349
Wild	3	10005	4399	15335	10936
NB/Wild	6	53561.2	24147	95046	70899
299/Wild	11	66037.58333	55353	149287	93934
303/Wild	3	54455.66667	49313	60953	11640
CL18/Wild	5	40904.8	13176	74089	60913
136/Wild	8	57556.125	10259	147136	136877

VIII. APPENDIX: FIGURES

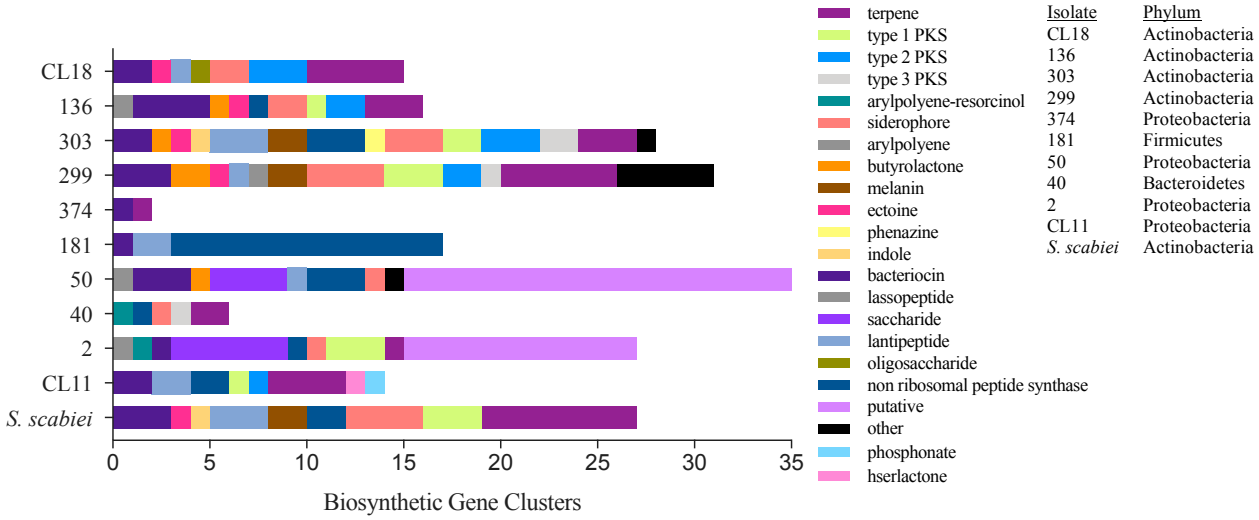


Figure 3.1. antiSMASH [31] strain genome analysis reveals unique biosynthetic gene clusters and potential metabolites.

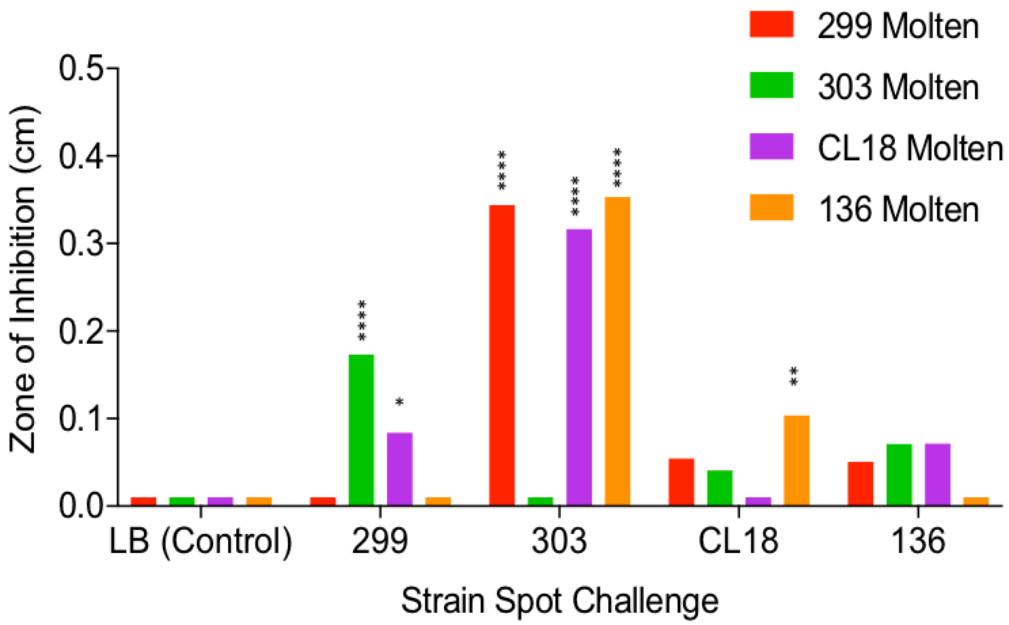


Figure 3.2. Streptomyces interactions demonstrate potential growth inhibition.

When 303 is spotted on top, growth of each other isolate is significantly inhibited. When 299 is spotted on top, growth of 303 and CL18 is inhibited. When spotted on top, CL18 inhibits the growth of 136. (2-way ANOVA, multiple comparisons, mean of 6 technical replicates, ($p<0.05$) *= $p<0.05$, **=$p<0.005$, ****=$p<0.0005$, indicates significance as compared to control n=6)

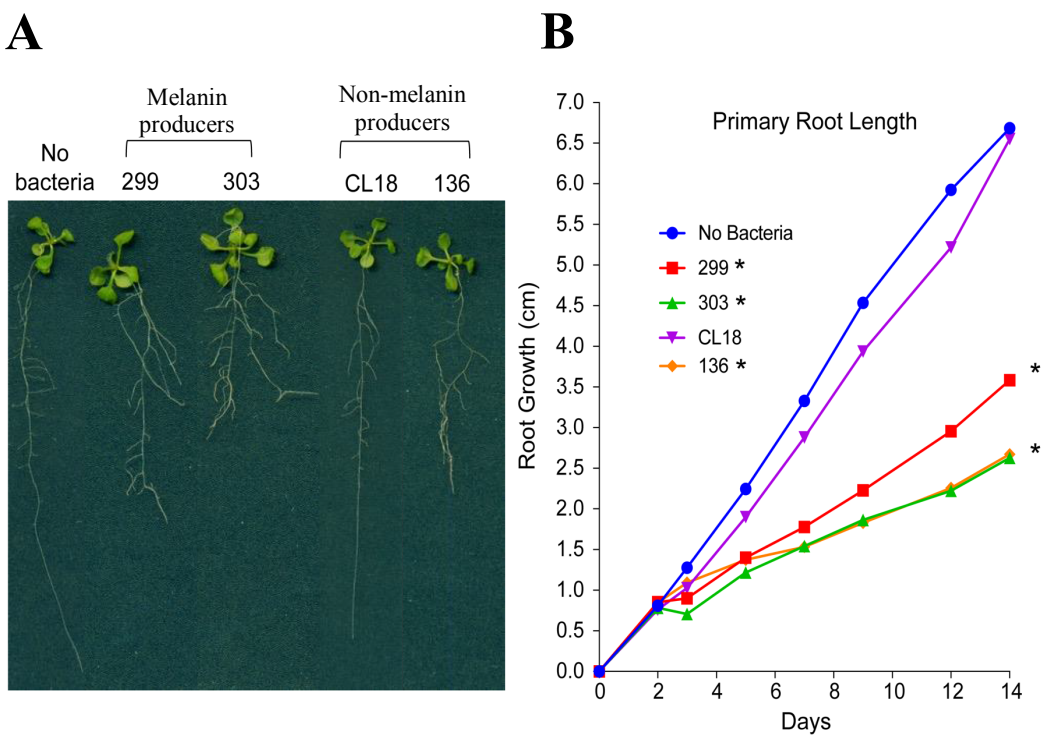


Figure 3.3. *Streptomyces* spp. differentially influence *A. thaliana* root morphology

Axenic 7-day old *A. thaliana* seedlings were inoculated with each of the four *Streptomyces* isolates and grown for 14 additional days. (A) Exemplar *A. thaliana* seedling root morphology following 14 day monoculture on agar plates of the strain listed above the seedling (B) Primary root length of 14 day old seedlings (1-Way ANOVA, multiple comparisons, mean of 9 replicates * indicates significance ($p<0.05$) as compared to no bacteria (NB).

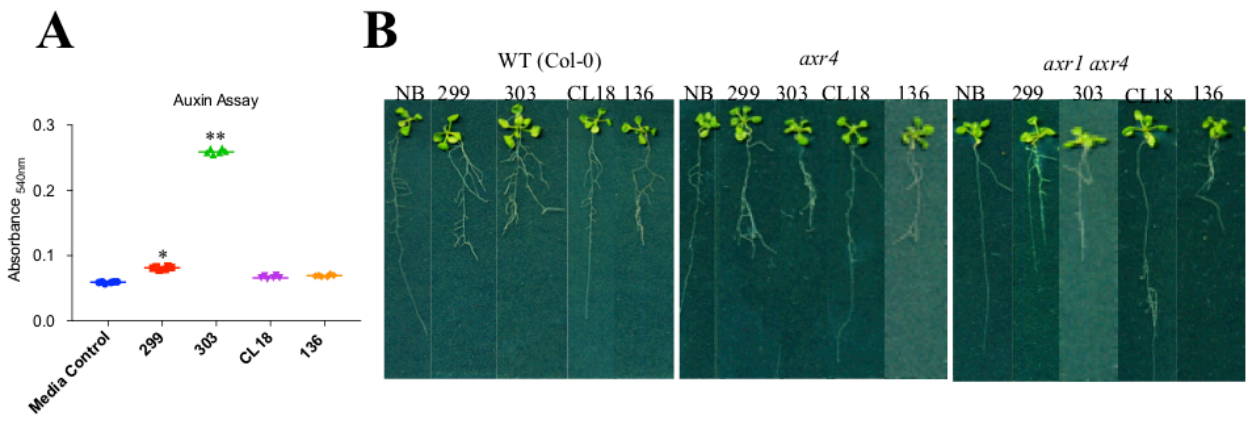


Figure 3.4. Microbial auxin production does not fully explain root phenotypes.

(A) (1-way ANOVA, multiple comparisons, mean of 6 replicates, ($p<0.0001$) (B) As compared to WT, auxin resistant mutants *axr4* and *axr1/4* show remarkably consistent root phenotypes.

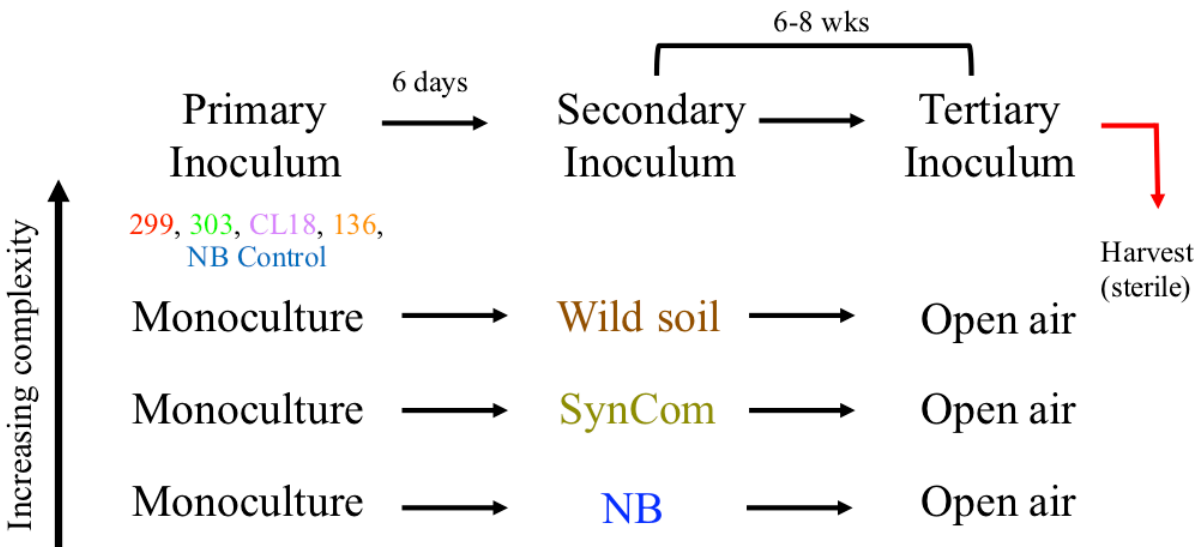


Figure 3.5. Experimental schematic for 16S rRNA amplicon sequencing samples.

A schematic of the experimental design to determine how different times and complexity of inoculum contribute to root microbiome assembly. First, axenic *A. thaliana* Col-0 seedlings were inoculated with a single *Streptomyces* strain or no bacteria (NB), Second, wild soil inoculum is wild soil slurry in sterile water (see Methods section), SynCom inoculum is detailed in Table 1.1, or NB was used to inoculate seedlings. Finally, all pots shared the same plant growth chamber where they could acquire inoculum from the air.

.

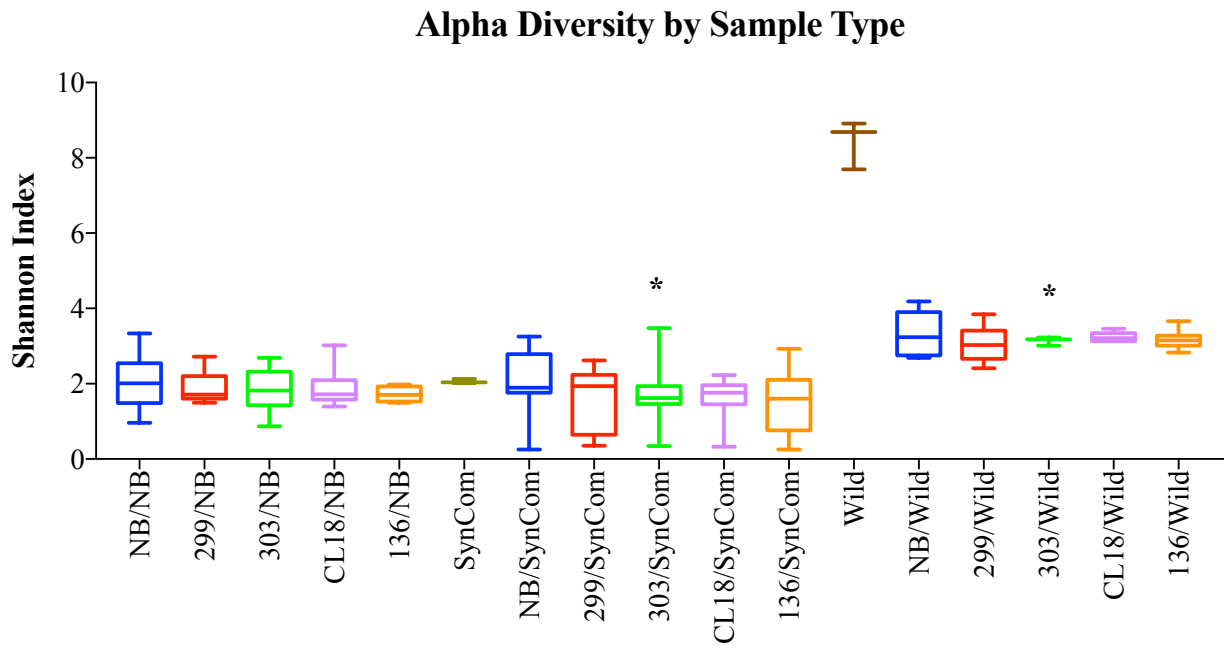


Figure 3.6. Alpha diversity indicates species richness by root microbiome sample.

Shannon indices calculated for each sample type (index calculated via QIIME2, accounts for ASV abundance and eveness). The x axis includes each sample type increasing in secondary inoculum complexity from left to right (NB, SynCom, then Wild). Blue boxes indicated NB primary inoculum, red boxes indicate 299 primary inoculum, green boxes indicated 303 primary inoculum, purple boxes indicated CL18 primary inoculum, orange boxes indicate 136 primary inoculum, the olive green box indicates SynCom inoculum alone, and the brown box indicates Wild inoculum alone. Box and whisker plots indicate average sample ASVs for each sample type, as well as standard deviations. * indicates that the Shannon index calculated for 303/SynCom and 303/Wild samples do not differ significantly whereas Shannon index differs significantly for all other *Streptomyces*/SynCom vs *Streptomyces*/Wild.

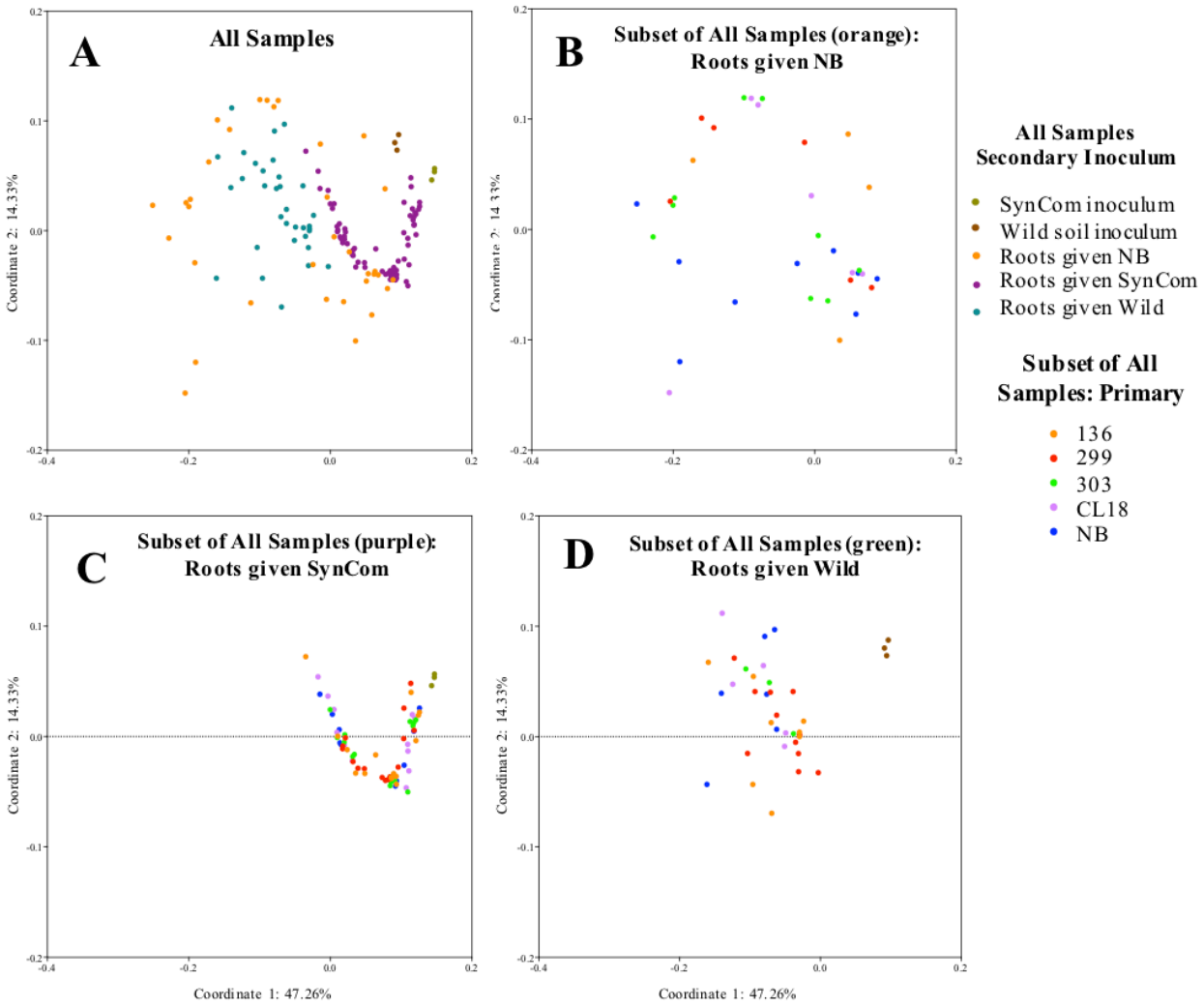


Figure 3.7. Principle coordinate analysis (PCoA) generated via weighted UniFrac distances shows diversity between samples.

(A) All samples, color indicates secondary inoculum (orange = NB, purple = SynCom, green = Wild) (B) Subset of all samples (orange samples in A), no secondary inoculum, color indicates primary inoculum (C) Subset of all samples (purple samples in A) SynCom secondary inoculum, color indicates primary inoculum (D) Subset of all samples (green samples in A) Wild secondary inoculum, color indicates primary inoculum (All samples given tertiary inoculum (i.e. open air)) Secondary colors are as follows: orange = 136, red = 299, green = 303, purple = CL18, and blue = NB.

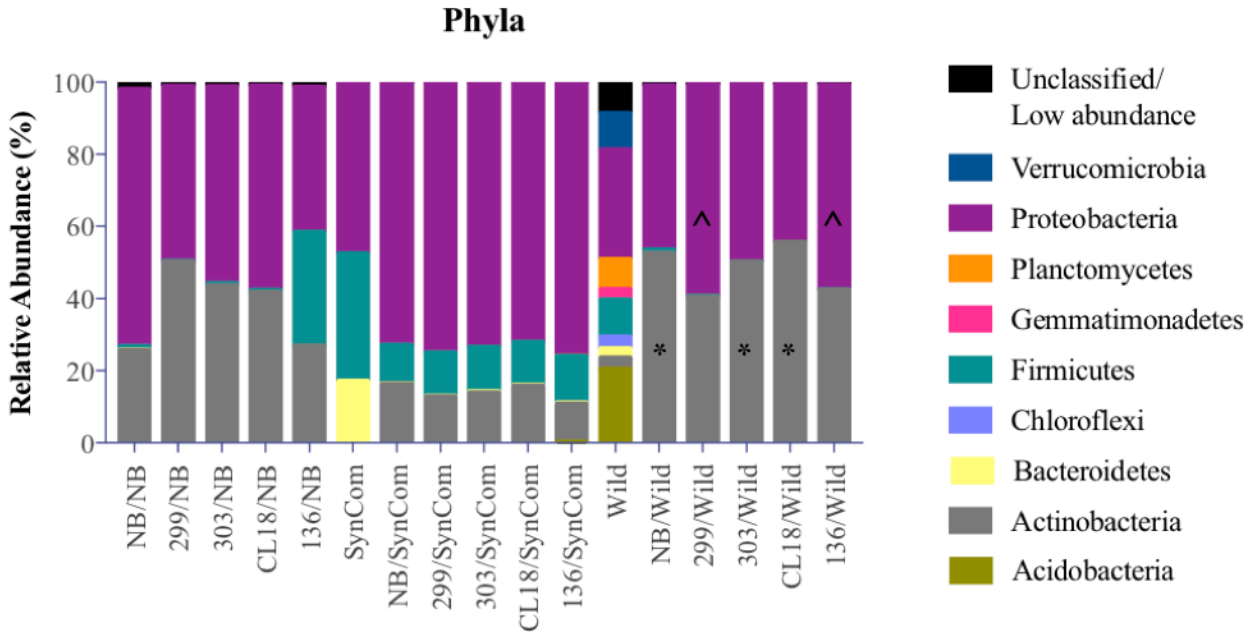


Figure 3.8. Relative abundance of phyla in root microbiome samples with Wild secondary inoculum differ.

Histogram shows the distribution of the relative abundances of each type of sample for the phylum-level ASV taxonomic assignment. ^ indicates relative abundance of Proteobacteria was significantly different from Wild inoculum alone. * indicates relative abundance of Actinobacteria differed significantly from Wild inoculum alone (Tukey's multiple comparisons $p<0.05$).

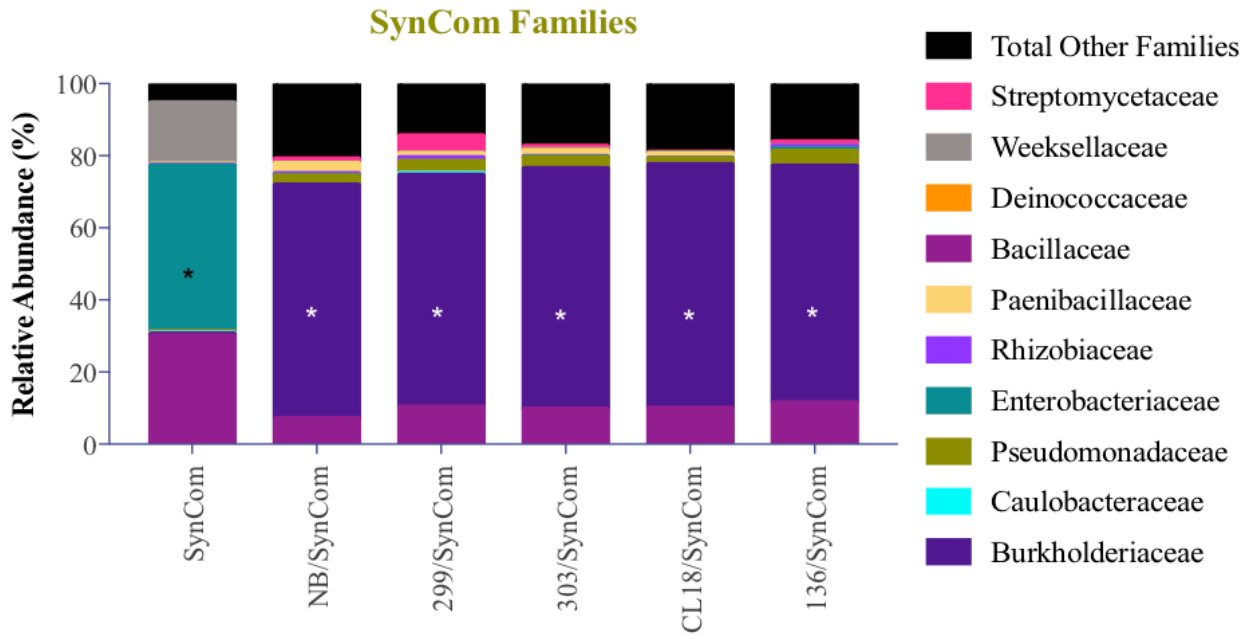


Figure 3.9. Relative abundance of families from samples secondarily inoculated with SynCom are different than the SynCom inoculum.

Histogram shows the distribution of the relative abundances of only samples that were inoculated with the SynCom for the family-level ASV taxonomic assignment for just families in the SynCom * indicates significant difference in relative abundance between SynCom inoculum and root microbiome sample. Dunnett's multiple comparisons, $p<0.05$.

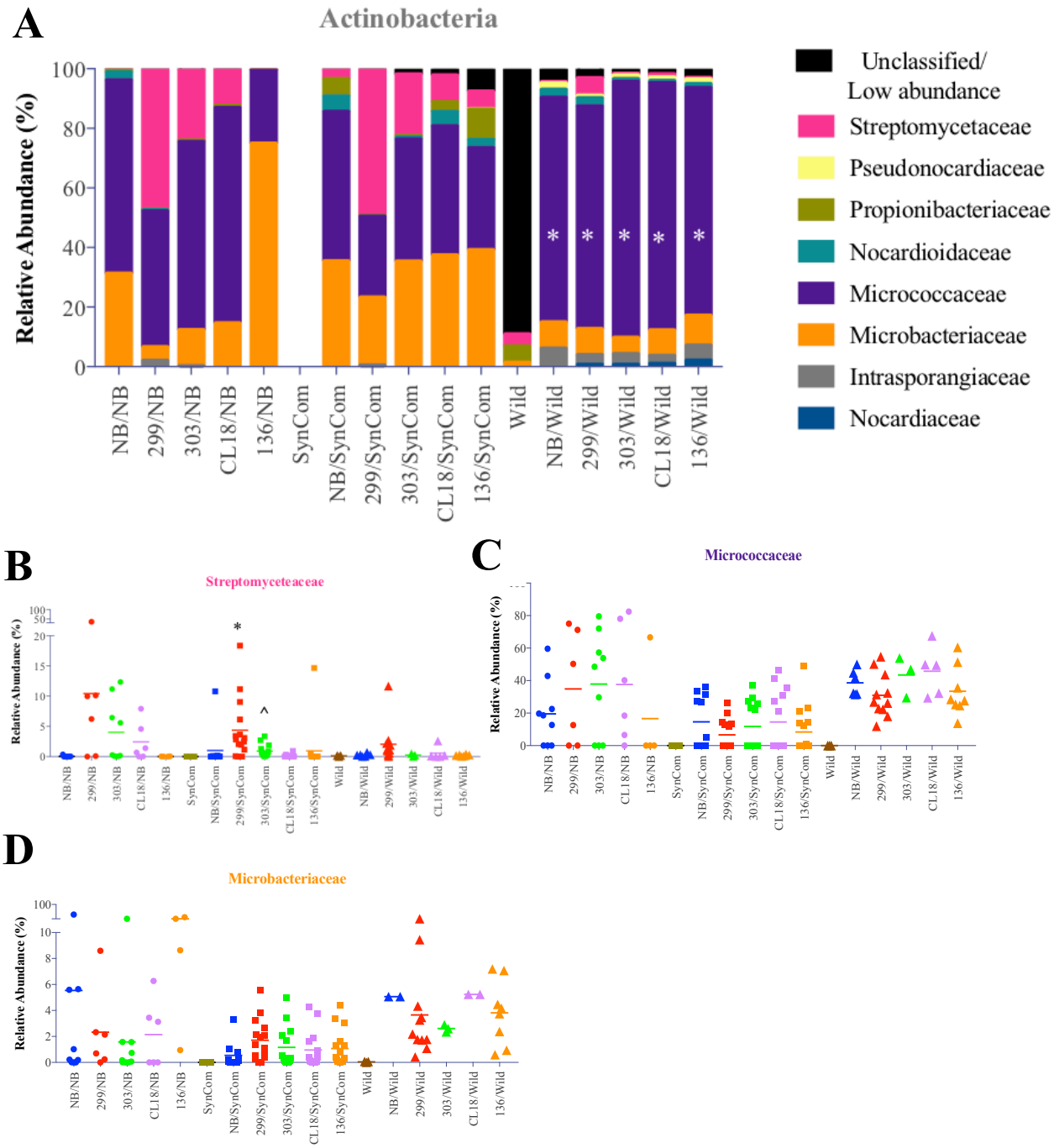


Figure 3.10. Relative abundance of Actinobacteria families in all samples.

Histogram shows the distribution of the relative abundances of each type of sample for only Actinobacteria families from the ASVs taxonomic assignment. Micrococcaceae are more abundant within root microbiomes as compared to Wild inoculum, Tukey's multiple comparisons, $p<0.05$ (A). * 299/SynCom samples have significantly different relative abundances of Streptomycetaceae than 136/SynCom and CL18/SynCom, ^ 303/SynCom samples are different in Streptomycetaceae

abundance as compared to 136/SynCom alone (Dunn's multiple comparisons, $p<0.05$) (B) Relative abundance of Micrococcaceae within each sample (C) Relative abundance of Microbacteriaceae within each sample (D).

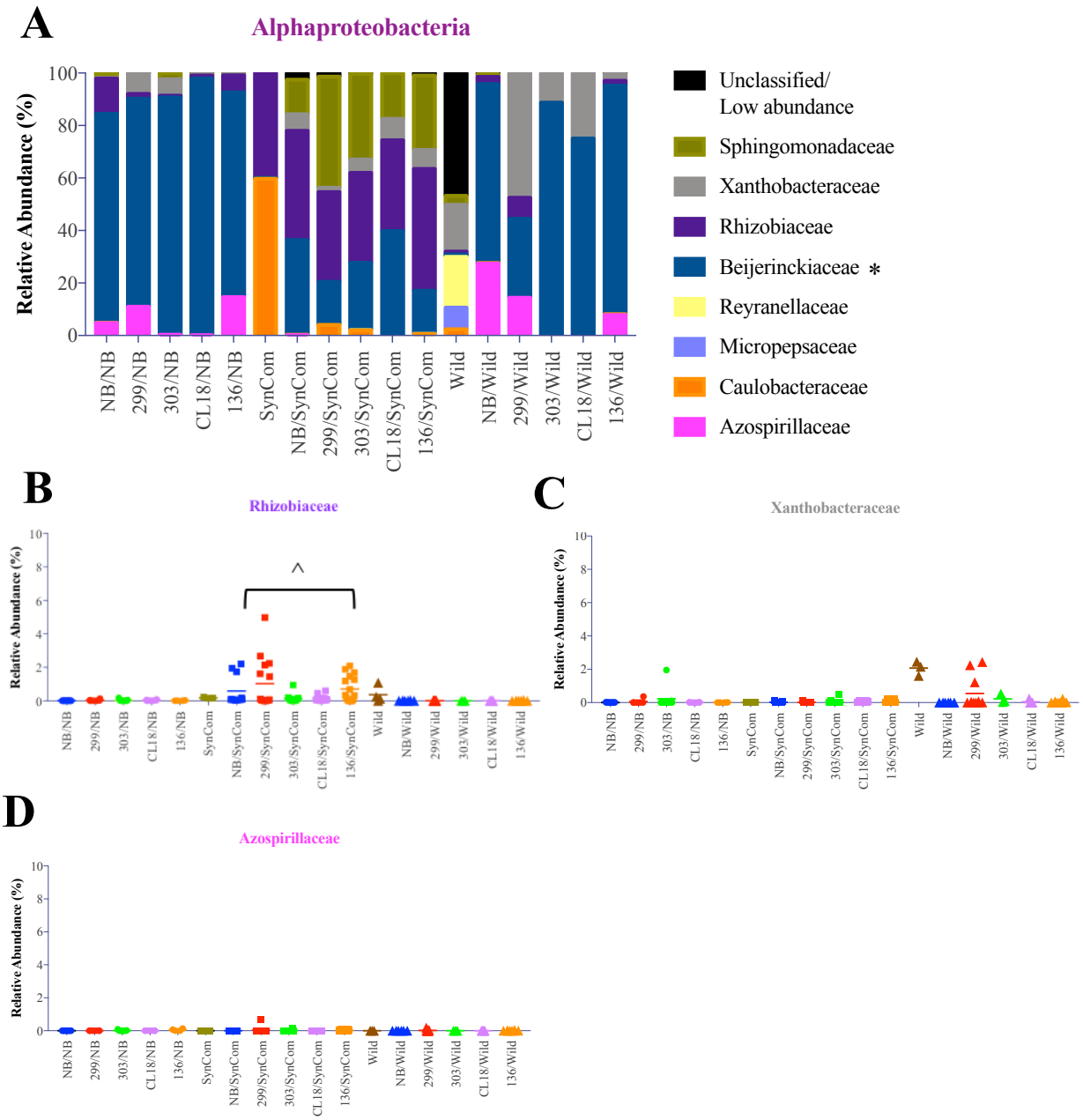


Figure 3.11. Relative abundances of Alphaproteobacteria families.

Histogram shows the distribution of the relative abundances of each type of sample for only Alphaproteobacteria families from the ASV taxonomic assignment Beijerinckiaceae relative abundances vary by primary inoculation with 303, CL18 and 136 and Wild or NB secondary inoculum, * Tukey's multiple comparisons, $p<0.05$ (A). Relative abundances of Rhizobiaceae in root microbiome samples with SynCom secondary inoculum significantly differ from samples with

Wild and NB secondary inoculum, ^ Dunn's multiple comparisons, $p<0.05$ (B). Relative abundances of Xanthobacteraceae (C) Relative abundances of Azospirillaceae (D).

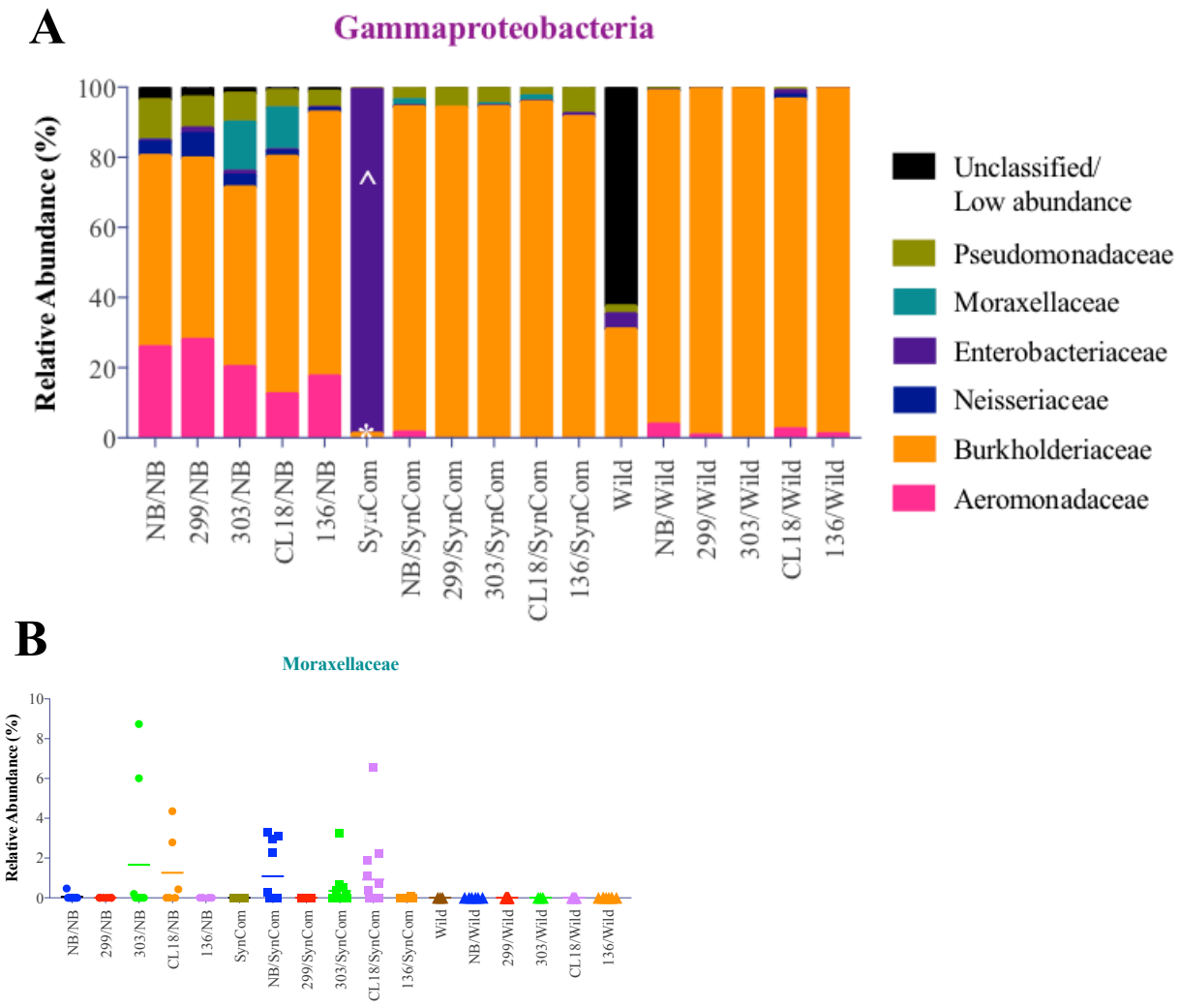


Figure 3.12. Gammaproteobacteria family relative abundances.

Histogram shows the distribution of the relative abundances of each type of sample for only Gammaproteobacteria families from the ASV taxonomic assignment. Relative abundances of Enterobacteriaceae are different in samples with Wild and SynCom secondary inoculum, and relative abundance of Burkholderia are different than samples with secondary Wild, SynCom or NB inoculum, ^* Tukey's multiple comparisons, $p<0.05$ (A). Relative abundances of Moraxellaceae (B).

CHAPTER FOUR - COMPOSITION OF THE GUT MICROBIOME REGULATES THE SEVERITY OF MALARIA

A VERSION OF THIS CHAPTER HAS BEEN PUBLISHED

Nicolas F. Villarino, Gary R. LeCleir, Joshua E. Denny, Stephen P. Dearth, Christopher L. Harding, Sarah S. Sloan (Chewning), Jennifer L. Gribble, Shawn R. Campagna, Steven W. Wilhelm, and Nathan W. Schmidt. "The composition of the gut microbiome modulates the severity of malaria." *PNAS.* 113(8): 2235-40.

10 individuals contributed to this chapter: Nicolas F. Villarino, Gary R. LeCleir, Joshua E. Denny, Stephen P. Dearth, Christopher, L. Harding, Sarah S. Sloan (Chewning), Jennifer L. Gribble, Shawn R. Campagna, Steven W. Wilhelm, and Nathan W. Schmidt. NFV, JED, and NWS designed experiments and analyzed the data; NFV, GRL, JED, SPD, CLH, SSC, and JLG performed experiments; GRL, JLG; SWW analyzed DNA sequencing; SPD and SRC analyzed the UPLC-HRMS data; NFV, GRL, SRC, SPD, SWW and NWS. wrote the manuscript. SSS contributions to experiments: Prepared antibiotic cocktails in mouse drinking water, helped prepare yogurt and probiotic treatments, harvested cecums from treated and untreated mice, homogenized cecal material for gavage, weighed mice, performed blood smears on treated and untreated mice, counted parasitized RBCs, culled mice when necessary. In addition, I added text to Introduction and Discussion sections for this document. SSC received approval from NFV and NWS to include this manuscript in her dissertation. The authors declare no competing financial interests.

I. ABSTRACT

Infectious diseases plague much of the developing world. Current efforts to advance our understanding of correlations between the gut microbiome and mediation of infectious disease are significant. Of particular interest are diseases for which we do not have an effective vaccine, such as malarial illnesses caused by infection with the parasite *Plasmodium*. *Plasmodium* infections result in clinical presentations that range from asymptomatic to severe malaria resulting in approximately one million deaths annually. In spite of this, the factors that determine disease severity remain poorly understood. Here we show that the gut microbiota of mice influences the pathogenesis of malaria. Genetically similar mice from different commercial vendors, which exhibited differences in their gut bacterial community, had significant differences in parasite burden and mortality after infection with multiple *Plasmodium* species. Germ-free mice that received cecal content transplants from 'resistant' or 'susceptible' mice had low and high parasite burdens, respectively, demonstrating the gut microbiota shaped the severity of malaria. Among differences in the gut flora were increased abundances of *Lactobacillus* and *Bifidobacterium* in resistant mice. Susceptible mice treated with antibiotics followed by yogurt made from these bacterial genera displayed a decreased parasite burden. Consistent with differences in parasite burden, resistant mice exhibited an elevated humoral immune response compared to susceptible mice. Collectively, these results identify the composition of the gut microbiota as a novel risk factor for severe malaria and modulation of the gut microbiota (*e.g*. probiotics) as a potential treatment to decrease parasite burden.

II. INTRODUCTION

Microbiomes across kingdoms have demonstrated remarkable similarity in their collective contributions to their hosts' survival [1-3]. As was described in chapter 1, the gut microbiota impacts multiple facets of host physiology [4] including shaping susceptibility to numerous diseases [5-13]. The effects of the gut microbiota on the mammalian host are strongly influenced by the collective composition of the bacterial populations [14] and commensal flora are known to affect local pathogen burdens and host immunity [15-17]. Microbiome studies in other systems, such as the plant model *Arabidopsis thaliana,* describe the essential contribution of microbe-microbe interactions on microbiome establishment and balance [18]. In addition to influencing local gut immunity, the gut microbiome also affects host immunity to extra-gastrointestinal tract viral infections [19], chronic diseases and a variety of infectious diseases [20, 21].

Plasmodium infections are a global health burden causing over 200 million cases of malaria and around one million deaths annually, with the vast majority of fatalities being children under the age of 5 living in sub-Saharan Africa [22]. Many *Plasmodium* infections are either asymptomatic or cause only mild malaria. Yet, some infections progress to severe malaria that most often manifest as impaired consciousness (cerebral malaria), respiratory distress, and severe anemia [23]. The best correlate of disease severity following *P. falciparum* infection in humans is parasite density [24, 25].

Recent studies also support that the gut microbiome modulates *Plasmodium* infections in humans. Anti-α-gal antibodies, induced by the gut pathobiont *E. coli* O86:B7, cross-react with sporozoites from human and rodent *Plasmodium* species that impair transmission of the parasite between the vector and vertebrate host; however, this cross-reactive immunity did not affect blood stage parasite burden [26]. Additionally, the stool bacteria composition of Malian children correlated prospectively with risk of *P. falciparum* infection, but not progression to febrile malaria [27]. Importantly, it remains unclear whether the gut microbiome also contributes to the development of severe malaria. As has been shown in plants, microbiomes change in response to infection, resulting in a beneficial consortium of bacteria [28]. This consortium can be altered via additions with probiotics or removal with antibiotic treatment. Use of probiotics has been shown to

beneficially influence both humoral and cellular systemic immunity in children via decrease of pro-inflammatory cytokines and increase in beneficial antibodies [29]. In addition, the use of probiotic therapies has been linked to benefits across a broad spectrum of diseases including HIV [30] and respiratory infections [31]. Similarly, here we used a probiotic cocktail to supplement the diet of mice treated with antibiotics. Collectively, our data demonstrate that the gut microbiome effects blood stage parasite burden and the subsequent severity of malaria.

III. MATERIALS AND METHODS

Animals and housing

Conventionally housed mice: Female C57BL/6J and BALB/cJ mice (6-8 weeks old) were purchased from The Jackson Laboratory (Bar Harbor, Maine); C57BL/6N and BALB/cN mice (6-8 weeks old) were purchased from the National Cancer Institute (Frederick, MD), Charles River Laboratories (Wilmington, MD), Harlan Laboratories (Indianapolis, IN) and Taconic (Hudson, NY). Mice were acclimatized for a minimum of 7 days prior to starting experiments.

Germ–free mice: Female C57BL/6J mice (8-10 weeks old) were purchased from The National Gnotobiotic Rodent Resource Center at the University of North Carolina-Chapel Hill. Upon arrival at the University of Tennessee the mice were kept in the transporting box until fecal transplant was done, then mice were housed in conventional (specific pathogen free) conditions. Animal experiments were carried out at The University of Tennessee adhering to the local and national regulations of laboratory animal welfare. Procedures involving the care or use of mice were reviewed and approved by The University of Tennessee Institutional Animal Care and Use Committee.

Diets

Unless noted otherwise mice were fed NIH-31 Modified Open Formula Mouse/Rat Irradiated Diet (Harlan 7913) (Harlan, Indianapolis, IN). In some experiments mice were fed Teklad 22/5 Rodent Diet (Harlan 8640; Harlan, Indianapolis, IN), Jackson Laboratory in-house diet (5K67; Cincinnati Lab & Pet Supply, Inc.; Cincinnati, OH) or NCI/CR in-house diet (5L79 Cincinnati Lab & Pet Supply, Inc.; Cincinnati, OH). Mice were placed on the respective diets upon arrival at the facility

and maintained on the different diets for at least one week prior to *P. yoelii* infection or removal of intestinal tissues for bacterial population analysis.

Plasmodium infection

Mice were infected with *P. yoelii* 17XNL, *P. chabaudi* AS, or *P. berghei* ANKA. For *P. yoelii* or *P. berghei* ANKA infections mice received $1x10^5$ parasitized red blood cells (intravenously) prepared from frozen/thawed stabilites. For *P. chabaudi* infections, experimental mice were infected intraperitoneally with freshly prepared $1x10^5$ parasitized red blood cells after one *in vivo* passage in C57BL/6 mice.

Evaluation of parasitemia

Blood samples were taken from the tail at regular intervals from 3 to 35 days post-infection. Parasitemia was assessed by evaluation of thin blood smears or flow cytometry. Thin blood smears–at least 5 high-power (1000x) fields were assessed for each sample. Total red blood cells and parasitized red blood cells were counted in each field. Flow cytometry–about 5-10 µl of blood was added to PBS and then fixed with 0.00625%% gluteraldehyde. Cells were stained with CD45.2-APC (clone 104; Biolegend; San Diego, CA), Ter119-APC/Cy7 (clone TER-119; Biolegend; San Diego, CA), dihydroethidium (Sigma Aldrich; St. Louis, MO), and Hoechst 33342 (Sigma Aldrich; St. Louis, MO). Red blood cells ($CD45.2^-Ter119^+$) were gated on and *Plasmodium* infected cells were subsequently identified as $dihydroethium^+Hoechst\ 33342^+$. Parasitemia represents the percentage of red blood cells infected with *P. yoelii*, *P. chabaudi* or *P. berghei*.

Enumeration of red blood cells and parasitized red blood cells

Blood samples were collected and used to quantify red blood cells per mL using a hemocytometer, and percent parasitemia. Red blood cells per mL and percent parasitemia were used to calculate the number of parasitized red blood cells per mL of blood.

Cecum transplant

Cecal content was squeezed from donor mice (n=3-5 mice per group) into a sterile petri dish. Immediately after harvesting the cecum material, it was diluted with sterile saline (2 mL) and mixed gently for ~30 seconds. Each germ-free mouse received the diluted cecum material (200 µL/mouse) administered by oral gavage. For each mouse, a new sterile oral gavage needle was used. After the cecal transplant, mice were housed using conventional conditions. Mice were infected with *P. yoelii* 3 weeks after the cecal transplant.

Gut microbiota analysis

Tissue collection: The distal half of the small intestine, cecum, and colon were excised from mice and flash frozen in liquid nitrogen. Samples were then stored at -80°C.

DNA isolation: DNA was extracted from samples using the MoBio PowerSoil DNA Isolation Kit (MoBio Laboratories Inc., Carlsbad, CA) according to manufacturer's protocols. No effort was made to separate mouse tissue from the bacterial component so as not to select against bacteria that were in close association with mouse tissue.

Ribosomal 16S sequencing: For amplification of bacterial 16S rRNA genes, bacteria specific PCR primers targeting the V4 region (bases 515-806) were used.

Amplification, barcoding and sequencing were completed by the Genome Sequencing Center at the Hudson-Alpha Institute for Biotechnology (Huntsville, AL) using the MiSeq platform with 150 bp paired-end reads.

Community analysis.: We used the Mothur software package (version 1.33.1) [42] to process sequences of sufficient length and quality similarly to the Schloss MiSeq SOP (http://www.mothur.org/wiki/MiSeq_SOP). Mothur was also used to cluster sequences into phylotypes and for phylogenetic classification and to sort our sequences into groups based on the region of the digestive tract from which the DNA was extracted. The Primer-E software package (Version 6; [43]) was used to interrogate the relationships between phylotypes across samples and to derive correlations between phylotype presence/abundance and other parameters. The ".shared" file (a matrix file containing phylotype abundances for each sample), created by Mothur, was imported directly into the Primer-E software package. All phylotype abundances were standardized to the total number of sequences per barcoded library (proportional abundances).

Standardized abundances were square-root transformed to partially deemphasize more highly abundant phylotypes. A Bray-Curtis similarity matrix was constructed and used to perform non-metric multidimensional scaling analysis (NMDS) for visualization of community structure relationships between the different samples. Detection of "biomarker" sequences was performed using the software package LEfSe (http://huttenhower.sph.harvard.edu/galaxy/) [26].

Metabolomics analysis

Collection of small intestine and cecum content samples: Immediately after euthanasia, the abdominal cavity was exposed and the small intestine and the cecum were dissected from the other intestinal sections. The small intestine and cecum contents were collected into petri dishes by squeezing the tissues from the proximal to distal ends of the organs. In addition, extraction solvent (1mL) (40:40:20 HPLC grade methanol, acetonitrile, water with 0.1% formic acid) was used to flush the small intestine and the cecum using a needle and syringe. The intestine contents were then transferred into separate cryotubes and flash frozen in liquid nitrogen. The samples were kept on ice for approximately one hour until extraction.

Collection of plasma samples: Blood was collected from the peri-orbital sinus using heparinized capillary tubes under general anesthesia with isoflurane. Immediately after collection, blood samples were transferred to centrifuge tubes and centrifuged for 10 minutes at 2,000 x g at room temperature. Following centrifugation, plasma samples were transferred to cryotubes and flash frozen in liquid nitrogen. The samples were kept on ice for approximately one hour until extraction.

Sample extraction and analysis: Extraction of samples was allowed to proceed at -78°C for 20 minutes. Samples were then centrifuged for 5 minutes (16.1 rcf) at 4°C. The supernatant was transferred to new vials and the sample pellet was resuspended in 200 µL of chilled (4°C) extraction solvent. The extraction was allowed to proceed for 15 min at -20°C at which time the samples were centrifuged for 5 min (16.1 rcf) at 4°C. The supernatant was transferred to vials and another 50 µL of extraction solvent was added to the sample pellet where the extraction was repeated once more. Vials containing all of the collected supernatant were dried under a stream of N_2 until the extraction solvent had evaporated. Solid residue was resuspended in 300 µL of

sterile water and transferred to autosampler vials. Samples were immediately placed in autosampler trays for mass spectrometric analysis.

Ultra Performance Liquid Chromatograpy—High Resolution Mass Spectrometric (UPLC-MS) Analysis: Samples were placed in autosampler trays and kept at 4°C. A 10 µL aliquot of each was injected through a Synergi 2.5 micron Hydro-RP 100, 100 x 2.00 mm LC column (Phenomenex) kept at 25°C. The eluent was introduced into the MS via an electrospray ionization source conjoined to a Thermo Scientific Exactive Plus Orbitrap MS through a 0.1 mm internal diameter fused silica capillary tube, and the MS was run in fullscan mode with negative mode ionization using a method adapted from Rabinowitz [44]. Briefly, the samples were run with a spray voltage was 3 kV. The nitrogen sheath gas was set to a flow rate of 10 psi with a capillary temperature of 320°C. AGC target was set to 3e6. The samples were analyzed with a resolution of 140,000 and a scan window of 85 to 800 *m/z* for from 0 to 9 minutes and 110 to 1000 m/z from 9 to 25 minutes. Solvent A consisted of 97:3 water:methanol, 10 mM tributylamine, and 15 mM acetic acid. Solvent B was methanol. The gradient from 0 to 5 minutes was 0% B, from 5 to 13 minutes was 20% B, from 13 to 15.5 minutes was 55% B, from 15.5 to 19 minutes was 95% B, and from 19 to 25 minutes was 0% B with a flow rate of 200 µL/min.

Metabolite feature extraction and data processing: The RAW files generated by the instrumental data collection software Xcalibur (Thermo Scientific) were converted to the mzML format [45] using the ProteoWizard package [46]. The MAVEN software package (Princeton University) was used to automatically align the total ion chromatograms using the retention times of annotated metabolites and other dominant features from each sample [47, 48]. Metabolites were manually identified and integrated using known masses (± 5 ppm mass tolerance) and retention times ($\Delta \leq$ 1.5 min). Metabolite ion counts were normalized via mass for cecum and small intestine samples, and fold changes were calculated between samples. The resulting data were clustered using Cluster 3.0 [49] and heatmaps were then generated from clustered data using Java Treeview [50] software. PCA analyses were performed and figures were generated using the statistical package R along with the ggplot2 [51] and ggbiplot [52] packages. PLS-DA plots were also generated via R along with the mixOmics [53] package using metabolite areas as the predictors and mouse type as the discrete outcomes with a tolerance of 1×10^{-6} and a max iteration of 500.

Yogurt treatment

Antibiotic treated mice were treated orally with an antibiotic cocktail consisting of ampicillin (0.5 mg/ml) (Sigma Aldrich; St. Louis, MO), vancomycin (0.25 mg/ml) (Amnesco; Solon, OH), metronidazole (0.5 mg/ml) (Spectrum Chemical Mfg. Comp.; Gardena, CA), neomycin sulfate (0.5 mg/ml) (EMD Millipore; Billerica, MA), and gentamycin sulfate (0.5 mg/ml) (Corning; Manassas, VA). Mice were treated *ad libitum* for 3 weeks. Water bottles containing the antibiotic cocktail were changed weekly. After 3 weeks antibiotic treatment ceased and half of the antibiotic treated mice were then treated with yogurt for 3 weeks prior to the *P. yoelii* infection. Yogurt was made using a starter culture containing *Lactobacillus bulgaricus*, *L. acidophilus*, *L. lactis, Bifidobacterium lactis*, and *Streptococcus thermophilus* (Yogurt Starter Culture #2, Custom Probiotics, Glendale, CA). In addition, yogurt was enriched with a probiotic powder supplement containing *L. acidophilus*, *L. rhamnosus*, *L. salivarius*, *L. plantarum*, *L. casei*, *L. lactis*, *B. breve*, *B. infantis*, *B. longum*, *B. bifidum*, and *B. lactis* (11 Strain Probiotic Powder, Custom Probiotics, Glendale, CA). Fresh yogurt was made for each treatment by adding the starter culture (1.2 grams) and the probiotic supplement (1.2 grams) to 15 mL of 2% reduced fat milk (Mayfield, Athens, TN) or organic 2% reduced fat milk–antibiotic pretreatment experiment (Organic Valley; La Farge, WI). The yogurt was then incubated at 37°C for 6-8 hours before administration. Mice were treated with yogurt as described in figure legends with 0.2 ml administered by oral gavage.

Isolation and sequencing of Lactobacillus

Fecal pellets from Jackson and NCI mice were processed separately. Pellets were homogenized in buffered saline solution and plated onto lactobacillus selective MRS agar. Plates were subsequently incubated at 37°C in anaerobic culture jars. Single colonies were re-streaked three times to purify the strains. DNA was extracted from bacterial colonies, lab-cultured yogurt, and probiotic powder using the MoBio Powersoil DNA extraction kit (MoBio, Carlsbad, CA) according to the manufacturer's protocols. An approximately 1500 bp segment of the 16S rRNA gene was amplified from isolate DNA, via PCR, using the 9F-1522R primer set. PCR products were purified using the Qiaquick PCR purification kit (Qiagen, Valencia, CA) and sequenced at the University of Tennessee Molecular Biology Resource Facility using Sanger sequencing.

Cellular immune response

Spleens were disrupted to generate single-cell suspensions in Hyclone RPMI 1640 media (Thermo Fisher Scientific Inc., Waltham, MA) supplemented with 10% fetal bovine serum (FBS) (Atlanta Biologicals, Inc., Lawrenceville, GA). RPMI 1640 was also supplemented with 1.19 mg/ml HEPES (Thermo Fisher Scientific Inc., Waltham, MA), 0.2 mg/ml L-glutamine (Research Products International Corp., Mt. Prospect, IL), (0.05 units/ml & 0.05 mg/ml) penicillin/streptomycin (Invitrogen, Grand Island, NY), 0.05 mg/ml gentamicin sulfate (Invitrogen, Grand Island, NY), and 0.05 μM 2-Mercaptoethanol (Thermo Fisher Scientific Inc., Waltham, MA). Single cell suspensions were treated with ammonium chloride potassium to lyse red blood cells. Spleens were harvested as indicated at the number of days post infection.

Cells were stained with Fc block (anti-CD16/32; clone 2.4G2) and the following fluorescence-conjugated antibodies (CD45.2; clone 104, CD4; clone RM4-5, CD8; clone 53-6.7, CD3; clone 17A2, CD19; clone 6D5, Ter119; clone Ter-119, CD11a; clone M17/4, CD49d; clone R1-2, PD-1; clone 29F.1A12, CD95; clone Jo2, GL7; clone GL7, biotion-CXCR5; clone 2G8, CD44; clone IM7) purchased from Biolegend (San Diego, CA) and BD Biosciences (San Diego, CA). For CXCR5 staining cells were stained with biotinylated-CXCR5 for 30 minutes at room temperature prior to staining with fluorescence-conjugated streptavidin. Antibodies were resuspended in FACS buffer (1x PBS, 1% FBS, 0.02% sodium azide) and cells were stained for 30 minutes at 4°C. Following staining cells were fixed and permeabilized with Fixation Buffer (Biolegend, San Diego, California). Cells were acquired through an LSR II (BD Biosciences). Data were analyzed by FlowJo software (Tree Star, Ashland, OR).

Detection of P. yoelii $MSP1_{19}$-specific antibodies

Serum was collected on the indicated days post *P. yoelii* infection and stored at -20°C. MaxiSorp Immuno plates (Thermo Scientific) were coated with 1 μg/ml recombinant $MSP1_{19}$ (The following reagent was obtained through the MR4 as part of the BEI Resources Repository, NIAID, NIH: *Plasmodium yoelii* yP.y.MSP1-19(XL)/VQ1, MRA-48, deposited by DC Kaslow.) Dilutions of serum were added to wells. Total $MSP1_{19}$-specific IgM, IgG1, IgG2b, IgG2c, and IgG3 antibodies were detected with horseradish peroxidase–conjugated goat anti–mouse IgM, IgG1, IgG2b, IgG2c,

and IgG3, respectively, (Jackson ImmunoResearch) and 3,3′,5,5′-tetramethylbenzidine substrate (Arcos Organics). Reactions were stopped by addition of 2M H_2SO_4. Results are presented as average endpoint titers with absorbance readings below 0.1 (absorbance at 450 nm).

Statistical analysis

Descriptive and comparative statistical analyses of data, except the gut microbiota and metabolomics data, were done using GraphPad Software version 6 (La Jolla, CA, USA). The area under the parasitemia curve (AUC) was estimated for each group following the trapezoidal rule with the following equation [54, 55].

$$AUC_{t1\text{-}t\text{-}last} = 0.5 \Sigma (Y_i + Y_{i+1}) * (t_{i+1} - t_i)$$

Where "t" was sampling time and "y" the observed outcome (e.g., % parasitemia).

IV. RESULTS

Mice from different vendors exhibit differential susceptibility to malaria.

Genetically similar inbred strains of mice (C57BL/6) maintained by different vendors (Jackson Laboratories and Taconic) have differences in their gut bacterial communities [32, 33]. To determine whether these differences had any effect on *Plasmodium* infections C57BL/6 mice from Jackson Laboratories (Jax), Taconic (Tac), National Cancer Institute/Charles River (NCI) and Harlan (Har) were infected with *P. yoelii*. Following infection, profound differences in parasitemia (the fraction of red blood cells infected with *P. yoelii*) were observed among the four groups of mice (Figure 4.1A,B). Whereas resistant mice (Jax and Tac) exhibited a maximum of approximately 10% parasitemia, they had no signs of morbidity (weight loss) or mortality, which was in contrast to the substantial weight loss and mortality observed in susceptible mice (NCI and Har) where parasitemia was >60% (Figure 4.1C,D). Moreover, NCI and Har mice exhibited more profound and longer lasting anemia (loss of red blood cells (RBCs) per mL) compared to Jax and Tac mice (Figure 4.S1A). Additionally, when total number of RBCs per mL was used to derive total pathogen burden, similarities were noted between the parasite burden as detected by parasitemia or parasitized RBCs (pRBCs) per mL of blood (Figure 4.S1B-E). Of note, mice infected with different doses of *P. yoelii* pRBCs showed similar parasitemia kinetics between the

different doses and susceptibility to infection (Figure 4.S2) suggesting mice from different vendors are differentially susceptible to progression to severe malaria but not to blood stage infection.

To determine the broader applicability of these data, another mouse strain and two *Plasmodium* species were tested. BALB/c mice from Jax, Tac, Charles River (CR) and Har were infected with *P. yoelii*. Mice were purchased from CR *in lieu* of NCI/CR. Of note, C57BL/6 mice purchased from CR exhibit similar parasitemia and morbidity as NCI mice following infection with *P. yoelii* (Figure 4.S3). Consistent with *P. yoelii* infections in C57BL/6 mice (Figure 4.S3), BALB/c mice from Jax and Tac exhibit reduced *P. yoelii* parasitemia compared to mice from CR and Har (Figure 5.S4A,B). Furthermore, C57BL/6 mice from Jax and Tac exhibited reduced parasitemia compared to CR and Har following *Plasmodium chabaudi* infection (Figure S4.4C,D). Finally, we assessed the development of experimental cerebral malaria (ECM) in C57BL/6 mice infected with *Plasmodium berghei* ANKA. Jax and Tac mice trended towards reduced parasitemia compared to NCI and Har mice at early time points, moreover there was a significant (p=0.04) difference in survival between these groups of mice (Figure 4.S4E,F). In sum, these data indicate the severity of malaria was dependent on the source of mice.

Diet is a strong modulator of organismal health as well as of the gut microbiome and its function [34]. To determine whether the diet could shape the severity of malaria, Jax and NCI mice were fed one of two commercially available rodent diets, either NIH-31 (used in Figure 4.1A-D or Teklad 22/5. Parasitemia in NCI mice was unaffected; however, Jax mice had high levels of parasitemia when fed Teklad 22/5 (Figure 4.1E,F). Consistent with the parasitemia data, Jax mice fed Teklad 22/5 also exhibited substantial weight loss and elevated mortality compared to Jax mice fed NIH-31 (Figure 4.1G,H). Since these diets had no effect on parasite burden in NCI mice, the changes in parasitemia in Jax mice were unlikely due to a direct effect of these diets on the parasite burden. Moreover, high parasite burdens in NCI mice fed NIH-31, suggest this diet supported the proliferative expansion of *P. yoelii*. When Jax and NCI mice were placed on the reciprocal vendor-specific diet and then infected with *P. yoelii* we noted a modest increase in parasite burden in Jax mice fed the NCI in-house diet, but no effect of the Jax in-house diet on NCI mice (Figure 4.S5).

Collectively, these data sets led to the hypothesis that the gut microbiota influenced *Plasmodium* infections.

Gut bacterial community structure and function are different in resistant and susceptible mice.

To directly test for differences in the gut microbiome, sections of the gastrointestinal tract from resistant (Jax and Tac) and susceptible (NCI and Har) mice were collected and the bacterial communities were characterized using 16S rRNA gene analysis (Figure 4.S15). There was a high degree of similarity between the microbial community assemblages found within the cecum and the colon of mice from the same vendor (Figure 4.S6A), while there were clear differences between the microbial communities of these regions compared to the distal half of the small intestine within the same vendor. Moreover, significant differences between mice from all vendors were apparent in the non-metric multidimensional scaling (NMDS) analysis of population structure within the cecum, with the susceptible NCI and Har libraries showing a comparative overlap with each other yet distinct differences when compared to the resistant Jax and Tac communities (Figure 4.S6B). Analysis of the cecal bacterial communities at the family level revealed substantial differences, with Clostridiaceae, Erysipelotrichaceae, Lactobacillaceae, and Peptostreptococcaceae (members of the Firmicutes phylum) being proportionally more abundant in resistant (Jax and Tac) mice, whereas Bacteroidaceae and Prevotellaceae (members of Bacteroidetes phylum), and Sutterellaceae (member of Proteobacteria phylum) were proportionally more abundant in susceptible (NCI and Har) mice (Figure 4.2A,B). Finally, dietary changes are capable of inducing significant changes in the gut microbiome [35] that reach steady state within 3-4 days in mice [36]. Consistent with these reports, we observed defined changes in the gut bacterial communities in Jax mice fed Teklad 22/5 or NIH-31 (Figure 4.S7-S8). In Jax mice fed the Teklad diet, there was a noted decrease in Peptostreptococcaceae below that observed in either Jax or Tac mice resulting in an increased similarity to the susceptible NCI and Har mice (Figure 4.S7C). These changes coincide with a shift in the severity of malaria between these two groups of mice (Figure 4.1E-H).

Consistent with changes in the gut bacterial community, analysis of metabolites in the small intestine, cecum, and plasma of Jax and NCI mice revealed differential expression between each tissue (Figure 4.S9A). An F-test of partial least squared discriminant analysis (PLS-DA) [37] used

to probe variation between metabolite profiles in Jax and NCI mice on a per tissue basis confirmed that the means of the variate-1 (component 1), which differentiated Jax from NCI mice in all tissues, were significantly different ($p \leq 0.0003$, 0.0001, 0.0001) for the small intestine, cecum, and plasma, respectively, (Figure 4.S9B-D; Figure 4.S16). Several metabolites exhibited large (≥1.5 fold) and statistically significant ($p \leq 0.1$) differences between Jax and NCI mice, with the top 25% of metabolites associated with distinct metabolic pathways (Figure 4.S9E,F; Figure 4.S173-S19). Therefore, differences in the gut bacterial populations and metabolites support the hypothesis that the severity of malaria was modulated by differences in gut bacterial communities.

Differences in the gut microbiome shape susceptibility to malaria.

To directly test this hypothesis, genetically identical germ-free (GF) C57BL/6 mice received cecal content transplants from either Jax or NCI mice. Of note, GF C57BL/6J mice exhibited no difference in parasitemia compared to conventional C57BL/6J mice following infection with *P. yoelii* nigeriensis [38]. Sequence analyses demonstrated the bacterial communities in colonized, germ-free mice reflected that of the donor communities and were different than the communities in germ-free mice exposed to only environmental microbes (Figure 4.3A). Furthermore, there was only a slight decrease in community diversity between respective donor and colonized germ-free mice (Figure 4.S10). Following *P. yoelii* infection, germ-free mice that received either Jax or NCI cecal transplants had parasite burdens similar to control Jax and NCI mice (Figure 4.3B,C). Both NCI control mice and germ-free mice that received NCI cecal transplants also had decreased survival compared to the Jax control mice and germ-free mice that received Jax cecal transplants (Figure 4.3D). Collectively, these data provided a direct demonstration that the severity of malaria was modulated by the gut microbiota.

Decreased parasite burden in mice treated with Lactobacillus and Bifidobacterium.

To identify individual microbial phylotypes that may shape the severity of malaria, a deeper analysis was performed on the bacterial communities in the cecum. When pooled by resistance (Jax/Tac) or susceptibility (NCI/Har) to *P. yoelii,* several phylotypes (referred to here as Operational Taxonomic Units, OTUs) emerged from a linear discriminant analysis (LDA) effect size (LEfSe)-driven analysis [39] as biomarkers of the resistant or susceptible phenotype. Among

those differences, *Lactobacillus* and *Bifidobacterium* were overly abundant in the resistant mice compared to susceptible mice (Figure 4.S11), with differences in *Lactobacillus* being the greatest driver of the differential community structure between resistant and susceptible mice (Figure 4.S11B).

To evaluate the linkage between *Lactobacillus* and *Bifidobacterium* towards resistance to severe malaria, Jax and NCI mice were treated with lab-cultured yogurt supplemented with probiotics that contained *Lactobacillus* and *Bifidobacterium* species prior to and following infection with *P. yoelii*. DNA sequencing of *Lactobacillus* isolated from fecal pellets from Jax and NCI mice or lab-cultured yogurt demonstrated phylogenetic congruence (Figure 4.S12). Consumption of *Lactobacillus* and *Bifidobacterium* can modulate the gut microbial community structure [40] or function [41]. Following infection with *P. yoelii,* both Jax and NCI mice treated with yogurt had a modest, but significant (Jax $p<0.0001$; NCI $p=0.0418$), decrease in parasite burden compared to control untreated mice (Figure 4.S13). Jax and NCI mice treated with milk used to make the yogurt showed a similar parasite burden as control Jax and NCI mice (mean $AUC_{Day\ 5\text{-}34}$: Jax control (n=4) 107.2±11.39 (S.D.) versus Jax milk (n=4) 83.55±24.83 (S.D.) $p = 0.13$; NCI control (n=4) 447.1±85.65 (S.D.) versus NCI milk (n=3) 384.8±73.08 (S.D.) $p = 0.36$). However, when mice were treated with antibiotics prior to yogurt treatment we observed a profound decrease (14-fold) in parasite burden in the susceptible NCI mice (Figure 4.4A-B), and no weight loss in those mice was noted when compared to the other NCI groups (Figure 4.4C). These data support the ability of *Lactobacillus* and *Bifidobacterium* to contribute towards the modulation of *Plasmodium* parasite burden, yet other constituents of the gut microbiota may also contribute to regulating the severity of malaria.

Severity of malaria tracts with the magnitude of the host immune response.

The gut microbiota can shape host immunity to systemic viral infections [19], and T follicular helper (Tfh) produced IL-21 is required for GC B cell help and clearance of murine *Plasmodium* infections [42]. Consistent with these observations, resistant Jax mice exhibited an elevated *P. yoelii*-specific CD4+ T cell ($CD49d^{hi}CD11a^{hi}$ [293], Tfh cell, and GC B cell responses compared to susceptible NCI mice (Figure 5.5A-C; Figure 5.S14). Jax and NCI mice had similar titers of

IgM specific for the 19-kDa fragment of merozoite surface protein 1 ($MSP1_{19}$) from *P. yoelii* (Figure 4.5D), suggesting similar activation of B cell in both groups. In contrast, Jax mice exhibited accelerated antibody class switching from $MSP1_{19}$-specific IgM to IgG isotypes, 4- to 10-fold higher titers at day 14 post-infection, compared to NCI mice (Figure 4.5D). Thus, one mechanism by which the gut microbiome shapes the severity of malaria following *P. yoelii* infection may be through modulation of the host immune response.

V. DISCUSSION

This study demonstrates that the murine gut microbiome influences the parasite burden of *Plasmodium* rodent species and modulates the severity of malaria in mice. Importantly, parasite burden is currently the best-known correlate of disease severity following *P. falciparum* infection in humans [24, 25]. An association between the gut microbial community and *Plasmodium* parasites has been previously recognized in the mosquito vector [44-48]. Interestingly, the unique assemblage of skin bacteria on human skin, and particularly volatiles produced by these bacteria, have also been shown to impact the attractiveness of *Anopheles* mosquitoes to particular individuals [49-51].

Studies that followed this work further support that the gut microbiota affects mammalian stages of the *Plasmodium* life cycle. Overall, the studies concluded that malarial infection reshapes the gut microbiome via influencing parasite fitness [52]. One study demonstrated that specific gut bacteria could impact the transmission of *P. berghei* sporozoites from mosquitos to mice [26]. The authors showed that the gut pathobiont, *E. coli* O86:B7, induced the production of anti-α-gal antibodies. When *Plasmodium*-infected mosquitoes injected sporozoites into the dermal tissue during a blood meal the anti-α-gal antibodies bound to the *Plasmodium* sporozoites, which prevented their migration to the liver [26]. These results also extended to humans where the presence of anti-α-gal IgM antibodies correlated with protection against *P. falciparum* infection. The effect of *E. coli* O86:B7 on *Plasmodium* infection was limited to transmission of sporozoites as there was no effect of the anti-α-gal antibodies on *the symptomatic blood stage of the infection.* Consistent with these findings, another report demonstrated that the unique composition of stool bacteria in Malian children correlated with prospective risk of *P. falciparum* infection, although

not progression to febrile malaria [27]. Although the mechanism responsible for this observation is unknown, the similarities between these two studies (i.e., susceptibility to infection but not severity of blood stage infection) suggest the prospective risk of *P. falciparum* infection differentiated by stool bacteria composition may be attributed to differences in anti-α-gal IgM antibodies. In contrast to the details of the two publications described above, we show that the gut microbiota modulates the severity of *P. yoelii* blood stage infections in mice, implying a novel and independent mechanism. Moreover, our findings show that the influence of the gut microbiome on *Plasmodium* infections is broad and not limited to the transmission of the parasite. Taken together our observation and those of Yilmaz et al. [26], result in the intriguing speculation that the human intestinal microbiota might impact different stages of the *Plasmodium* life cycle in humans. In conclusion, our findings confirm and support the ability of the gut microbiome to affect *Plasmodium* parasite fitness.

One potential mechanism by which the gut microbiota regulates the severity of malaria is a direct effect on the parasite itself where gut microbiota-derived products either promote or inhibit its growth. Whereas this possibility has not been formally excluded, we observe similar parasitemia expansion kinetics, when plotted on a log-scale, between days 5 and 11 post-infection in both resistant and susceptible mice. This observation suggests that the gut microbiota does not have a direct effect on the parasite. Consequently, it is more likely that the gut microbiota impacts the severity of malaria by modulating the host immune response to *Plasmodium*. Consistent with this possibility, resistant Jax mice exhibited an elevated anti-*Plasmodium* immune response compared to susceptible NCI mice. While these data correlate with the parasite burden in these mice, further experiments will be necessary to demonstrate the differential immune response is responsible for the difference in severity, and if so, how the gut microbiota modulates the host immune response to this extra-gastrointestinal infection. It has been previously shown that the gut microbiome provides signals to monocytes/macrophages that primed those cells to respond to and help control systemic lymphocytic choriomeningitis virus infections [19]. Whether the gut microbiome modulates host immunity to *Plasmodium* through similar or different effects on the host immune system remains to be determined.

As mentioned above, diet has a major role in shaping the composition and activity of the gut microbiota [35, 53, 54]. Consequently, manipulating the structure and function of these complex communities through the diet provides an opportunity to manipulate the host immune system [53]. In our study, we identified that *Lactobacillus* and *Bifidobacterium* species in cecal content could have a protective role by modulating the parasite burden and attenuating the severity of the disease. It is also possible that these bacterial genera correlate with decreased parasitemia through niche competition that decreases the abundance of bacterial genera that cause elevated parasitemia. Since antibiotic treatment followed by yogurt treatment triggered a 14-fold reduction in parasite burden in susceptible mice, the results suggest that through optimization (*e.g*., identifying and treating with the most effective 'protective' bacterial species or eliminating bacteria that contribute to high parasitemia), modulating the gut microbiome has the potential be a novel prophylaxis to prevent severe malaria. Consistent with this possibility, prior work has shown that children in a rural African village in Burkina Faso have an enrichment of the Bacteroidetes phylum and a depletion of the Firmicutes phylum, which contains *Lactobacillus*, compared to European children [55]. This resembles the community structure in susceptible mice that have increased Bacteroidetes and reduced Firmicutes compared to resistant mice (Figure 4.4S11). Therefore, the commonality between the bacterial community structure in African children and *Plasmodium* susceptible mice suggests the possibility that probiotic modulation of the gut microbiota in mice to control severe malaria may work in humans. To that end, there is great opportunity for future studies aimed at development of feasible and tractable probiotic interventions. The plant microbiome is known to house bacterial taxa protective against *Plasmodium* infection, namely Firmicutes [56]. Yet to be explored are the viability and effectiveness of the use of edible or agricultural plants as probiotics. Studies designed to determine plant colonization of mammalian immune-beneficial microbe and subsequent survival through the mammalian gastrointestinal tract are lacking.

This report demonstrates the novel observation that the severity of malaria in mice is profoundly impacted by the composition of the gut microbiota. The data lead to the hypothesis that differences in the gut microbiota may explain why some humans infected with *Plasmodium* progress to severe disease while others do not. The results also support the possibility that manipulating the gut

microbiota has the potential to control the severity of malaria in humans. Whereas modulating the gut microbiota may not prevent *Plasmodium* infections, altering the gut microbiome has the potential to ameliorate severe disease and save thousands of lives annually.

VI. ACKNOWLEDGEMENTS

We thank Bruce Applegate and Whitney Powell for technical assistance. The authors thank Dr. Sarah Lebeis and Dr. Yousef Abu Kwaik for reviewing the manuscript. This work was supported by grants from the NIH (1R21AI113386) and the American Cancer Society (Research Scholar Grant, RSG-14-057-01-MPC) (N.W.S.), and the Kenneth & Blair Mossman Professorship (S.W.W.). The National Gnotobiotic Rodent Resource Center at the University of North Carolina-Chapel Hill was supported by 5-P39-DK034987 and 5-P40-OD010995.

VII. REFERENCES

1. Hacquard, S., et al., *Microbiota and Host Nutrition across Plant and Animal Kingdoms.* Cell Host Microbe, 2015. **17**(5): p. 603-16.
2. Groussin, M., et al., *Unraveling the processes shaping mammalian gut microbiomes over evolutionary time.* Nature Communications, 2017. **8**.
3. Finkel, O.M., et al., *Understanding and exploiting plant beneficial microbes.* Current Opinion in Plant Biology, 2017. **38**: p. 155-163.
4. Honda, K. and D.R. Littman, *The microbiome in infectious disease and inflammation.* Annual review of immunology, 2012. **30**: p. 759-95.
5. Turnbaugh, P.J., et al., *An obesity-associated gut microbiome with increased capacity for energy harvest.* Nature, 2006. **444**(7122): p. 1027-31.
6. Wen, L., et al., *Innate immunity and intestinal microbiota in the development of Type 1 diabetes.* Nature, 2008. **455**(7216): p. 1109-13.
7. Hsiao, E.Y., et al., *Microbiota modulate behavioral and physiological abnormalities associated with neurodevelopmental disorders.* Cell, 2013. **155**(7): p. 1451-63.
8. Johnson, C.C., et al., *Antibiotic exposure in early infancy and risk for childhood atopy.* The Journal of allergy and clinical immunology, 2005. **115**(6): p. 1218-24.
9. Joffe, T.H. and N.A. Simpson, *Cesarean section and risk of asthma. The role of intrapartum antibiotics: a missing piece?* The Journal of pediatrics, 2009. **154**(1): p. 154.
10. Fujimura, K.E., et al., *House dust exposure mediates gut microbiome Lactobacillus enrichment and airway immune defense against allergens and virus infection.* Proceedings of the National Academy of Sciences of the United States of America, 2014. **111**(2): p. 805-10.
11. Manichanh, C., et al., *Reduced diversity of faecal microbiota in Crohn's disease revealed by a metagenomic approach.* Gut, 2006. **55**(2): p. 205-11.
12. Frank, D.N., et al., *Molecular-phylogenetic characterization of microbial community imbalances in human inflammatory bowel diseases.* Proceedings of the National Academy of Sciences of the United States of America, 2007. **104**(34): p. 13780-5.
13. Peterson, D.A., et al., *Metagenomic approaches for defining the pathogenesis of inflammatory bowel diseases.* Cell host & microbe, 2008. **3**(6): p. 417-27.

14. Nicholson, J.K., et al., *Host-gut microbiota metabolic interactions.* Science, 2012. **336**(6086): p. 1262-7.
15. Kamada, N., et al., *Control of pathogens and pathobionts by the gut microbiota.* Nature Immunology, 2013. **14**(7): p. 685-690.
16. Benson, A., et al., *Gut commensal bacteria direct a protective immune response against Toxoplasma gondii.* Cell host & microbe, 2009. **6**(2): p. 187-96.
17. Naik, S., et al., *Compartmentalized control of skin immunity by resident commensals.* Science, 2012. **337**(6098): p. 1115-9.
18. Hassani, M.A., P. Duran, and S. Hacquard, *Microbial interactions within the plant holobiont.* Microbiome, 2018. **6**.
19. Abt, M.C., et al., *Commensal bacteria calibrate the activation threshold of innate antiviral immunity.* Immunity, 2012. **37**(1): p. 158-70.
20. Shi, N., et al., *Interaction between the gut microbiome and mucosal immune system.* Military Medical Research, 2017. **4**.
21. Yoo, B.B. and S.K. Mazmanian, *The Enteric Network: Interactions between the Immune and Nervous Systems of the Gut.* Immunity, 2017. **46**(6): p. 910-926.
22. Murray, C.J., et al., *Global malaria mortality between 1980 and 2010: a systematic analysis.* Lancet, 2012. **379**(9814): p. 413-31.
23. Crompton, P.D., et al., *Malaria immunity in man and mosquito: insights into unsolved mysteries of a deadly infectious disease.* Annu Rev Immunol, 2014. **32**: p. 157-87.
24. Dondorp, A.M., et al., *Estimation of the total parasite biomass in acute falciparum malaria from plasma PfHRP2.* PLoS Med, 2005. **2**(8): p. e204.
25. Hanson, J., et al., *Relative contributions of macrovascular and microvascular dysfunction to disease severity in falciparum malaria.* J Infect Dis, 2012. **206**(4): p. 571-9.
26. Yilmaz, B., et al., *Gut Microbiota Elicits a Protective Immune Response against Malaria Transmission.* Cell, 2014. **159**(6): p. 1277-89.
27. Yooseph, S., et al., *Stool microbiota composition is associated with the prospective risk of Plasmodium falciparum infection.* BMC Genomics, 2015. **16**(1): p. 631.
28. Berendsen, R.L., et al., *Disease-induced assemblage of a plant-beneficial bacterial consortium.* Isme Journal, 2018. **12**(6): p. 1496-1507.

29. Huang, S.C. and Y.J. Yang, *Probiotics-containing yogurt ingestion modulates systemic cellular and humoral immunity in children.* Journal of Immunology, 2012. **188**.
30. Carter, G.M., et al., *Probiotics in Human Immunodeficiency Virus Infection: A Systematic Review and Evidence Synthesis of Benefits and Risks.* Open Forum Infectious Diseases, 2016. **3**(4).
31. Pu, F.F., et al., *Yogurt supplemented with probiotics can protect the healthy elderly from respiratory infections: A randomized controlled open-label trial.* Clinical Interventions in Aging, 2017. **12**: p. 1223-1231.
32. Ivanov, II, et al., *Specific microbiota direct the differentiation of IL-17-producing T-helper cells in the mucosa of the small intestine.* Cell host & microbe, 2008. **4**(4): p. 337-49.
33. Ivanov, II, et al., *Induction of intestinal Th17 cells by segmented filamentous bacteria.* Cell, 2009. **139**(3): p. 485-98.
34. David, L.A., et al., *Diet rapidly and reproducibly alters the human gut microbiome.* Nature, 2014. **505**(7484): p. 559-63.
35. Turnbaugh, P.J., et al., *The effect of diet on the human gut microbiome: a metagenomic analysis in humanized gnotobiotic mice.* Science translational medicine, 2009. **1**(6): p. 6ra14.
36. Carmody, R.N., et al., *Diet dominates host genotype in shaping the murine gut microbiota.* Cell Host Microbe, 2015. **17**(1): p. 72-84.
37. Perez-Enciso, M. and M. Tenenhaus, *Prediction of clinical outcome with microarray data: a partial least squares discriminant analysis (PLS-DA) approach.* Human genetics, 2003. **112**(5-6): p. 581-92.
38. Mooney, J.P., et al., *Inflammation-associated alterations to the intestinal microbiota reduce colonization resistance against non-typhoidal Salmonella during concurrent malaria parasite infection.* Sci Rep, 2015. **5**: p. 14603.
39. Segata, N., et al., *Metagenomic biomarker discovery and explanation.* Genome biology, 2011. **12**(6): p. R60.
40. Cox, M.J., et al., *Lactobacillus casei abundance is associated with profound shifts in the infant gut microbiome.* PloS one, 2010. **5**(1): p. e8745.

41. McNulty, N.P., et al., *The impact of a consortium of fermented milk strains on the gut microbiome of gnotobiotic mice and monozygotic twins.* Science translational medicine, 2011. **3**(106): p. 106ra106.
42. Perez-Mazliah, D., et al., *Disruption of IL-21 Signaling Affects T Cell-B Cell Interactions and Abrogates Protective Humoral Immunity to Malaria.* PLoS Pathog, 2015. **11**(3): p. e1004715.
43. Butler, N.S., et al., *Therapeutic blockade of PD-L1 and LAG-3 rapidly clears established blood-stage Plasmodium infection.* Nature immunology, 2012. **13**(2): p. 188-95.
44. Azambuja, P., E.S. Garcia, and N.A. Ratcliffe, *Gut microbiota and parasite transmission by insect vectors.* Trends Parasitol, 2005. **21**(12): p. 568-72.
45. Dong, Y., F. Manfredini, and G. Dimopoulos, *Implication of the mosquito midgut microbiota in the defense against malaria parasites.* PLoS Pathog, 2009. **5**(5): p. e1000423.
46. Cirimotich, C.M., et al., *Natural microbe-mediated refractoriness to Plasmodium infection in Anopheles gambiae.* Science, 2011. **332**(6031): p. 855-8.
47. Boissiere, A., et al., *Midgut microbiota of the malaria mosquito vector Anopheles gambiae and interactions with Plasmodium falciparum infection.* PLoS Pathog, 2012. **8**(5): p. e1002742.
48. Bahia, A.C., et al., *Exploring Anopheles gut bacteria for Plasmodium blocking activity.* Environ Microbiol, 2014. **16**(9): p. 2980-94.
49. Verhulst, N.O., et al., *Cultured skin microbiota attracts malaria mosquitoes.* Malar J, 2009. **8**: p. 302.
50. Verhulst, N.O., et al., *Composition of human skin microbiota affects attractiveness to malaria mosquitoes.* PLoS One, 2011. **6**(12): p. e28991.
51. Busula, A.O., et al., *Variation in host preferences of malaria mosquitoes is mediated by skin bacterial volatiles.* Medical and Veterinary Entomology, 2017. **31**(3): p. 320-326.
52. Ippolito, M.M., et al., *Malaria and the microbiome: a systematic review.* Clinical infectious diseases : an official publication of the Infectious Diseases Society of America, 2018.
53. Kau, A.L., et al., *Human nutrition, the gut microbiome and the immune system.* Nature, 2011. **474**(7351): p. 327-36.

54. Brestoff, J.R. and D. Artis, *Commensal bacteria at the interface of host metabolism and the immune system.* Nat Immunol, 2013. **14**(7): p. 676-84.
55. De Filippo, C., et al., *Impact of diet in shaping gut microbiota revealed by a comparative study in children from Europe and rural Africa.* Proceedings of the National Academy of Sciences of the United States of America, 2010. **107**(33): p. 14691-6.
56. Turner, T.R., E.K. James, and P.S. Poole, *The plant microbiome.* Genome Biology, 2013. **14**(6).

VIII. APPENDIX: FIGURES

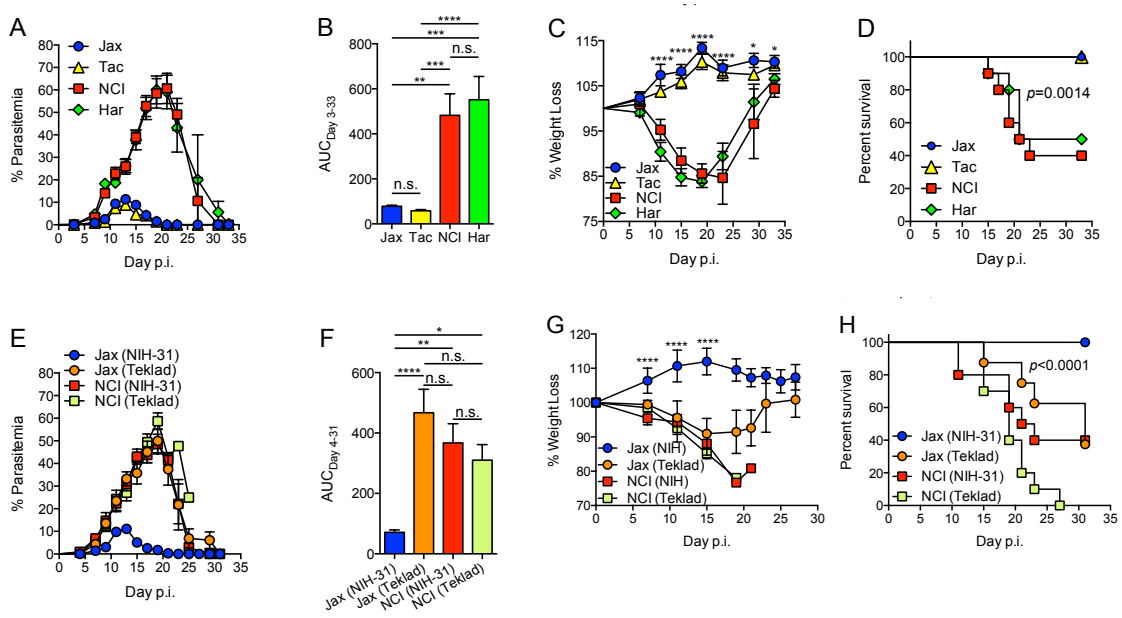


Figure 4.1. Plasmodium parasite burden, morbidity and mortality vary by mouse vendor and diet.

C57BL/6 mice were infected with *P. yoelii* parasitized red blood cells. (A) Fraction of red blood cells infected with *P. yoelii* (% parasitemia). (B) Area under the parasitemia curve (AUC) analysis. Data were analyzed by one-way ANOVA and Tukey's multiple comparison post-test. (C) Percent weight loss following infection. Data were analyzed by one-way ANOVA. (D) Survival of mice following infection. Survival curves were analyzed by Log-rank (Mantel-Cox) test. (E-H) Mice were fed either NIH-31 or Teklad 22/5 diets before and after *P. yoelii* infection. (E) Percent parasitemia following *P. yoelii* infection. (F) AUC analysis. Data were analyzed by one-way ANOVA and Tukey's multiple comparison post-test. (G) Percent weight loss following infection. Data were analyzed by one-way ANOVA. (H) Survival of mice following infection. Survival curves were analyzed by Log-rank (Mantel-Cox) test. (A-F, H) Data (mean±S.E.) are cumulative results (n=8-10 mice/group) from two experiments. (G) Data (mean±S.D.) are from 4-5 mice per group from one experiment. * $p < 0.05$, ** $p < 0.01$, *** $p < 0.001$, **** $p < 0.0001$, n.s. = not significant.

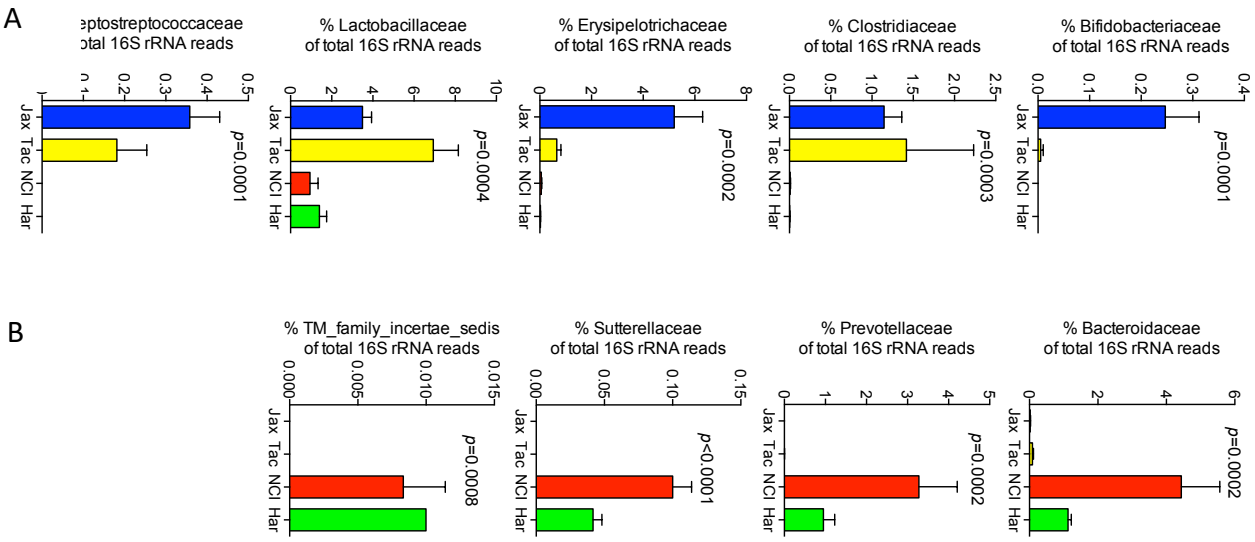


Figure 4.2. Susceptibility to malaria correlates with differences in cecal bacteria populations.

(A) Bacterial families that were identified as being significantly enriched in Jackson or Taconic mice. (B) Bacterial families identified as being significantly enriched in NCI or Harlan mice. (A-B) Data (mean±S.E.) are from 6 mice per group and extracted from analysis in Figure S6c. Data were analyzed by Kruskal-Wallis test.

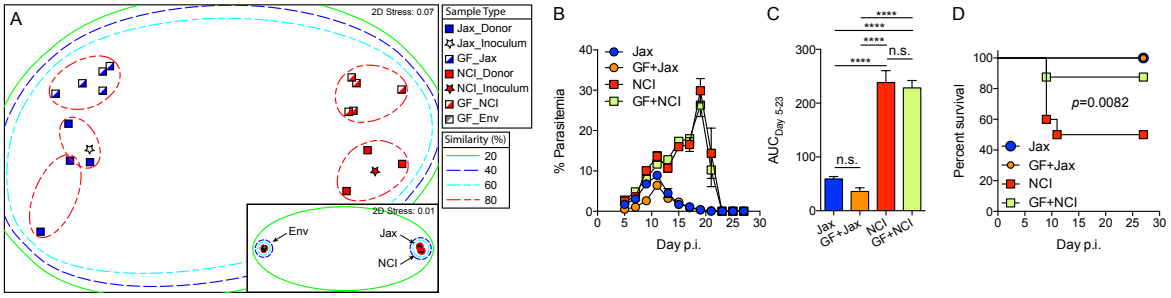


Figure 4.3. Gut microbiome shapes susceptibility to severe malaria.

Germ-free mice were colonized with cecal contents from Jax or NCI mice. (A) Bacterial population analysis was performed using NMDS, as described in Figure S6. (B-D) Colonized germ-free mice and control Jax and NCI mice were infected with *P. yoelii*. (B) Percent parasitemia following *P. yoelii* infection. (C) AUC analysis. (B-C) Data (mean±S.E.) from 4-5 mice/group are representative of two experiments. Data were analyzed by one-way ANOVA and Tukey's multiple comparison post-test. (D) Survival of mice following infection. Data are cumulative results (n=8-10 mice/group) from two experiments. Survival curves were analyzed by Log-rank (Mantel-Cox) test. **** $p < 0.0001$, n.s. = not significant.

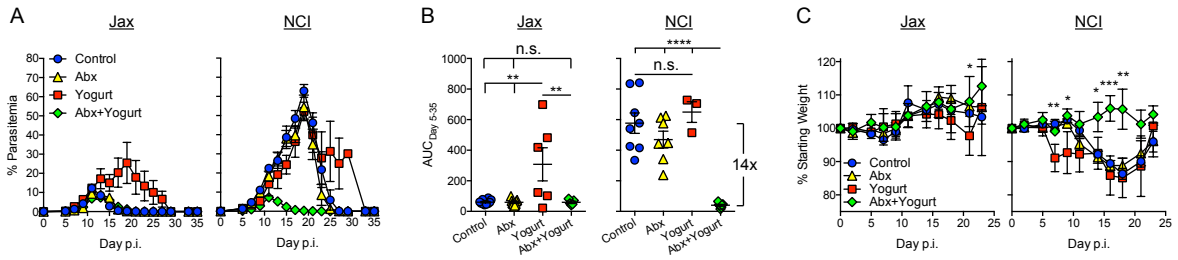


Figure 4.4. Susceptible mice treated with yogurt have decreased parasitemia and morbidity.

Jax and NCI mice were left untreated (control), treated with antibiotics for three-weeks then left untreated for three additional weeks (Abx), left untreated for three-weeks followed by treatment with yogurt 5 times per week for three-weeks (Yogurt), or treated with antibiotics for three-weeks followed by treatment with yogurt 5 times per week for three-weeks (Abx+Yogurt). Mice were then infected with *P. yoelii*. Yogurt treated mice continued to receive yogurt 5 times per week following infection. (A) Percent parasitemia following *P. yoelii* infection. (B) AUC analysis. Data were analyzed by one-way ANOVA and Tukey's multiple comparison post-test. (C) Percent weight loss following infection. Data were analyzed by one-way ANOVA. (A-C) Data (mean±S.E.) are cumulative results (n=3-10 mice/group) from two experiments. * $p < 0.05$, ** $p < 0.01$, *** $p < 0.001$, **** $p < 0.0001$, n.s. = not significant.

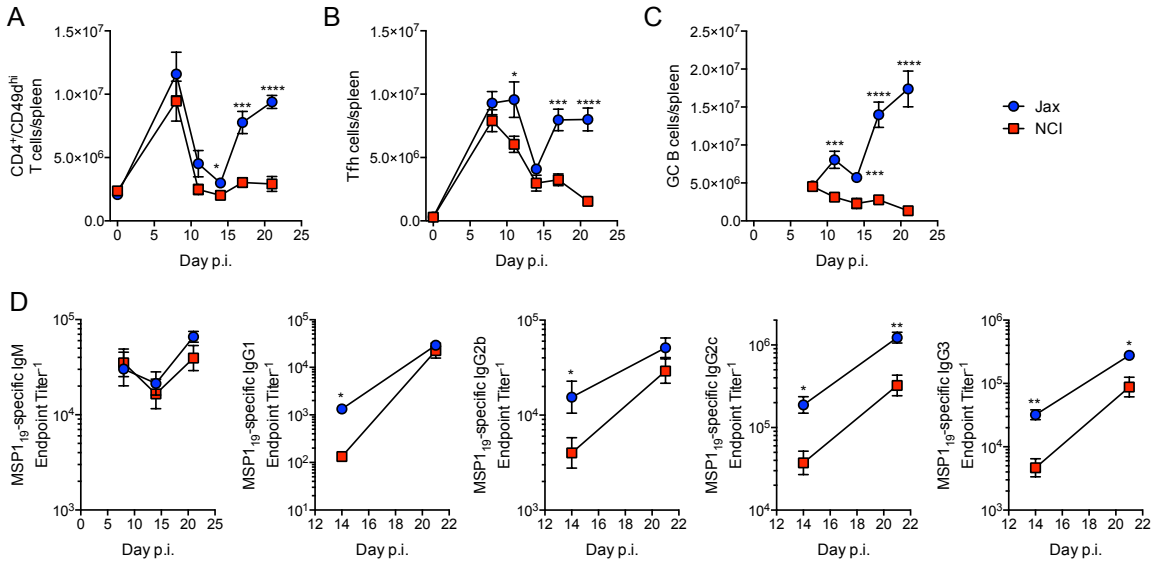


Figure 4.5. Resistant Jax mice have an elevated cellular and humoral immune response to Plasmodium.

Jax and NCI mice were infected with *P. yoelii*. Total number of CD4+CD11ahiCD49dhi cells (A) T follicular helper cells (B) and germinal center (GC) B cells (C) per spleen on the indicated day. Data (mean±S.E.) are cumulative results (n=5-10 mice/data point) from three experiments. (D) Serum $MSP1_{19}$-specific antibody endpoint titers. Data (mean±S.E.) are cumulative results (n=3-7 mice/data point) from two experiments. Numbers in the panels represent the fold difference between the means of the Jax and NCI mice. Data were analyzed by unpaired two-tailed *t* test. * $p < 0.05$, ** $p < 0.01$, *** $p < 0.001$, **** $p < 0.0001$

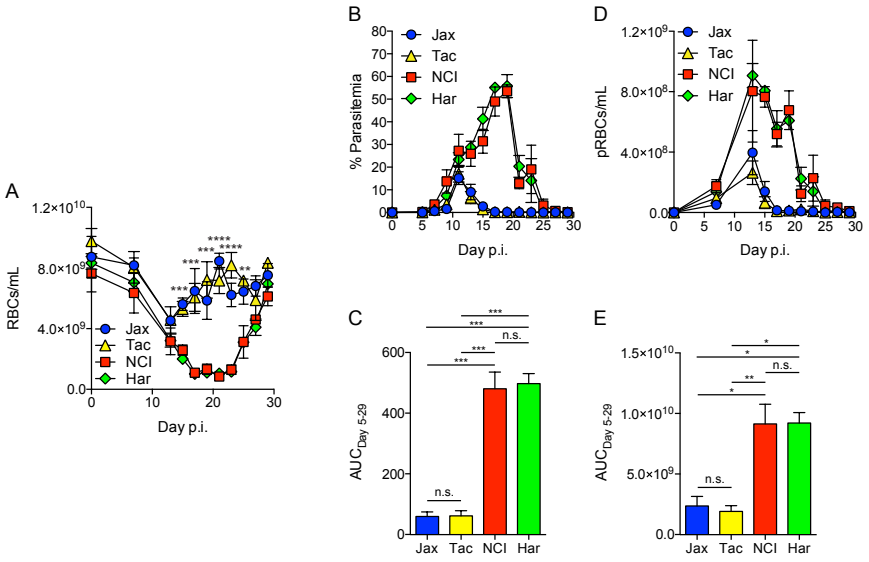
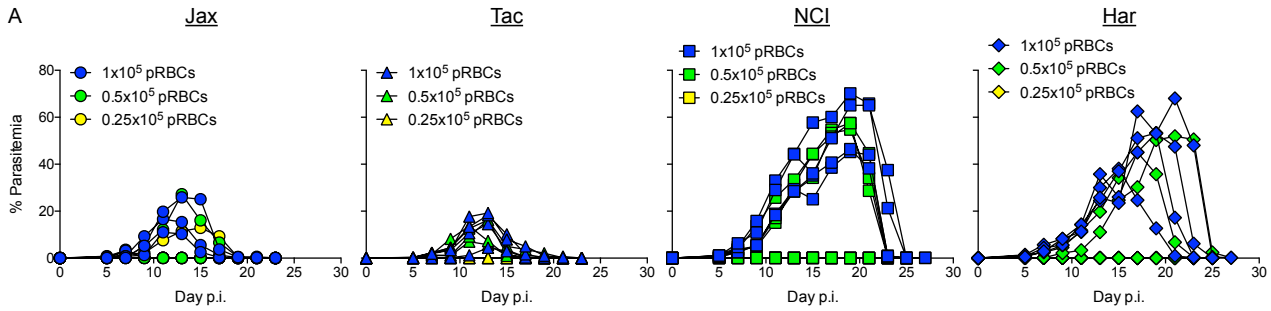


Figure 4.S1. Differential anemia and circulating parasitized red blood cells between mice from different vendors.

C57BL/6 mice were infected with 1x10^5 *P. yoelii* parasitized red blood cells. (A) Number of red blood cells (RBCs) per mL of blood. (B) Fraction of red blood cells infected with *P. yoelii* (% parasitemia). (C) Percent parasitemia AUC analysis. (D) Number of parasitized red blood cells (pRBCs) per mL of blood. (E) pRBCs/mL of blood AUC analysis. (A-E) Data (mean±S.E.) are from 3-4 mice/group. (A,C, and E) Data were analyzed by one-way ANOVA and Tukey's multiple comparison post-test. * $p < 0.05$, ** $p < 0.01$, *** $p < 0.001$, **** $p < 0.0001$, n.s. = not significant.



B

	Jax	Tac	NCI	Har	
	Infected/Total	Infected/Total	Infected/Total	Infected/Total	Fischer's Exact Test
1.00x10^5 pRBCs	7/8	8/8	8/8	6/8	6/8 vs. 8/8 p = 0.47
0.50x10^5 pRBCs	5/8	6/8	4/8	3/8	3/8 vs. 6/8 p = 0.31
0.25x10^5 pRBCs	2/8	2/8	0/8	0/8	0/8 vs. 2/8 p = 0.47

Figure 4.S2. Similar susceptibility to parasitized red blood cell infection between C57BL/6 mice from different vendors.

C57BL/6 mice from the indicated vendors were infected with the indicated number of *P. yoelii* parasitized red blood cells (pRBCs). (A) Fraction of RBCs infected with *P. yoelii* (% parasitemia). Each line represents parasitemia kinetics from an individual mouse (n=4 mice/dose/vendor). Data are representative of two experiments. (B) Number of mice from each vendor infected with the indicated dose of pRBCs and the total number of mice injected. Data are cumulative results from two experiments. Susceptibility to infection at the different doses between vendors was analyzed by two-tailed Fisher's Exact Test.

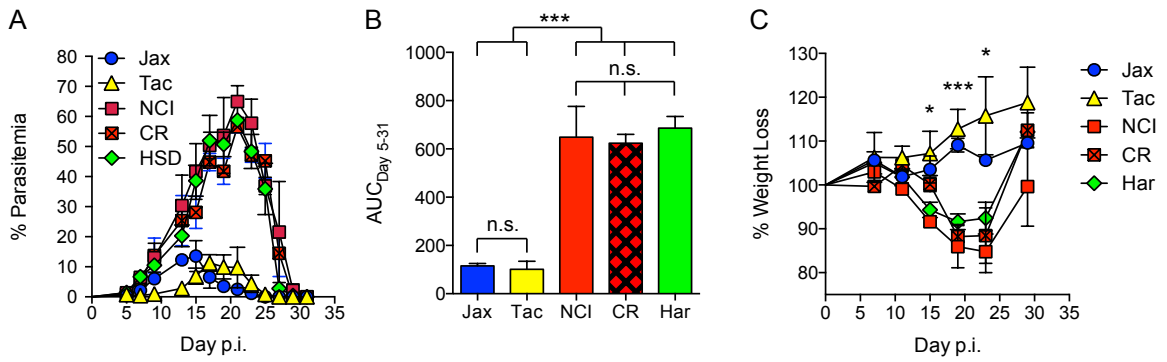


Figure 4.S3. C57BL/6 mice from Charles River are susceptible to high P. yoelii parasite burden.

C57BL/6mice were infected with 1x10^5 *P. yoelii* parasitized red blood cells. (A) Fraction of red blood cells infected with *P. yoelii* (% parasitemia). (B) Area under the parasitemia curve (AUC) analysis. Data were analyzed by one-way ANOVA and Tukey's multiple comparison test. (C) Percent weight loss following infection. Data were analyzed by one-way ANOVA. (A-C) Data (mean±S.E.) are from 3-5 mice/group and representative of two experiments. * $p < 0.05$, *** $p < 0.001$, n.s. = not significant.

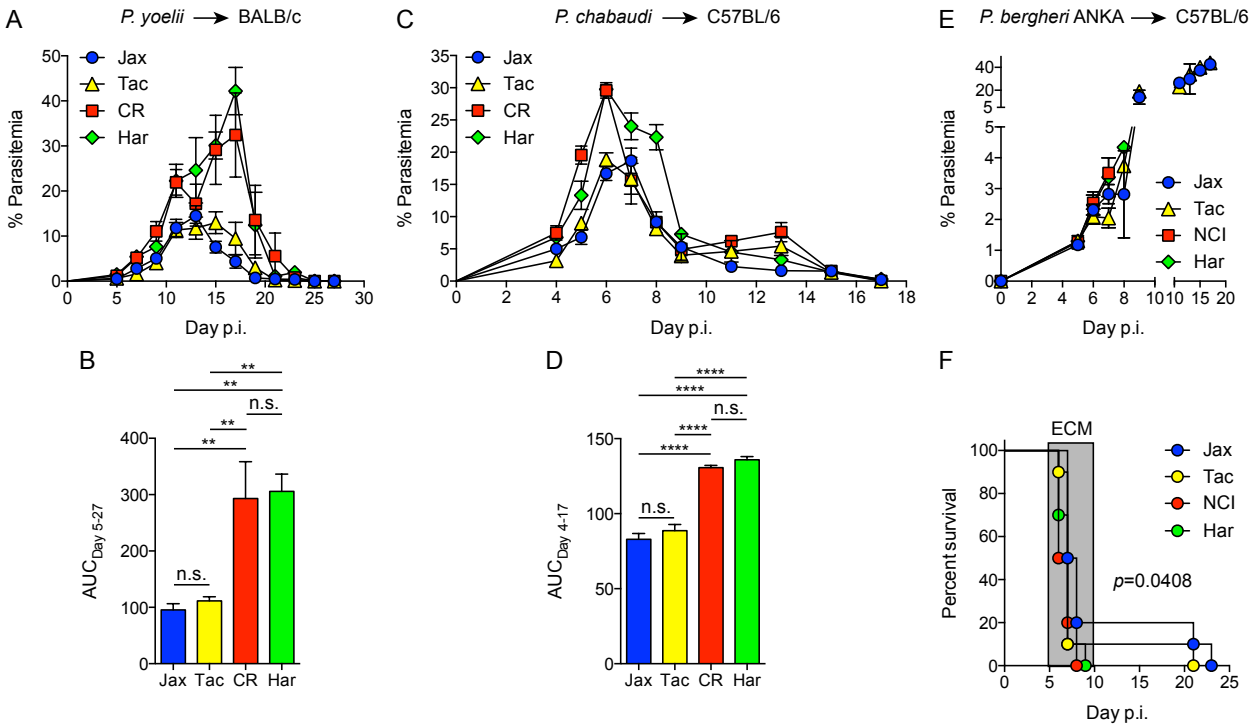


Figure 4.S4. Modulation of malaria pathogenesis by the gut microbiota is generalizable to another mouse strain and Plasmodium species.

Figure (A-B) BALB/c mice were infected with 1x10^5 *P. yoelii* parasitized red blood cells. (A) Fraction of red blood cells infected with *P. yoelii* (% parasitemia). (B) Area under the parasitemia curve (AUC) analysis. Data were analyzed by one-way ANOVA and Tukey's multiple comparison test. (A-B) Data (mean±S.E.) are cumulative results (n=8 mice/group) from two experiments. (C-D) C57BL/6 mice were infected with 1x10^5 *P. chabaudi* parasitized red blood cells. (C) Fraction of red blood cells infected with *P. chabaudi* (% parasitemia). (D) Area under the parasitemia curve (AUC) analysis. Data were analyzed by one-way ANOVA and Tukey's multiple comparison test. (C-D) Data (mean±S.E.) are from 3-4 mice/group and representative of two experiments. (E-F) C57BL/6 mice were infected with 1x10^5 *P. berhgei* ANKA parasitized red blood cells. (E) Fraction of red blood cells infected with *P. berghei* (% parasitemia) from surviving mice. Data (mean±S.E.) are cumulative results (n=10 mice/group) from two experiments. (F) Survival of mice following infection (n=10 mice/group). Survival curves were analyzed by Log-rank (Mantel-Cox) test. ** $p < 0.01$, **** $p < 0.0001$, n.s. = not significant.

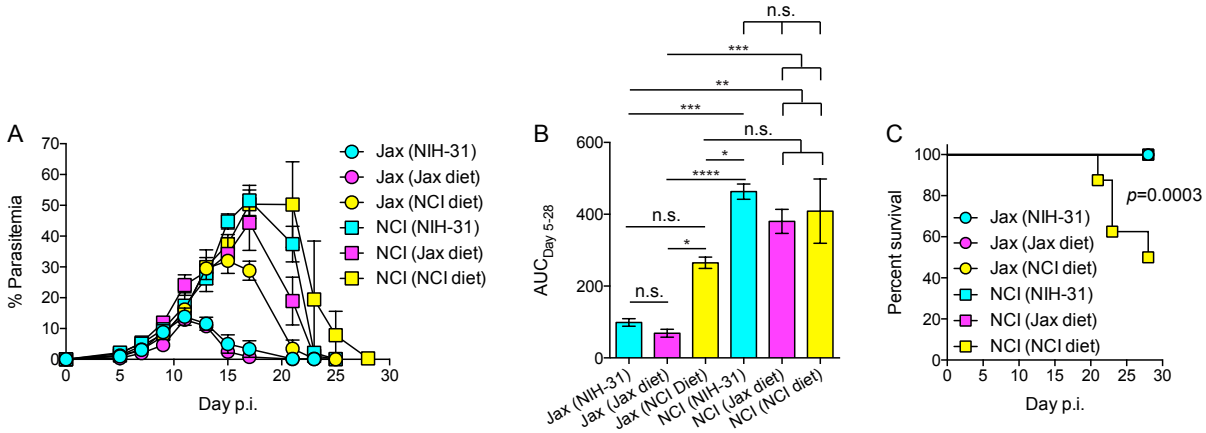


Figure 4.S5. Inversion of Jax and NCI in-house diets minimally effects severity of P. yoelii infection.

C57BL/6 mice were placed on one of three different rodent chows; NIH-31, Jax in-house diet, or NCI in-house diet, for one-week prior to infection through resolution of infection. Mice were infected with $1x10^5$ *P. yoelii* parasitized red blood cells. (A) Fraction of red blood cells infected with *P. yoelii* (% parasitemia). (B) Area under the parasitemia curve (AUC) analysis. (A-B) Data (mean±S.E.) are from 3-4 mice/group and representative of two experiments. * $p < 0.05$, ** $p < 0.01$, *** $p < 0.001$, **** $p < 0.0001$, n.s. = not significant. (C) Survival of mice following infection (n=7-8 mice/group) from two experiments. Survival curves were analyzed by Log-rank (Mantel-Cox) test.

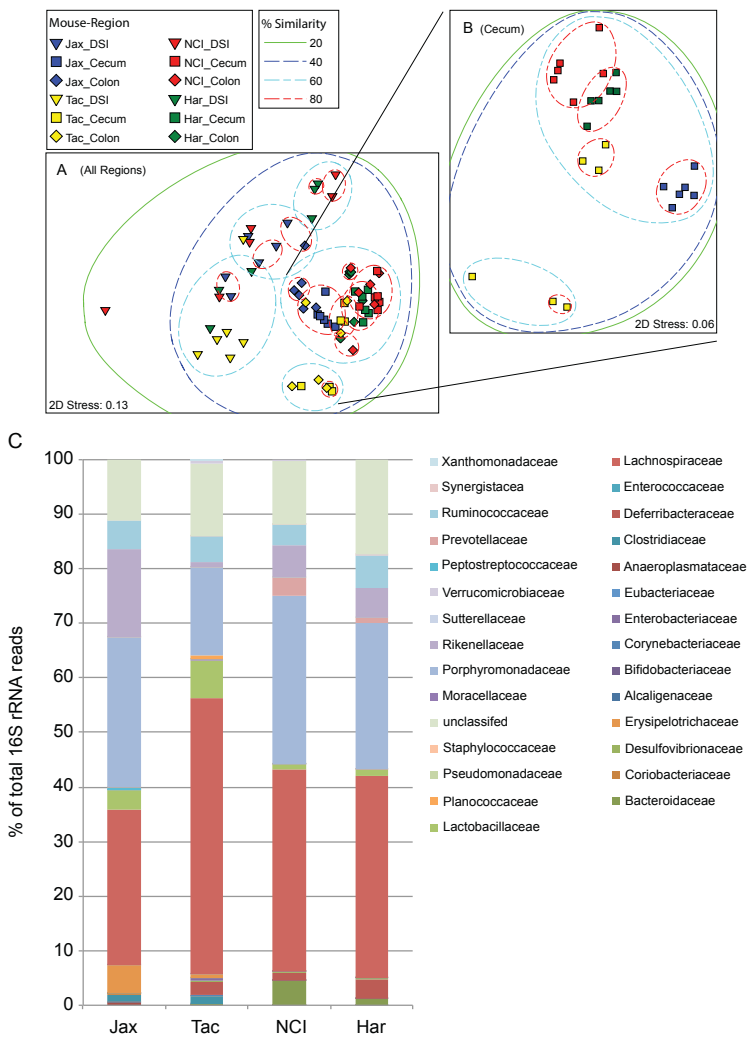


Figure 4.S6. Susceptibility to malaria correlates with differences in the gut microbial community structure.

Bacterial population analysis was performed using NMDS. The closer together two points are the more similar the libraries are to one another. Libraries with similarities greater than 20%, 40%, 60% or 80% are encircled with green, blue, teal or red dotted lines, respectively. Triangle=distal portion of the small intestine (DSI); Square=cecum; Diamond=colon (A) Analysis of all three regions of the digestive tract. (B) Analysis of only the cecum bacterial populations. (C) Percentage of 16S rRNA gene reads of bacterial families comprising at least 0.01% of reads from at least 1 sample. Abundances of 16S reads at the Family level were first normalized to proportional abundances and then the average proportional abundance (n=6) for each family was calculated for mice from each of the four vendors.

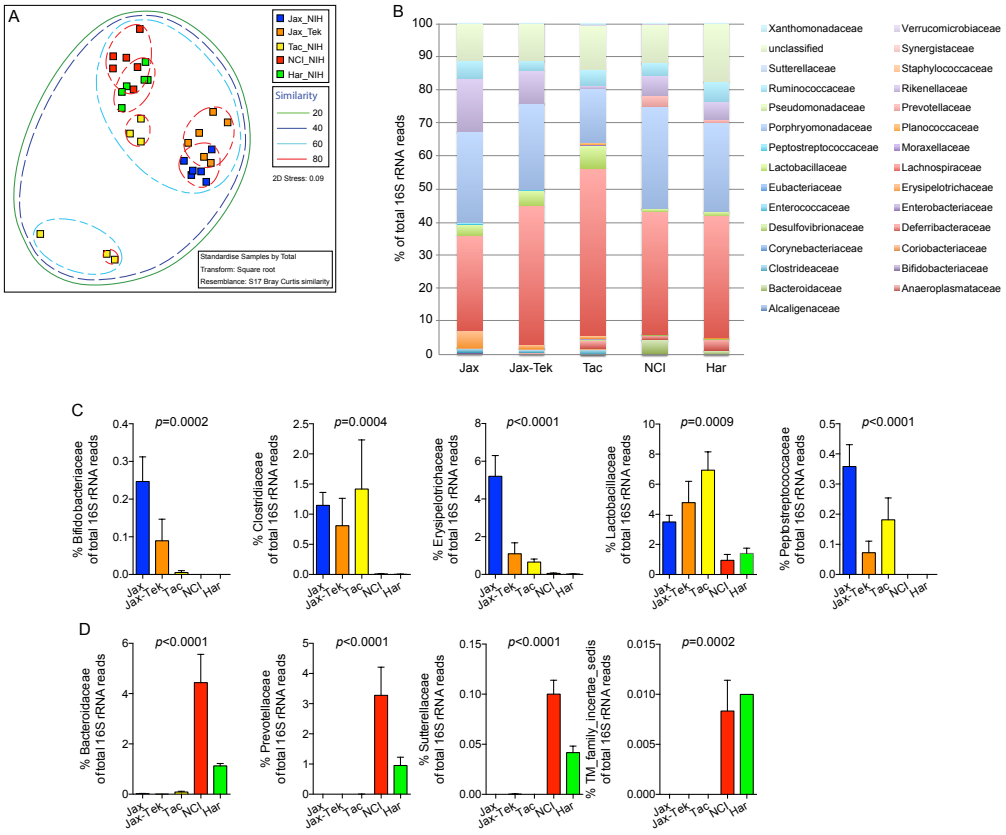


Figure 4.S7. Jackson mice fed Teklad 22/5 diet exhibit defined changes in cecal bacterial populations.

All mice were fed NIH-31, except one group of Jackson mice that received Teklad 22/5 (Jax-Tek). (A) Cecal cacterial population analysis was performed using NMDS. The closer together two points are the more similar the libraries are to one another. Libraries with similarities greater than 20%, 40%, 60% or 80% are encircled with green, blue, teal or red dotted lines, respectively. Analysis of cecal bacterial populations. Each symbol represents an individual mouse. (B) Percentage of 16S rRNA gene reads of bacterial families comprising at least 0.01% of reads from at least 1 sample. Abundances of 16S reads at the Family level were first normalized to proportional abundances and then the average proportional abundance (n=6) for each family was calculated for mice from each of the groups. (C) Bacterial families that were identified as being significantly enriched in Jackson or Taconic mice. (D) Bacterial families identified as being significantly enriched in NCI or Harlan mice. (C-D) Data (mean±S.E.) are from 6 mice per group and extracted from analysis in panel B. Data were analyzed by Kruskal-Wallis test.

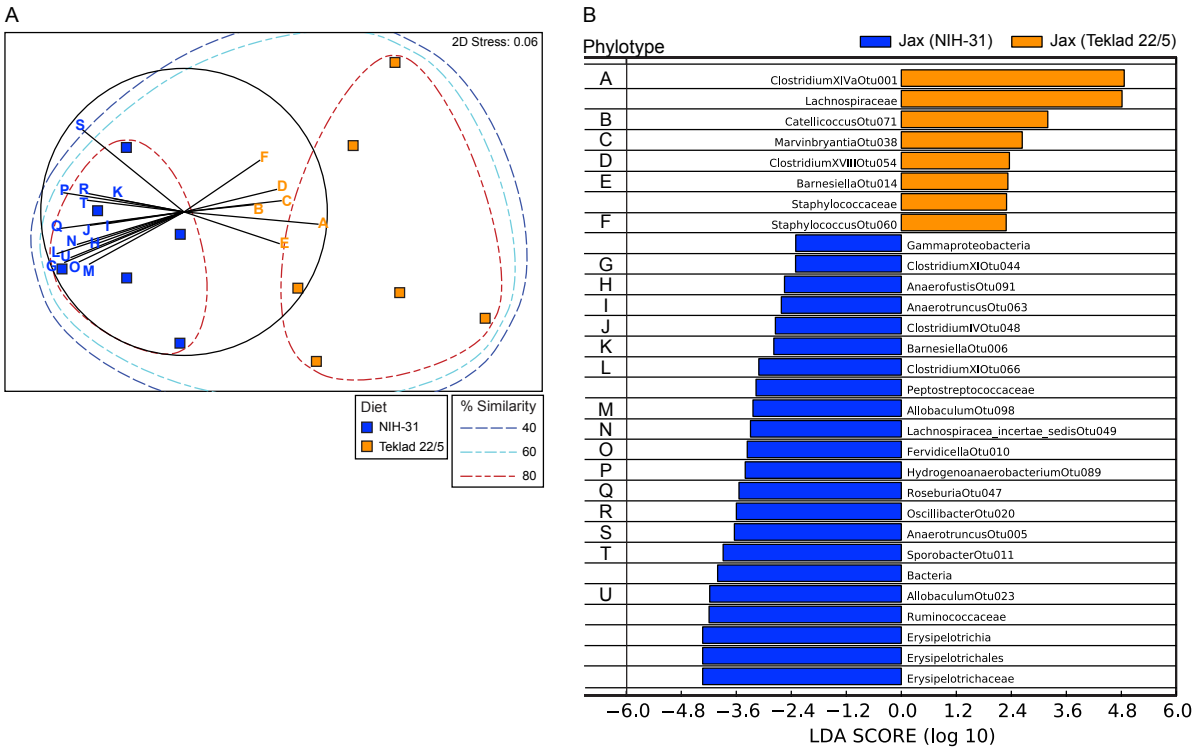


Figure 4.S8. Distinct bacterial community structure in Jackson mice fed separate diets.

C57BL/6 mice from Jackson Laboratory (Jax) were fed two separate diets (NIH-31 (n=6) or Teklad 22/5 (n=6)) for one to three weeks prior to removal of gut contents and analysis of gut bacterial community. (A) NMDS plot displaying the similarity between bacterial populations within the cecum of mice fed the different diets. Each symbol represents a single mouse. The closer together two points are in the figure, the more similar the libraries are to one another. Libraries with similarities greater than 40%, 60% or 80% are encircled with blue, teal or red dashed lines, respectively. Selected vectors (lettered A-U), overlaid on the figure, were taken from a PCA plot made from all phylotype abundances in this study after identification by LEfSe analysis as having statistically significant differential abundances in mice fed different diets. (B) LEfSe output highlighting differentially abundant phylotypes between Jax mice fed the two separate diets. Some of these phylotypes are included in (A) as vectors.

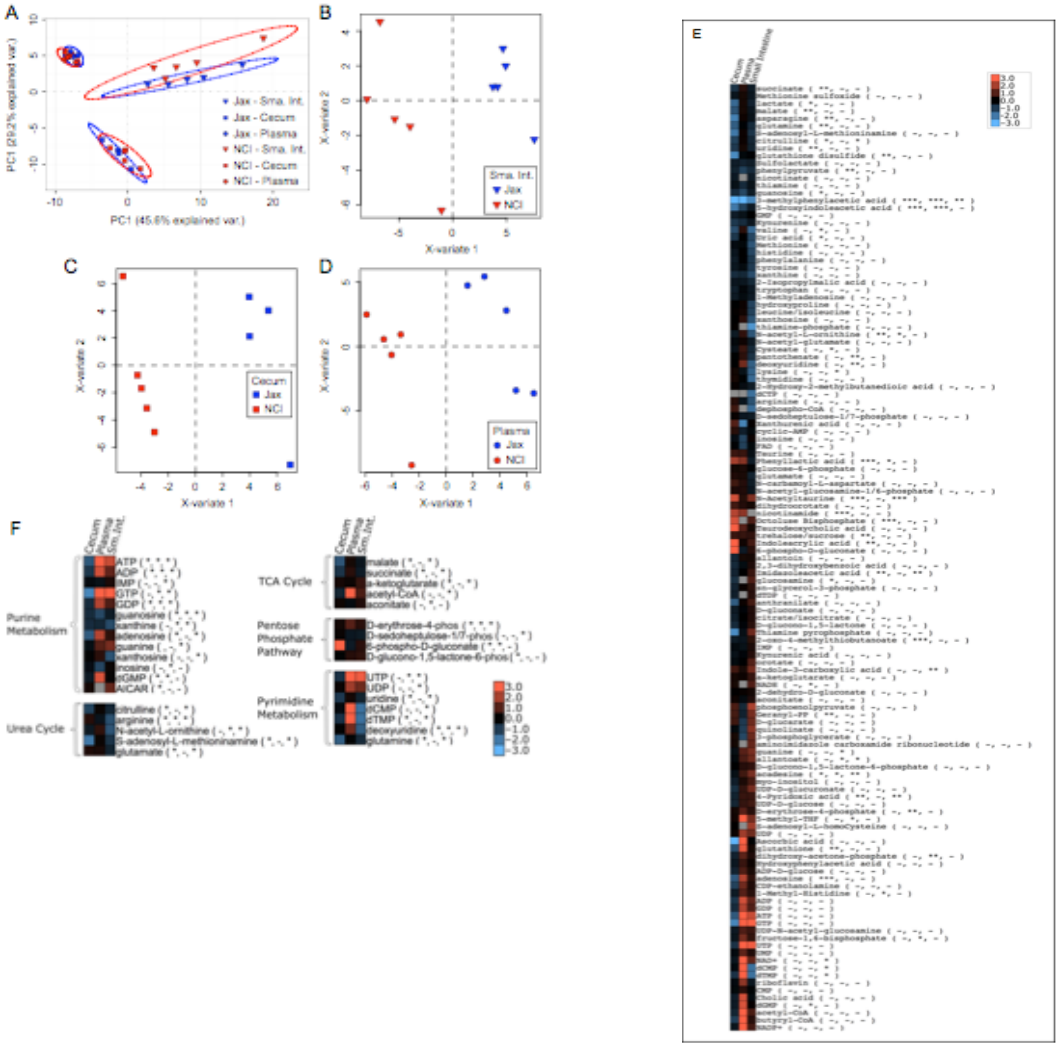


Figure 4.S9. Changes in the gut microbial community structure correlate with changes in the gut and plasma metabolome in resistant and susceptible mice.

(A) Principal component analysis of metabolite profiles for all sample types. Ellipses size indicates 95% normal probability. Triangle=small intestine, square=cecum, circle=plasma. Each symbol represents an individual mouse. (B-D) Partial least squares discriminant analysis within individual samples types: small intestine, cecum, and plasma, respectively. Separation between points indicates relative amount of variability. (E) Color intensity indicates magnitude of the fold change with red being an increase and blue being a decrease in metabolite concentrations of Jax with respect to NCI mice. Asterisks in parentheses next to metabolite names indicate significance for the change for the corresponding row and column. *** $p \leq 0.01$, ** $p \leq 0.05$, * $p \leq 0.10$, (–) not significant. (F) Metabolites grouped according to metabolic pathways that were major drivers in

the differentiation of resistant and susceptible mice using PLS-DA. Data are expressed as a ratio of Jax/NCI with red shades representing metabolites higher in Jax mice and blue shades representing metabolites higher in NCI mice. (*) = Metabolite that was a driving factor in differentiating resistant and susceptible mice, respective to column order. (–) = Metabolite that was not a driving factor in variation for the respective column.

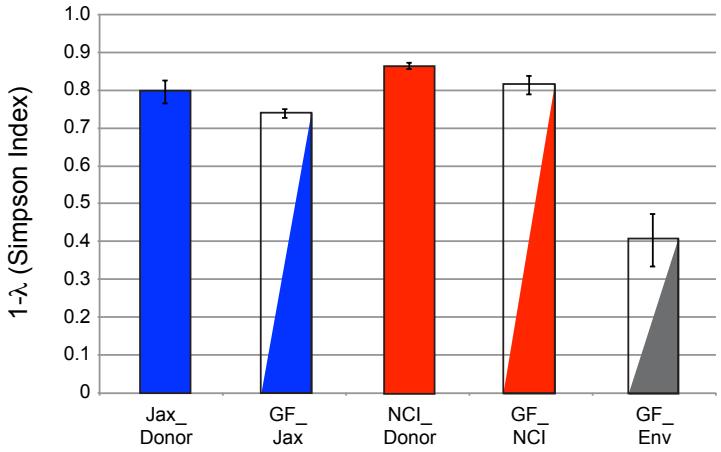


Figure 4.S10. Germ-free mice colonized wtih cecal content have similar bacterial diversity as donor sample.

Germ-free mice were colonized with cecal contents from Jax or NCI mice.The 1-λ (Simpson Index) was calculated for 5 different mouse types (Jax-Donors (n=4), GF-Jax recipients post-cecal transplant (n=5), NCI Donors (n=3), GF-NCI recipients post-cecal transplant (n=5) and GF mice receiving no transplant (n=5)). Data are mean±SD. Communities with values closer to 1 are considered to be more diverse.

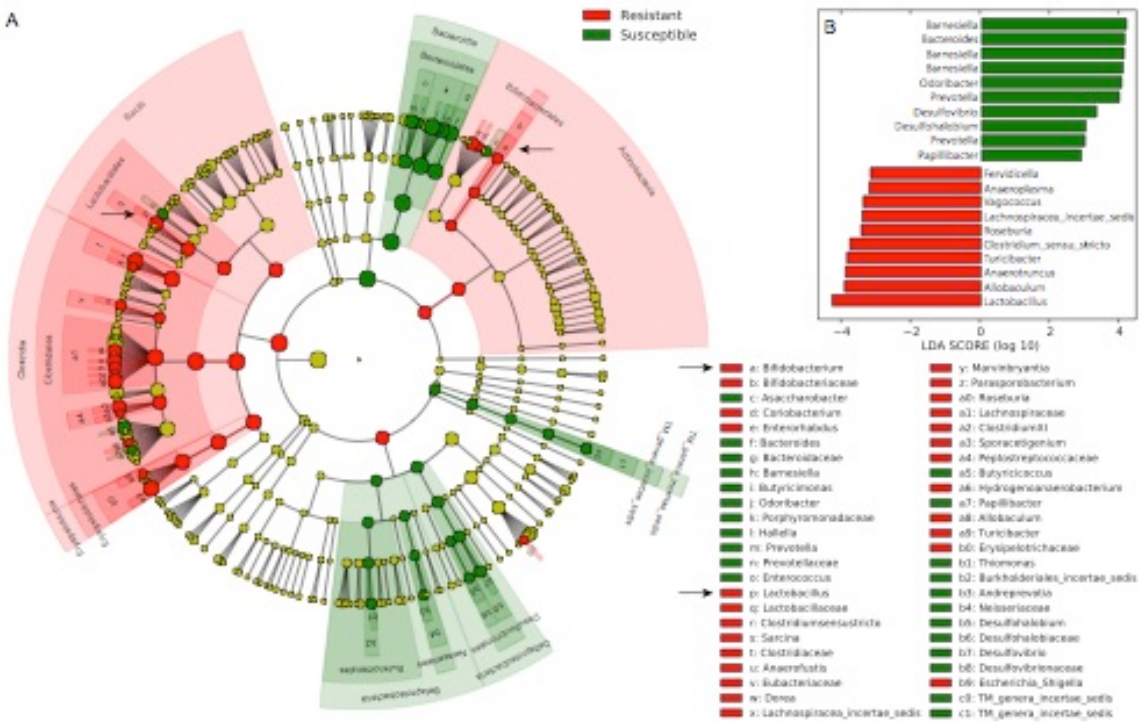


Figure 4.S11. Lactobacillus and Bifidobacterium are among the bacteria that drive differences between the gut-associated bacterial communities of resistant and susceptible mice.

(A) LEfSe cladogram illustrating all 313 phylotypes in this study. Red identifies phylotype biomarkers for resistance to malaria and green identifies phylotype biomarkers for susceptibility to malaria. Circle size reflects the sequence abundance within the samples. (B) Top ten phylotypes with largest effect sizes for susceptibility and resistance to malaria.

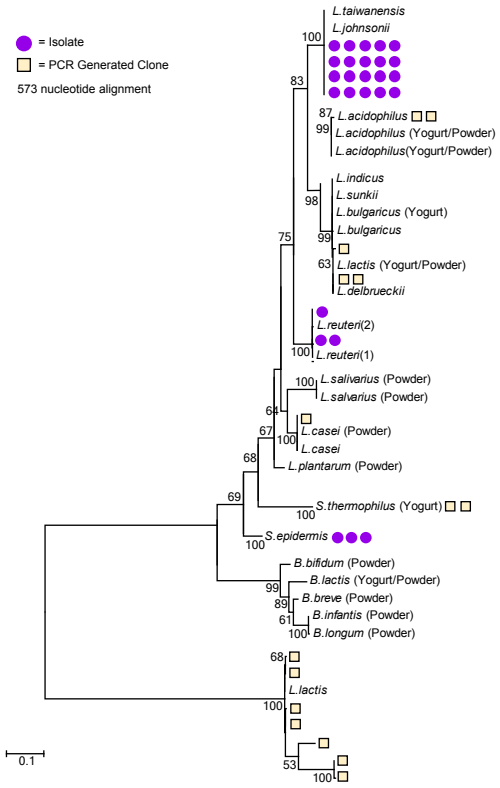


Figure 4.S12. Phylogenetic tree of bacteria isolated from stool samples and lab-cultured yogurt.

A maximum likelihood tree was constructed from an alignment of 16S rRNA gene sequences approximately 573 base pairs long. Sequences used to construct the tree were obtained from bacterial isolates (cultured from Jackson and NCI mouse fecal pellets) and from PCR amplicons retrieved from DNA extracted from lab-cultured yogurt containing probiotic powder. Isolate sequences = purple circles, clone sequences (yogurt or powder) = tan squares. Distance bar represents 0.1 substitutions per base.

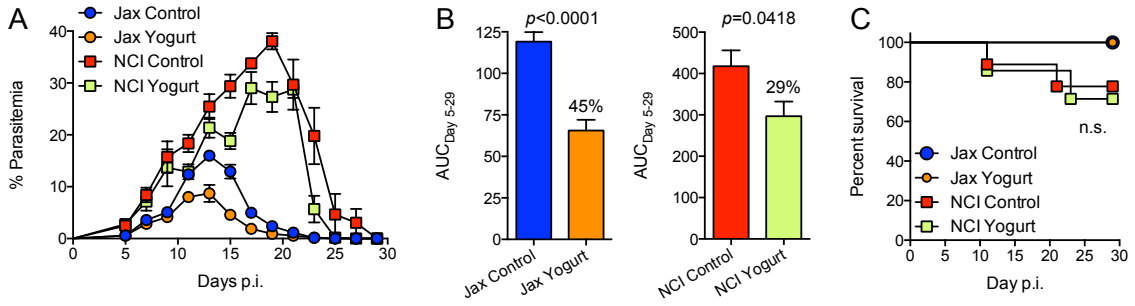


Figure 4.S13. Treatment of gut microbiota intact mice with yogurt has a modest effect on parasite burden.

Mice were treated 5-6 times/week with yogurt for 3 weeks prior to *P. yoelii* infection and 3 times per week following infection. (A) Percent parasitemia following *P. yoelii* infection. (B) AUC analysis. Data were analyzed by unpaired two-tailed *t* test. (C) Survival of mice following infection. Survival curves were analyzed by Log-rank (Mantel-Cox) test. (A-C) Data (mean±S.E.) from 7-9 mice/group are cumulative data from two experiments.

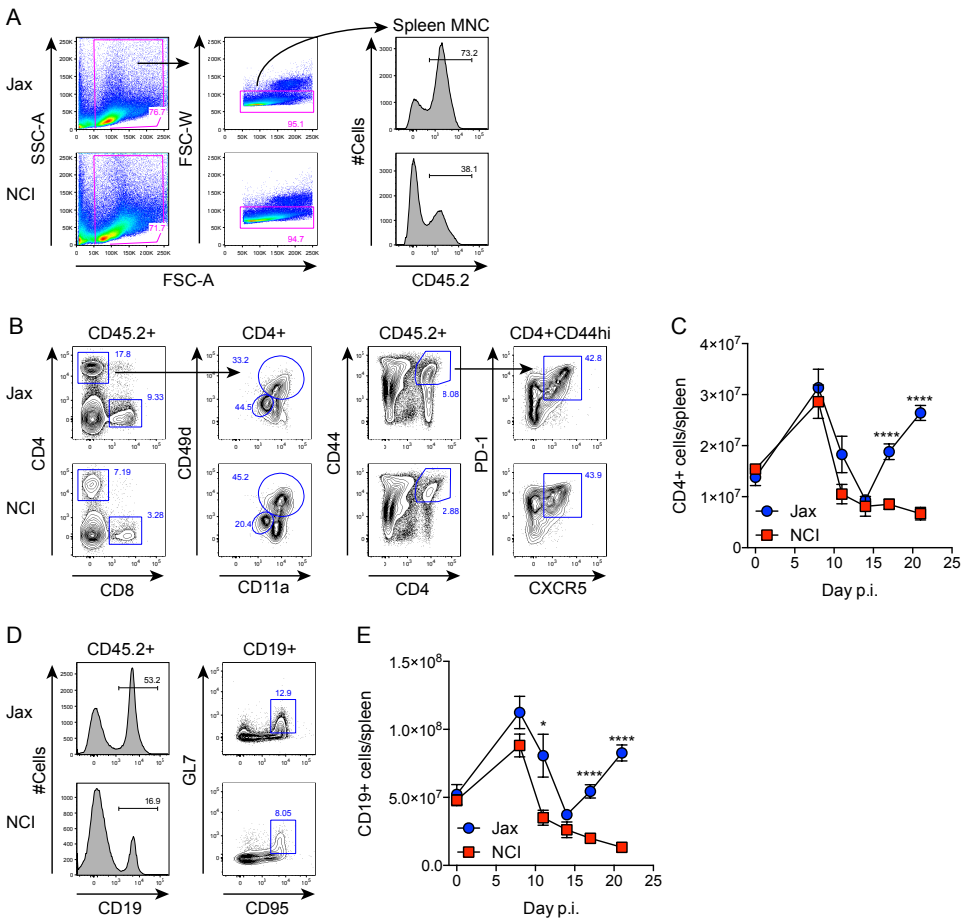


Figure 4.S14. Gating strategy for T cell and B cell populations in Jax and NCI mice infected with P. yoelii.

Jax and NCI mice were infected with *P. yoelii*. Representative contour plots and histograms are from day 21-post infection. (A) Representative contour plots and histograms showing gating strategy of CD45.2+ cells. (B) Representative contour plots showing gating strategy for T cell subsets: CD4+ T cells, *P. yoelii*-specific CD4+ T cells (CD4+CD49d^{hi}CD11a^{hi}), and T follicular helper (Tfh) cells (CD4+ CD44^{hi}CXCR5+PD-1+). (C) Total number of CD4+ cells per spleen. (D) Representative contour plots and histograms showing gating strategy of B cell subsets: CD19+ B cells and GC B cells (CD19+GL7+CD95+). (E) Total number of CD19+ cells per spleen. Data (mean±S.E.) are cumulative results (n=5-10 mice/data point) from three experiments. Data were analyzed by unpaired two-tailed *t* test. * $p<0.05$, **** $p<0.0001$.

Sample ID	Mouse	Region	Resistant?	S	N	d	J'	H'(log10)	1/λ
H_4612	**Har**	DSI	N	85	103,055	7.28	0.25	0.48	0.52
H_4613	**Har**	Cecum	N	85	191,572	6.91	0.51	0.99	0.82
H_4614	**Har**	Colon	N	88	246,215	7.01	0.44	0.85	0.69
H_4622	**Har**	DSI	N	95	26,498	9.23	0.47	0.93	0.79
H_4623	**Har**	Cecum	N	77	144,414	6.40	0.51	0.97	0.78
H_4624	**Har**	Colon	N	123	140,969	10.29	0.49	1.03	0.77
H_4632	**Har**	DSI	N	94	22,480	9.28	0.49	0.96	0.82
H_4633	**Har**	Cecum	N	85	310,706	6.64	0.54	1.05	0.84
H_4634	**Har**	Colon	N	82	63,897	7.32	0.60	1.14	0.89
H_4712	**Har**	DSI	N	56	1,534	7.50	0.58	1.01	0.81
H_4713	**Har**	Cecum	N	89	299,579	6.98	0.47	0.92	0.79
H_4714	**Har**	Colon	N	80	188,189	6.50	0.48	0.91	0.79
H_4722	**Har**	DSI	N	63	44,509	5.79	0.27	0.49	0.50
H_4723	**Har**	Cecum	N	82	188,386	6.67	0.48	0.91	0.78
H_4724	**Har**	Colon	N	88	335,328	6.84	0.46	0.90	0.78
H_4732	**Har**	DSI	N	72	41,215	6.68	0.28	0.52	0.46
H_4733	**Har**	Cecum	N	74	168,137	6.07	0.51	0.96	0.81
H_4734	**Har**	Colon	N	84	215,138	6.76	0.50	0.97	0.80
J_4612	**Jax**	DSI	Y	58	10,220	6.17	0.50	0.89	0.76
J_4613	**Jax**	Cecum	Y	83	212,544	6.68	0.50	0.96	0.82
J_4614	**Jax**	Colon	Y	109	144,423	9.09	0.45	0.92	0.76
J_4622	**Jax**	DSI	Y	69	6,396	7.76	0.53	0.97	0.78
J_4623	**Jax**	Cecum	Y	74	290,135	5.80	0.50	0.94	0.81
J_4624	**Jax**	Colon	Y	87	171,168	7.14	0.53	1.03	0.85
J_4632	**Jax**	DSI	Y	78	32,429	7.41	0.32	0.61	0.53
J_4633	**Jax**	Cecum	Y	73	163,210	6.00	0.54	1.00	0.84
J_4634	**Jax**	Colon	Y	74	38,128	6.92	0.44	0.82	0.68
J_4712	**Jax**	DSI	Y	66	141,766	5.48	0.45	0.82	0.72
J_4713	**Jax**	Cecum	Y	98	147,576	8.15	0.51	1.02	0.84
J_4714	**Jax**	Colon	Y	91	97,286	7.84	0.50	0.98	0.79
J_4722	**Jax**	DSI	Y	77	17,265	7.79	0.46	0.87	0.73
J_4723	**Jax**	Cecum	Y	73	128,780	6.12	0.45	0.84	0.75
J_4724	**Jax**	Colon	Y	81	149,433	6.71	0.50	0.96	0.81
J_4732	**Jax**	DSI	Y	69	17,351	6.97	0.24	0.44	0.35
J_4733	**Jax**	Cecum	Y	71	176,751	5.79	0.53	0.98	0.81
J_4734	**Jax**	Colon	Y	70	83,812	6.09	0.27	0.49	0.40
N_4612	**NCI**	DSI	N	78	5,862	8.87	0.57	1.08	0.81
N_4613	**NCI**	Cecum	N	81	153,710	6.70	0.48	0.91	0.75

Figure 4.S15. Sequencing and diversity metrics from Jax, Har, NCI, and Tac mice.

Total number of sequences from all samples = 8,665,599. S = species richness; N = number of sequences; d = Margalef species richness; J' = Pielou's evenness; H' = Shannon index; 1/λ = Inverse Simpson.

Sample ID	Mouse	Region	Resistant?	S	N	d	J'	H'(log10)	1/λ
N_4614	**NCI**	Colon	N	73	60,882	6.54	0.53	0.99	0.83
N_4622	**NCI**	DSI	N	129	32,346	12.33	0.57	1.20	0.90
N_4623	**NCI**	Cecum	N	92	196,467	7.47	0.51	1.01	0.83
N_4624	**NCI**	Colon	N	88	155,236	7.28	0.53	1.02	0.84
N_4632	**NCI**	DSI	N	80	6,446	9.01	0.47	0.90	0.72
N_4633	**NCI**	Cecum	N	82	160,507	6.76	0.50	0.96	0.78
N_4634	**NCI**	Colon	N	85	170,630	6.97	0.47	0.91	0.79
N_4712	**NCI**	DSI	N	83	140,322	6.92	0.33	0.63	0.70
N_4713	**NCI**	Cecum	N	87	134,246	7.28	0.46	0.89	0.77
N_4714	**NCI**	Colon	N	149	148,733	12.43	0.39	0.84	0.61
N_4722	**NCI**	DSI	N	67	7,778	7.37	0.34	0.63	0.51
N_4723	**NCI**	Cecum	N	78	196,757	6.32	0.53	1.01	0.84
N_4724	**NCI**	Colon	N	76	219,072	6.10	0.57	1.07	0.87
N_4732	**NCI**	DSI	N	75	54,099	6.79	0.37	0.69	0.73
N_4733	**NCI**	Cecum	N	76	346,990	5.88	0.52	0.97	0.83
N_4734	**NCI**	Colon	N	77	170,635	6.31	0.48	0.90	0.75
T_4612	**Tac**	DSI	Y	72	10,268	7.69	0.41	0.77	0.62
T_4613	**Tac**	Cecum	Y	82	129,923	6.88	0.50	0.95	0.79
T_4614	**Tac**	Colon	Y	89	119,367	7.53	0.46	0.90	0.73
T_4622	**Tac**	DSI	Y	71	3,309	8.64	0.62	1.15	0.84
T_4623	**Tac**	Cecum	Y	80	160,273	6.59	0.49	0.94	0.77
T_4624	**Tac**	Colon	Y	77	137,109	6.43	0.52	0.98	0.82
T_4632	**Tac**	DSI	Y	68	1,852	8.90	0.76	1.38	0.93
T_4633	**Tac**	Cecum	Y	85	176,059	6.95	0.49	0.94	0.80
T_4634	**Tac**	Colon	Y	44	8,525	4.75	0.56	0.92	0.78
T_4712	**Tac**	DSI	Y	92	5,302	10.61	0.71	1.39	0.93
T_4713	**Tac**	Cecum	Y	140	165,425	11.57	0.43	0.93	0.71
T_4714	**Tac**	Colon	Y	81	147,027	6.72	0.46	0.88	0.76
T_4722	**Tac**	DSI	Y	57	2,676	7.10	0.60	1.05	0.80
T_4723	**Tac**	Cecum	Y	83	129,267	6.97	0.46	0.89	0.72
T_4724	**Tac**	Colon	Y	88	90,087	7.63	0.55	1.06	0.87
T_4732	**Tac**	DSI	Y	50	1,385	6.77	0.70	1.18	0.86
T_4733	**Tac**	Cecum	Y	68	130,609	5.69	0.49	0.90	0.74
T_4734	**Tac**	Colon	Y	90	125,924	7.58	0.46	0.90	0.74

Figure 4.S15. Continued

Small Intestine

Jax Variability		NCI Variability	
Variate 1	**Variate 2**	**Variate 1**	**Variate 2**
3.84	5.23	6.90	10.86

	Jax – NCI Variability	
	Variate 1	**Y**
Avg. Distance	10.03	1.72
p-value	0.000269	0.411425

Cecum

Jax Variability		NCI Variability	
Variate 1	**Variate 2**	**Variate 1**	**Variate 2**
3.03	12.35	2.32	11.47

	Jax – NCI Variability	
	Variate 1	**Variate 2**
Avg. Distance	9.12	1.76
p value	0.000145	0.629464

Plasma

Jax Variability		NCI Variability	
Variate 1	**Variate 2**	**Variate 1**	**Variate 2**
4.93	9.08	3.34	11.71

	Jax – NCI Variability	
	Variate 1	**Variate 2**
Avg. Distance	8.23	2.36
p value	0.000104	0.432392

Figure 4.S16. Variability in each sample type for PLS-DA.

For each sample type, the intra condition distance between the extreme values in each dimension are listed. Comparison is also shown for the distance between the average of the points for each condition in each dimension. Additionally, the p values are shown for the inter conditional comparison. Results show a high level of significance between the Jax and NCI samples in the variate 1 dimension.

	Jax		NCI	
Metabolite	**Average**	**RSD (%)**	**Average**	**RSD (%)**
lactate	1.12E+07	33.2	1.82E+07	43.1
succinate	4.01E+06	22.6	5.72E+06	16.7
valine	1.02E+05	72.0	3.22E+05	47.7
nicotinamide	N.D.	N.D.	4.39E+03	N.D.
nicotinate	1.43E+05	83.0	1.51E+05	59.7
Taurine	2.32E+06	37.0	3.05E+06	39.2
hydroxyproline	7.51E+05	41.3	1.63E+06	26.4
leucine/isoleucine	7.75E+05	44.8	1.66E+06	31.3
asparagine	6.12E+05	42.4	6.67E+05	84.4
malate	3.44E+06	34.3	4.46E+06	37.6
anthranilate	1.05E+05	61.0	7.04E+04	47.8
Imidazoleacetic acid	1.43E+05	22.2	1.08E+05	53.7
α-ketoglutarate	3.46E+08	56.0	2.18E+08	43.5
glutamine	1.09E+08	106.2	2.07E+08	79.6
lysine	3.10E+07	48.0	9.79E+07	45.1
glutamate	4.94E+09	43.4	7.34E+09	31.7
2-oxo-4-methylthiobutanoate	1.27E+06	69.1	1.02E+06	50.7
2-Hydroxy-2-methylbutanedioic acid	1.58E+08	31.7	2.23E+08	31.4
methionine	1.77E+08	36.8	4.47E+08	45.0
3-methylphenylacetic acid	4.06E+06	44.7	2.18E+07	60.5
guanine	4.10E+06	49.4	1.44E+06	56.7
xanthine	1.83E+08	31.5	4.28E+08	46.4
Hydroxyphenylacetic acid	1.61E+06	14.6	1.61E+06	22.8
2,3-dihydroxybenzoic acid	6.52E+07	46.5	6.37E+07	75.5
histidine	3.83E+07	50.3	8.95E+07	39.5
orotate	2.28E+07	94.4	1.31E+07	114.1
dihydroorotate	2.80E+06	74.7	2.85E+06	83.9
allantoin	8.37E+07	46.2	7.90E+07	48.5
Indole-3-carboxylic acid	3.09E+06	22.6	1.19E+06	42.0
phenylpyruvate	2.40E+07	66.8	4.17E+07	39.2
methionine sulfoxide	2.90E+06	27.9	4.17E+06	41.5
phenylalanine	8.78E+08	16.8	1.72E+09	26.0
Phenyllactic acid	1.09E+07	81.1	1.73E+07	39.5
quinolinate	8.94E+07	110.6	3.48E+07	54.3
N-Acetyltaurine	4.74E+08	25.8	1.75E+08	22.0
phosphoenolpyruvate	4.22E+06	116.7	1.20E+06	41.5
uric acid	2.79E+08	20.5	6.48E+08	41.2
cysteate	3.12E+06	38.3	5.83E+06	52.9
1-Methyl-Histidine	5.14E+05	69.6	4.27E+05	54.7
Sulfolactate	5.32E+07	29.3	8.83E+07	67.5
dihydroxy-acetone-phosphate	1.52E+08	93.8	1.18E+08	57.8
sn-glycerol-3-phosphate	3.80E+09	41.0	2.74E+09	21.3
aconitate	1.52E+08	53.2	1.35E+08	28.7
N-acetyl-L-ornithine	7.59E+06	32.6	2.01E+07	34.6
arginine	7.78E+07	47.5	2.04E+08	39.3
citrulline	8.51E+06	37.7	1.56E+07	35.0
ascorbic acid	4.94E+09	60.1	5.38E+09	47.9
N-carbamoyl-L-aspartate	1.16E+07	66.5	1.89E+07	73.5

Figure 4.S17. Average small intestine metabolite ion counts and relative standard deviations (RSD) for Jax (n=5) and NCI (n=5) mice.

Metabolite	Jax		NCI	
	Average	RSD (%)	Average	RSD (%)
allantoate	9.06E+06	63.4	4.25E+06	62.4
2-Isopropylmalic acid	3.92E+06	32.1	7.89E+06	80.7
glucono-1,5-lactone	5.72E+08	56.8	4.60E+08	47.5
glucosamine	8.14E+05	73.6	5.28E+05	113.1
myo-inositol	1.18E+09	63.1	8.00E+08	49.8
tyrosine	6.65E+08	22.9	1.33E+09	41.8
4-Pyridoxic acid	4.11E+08	27.4	2.98E+08	44.7
3-phosphoglycerate	4.79E+07	104.9	2.09E+07	59.5
indoleacrylic acid	3.00E+04	89.4	2.55E+04	44.1
kynurenic acid	3.75E+06	38.4	3.06E+06	44.3
N-acetyl-glutamate	2.88E+08	57.6	3.97E+08	25.0
5-hydroxyindoleacetic acid	8.00E+07	28.0	1.31E+08	57.8
citrate/isocitrate	2.37E+09	62.5	1.73E+09	52.8
2-dehydro-D-gluconate	4.88E+08	40.0	3.96E+08	42.2
D-gluconate	1.51E+09	81.8	1.24E+09	37.3
D-erythrose-4-phosphate	2.22E+05	48.8	1.70E+05	29.5
Tryptophan	5.54E+08	21.6	7.72E+08	26.3
xanthurenic acid	4.23E+06	24.4	4.34E+06	51.6
Kynurenine	5.47E+05	40.7	7.39E+05	20.3
D-glucarate	2.04E+08	107.9	9.91E+07	59.1
pantothenate	4.01E+08	37.4	7.13E+08	28.6
deoxyuridine	4.82E+06	79.8	1.30E+07	74.7
Thymidine	2.56E+06	113.0	8.05E+06	70.5
Uridine	2.26E+07	33.7	3.47E+07	17.5
D-glucono-1,5-lactone-6-phosphate	1.06E+07	39.1	8.49E+06	40.3
Acadesine	1.50E+06	42.3	7.16E+05	78.2
glucose-6-phosphate	1.49E+08	74.3	1.62E+08	25.1
Thiamine	8.16E+06	46.2	1.06E+07	24.2
Adenosine	3.85E+06	27.9	2.71E+06	35.6
Inosine	3.85E+08	51.7	3.58E+08	30.8
6-phospho-D-gluconate	4.34E+07	63.7	3.31E+07	32.6
1-methyladenosine	5.30E+06	55.5	8.70E+06	66.0
guanosine	2.51E+07	34.5	3.16E+07	58.6
xanthosine	2.83E+06	51.7	7.52E+06	65.3
D-sedoheptulose-1/7-phosphate	8.44E+06	34.0	1.21E+07	14.1
N-acetyl-glucosamine-1/6-phosphate	7.25E+07	44.6	9.33E+07	31.8
dCMP	7.57E+06	108.0	3.06E+07	53.9
glutathione	1.39E+09	38.6	1.21E+09	33.2
Geranyl-PP	8.73E+07	89.7	4.08E+07	76.4
dTMP	1.40E+07	97.9	5.39E+07	51.6
CMP	7.11E+07	62.0	7.53E+07	38.4
UMP	5.08E+08	43.9	3.81E+08	46.7
cyclic-AMP	5.33E+06	73.6	6.60E+06	39.1
AICAR	1.59E+07	138.0	7.27E+06	71.3
fructose-1-6-bisphosphate	7.71E+07	103.1	4.48E+07	97.5
trehalose/sucrose	5.61E+07	22.8	4.55E+07	61.7
thiamine-phosphate	6.50E+06	177.7	2.78E+07	113.1
dGMP	2.45E+09	52.9	2.21E+09	47.6
IMP	1.13E+08	43.0	8.29E+07	67.4
S-adenosyl-L-methioninamine	1.78E+06	93.5	4.25E+06	84.5
GMP	2.57E+08	77.5	2.49E+08	55.9
riboflavin	8.67E+06	23.3	1.18E+07	33.5
S-adenosyl-L-homocysteine	1.21E+07	122.5	3.99E+06	114.8
octoluse bisphosphate	5.01E+06	61.3	3.11E+06	72.1

Figure 4.S17. Continued

Metabolite	Jax		NCI	
	Average	RSD (%)	Average	RSD (%)
dTDP	3.22E+05	48.4	2.37E+05	57.3
UDP	4.83E+06	70.7	2.13E+06	49.1
Cholic acid	4.67E+10	95.8	5.50E+10	52.7
Thiamine pyrophosphate	4.69E+06	143.0	2.55E+06	75.8
ADP	3.88E+08	72.6	1.64E+08	71.7
GDP	1.96E+07	89.7	8.97E+06	89.4
CDP-ethanolamine	1.30E+07	62.7	1.09E+07	40.3
5-methyl-THF	4.72E+06	87.5	2.02E+06	40.0
dCTP	1.51E+05	12.3	2.21E+05	185.0
UTP	1.28E+07	89.6	2.03E+06	151.3
taurodeoxycholic acid	7.36E+10	15.2	6.05E+10	39.2
ATP	1.16E+08	87.5	2.15E+07	107.4
GTP	7.16E+06	79.0	6.73E+05	126.0
UDP-D-glucose	2.67E+08	49.8	1.66E+08	45.7
UDP-D-glucuronate	1.34E+08	64.2	5.55E+07	48.5
ADP-D-glucose	2.08E+07	69.0	1.80E+07	36.9
UDP-*N*-acetyl-glucosamine	5.12E+08	44.0	3.42E+08	52.9
glutathione disulfide	6.76E+07	50.1	8.28E+07	99.5
NAD^+	5.17E+07	39.8	2.68E+07	62.5
NADH	1.54E+07	54.1	8.20E+06	56.3
dephospho-CoA	1.15E+07	56.7	3.72E+07	61.9
$NADP^+$	1.03E+07	74.8	6.33E+06	49.5
FAD	8.96E+06	50.2	1.04E+07	36.2
acetyl-CoA	9.78E+06	52.2	6.30E+06	66.3
butyryl-CoA	3.72E+06	108.5	3.30E+06	133.6

Figure 4.S17. Continued

	Jax		NCI	
Metabolite	**Average**	**RSD (%)**	**Average**	**RSD (%)**
lactate	5.88E+05	166.1	1.60E+06	59.4
succinate	2.44E+06	29.4	3.46E+06	29.6
valine	8.80E+03	35.1	1.12E+04	44.7
nicotinamide	9.65E+05	45.6	1.70E+05	47.2
nicotinate	6.21E+05	19.3	6.73E+05	53.8
Taurine	1.22E+06	48.8	5.98E+05	40.2
hydroxyproline	4.02E+04	45.3	3.31E+04	30.8
leucine/isoleucine	4.16E+04	51.5	3.07E+04	51.3
asparagine	7.73E+04	79.6	2.83E+05	64.0
malate	1.87E+06	35.9	3.78E+06	37.6
anthranilate	1.58E+06	128.8	3.62E+06	98.1
Imidazoleacetic acid	7.05E+05	21.2	8.54E+05	22.2
α-ketoglutarate	1.28E+09	38.7	9.21E+08	50.8
glutamine	4.56E+07	24.9	1.16E+08	46.4
lysine	8.64E+06	37.8	5.88E+06	45.1
glutamate	1.09E+10	28.1	7.20E+09	25.1
2-oxo-4-methylthiobutanoate	7.00E+05	33.5	7.43E+05	22.0
2-hydroxy-2-methylbutanedioic acid	1.68E+09	19.4	1.33E+09	14.1
methionine	5.04E+07	29.2	4.51E+07	25.9
3-methylphenylacetic acid	3.60E+07	45.0	6.00E+09	35.4
guanine	1.08E+07	32.5	9.73E+06	35.0
xanthine	1.63E+08	34.6	2.07E+08	56.8
hydroxyphenylacetic acid	1.49E+07	48.8	1.50E+07	26.9
2,3-dihydroxybenzoic acid	2.99E+08	40.6	3.87E+08	57.6
histidine	3.85E+06	50.9	3.95E+06	71.0
orotate	5.31E+07	41.2	5.09E+07	56.3
dihydroorotate	5.35E+06	44.4	2.64E+06	72.4
allantoin	1.93E+06	87.1	2.59E+06	41.6
indole-3-carboxylic acid	1.51E+07	16.9	7.40E+06	45.7
phenylpyruvate	2.09E+06	10.4	2.52E+06	27.0
methionine sulfoxide	1.93E+07	72.0	1.92E+07	26.9
phenylalanine	5.28E+07	54.2	5.40E+07	43.6
phenyllactic acid	1.14E+10	29.1	2.37E+09	43.4
quinolinate	5.08E+07	46.3	4.57E+07	30.6
N-Acetyltaurine	1.53E+09	24.2	2.30E+08	69.7
phosphoenolpyruvate	4.24E+07	94.6	2.31E+07	63.3
uric acid	2.53E+07	53.8	3.75E+07	37.3
cysteate	7.38E+07	39.1	7.81E+07	38.1
1-methyl-histidine	4.90E+05	66.1	4.97E+05	61.5
sulfolactate	1.21E+08	32.4	1.31E+08	42.1
dihydroxy-acetone-phosphate	4.24E+07	50.1	5.63E+07	49.8
sn-glycerol-3-phosphate	5.90E+08	33.8	7.63E+08	44.7
aconitate	9.50E+07	85.0	7.01E+07	56.0
N-acetyl-L-ornithine	5.22E+06	33.9	5.47E+06	24.3
arginine	9.06E+06	29.4	5.32E+06	65.1
citrulline	9.84E+06	74.0	1.54E+07	57.7
ascorbic acid	6.55E+06	23.3	3.64E+07	168.3
N-carbamoyl-L-aspartate	3.36E+07	42.1	1.68E+07	52.0

Figure 4.S18. Average cecum metabolite ion counts and relative standard deviations (RDS) for Jax (n=4) and NCI (n=5) mice.

Metabolite	Jax		NCI	
	Average	RSD (%)	Average	RSD (%)
allantoate	2.21E+05	100.0	2.50E+05	66.9
2-Isopropylmalic acid	2.04E+08	69.0	2.01E+08	72.3
glucono-1,5-lactone	3.20E+08	28.2	4.09E+08	44.2
glucosamine	1.35E+06	87.3	1.59E+06	40.7
myo-inositol	1.35E+09	37.2	1.49E+09	38.0
tyrosine	7.94E+07	31.6	8.28E+07	22.8
4-pyridoxic acid	1.29E+09	13.6	1.55E+09	19.1
3-phosphoglycerate	1.32E+08	116.6	1.14E+08	44.3
indoleacrylic acid	6.97E+05	49.6	3.51E+04	68.7
kynurenic acid	1.38E+07	60.1	1.42E+07	70.5
N-acetyl-glutamate	1.58E+09	30.7	1.54E+09	24.6
5-hydroxyindoleacetic acid	8.76E+08	33.3	2.66E+09	25.2
citrate/isocitrate	4.46E+08	21.4	5.46E+08	90.3
2-dehydro-D-gluconate	6.62E+07	23.5	5.30E+07	36.3
D-gluconate	1.05E+08	53.4	1.30E+08	50.8
D-erythrose-4-phosphate	8.66E+05	39.5	6.65E+05	25.5
tryptophan	4.33E+07	41.7	5.00E+07	41.2
xanthurenic acid	1.14E+07	71.1	5.07E+06	49.5
kynurenine	2.52E+04	107.7	4.10E+04	84.9
D-glucarate	2.78E+06	125.1	1.76E+06	120.4
pantothenate	4.25E+08	43.5	3.35E+08	30.6
deoxyuridine	4.12E+06	41.0	3.25E+06	52.3
thymidine	4.01E+06	49.1	2.51E+06	52.9
uridine	2.63E+06	42.3	3.90E+06	43.6
D-glucono-1,5-lactone-6-phosphate	4.94E+07	20.9	4.10E+07	15.9
acadesine	4.55E+06	33.8	4.19E+06	19.7
glucose-6-phosphate	3.96E+08	46.9	3.09E+08	54.2
thiamine	8.28E+06	66.0	7.20E+06	34.0
adenosine	1.57E+07	37.5	3.36E+07	31.3
inosine	2.33E+08	25.8	2.21E+08	49.6
6-phospho- D-gluconate	7.61E+05	147.6	1.11E+05	74.4
1-methyladenosine	7.74E+06	51.7	8.61E+06	52.6
guanosine	2.52E+07	14.3	3.47E+07	32.6
xanthosine	8.31E+06	61.7	6.16E+06	61.9
D-sedoheptulose-1/7-phosphate	5.73E+07	54.0	4.90E+07	45.2
N-acetyl-glucosamine-1/6-phosphate	4.60E+08	32.6	3.17E+08	13.9
dCMP	1.54E+06	40.8	1.52E+06	70.1
glutathione	1.12E+08	52.1	2.47E+08	34.6
geranyl-PP	5.23E+07	41.1	2.25E+07	29.0
dTMP	1.35E+07	46.6	2.12E+07	38.6
CMP	2.51E+07	26.4	2.33E+07	22.2
UMP	1.43E+08	34.1	1.40E+08	23.4
cyclic-AMP	2.82E+05	59.2	1.73E+05	95.6
AICAR	1.59E+06	9.1	1.10E+06	24.9
fructose-1-6-bisphosphate	1.32E+07	94.5	1.53E+07	73.1
trehalose/sucrose	4.72E+07	39.9	2.31E+07	49.0
thiamine-phosphate	6.54E+05	37.6	5.43E+05	85.1
dGMP	4.88E+08	42.8	5.82E+08	27.7
IMP	2.69E+07	47.1	2.58E+07	23.6
S-adenosyl-L-methioninamine	3.92E+05	138.2	9.79E+05	100.7
GMP	2.73E+07	48.6	3.25E+07	32.1
riboflavin	1.40E+06	31.3	1.29E+06	24.7
S-adenosyl-L-homocysteine	1.35E+06	34.1	1.02E+06	39.2
octoluse bisphosphate	1.41E+06	39.8	1.91E+05	54.6

Figure 4.S18. Continued

Metabolite	Jax		NCI	
	Average	RSD (%)	Average	RSD (%)
dTDP	4.88E+06	79.7	6.85E+06	85.5
UDP	9.10E+05	71.1	7.80E+05	74.5
cholic acid	2.44E+09	49.4	2.91E+09	56.6
thiamine pyrophosphate	5.60E+04	135.8	1.72E+05	110.0
ADP	3.52E+07	72.7	6.28E+07	68.9
GDP	1.20E+06	140.5	2.10E+06	89.5
CDP-ethanolamine	4.18E+05	50.1	7.92E+05	56.8
5-methyl-THF	1.07E+06	91.8	5.97E+05	46.4
dCTP	N.D.	N.D.	N.D.	N.D.
UTP	1.95E+06	132.2	3.67E+06	128.5
taurodeoxycholic acid	3.16E+09	77.6	3.64E+08	33.7
ATP	4.59E+06	111.7	1.23E+07	90.4
GTP	1.00E+05	N.D.	2.23E+05	97.0
UDP-D-glucose	6.35E+07	35.8	8.77E+07	68.5
UDP-D-glucuronate	5.17E+06	48.1	8.12E+06	86.0
ADP-D-glucose	4.30E+06	41.1	5.86E+06	58.9
UDP-*N*-acetyl-glucosamine	2.00E+08	31.3	2.39E+08	52.5
glutathione disulfide	2.37E+06	75.1	1.00E+07	55.2
NAD^+	5.65E+07	18.1	6.10E+07	70.6
NADH	2.10E+06	68.1	1.47E+06	86.2
dephospho-CoA	1.54E+07	97.6	9.03E+06	33.9
$NADP^+$	9.81E+06	47.1	1.16E+07	74.8
FAD	3.31E+07	25.5	3.06E+07	53.8
acetyl-CoA	5.55E+07	48.3	7.84E+07	98.7
butyryl-CoA	3.00E+07	52.1	5.82E+07	135.0

Figure 4.S18 Continued

	Jax		NCI	
Metabolite	**Average**	**RSD (%)**	**Average**	**RSD (%)**
lactate	4.14E+06	16.2	3.43E+06	40.5
succinate	6.30E+05	42.4	4.53E+05	31.6
valine	6.67E+04	25.1	4.71E+04	33.8
nicotinamide	6.91E+03	22.1	4.36E+03	N.D.
nicotinate	N.D.	N.D.	N.D.	N.D.
taurine	3.66E+05	48.7	2.31E+05	73.2
hydroxyproline	9.15E+04	30.6	8.26E+04	22.2
leucine/isoleucine	9.92E+04	29.5	8.62E+04	17.0
asparagine	1.10E+05	32.8	9.79E+04	39.5
malate	9.03E+05	57.4	7.42E+05	28.4
anthranilate	3.00E+04	66.8	2.73E+04	27.8
imidazoleacetic acid	5.41E+03	14.6	5.53E+03	6.0
α-ketoglutarate	6.83E+08	46.1	6.14E+08	20.7
glutamine	6.38E+08	13.5	6.74E+08	12.8
lysine	3.56E+06	32.6	4.40E+06	40.4
glutamate	2.26E+08	22.1	1.82E+08	43.4
2-oxo-4-methylthiobutanoate	1.21E+05	68.7	1.55E+05	27.7
2-hydroxy-2-methylbutanedioic acid	1.24E+08	28.3	1.44E+08	53.9
methionine	1.16E+08	26.9	1.28E+08	19.1
3-methylphenylacetic acid	1.74E+06	84.7	3.46E+07	23.3
guanine	2.04E+04	90.5	9.86E+03	52.1
xanthine	5.63E+07	97.6	8.89E+07	39.5
hydroxyphenylacetic acid	5.21E+06	43.2	3.29E+06	21.5
2,3-dihydroxybenzoic acid	6.49E+07	35.3	7.53E+07	35.5
histidine	2.54E+06	24.0	2.55E+06	26.7
orotate	1.33E+07	40.6	1.38E+07	33.6
dihydroorotate	5.11E+05	34.4	3.85E+05	29.8
allantoin	1.24E+08	21.4	1.03E+08	21.3
indole-3-carboxylic acid	5.50E+05	39.6	4.45E+05	25.9
phenylpyruvate	2.13E+06	48.0	4.53E+06	65.6
methionine sulfoxide	1.11E+07	134.3	9.10E+06	45.1
phenylalanine	2.03E+08	22.9	2.09E+08	13.9
phenyllactic acid	1.48E+07	58.8	4.90E+06	35.0
quinolinate	7.89E+05	67.0	1.60E+06	82.4
N-acetyltaurine	4.69E+07	32.3	3.41E+07	29.9
phosphoenolpyruvate	5.96E+06	132.3	9.50E+06	175.9
uric acid	1.92E+08	23.7	1.97E+08	21.8
cysteate	1.84E+05	30.9	1.15E+05	30.6
1-methyl-histidine	1.08E+05	42.1	6.62E+04	42.5
sulfolactate	2.24E+06	36.9	3.35E+06	53.2
dihydroxy-acetone-phosphate	1.62E+07	33.9	7.62E+06	57.8
sn-glycerol-3-phosphate	1.64E+08	29.2	1.51E+08	32.7
aconitate	1.78E+08	28.5	2.03E+08	34.8
N-acetyl-L-ornithine	4.09E+06	27.0	2.76E+06	15.0
arginine	2.56E+06	36.1	3.22E+06	45.1
citrulline	6.72E+07	24.1	6.06E+07	33.1
ascorbic acid	4.81E+06	134.9	9.80E+04	55.5
N-carbamoyl-L-aspartate	5.98E+05	62.1	4.41E+05	13.4

Figure 4.S19. Average plasma metabolite ion counts and relative standard deviations (RSD) for Jax (n=5) and NCI (n=5) mice.

Metabolite	Jax		NCI	
	Average	RSD (%)	Average	RSD (%)
allantoate	2.81E+05	46.1	1.51E+05	25.4
2-isopropylmalic acid	5.97E+06	51.5	7.82E+06	76.9
glucono-1,5-lactone	1.54E+06	35.9	1.65E+06	37.1
glucosamine	3.02E+04	N.D.	N.D.	N.D.
myo-inositol	4.86E+07	9.8	3.85E+07	38.0
tyrosine	1.96E+08	30.0	2.23E+08	14.2
4-pyridoxic acid	5.91E+06	48.7	3.75E+06	19.9
3-phosphoglycerate	4.18E+07	54.2	9.50E+07	133.5
indoleacrylic acid	7.75E+05	47.8	6.79E+05	34.9
kynurenic acid	3.54E+05	42.3	3.82E+05	47.7
N-acetyl-glutamate	1.20E+07	34.2	1.06E+07	28.7
5-hydroxyindoleacetic acid	1.08E+06	44.0	2.31E+06	12.1
citrate/isocitrate	8.59E+09	27.2	8.66E+09	25.8
2-dehydro-D-gluconate	1.98E+07	25.5	1.86E+07	19.6
D-gluconate	1.54E+08	19.4	1.64E+08	18.9
D-erythrose-4-phosphate	4.01E+06	31.7	1.96E+06	50.4
tryptophan	1.74E+08	33.4	1.91E+08	14.9
xanthurenic acid	2.41E+05	60.1	1.08E+06	160.5
kynurenine	5.00E+05	40.6	8.34E+05	51.6
D-glucarate	4.34E+06	62.4	8.36E+06	112.4
pantothenate	2.87E+08	20.8	1.98E+08	13.7
deoxyuridine	5.99E+06	34.0	2.34E+06	36.7
thymidine	1.17E+06	88.6	1.23E+06	33.3
uridine	9.53E+06	26.5	7.90E+06	7.3
D-glucono-1,5-lactone-6-phosphate	1.59E+04	61.1	1.46E+04	37.4
acadesine	3.80E+04	39.2	2.24E+04	14.8
glucose-6-phosphate	2.02E+07	28.6	1.63E+07	45.4
thiamine	1.30E+05	50.1	2.12E+05	62.6
adenosine	7.65E+03	50.9	3.51E+03	N.D.
inosine	6.87E+06	106.4	1.53E+07	56.7
6-phospho- D-gluconate	1.72E+06	85.1	2.33E+06	62.1
1-methyladenosine	4.73E+05	33.8	5.47E+05	20.7
guanosine	2.64E+05	128.1	6.02E+05	61.0
xanthosine	1.19E+05	86.2	8.36E+04	90.0
D-sedoheptulose-1/7-phosphate	1.61E+06	90.1	2.11E+06	162.7
N-acetyl-glucosamine-1/6-phosphate	7.37E+06	27.8	5.61E+06	34.4
dCMP	4.08E+05	163.7	1.92E+04	106.8
glutathione	1.73E+07	173.8	2.49E+06	110.8
geranyl-PP	6.31E+04	78.9	9.28E+04	147.2
dTMP	7.99E+05	123.3	7.03E+03	39.0
CMP	2.98E+06	32.2	2.09E+06	80.0
UMP	6.54E+06	86.5	3.02E+06	162.4
cyclic-AMP	5.31E+04	36.7	7.49E+04	63.0
AICAR	5.32E+03	N.D.	N.D.	N.D.
fructose-1-6-bisphosphate	3.44E+07	58.8	1.30E+07	54.1
trehalose/sucrose	1.13E+06	63.9	7.31E+05	43.3
thiamine-phosphate	N.D.	N.D.	N.D.	N.D.
dGMP	4.16E+07	80.2	7.03E+06	172.1
IMP	4.84E+06	120.2	5.97E+06	201.2
S-adenosyl-L-methioninamine	4.38E+07	30.5	3.97E+07	34.5
GMP	6.15E+06	59.4	7.59E+06	165.9
riboflavin	8.96E+03	9.3	5.60E+03	N.D.
S-adenosyl-L-homoCysteine	2.12E+03	5.9	N.D.	N.D.

Figure 4.S19. Continued

	Jax		NCI	
Metabolite	**Average**	**RSD (%)**	**Average**	**RSD (%)**
octoluse Bisphosphate	N.D.	N.D.	5.09E+03	15.1
dTDP	1.23E+05	111.3	N.D.	N.D.
UDP	2.73E+04	112.7	1.48E+04	26.0
Cholic acid	8.82E+07	130.8	1.57E+07	71.2
thiamine pyrophosphate	1.30E+06	100.1	1.54E+06	78.9
ADP	3.77E+07	100.8	6.70E+06	70.7
GDP	3.16E+06	135.6	7.24E+05	141.8
CDP-ethanolamine	1.84E+05	84.5	7.31E+04	122.4
5-methyl-THF	4.43E+04	57.4	9.40E+03	N.D.
dCTP	N.D.	N.D.	N.D.	N.D.
UTP	5.72E+05	127.6	9.94E+03	17.7
taurodeoxycholic acid	2.04E+07	70.4	1.00E+07	62.8
ATP	1.85E+07	116.3	1.70E+06	79.7
GTP	2.15E+06	177.7	9.97E+04	79.7
UDP-D-glucose	1.31E+06	111.5	8.52E+05	164.0
UDP-D-glucuronate	1.41E+05	138.4	1.15E+05	174.6
ADP-D-glucose	1.49E+05	85.2	7.88E+04	132.1
UDP-*N*-acetyl-glucosamine	1.56E+06	52.7	8.15E+05	106.9
glutathione disulfide	5.14E+07	50.0	5.66E+07	56.2
NAD^+	2.71E+05	157.1	3.24E+04	58.0
NADH	1.03E+04	13.6	N.D.	N.D.
dephospho-CoA	9.94E+04	92.2	N.D.	N.D.
$NADP^+$	7.06E+05	113.1	1.63E+05	N.D.
FAD	1.18E+06	42.2	2.48E+06	68.8
acetyl-CoA	1.87E+07	159.6	9.90E+03	N.D.
butyryl-CoA	3.56E+07	173.1	7.96E+04	N.D.

Figure 4.S19. Continued

CHAPTER FIVE - CONCLUSIONS AND FUTURE DIRECTIONS

Distinct microbiomes are found within various host tissues and in free living environments. Assemblages of microbes inhabit multiple surfaces and sites within and on hosts across kingdoms of life [1]. Due to a number of selective pressures, host-associated microbiomes are often very different than their surrounding environmental inocula [2]. Further, internal and external host microenvironments vary and may sometimes functionally overlap, suggesting niche microbial modifications to best serve the host and the microbiome. [3-6]. Perhaps not surprisingly, the human gut alone is the home to bacterial abundances in accordance with whole human body cell totals [7]. Thus, microbial influence on hosts and other microbes is a fundamental component of life on Earth. Host and microbe co-evolution has allowed for optimization of these relationships, often resulting in shared benefits such as nutrient acquisition [8], abiotic stress tolerance (e.g. drought) [9], and protection from pathogens [10, 11]. Taxa comprising microbiomes are often host-specific and can tip the balance from host death to survival [12, 13]. Significantly, taxa abundance within a microbiome does not always correlate with influence or importance, as rare or transient members sometimes disproportionately influence their host [14]. Exploration of composition in relation to function suggest that less important is the individual taxa, rather of significance is what the microbe can do to meet a functional need of the community and host [3, 6, 15-17].

Microbiome assembly and stability cues are complex, and many are largely unknown. Host-microbe interactions and commensal community establishment requires contributions from both microbes and hosts, namely immune modulation of the host and microbial tolerance of co-dwelling members. Of note, assembly timing is host-specific [18, 19] and may be dynamic. Stability is not always achievable, and resulting dysbiosis is known to disrupt microbiomes and can result in host pathology [4, 20-23] and even seemingly unrelated host physiologies [24]. The powerful relationships between hosts and microbiomes offer endless opportunities to determine functional and mechanistic microbiome assemblage attributes for application in therapies to improve health and wellness.

Microbial treatment of plants to improve plant health or disease resistance is not novel, and technological advancements have highlighted the importance of identification of plant growth

promoting (PGP) genes as well as application of our current knowledge of disease-suppressive organisms such as strains of *Pseudomonas* spp [25-28]. Discovery of plant-mediated microbiome modifications to control diseases are ongoing. For example, tomato plants root exudate profiles change in the presence of a pathogen, resulting in altered microbiome composition [29]. Also, barley increases antifungal traits when infected with a root pathogen [30]. Disease suppressive soils are known to influence pathogen survival and contribute to plant health [12]. Common microbial members of disease suppressive soils are Pseudomonales, Streptomycetaceae and Micromonosporaceae [12]. Study of three potato cultivars in two different soils found taxonomic differences in rhizosphere microbiomes. Specifically, the authors discovered an abundance of disease-suppressive taxa listed above, suggesting plant genotype can influence plant selection of microbes for protective purposes [31]. We suggest that new approaches and strategies in sustainable agriculture may soon be called for. A recent review details the use of beneficial microbes as seed coats prior to use in agriculture [32]. The review highlights the possibilities of using endophytic and rhizosphere-associated organisms, such as endophytic *Achromobacter xylosoxidans* for treatment of rice [33] and *Beauveria bassiana* for treatment of pine trees [34].

While the potential exists, specific challenges related to scale, production and ultimately colonization and microbial survival persist. Considerations of beneficial consortia versus individual taxa further create complexity [25]. Phyla with beneficial potential are growing and regularly include Proteobacteria, Firmicutes, Bacteroidetes and Actinobacteria [10, 25]. While not abundant in the root microbiome, members of the Actinobacteria phylum, *Streptomyces* are being recognized for their potential application [10]. Known for their robust metabolic potential [35] as well as presence within roots of a variety of plants [36-38], Actinobacteria are routinely included in plant-beneficial consortia [39]. Thus far, and largely legitimately, many Actinobacteria communities for agricultural application are composed of larger grouping of phyla members, with the intention of generalized treatment to maximize plant benefit. While these strategies may work, they may not achieve optimal results, meaning plant energy output dedicated to assimilation of many different microbes may outweigh benefit. As described in Chapter 3, we propose that microbial interactions may influence treatment potency and suggest the need for targeted exploration of Actinobacteria isolate monoapplications. In addition, unique microbial metabolites,

such as melanin (Chapter 2) or those predicted via antiSMASH (Chapter 3), may induce the desired plant-beneficial outcome and thus necessitate more simplified applications of fewer taxa or even the product itself. Much can be learned from lower complexity and monoculture experiments. As we discover more about lower complexity relationships, the opportunity exists to identify functional benefits and construct consortia with exponential host benefits. However, complex agriculture systems will likely require fine-tuned, consistent and tractable applications, regardless of the diversity of the proposed beneficial bacteria.

Additional sequencing results of samples treated as described in Chapter 3 were recently made available to our lab for inclusion in our community studies. In some cases, these samples will contribute to our power via addition of new technical replicates, and in other cases, we will add new experimental samples to our studies. We will use the QIIME 2 pipeline and analyses described above to determine appropriate inclusion and new results. In addition, we anticipate monoinoculation vertical plate assays with members of our 11 isolate synthetic community (SynCom, Chapter 3) for assessment of root morphology, as well as colonization phenotypes. Our collection of isolates as well as those of collaborators allow additional testing of new isolates from genera identified in individual family relative abundances in Chapter 3. We are specifically interested in plant associated Azospirillaceae and Moraxellaceae as these genera proved inconsistent colonizers, and they both originated from the tertiary open-air inoculum or secondary wild soil slurry (Chapter 3). These experiments would help tease apart genus from species influence and further inform isolates include in future low complexity SynCom.

To make functional and mechanistic microbiome assembly and stability inferences, we must move beyond identification of genes suspected to be important to transcriptional studies. We will design experiments to determine transcriptional profiles from our four *Streptomyces* and select SynCom members when challenged with other *Streptomyces* or SynCom isolates as well as in the context of the plant. We are particularly interested in transcriptomic profiles of 299 and 303 as they were shown to be a significant primary inoculum with potential microbiome sculpting activities both via alpha diversity metrics and relative abundances of Streptomycetaceae (Chapter 3). Additionally, we will select members from each family of interest for transcriptional profiling.

Ultimately, building on our 16S rRNA gene sequence databases, we would like to identify genes up and downregulated during microbiome colonization events, helping to tease apart plant from microbial-driven microbiome assemblage mechanisms.

Significantly, antiSMASH results provide a rich set of data primed for hypothesis generation and testing. AntiSMASH provided valuable evidence that the pigmentation in 299 and 303 cultures was as a result of melanin production (Chapter 2). In addition, the analysis predicted various strain-specific antimicrobial metabolites, several of which are overlapping, suggesting resistance, and functional redundancy. These discoveries provide possibilities of testing functional groups of organisms for comparison to taxonomically defined groups.

The use of lower complexity SynCom, co-culture *in vitro,* and monoculture *in vivo* studies to inform community level interactions is generating more attention [40]. We suggest that these techniques combined with community genomics and transcriptomics will provide increasingly robust conclusions and identification of important mechanisms that can be developed into applications improving plant growth and productivity. These techniques should also be considered in relation to study of the mammalian microbiome. Complexity of plant-microbiome interactions are similar to those described when attempting to determine the individual and combined influence of multiple and often simultaneous environmental exposures in humans [41]. Though host systems are distinct, strategies for making mechanistic conclusions and development of applications/therapies may align across host systems and have begun to be explored in various experimental forums [8, 42].

With these things in mind, strategies to combine plant and gut microbiome benefits seem likely. Increasingly, disease etiologies are associated with dysbiosis [43-45]. If not dysbiosis, as in the case of malaria (Chapter 4) protective and susceptible disease phenotypes correlate with divergent microbiome composition and abundances [46]. Capitalizing on data such as these suggest the need to development of therapies joining plant and gut microbiome research. The previously described use of probiotic seed coating to protect crops from specific pathogens provides a starting point for efforts such as these [32]. I would suggest the need to bridge the gap between diseases such as

malaria and probiotic therapies *in planta*. Perhaps seed coatings that are crop and gut beneficial and anti-malarial could both feed and protect individuals. Alternatively, studies of plant microbes that induce host genes involved in pathogen suppression may inform recognition similar patterns in mammals, creating opportunities to develop targeted functional microbial therapies. For example, further exploration of *Lactobacillus* genes significant in modulation of malarial illness could allow identification of agriculturally relevant plant-specific taxa harboring homologous gene(s). Growing evidence of microbiome assembly structures and cues across plant species, provides great opportunity for advancements in paired plant-mammal microbiome therapeutics.

Here we have provided evidence of microbiome potential in influencing hosts or competing microbes. Significantly, we suggest the metabolic potential of *Streptomyces* to both protect themselves from common plant root phenolics (Chapter 2) and persist when challenged with communities of varying complexities (Chapter 3). While not robust colonizers, *Streptomyces'* consistent presence in microbiomes across plant species suggests their importance and signals their value for further explorations. Further, it affirms that abundance may not be as influential as function or capability of less abundant taxa. These studies also suggest the value of employing multiple techniques to more fully understand microbial relationships. Further, using communities with varying levels of complexity provides insights that could otherwise be overlooked. Similarly, while mammalian gut taxa have been previously identified as beneficial for gut health, complex gut microbiomes are not well understood. Probiotic therapies are not regulated and still not well understood. Further, even less is known about how gut microbiome composition modulates pathogen infection. In Chapter 4 we describe that gut microbiome taxa abundances are divergent for malaria-susceptible and malaria-resistant mice. However, we know much less about the mechanisms involved in these phenotypes. Application of reductionist approaches, multiple levels of microbiome complexity and employing various techniques may help to tease apart functions of taxa aligned with disease suppression. Great opportunity exists to extend our knowledge of microbiomes and host associations across kingdoms of life. Likely a central node linking these studies are network analyses, identifying overlapping genes and functions.

My future research efforts will likely focus on the overlap of the mammalian microbiome and liver diseases. I am interested in development of microbial therapies to reduce T-cell mediated allograft rejection of transplanted livers. The ideas explored throughout my dissertation significantly contribute to the direction and intention of my future work. Likely with much assistance and training, I intend to apply emerging ideas suggesting the importance of network analyses to create a network of mammalian gut and *A. thaliana* root genes. These systems are similar in that they require host immune modulation for microbe assimilation. I can then introduce known microbiome members in each system and query the network for genes significant in immune regulation. I also plan to design SynCom for mammalian application using methods learned here, and further look for functional redundancy to determine taxonomic versus functional host-mediated selective pressures. Overall, I intend to design agricultural microbial therapies that can be applied in mammalian systems to provide specific immune suppression. Opportunities for cross kingdom investigation are great. However, use of a less complex plant system for application to a more complex mammalian system is be challenging. Studies of microbiomes must be more dynamic and multidisciplinary to incorporate the needs of a growing population with increased demands on crop production as well as rising chronic and infectious disease prevalence.

I. REFERENCES

1. Rosenberg, E. and I. Zilber-Rosenberg, *The hologenome concept of evolution after 10 years.* Microbiome, 2018. **6**.
2. Adair, K.L. and A.E. Douglas, *Making a microbiome: the many determinants of host-associated microbial community composition.* Current Opinion in Microbiology, 2017. **35**: p. 23-29.
3. Bai, Y., et al., *Functional overlap of the Arabidopsis leaf and root microbiota.* Nature, 2015. **528**(7582): p. 364-9.
4. O'Dwyer, D.N., R.P. Dickson, and B.B. Moore, *The Lung Microbiome, Immunity, and the Pathogenesis of Chronic Lung Disease.* Journal of Immunology, 2016. **196**(12): p. 4839-4847.
5. Wolz, C.R.M., et al., *Effects of host species and environment on the skin microbiome of Plethodontid salamanders.* Journal of Animal Ecology, 2018. **87**(2): p. 341-353.
6. van der Heijden, M.G. and M. Hartmann, *Networking in the Plant Microbiome.* PLoS Biol, 2016. **14**(2): p. e1002378.
7. Sender, R., S. Fuchs, and R. Milo, *Revised Estimates for the Number of Human and Bacteria Cells in the Body.* Plos Biology, 2016. **14**(8).
8. Hacquard, S., et al., *Microbiota and Host Nutrition across Plant and Animal Kingdoms.* Cell Host Microbe, 2015. **17**(5): p. 603-16.
9. Naylor, D. and D. Coleman-Derr, *Drought Stress and Root-Associated Bacterial Communities.* Frontiers in Plant Science, 2018. **8**.
10. Viaene, T., et al., *Streptomyces as a plant's best friend?* FEMS Microbiol Ecol, 2016. **92**(8).
11. King, K.C., et al., *Rapid evolution of microbe-mediated protection against pathogens in a worm host.* Isme Journal, 2016. **10**(8): p. 1915-1924.
12. Berendsen, R.L., C.M.J. Pieterse, and P. Bakker, *The rhizosphere microbiome and plant health.* Trends in Plant Science, 2012. **17**(8): p. 478-486.
13. Blaser, M.J., *Who are we? Indigenous microbes and the ecology of human diseases.* Embo Reports, 2006. **7**(10): p. 956-960.

14. Shade, A. and J.A. Gilbert, *Temporal patterns of rarity provide a more complete view of microbial diversity.* Trends Microbiol, 2015. **23**(6): p. 335-40.
15. Tripathi, B.M., et al., *Trends in Taxonomic and Functional Composition of Soil Microbiome Along a Precipitation Gradient in Israel.* Microb Ecol, 2017. **74**(1): p. 168-176.
16. Borer, E.T., et al., *The world within: Quantifying the determinants and outcomes of a host's microbiome.* Basic and Applied Ecology, 2013. **14**(7): p. 533-539.
17. Bakker, P.A.H.M., et al., *The rhizosphere revisited: root microbiomics.* Frontiers in Plant Science, 2013. **4**.
18. Milani, C., et al., *The First Microbial Colonizers of the Human Gut: Composition, Activities, and Health Implications of the Infant Gut Microbiota.* Microbiology and Molecular Biology Reviews, 2017. **81**(4).
19. Chaparro, J.M., et al., *Root exudation of phytochemicals in Arabidopsis follows specific patterns that are developmentally programmed and correlate with soil microbial functions.* PLoS One, 2013. **8**(2): p. e55731.
20. Huttenhower, C., et al., *Structure, function and diversity of the healthy human microbiome.* Nature, 2012. **486**(7402): p. 207-214.
21. Jiang, W., M.M. Lederman, and P. Hunt, *Plasma levels of bacterial DNA correlate with immune activation and the magnitude of immune restoration in persons with antiretroviral-treated HIV infection (vol 199, pg 1177, 2009).* Journal of Infectious Diseases, 2009. **200**(1): p. 160-160.
22. Chen, Y., et al., *Characterization of Fecal Microbial Communities in Patients with Liver Cirrhosis.* Hepatology, 2011. **54**(2): p. 562-572.
23. Klein, E., et al., *Soil suppressiveness to fusarium disease: shifts in root microbiome associated with reduction of pathogen root colonization.* Phytopathology, 2013. **103**(1): p. 23-33.
24. Caputi, V., et al., *Antibiotic-induced dysbiosis of the microbiota impairs gut neuromuscular function in juvenile mice.* British Journal of Pharmacology, 2017. **174**(20): p. 3623-3639.

25. Finkel, O.M., et al., *Understanding and exploiting plant beneficial microbes.* Current Opinion in Plant Biology, 2017. **38**: p. 155-163.
26. Lareen, A., F. Burton, and P. Schafer, *Plant root-microbe communication in shaping root microbiomes.* Plant Mol Biol, 2016. **90**(6): p. 575-87.
27. Schlatter, D., et al., *Disease Suppressive Soils: New Insights from the Soil Microbiome.* Phytopathology, 2017. **107**(11): p. 1284-1297.
28. Mauchline, T.H. and J.G. Malone, *Life in earth - the root microbiome to the rescue?* Current Opinion in Microbiology, 2017. **37**: p. 23-28.
29. Gu, Y., et al., *Pathogen invasion indirectly changes the composition of soil microbiome via shifts in root exudation profile.* Biology and Fertility of Soils, 2016. **52**(7): p. 997-1005.
30. Dudenhoffer, J.H., S. Scheu, and A. Jousset, *Systemic enrichment of antifungal traits in the rhizosphere microbiome after pathogen attack.* Journal of Ecology, 2016. **104**(6): p. 1566-1575.
31. Weinert, N., et al., *PhyloChip hybridization uncovered an enormous bacterial diversity in the rhizosphere of different potato cultivars: many common and few cultivar-dependent taxa.* Fems Microbiology Ecology, 2011. **75**(3): p. 497-506.
32. O'Callaghan, M., *Microbial inoculation of seed for improved crop performance: issues and opportunities.* Applied Microbiology and Biotechnology, 2016. **100**(13): p. 5729-5746.
33. Montanez, A., et al., *Characterization of cultivable putative endophytic plant growth promoting bacteria associated with maize cultivars (Zea mays L.) and their inoculation effects in vitro.* Applied Soil Ecology, 2012. **58**: p. 21-28.
34. Brownbridge, M., et al., *Persistence of Beauveria bassiana (Ascomycota: Hypocreales) as an endophyte following inoculation of radiata pine seed and seedlings.* Biological Control, 2012. **61**(3): p. 194-200.
35. Barka, E.A., et al., *Taxonomy, Physiology, and Natural Products of Actinobacteria.* Microbiol Mol Biol Rev, 2016. **80**(1): p. 1-43.
36. Lundberg, D.S., et al., *Defining the core Arabidopsis thaliana root microbiome.* Nature, 2012. **488**(7409): p. 86-90.
37. Kirby, R., *Actinomycetes and lignin degradation.* Adv Appl Microbiol, 2006. **58**: p. 125-68.

38. Golinska, P., et al., *Endophytic actinobacteria of medicinal plants: diversity and bioactivity.* Antonie Van Leeuwenhoek, 2015. **108**(2): p. 267-89.
39. Sathya, A., R. Vijayabharathi, and S. Gopalakrishnan, *Plant growth-promoting actinobacteria: a new strategy for enhancing sustainable production and protection of grain legumes.* 3 Biotech, 2017. **7**.
40. Vorholt, J.A., et al., *Establishing Causality: Opportunities of Synthetic Communities for Plant Microbiome Research.* Cell Host & Microbe, 2017. **22**(2): p. 142-155.
41. Robinson, O., et al., *The Pregnancy Exposome: Multiple Environmental Exposures in the INMA-Sabadell Birth Cohort.* Environmental Science & Technology, 2015. **49**(17): p. 10632-10641.
42. Zeng, Q.L., et al., *Models of microbiome evolution incorporating host and microbial selection.* Microbiome, 2017. **5**.
43. Littman, D.R. and E.G. Pamer, *Role of the commensal microbiota in normal and pathogenic host immune responses.* Cell Host Microbe, 2011. **10**(4): p. 311-23.
44. Zhu, W.H., et al., *Precision editing of the gut microbiota ameliorates colitis.* Nature, 2018. **553**(7687): p. 208-+.
45. Shi, N., et al., *Interaction between the gut microbiome and mucosal immune system.* Military Medical Research, 2017. **4**.
46. Villarino, N.F., et al., *Composition of the gut microbiota modulates the severity of malaria.* Proceedings of the National Academy of Sciences of the United States of America, 2016. **113**(8): p. 2235-2240.

VITA

Sarah Stuart Chewning was born in Virginia Beach, VA to Craig and Susan Chewning. She loved being outdoors and exploring the woods and local waterways. Her interest in science blossomed in middle school in Kennesaw, GA. There she found that she enjoyed learning about the scientific world and began considering a future in science. The generosity and kindness of her 7th grade science teacher gave her confidence and inspired her to continue her interests in science.

She attended the University of Georgia and graduated in 2004 with a bachelor of science in Environmental Health. Her studies required a course in Epidemiology, in which she excelled and enjoyed very much. This led her to earn a Master of Public Health at the Rollins School of Public Health at Emory University in 2004. In 2003 she began an internship with the Centers for Disease Control and Prevention Agency for Toxic Substances and Disease Registry. She had found her passion in Public Health and was promoted to an ORISE Fellowship in 2004. She continued her work with CDC for two years, at which time she decided to pursue an opportunity to work as an infectious disease Epidemiologist at the Chattanooga-Hamilton County Health Department. She served there 6 years and loved the dynamic nature of outbreak investigations as well as teaching and training staff. During that time she also began teaching Epidemiology and other courses as adjunct faculty at the University of Tennessee Chattanooga. She was offered a full time faculty position and took the opportunity to explore a career in academia. It was then that she knew she would pursue a Doctor of Philosophy. She chose Microbiology as she desired a research career in science that would allow her to learn and answer questions in Immunology. She began her PhD at the University of Tennessee Knoxville in 2013 and joined the Schmidt lab studying malaria immunology. In 2014 she had the opportunity to be the inaugural graduate student of Sarah Lebeis and explore plant immunology as well as plant microbiome science. She enjoyed the opportunity learn two model systems and apply the knowledge and techniques gained in mammalian immunology to her new system. She found she very enjoyed being a member of a research laboratory and decided that despite her previous intentions to immediately rejoin traditional public health workforce, she would pursue a Post-Doctoral Fellowship.

Sarah Stuart will begin her Post-Doctoral Fellowship in the laboratory of Arash Grakoui with Emory University's Vaccine Center. She will again research mammalian immunology and anticipates pursing a project exploring the correlation between liver allograft rejection and the gut microbiome.